

Durham E-Theses

Transient interaction and control scheduling in multimachine power systems

Bumby, J. R.

How to cite:

Bumby, J. R. (1974) *Transient interaction and control scheduling in multimachine power systems*, Durham theses, Durham University. Available at Durham E-Theses Online:
<http://etheses.dur.ac.uk/8239/>

Use policy

The full-text may be used and/or reproduced, and given to third parties in any format or medium, without prior permission or charge, for personal research or study, educational, or not-for-profit purposes provided that:

- a full bibliographic reference is made to the original source
- a [link](#) is made to the metadata record in Durham E-Theses
- the full-text is not changed in any way

The full-text must not be sold in any format or medium without the formal permission of the copyright holders.

Please consult the [full Durham E-Theses policy](#) for further details.

TRANSIENT INTERACTION AND CONTROL
SCHEDULING IN MULTIMACHINE
POWER SYSTEMS

by

J.R. BUMBY, B.Sc.

Thesis submitted for the Degree of Doctor of
Philosophy in the Faculty of Science,
University of Durham.

The copyright of this thesis rests with the author.
No quotation from it should be published without
his prior written consent and information derived
from it should be acknowledged.

April, 1974.



ABSTRACT

TRANSIENT INTERACTION AND CONTROL SCHEDULING
IN MULTIMACHINE POWER SYSTEMS

by

J.R. BUNBY

The thesis describes new methods of determining control schemes for multimachine power systems by using Linear Multivariable Control Theory.

The initial stages of the work includes a review of the different modelling techniques available for studying the performance of synchronous machines by analogue or digital computation. Based on this review a non-linear digital program that describes any multimachine power system is produced. For control work a linearised version of this program is available.

A review of the mathematical theory behind Linear Multivariable Control methods is given emphasising its link with the classical approach of Nyquist Analysis.

The control theory is interfaced with the digital model of the power system to produce a series of designs by which control is achieved by either:

- (i) Impedance switching
- (ii) Fast valving
- (iii) Field Excitation

The different control designs are compared both with each other and with control schemes suggested by other authors. Working from a purely mathematical basis control schemes are postulated that produce improved operation to both small and large disturbances.

The advantages of fast valving as a control method is outlined and suggested as the most advantageous method of overall control for both single and multimachine power systems.

ACKNOWLEDGMENTS

The author would like to express his sincere gratitude to the following:

Mr. R. Gorley of the Computing Department, University of Durham.

The Engineering Science Department, University of Durham, for the facilities provided to make this work possible.

Dr. C. Preece, my supervisor, for his continued help and encouragement throughout this work.

The Science Research Council are acknowledged for providing the author with financial support.

CONTENTS

Page No.

List of Symbols

Chapter 1 - Introduction

1.1	The Transient Stability Problem	1
1.2	Methods of Improving Transient Stability								
1.2.1	The Control Problem	2
1.2.2	Impedance Switching	2
1.2.3	Excitation Control	3
1.2.4	Turbine Fast Valving	3
1.3	Control System Design Methods	4
1.4	Multivariable Control Methods	5
1.5	Formulation of the Design Problem	6
1.6	Stability Definitions								
1.6.1	General	7
1.6.2	Lyapunov Instability	7
1.6.3	Nyquist Instability	8
1.6.4	Definition of the Stability Limit				8
1.7	Development of Synchronous Machine Models								
1.7.1	General	9
1.7.2	Machine System Interface	9
1.7.3	Saturation of Machine Parameters	10
1.7.4	Machine Representation	10
1.7.5	Conclusion	14

Chapter 2 - A Non-Linear Multimachine Power System Computer Program

2.1	General Program Specification	15
2.2	Modelling Technique Synchronous Machine	15

2.3	Network Performance Model								
2.3.1	The Model Reference Frame	17
2.3.2	Busbar Representation	18
2.3.3	Representation of Loads	18
2.3.4	Synchronous Machine Connection	19
2.3.5	The Interconnection of Machine and Network Equations								19
2.4	Digital Program Solution Method	20
2.5	Control Equipment								
2.5.1	Alternator Field Excitation Regulator					20
2.5.2	Input Power Regulator	22
2.6	Numerical Methods								
2.6.1	Iteration Method	22
2.6.2	Iteration Stability	23
2.6.3	Integration Methods	23
2.6.4	Integration Instabilities	23
2.7	Program Verification	25
2.8	Conclusion	25

Chapter 3 - A Linear Multimachine Power System Computer Program

3.1	General	26
3.2	The Linearised Machine and Network Equations					26
3.3	Regulator Modelling	28
3.4	Solution Technique	28
3.5	Program Verification	28
3.6	The Plant Transfer Function Matrix					29
3.7	A Definition of Transient Response					29
3.8	The Output Equation	30
3.9	Formation of the Plant Transfer Function Matrices									
3.9.1	Control of Turbine Input Power	32
3.9.2	Control of Field Excitation	32
3.9.3	Transfer Function Matrices with Regulators					33

3.10	Conclusion	34
------	--------------------	----

Chapter 4 - Linear Multivariable Control Theory

4.1	General	35
4.2	The Control System	35
4.3	Vector Feedback Stability Criteria	
4.3.1	General Stability Definitions	36
4.3.2	Stability in Terms of the Return Difference Matrix ..	38
4.3.3	An Indirect Statement of Stability in Terms of the Return Difference Matrix	39
4.3.4	Stability in Terms of Open Loop and Closed Loop Transfer Function Matrices ,. .. .	40
4.4	Application of the Stability Criteria	43
4.5	Digital Computation of the Inverse Nyquist Diagrams ..	44
4.6	Design of Non-Interactive Controllers	44
4.6.1	Controller Design by Matrix Division	45
4.6.2	Compensation in The Feedback Matrix, $F(p)$..	45
4.6.3	Rosenbrock's Inverse Nyquist Array Design Method	45
4.6.4	Discussion	46
4.7	Conclusion	46

Chapter 5 - The Dynamic Interaction of Synchronous Machines

5.1	Introduction	47
5.2	Control Equipment	47
5.3	Transmission Systems Studied	48
5.4	A Qualitative Assessment of Parameter Variation on the Oscillation Frequency ..	48
5.5	Interaction Phenomena - A General Description	50
5.6	Synchronous Machine Models - The Effect of Neglecting Transient Saliency	51
5.7	Multiswing and First Swing Instability	54

	<u>Page No.</u>
5.8 The Effect of Damping Constants on Dynamic Interaction	54
5.9 The Effect of Flux Decrement on the Transient Interaction	55
5.10 Conclusion	57

Chapter 6 - A Transient Control Scheme by Impedance Switching

6.1 General	59
6.2 A Comparison Between The Linear/Non-Linear Equations	
6.2.1 The Effect of the Initial Conditions	59
6.2.2 The Effect of Fault Conditions	59
6.2.3 Conclusion	61
6.3 A Switched Series Impedance Control Scheme	61
6.4 Derivation of the Linear Equations	62
6.5 Compensator Design	64
6.6 Stability	65
6.7 Fault Conditions	65
6.8 Application of the Control Matrix	66
6.9 Implementation of a Switched Control Unit	66
6.10 Controlled Capacitor Insertion	67
6.11 Large Disturbances	68
6.12 Controller Versatility	68
6.13 Practical Difficulties Involved with Impedance Switching	69
6.14 Conclusions	70

Chapter 7 - A Non-Interactive Control Scheme - Small
Perturbation Study

7.1 General	72
7.2 System Disturbances	72
7.3 The Removal of Interaction Effects by Turbine Fast Valving	
7.3.1 The Design Scheme	73
7.3.2 Stability and Control	75

7.4	The Removal of Interaction Effects by Excitation Methods	
7.4.1	The Design Scheme	76
7.4.2	Controllability	78
7.5	A Measure of Damping	79
7.6	Fast Valving - The Effect of Regulator Models	
7.6.1	General	79
7.6.2	Direct Control of Turbine Power Input	80
7.6.3	Regulator Modelled by a First Order Lag	81
7.6.4	Second Order Regulator	82
7.7	Stabilisation of Velocity Feedback with an Additional Acceleration Term	84
7.8	The Removal of Interaction on 3% Faults of Short Duration	
7.8.1	General	86
7.8.2	The Benefit of Interaction Removal	86
7.9	Excitation Control	
7.9.1	General	88
7.9.2	Voltage Feedback	88
7.9.3	Velocity Feedback	90
7.9.4	Acceleration Feedback	92
7.10	Conclusion	92

Chapter 8 - A Non-Interactive Control Scheme - Large Disturbances

8.1	General	96
8.2	Fast Valving	
8.2.1	Acceleration Feedback	96
8.2.2	Velocity Feedback	99
8.2.3	Combined Velocity and Acceleration Feedback ..	100
8.3	Excitation Control	
8.3.1	The Alteration of First Load Angle Maximum	100
8.3.2	Subsequent Load Angle Reductions	103

8.4	The Effect of Interaction Removal on the Stability Limit	104
8.5	Conclusion	105

Chapter 9 - Reliability of the Non-Interactive Control Method

9.1	General	108
9.2	The Effect of the Cross Feedback Components	108
9.3	Application of the Non-Interactive Controller to REP 6	110
9.4	Sensitivity of the Control Unit to Changes in the Initial Operating Point	
9.4.1	Small Perturbations	111
9.4.2	Large Disturbances	112
9.5	Conclusion	112

Chapter 10 - Conclusion

10.1	Control Design Method	114
10.2	Impedance Switching	115
10.3	A Comparison Between Excitation Control and Fast Valving	115
10.4	Future Trends	118
10.5	Fast Valving	119
	References	121

Appendices

Appendix A - Development of the Synchronous Machine Model

A.1	5-Winding Model	131
A.2	3-Winding Model	134

Appendix B - The Network Equations

B.1	Steady State	136
B.2	Transient State	137

Appendix C - Development of the Linear System Model								
C.1	Machine Equations	138
C.2	System Equations	140
C.3	Connection of the Machine and Network Equations	..						141
C.4	Calculation of the Output Matrix for Voltage Feedback							144
Appendix D - A Description of the Multimachine Digital Program								145
Appendix E - A Description of the Linear Program								146
Appendix F - Digital Program to Plot Inverse Nyquist Diagrams								147
Appendix G - Machine and System Parameters								149
Appendix H								150

LIST OF SYMBOLS

GENERAL

- j - Complex Operator.
- p - Laplace Operator,
- $*$ - Complex conjugate.
- \hat{A} - Inverse of Matrix, A.
- Δ - Small change in a Parameter.

Capital letters depicting electrical quantities imply R.M.S. values and small letters instantaneous values,

e.g. I - R.M.S. current

i - instantaneous current.

p.u. quantities are used throughout.

SYNCHRONOUS MACHINE

- d - Machine direct-axis.
- q - Machine quadrature-axis.
- D - System direct-axis.
- Q - System quadrature-axis.
- E_h - Modelling voltage.
- E_{hd} - d-cmpt. of E_h .
- E_{hq} - q-cmpt. of E_h .
- E_T - Machine terminal voltage.
- e_d - d-axis cmpt. of terminal voltage.
- e_q - q-axis cmpt. of terminal voltage.
- E_i' - Voltage behind transient reactance.
- E_q', e_q' - q-axis component of E'
- E_d', e_d' - d-axis component of E'
- E' - Voltage behind x_d'
- E_{fd}, e_f - Field voltage.
- E_{q0} - Open circuit voltage.

e_q''	- q-axis voltage behind subtransient reactance.
e_d''	- d-axis voltage behind subtransient reactance.
f	- frequency, 50
H	- Inertia constant, KJ/KVA.
I_T, i_T	- Machine terminal Current.
I_d, i_d	- d-axis comp. of I_T, i_T
I_q, i_q	- q-axis comp. of I_T, i_T
I_f, i_f	- Field current.
i_D	- d-axis damper current.
i_Q	- q-axis damper current.
K_D	- Damping constant.
P_m	- Mechanical input power.
P_T	- Machine Terminal power, Real.
Q_T	- Machine Terminal power, Reactive.
P_L	- Power losses.
r	- Armature resistance/phase.
r_f	- Field resistance.
r_D	- d-axis damper resistance.
r_Q	- q-axis damper resistance.
T_{d0}'	- Field open circuit time constant.
T_d'	- Field short circuit time constant.
T_{d0}''	- Field subtransient open circuit time constant.
T_d''	- Field subtransient short circuit time constant.
T_{q0}''	- Quadrature axis subtransient short cct. time constant.
T_D	- Direct Axis Damper leakage time constant.
T_F	- Time of Fault.
T_{FC}	- Time of Fault clearing.
T_{FR}	- Time of Reclosure.

- ω - synchronous angular frequency = $2\pi.f$
- x_d - d-axis synchronous reactance.
- x_q - q-axis synchronous reactance.
- x_d' - d-axis transient reactance.
- x_q' - q-axis transient reactance.
- x_d'' - d-axis sub-transient reactance.
- x_q'' - q-axis sub-transient reactance.
- x_{ad} - Magnetising reactance between rotor and d-axis stator.
- x_{fd} - Magnetising reactance between field and d-axis damper.
- x_{aq} - Magnetising reactance between rotor and q-axis stator
- $x_d(p)$] - Operational Impedances.
- $x_q(p)$]
- $G(p)$]
- ω - Instantaneous angular frequency.
- δ - Rotor angle w.r.t. E'
- δ_q - Rotor angle w.r.t. to q-axis.
- ϕ_d - d-axis stator flux linkage.
- ϕ_f - Field flux linkage.
- ϕ_D - d-axis damper flux linkage.
- ϕ_q - q-axis stator flux linkage.
- ϕ_O - q-axis damper flux linkage.
- 1 - Machine 1.
- 2 - Machine 2.

REGULATOR MODELS

(a) FIELD EXCITATION REGULATOR

- e_r - Error voltage.
- E_{fd} - Alternator field voltage
- K_{fb} - Feedback Gain.

- K - Overall Exciter Gain.
- K_1 - Amplifier Gain.
- T_{fb} - Transducer time constant.
- T_1 - Amplifier time constant.
- T_2, T_3 - Rectifier time constants.
- T_{exc} - Overall Exciter time constant.
- V_{ref} - Exciter reference voltage.
- y_{fb} - Feedback parameter.

(b) INPUT POWER REGULATOR

- K_p - Overall Gain
- K_{fb} - Feedback Gain.
- T_v - Valve time constant.
- T_s - Time constant of Steam System.

TRANSMISSION SYSTEM

- E_k - Voltage at bus, K .
- E_{bus} - Matrix of bus voltages.
- I_{bus} - Matrix of bus currents.
- I_k - Current at bus, K .
- P_k - Real power at bus,
- P_{kl} - Real power flow between bus k and l .
- Q_k - Reactive power at bus,
- Q_{kl} - Reactive power flow between bus k and l .
- Y_{bus} - Bus admittance matrix.
- Y_{ij} - Component i, j of Y_{bus}
- y_{jk} - Admittance between bus j and k .
- y_k - Sum of line charging and shunt admittance at bus k .
- $\frac{1}{2} y'_{kl}$ - Line charging between bus k and l .

Y_{KSHUNT} - Shunt admittance at bus, K .

Y_{K0} - Load represented at bus, K , by static admittance to ground.

CONTROL SYSTEM DESIGN

A - $n \times n$ Plant Matrix.

B - $n \times m$ Driving Matrix (1)

C - $m \times n$ Output Matrix.

D - $n \times m$ Driving Matrix (2)

D_c - Contour in the Complex Plane.

$d(p), \underline{d}$ - $m \times 1$ Vector of inputs (2).

$d_i(p), \delta_i(p)$ - radius of d -circles at the complex frequency, p .

$e(p)$ - $m \times 1$ matrix of error transforms.

$E(p)$ - $m \times m$ Return Difference Matrix.

$e_{ij}(p)$ - Component i, j of $E(p)$.

$F(p)$ - $m \times m$ matrix of Feedback Transducer transfer functions.

$f_{ij}(p)$ - Component i, j of $F(p)$.

$G(p)$ - $m \times m$ matrix of Plant Transfer functions.

$h(p)$ - $m \times 1$ matrix of reference input transforms.

$H(p)$ - $m \times m$ Closed Loop Transfer Function Matrix.

I_m, I - Identity Matrix.

$K(p)$ - $m \times m$ matrix of Controller transfer functions.

$K_a, K_b(p), K_c(p)$ - Synthesised components of Controller Matrix, (p).

k_i, k_{fb_i} - Feedback gain in loop, i .

$L(p)$ - $m \times m$ post-compensator matrix.

m - Number of inputs/outputs.

n - Number of state variables.

$\hat{p}_i(p)$ - Transfer function seen in the i^{th} loop when this is open and all other loops closed.

- $Q(p)$ - $m \times m$ Open-loop Transfer function Matrix.
 $q_{ij}(p)$ - Component i, j of $Q(p)$.
 $T(p)$ - $m \times m$ Return Ratio Matrix.
 $t_{ij}(p)$ - Component i, j of $T(p)$.
 $u(p), \underline{u}$ - $m \times 1$ vector of inputs (i).
 ω - Angular frequency.
 $y(p), \underline{y}$ - $m \times 1$ Vector of outputs.
 $\phi_o(p)$ - Open-loop system characteristic polynomial.
 $\phi_2(p)$ - Closed-loop system characteristic polynomial.
 $\rho_i(p)$ - Eigen-value, i , of $E(p)$.
 $\lambda_i(p)$ - Eigen-value, i , of $T(p)$.

CHAPTER 1

INTRODUCTION

1.1 THE TRANSIENT STABILITY PROBLEM

In the early years of electric generation and transmission transient stability problems were not very significant as,

- (i) Transmission distances were either small or, over the longer distances low transmission powers were used.
- (ii) The inertia constant of the alternator was high.
- (iii) The characteristic generator impedance was low.

In more recent years transmission distances and powers have increased⁽¹²⁾ while the trend in alternator design has shown a decrease in inertia constant and an increase in the generator characteristic impedance⁽⁸²⁾₍₇₆₎. These facts render a system more susceptible to transient instability. Consequently there is an increasing need to analyse power systems while they are still in their design stage and to develop, new, improved control schemes to help overcome the transient stability problem.

In the case of multimachine power systems the flow of synchronising power between each individual alternator during the transient period can alter the transient stability limit. Work by Freece⁽²¹⁾ and Dingley and Morris⁽⁵¹⁾ has shown that multiswing instability can result in such systems. The most usual cause of dynamic interaction is when two, or more, machines are electrically close and their inertia constants differ. This condition arises in cross-compound sets with lines running at different speeds⁽⁵¹⁾ when typical inertia constants are; 2 KJ/KVA for the high speed line and 8 KJ/KVA for the low speed line.⁽⁵⁷⁾ Similar inertia differences can arise in a power system when a hydro station is electrically close to a large steam station.



In the developing countries it is not uncommon to have large transmission distances between the generating stations and the system load. In this type of study interaction phenomena are important as the electrical coupling between machines can be low compared with the coupling between the generators and the main system loads.

1.2 METHODS OF IMPROVING TRANSIENT STABILITY

1.2.1 THE CONTROL PROBLEM

For any synchronous machine in a multimachine power system the power balance at any instant is given by

$$H \cdot \ddot{\delta} = P_M - P_T - P_L \quad (1.1)$$

In the steady state $P_M = P_T + P_L$

When a fault occurs there is a change in the electrical output power and the rotor moves in such a way as to try and keep the energy balance. To counteract this rotor movement either the turbine input power, P_M , or the electrical power, P_L , can be altered in some determined way. Methods by which this can be done are now discussed.

1.2.2 IMPEDANCE SWITCHING

Quenching machine transients by inserting a capacitor in the transmission line has been shown to produce strong control. ⁽⁷⁵⁾⁽⁸⁴⁾⁽⁸¹⁾₍₅₃₎₍₅₂₎

Using capacitor insertion methods the system response can be either underdamped, overdamped or critically damped (posicast switching) depending on the fault size and capacitor used. ⁽⁸⁵⁾⁽⁸⁸⁾

Posicast switching is ideal as it requires the least amount of switching operations to reach the new steady state condition. Unfortunately because the optimum capacitance size is fault dependent posicast switching cannot be achieved for all fault conditions.

Capacitor control can be obtained in a number of ways by using

switched or continuously operating capacitors in either a shunt or series mode. However Kimbark⁽⁵¹⁾ has demonstrated that switched series capacitors require a lower rating to produce the same transient stability limit than either unswitched series or switched shunt capacitors.

1.2.3 EXCITATION CONTROL

Excitation control involves changing the magnitude of the machine internal voltage and hence the height of the operating locus in a determined manner.

Control of the field excitation is an established control means and was first introduced to help produce a stable terminal voltage. Control was achieved by feeding back a signal proportional to terminal voltage. It was later found that this control was also beneficial during the transient period.

More recent work⁽⁹⁾ using different feedback signals to the exciter has shown that the transient stability limit can be substantially improved by incorporating signals describing the machine's state in the feedback control signal.

1.2.4 TURBINE FAST VALVING

Fast valving refers to the opening and closing of special electrohydraulic valves in the steam system to control steam flow to the turbine and hence the mechanical power input to the alternator. Fast valving of the intercept valves in the reheat cycle is usually preferred as it causes fewer practical problems than valving the main steam flow yet controls approximately 70% of the total input power⁽⁵⁾

Electrohydraulic valves with closing times of 100 - 200 ms are available,⁽⁵⁾⁽²⁷⁾ while the opening times are approximately four times greater than the closing times. This is due to the valve control system

having to be drained of hydraulic fluid.

1.3 CONTROL SYSTEM DESIGN METHODS

To implement the control elements of section 1.2 it is necessary to design a control scheme. This design can be approached by two general methods,

- (i) By considering the systems non-linear dynamics different feedback control signals can be suggested and investigated on a computer model of the system⁽⁹⁾.
- (ii) Modern control theory can be applied to a linearised version of the machine and system equations to determine the necessary control action.

Optimal control methods have been favoured by a number of authors⁽²⁶⁾⁽¹⁾⁽⁴⁹⁾ whereby a quadratic performance index is proposed. This performance index includes weighting matrices which take account of the relative importance between the different inputs and outputs of the system. The performance index is minimised, generally by solution of the Matrix Ricatti equation,⁽⁵⁵⁾ to obtain the resulting control scheme. The designs proposed by the above authors differ due to the choice of weighting in the performance index.

As the design is carried out on a linear equation set, the control schemes are valid over a small operating region and has to be applied to large disturbances with caution. For instance, Anderson⁽¹⁾ obtained improved response for small disturbances but when the control scheme was subjected to a large disturbance it showed no improvement on the system response. This was due to the choice of weighting matrices. On the other hand De Sarkar and Dharma Rao⁽⁶¹⁾ produced a sub-optimal control scheme which exhibited improved response at both levels.

Optimum control methods suffer several disadvantages summarised by MacFarlane⁽⁶⁸⁾ as,

- (i) They require access to all the system states.
- (ii) They provide gain margins far in excess of those actually required for stability.
- (iii) They offer no means of providing dynamic compensation.

An alternative approach to optimal control methods is to use an extended classical approach developed at Manchester Institute of Science and Technology by MacFarlane and Rosenbrock. This is the approach taken in this work and is considered by investigating multi-machine systems.

For any multi input/output control problem MacFarlane⁽⁶⁷⁾ has shown that it is inadvisable to design separate control loops using single loop theory. Applying this control design method to multimachine power systems can aggravate interaction phenomena⁽⁶⁰⁾ and ultimately result in an inherently stable system being unstable.⁽⁵⁶⁾

In designing a control scheme for a multi input/output system all the inputs and outputs of the system and their respective effect on each other must be considered to avoid the kind of instability discussed above. Thus some form of group control scheme must be formulated.

1.4 MULTIVARIABLE CONTROL METHODS

The multivariable control methods applied in the present work involve a design technique in the frequency plane proposed by Rosenbrock⁽⁶⁵⁾⁽⁶⁶⁾ for linear multivariable control problems. Inverse Nyquist (I.N.) plots are utilised where interaction between channels can be investigated by changing the usual Nyquist line locus to that of a band. The width of this band being dependant on the amount of interaction between channels.

This design method has the advantage that well established

classical design methods can be used but instead of considering a line as the Nyquist locus this is replaced by the envelope of circles. One of the main advantages over optimal methods is that it does not require access to all the system states, which, in some cases can be difficult to obtain. It is for these reasons that the investigation of linear multivariable control theory applied to multimachine power systems was initiated.

1.5 FORMULATION OF THE DESIGN PROBLEM

The work presented in the following chapters will demonstrate how the multivariable approach produces a group control scheme to reduce interaction effects and allows dynamic compensation to be applied via the control elements of section 1.2. By reducing the interaction effects to a minimum dynamic compensation can be made without fear of introducing the possible instability referred to by MacFarlane in reference (67).

The overall control scheme is developed with special reference to;

- (i) Improvement of the overall system stability.
- (ii) Removal of interaction between machines in a multimachine power system.
- (iii) Improvement of the system response.

The approach taken allows for the investigation of different control signals to the regulators discussed in section 1.2 and their effect on both the steady and transient stability limits to be studied.

Initially the effect of interaction in multimachine systems is investigated in Chapter 5 while the remaining Chapters discuss the effect of the various control schemes on both small and large disturbances. As the conventional regulators are used their effect on the system both

with and without interaction present is considered in detail. This is important because in the event of any failure in the group control scheme the regulators themselves will be acting in their conventional mode. i.e. control being applied round each individual machine irrespective of the other machines in the system. It also provides a method to judge the performance of the group control by. Finally in Chapter 9 the overall reliability of the design method is discussed.

Before any control work can begin it is necessary to produce a digital computer program to represent any multimachine power system. This digital model is necessary both in its non-linear and linearised form. The early chapters of the work discuss the development of these two programs.

1.6 STABILITY DEFINITIONS

1.6.1 GENERAL

Feedback of certain signals to the regulators of section 1.2 have been shown to produce self-induced oscillations⁽³⁴⁾⁽⁷⁸⁾⁽⁹⁾ which can ultimately lead to an unstable system. Also because of the non-linear nature of the machine equations there is a specific region in the state space in which the system is stable. Once the system state is outside this region the system will be unstable.

It is necessary to differentiate between these two different types of instability.

1.6.2 LYAPUNOV INSTABILITY

It is not always necessary to have an explicit knowledge of the system equations to determine the stability boundary. Authors have applied the direct method of Lyapunov⁽³¹⁾⁽³²⁾⁽³³⁾⁽³⁵⁾ to determine the

transient stability boundary of simple power systems using different synchronous machine models.

The Lyapunov function produced by Gless⁽³¹⁾ yielded a stability boundary in the phase plane similar to that depicted in Fig. 1.1 where δ_{o1} , δ_{o2} are the initial and final steady values of rotor angle and δ_c is the rotor angle at fault clearance. At the onset of a fault the phase trajectory of the machine will take the path shown and if this fault trajectory travels outside the stable region the system will be unstable. However if the fault is cleared while the trajectory is in the stable region the post-fault trajectory will be stable as shown in the diagram with δ_{o2} as the focus. This model assumes no damping. If damping was present the post-fault trajectory would spiral into δ_{o2} and the system would be asymptotically stable.

A system producing this behaviour is said to be bounded and any instability due to inadequate fault clearance will be termed Lyapunov instability.

1.6.3 NYQUIST INSTABILITY

The term Nyquist instability is used to describe the instability caused by self-induced oscillations. These self-induced oscillations are produced by different feedback control signals to the regulators when incorrect gain and phase margins exist.

The onset of the self-induced oscillations can be related to a Nyquist plot of the system, as will be demonstrated in Chapters 7 and 8, and is consequently termed Nyquist instability.

1.6.4 DEFINITION OF THE STABILITY LIMIT

When a system is subjected to a three phase fault there is a critical period, termed the critical clearing time, after which fault

removal will result in an unstable system in the Lyapunov sense. For any large disturbance the critical clearing time is used as a measure of the overall system stability.

1.7 DEVELOPMENT OF SYNCHRONOUS MACHINE MODELS

1.7.1 GENERAL

The analysis of synchronous machines by Park⁽¹⁹⁾⁽²⁰⁾ and later extended by Doherty and Nickle⁽²⁹⁾⁽³⁰⁾ and Shackshaft⁽³⁶⁾ form a convenient basis on which to build computer models to predict the dynamic performance of power systems.

Different machine models can be obtained from successive approximations to Park's equations (Appendix A). The effect of these different approximations on the resulting accuracy and overall computer time are now discussed.

1.7.2 MACHINE, SYSTEM INTERFACE

The power system equations are generally represented by a set of algebraic equations which characterise its behaviour at frequencies close to fundamental frequency.⁽¹¹⁾

To match these algebraic network equations to the machine equations it has to be assumed that the stator quantities can be represented by slowly changing phasors, i.e. the system can be regarded as slowly passing from one steady state to another. The stator transients in the machine equations are neglected and because of the slowly changing phasor quantities large step lengths in the numerical integration procedure can be used.⁽³⁸⁾⁽¹⁷⁾

If the stator transients in equations (A.25) and (A.26) are not ignored then the system equations are no longer algebraic and have to take into account any transmission line and transformer inductive voltage drop

after a sudden change and become a set of differential equations.⁽³⁶⁾
Introducing the stator transients not only invalidates the assumption of slowly changing stator quantities but it also introduces the asymmetrical component of stator current⁽⁴¹⁾ It is now found that the axis quantities change at approximately supply frequency which, to avoid numerical instability necessitates a small numerical step length⁽³⁸⁾⁽¹¹⁾⁽³⁷⁾⁽⁴¹⁾ Typical values for this step length are of the order of 0.0005s to 0.001s as compared with 0.02s to 0.05s when stator transients are ignored.⁽¹¹⁾ Transforming into computer time means an increase of at least 25 for single machine studies and an increase of at least 100 for multimachine studies.⁽³⁸⁾

1.7.3 SATURATION OF MACHINE PARAMETERS

The refinement of representing machine saturation can be incorporated into all models. There are a variety of methods for incorporating saturation and are well documented in the literature.⁽³⁸⁾⁽²¹⁾⁽³⁶⁾

However Hammons and Winning⁽³⁸⁾ conclude that detailed simulation of saturation is not justified because of the increase in computer time and that saturated machine values, with the pre-fault conditions carefully defined, suffice. This same conclusion has been reached by other authors⁽²¹⁾⁽³⁸⁾

Saturation effects only become important when A.V.R. and high field forcing is considered.⁽²¹⁾⁽⁴⁾

1.7.4 MACHINE REPRESENTATION

The complete synchronous machine model uses the full five winding Park's equation. Equations (A.1) to (A.12). As this model incorporates stator transients its biggest disadvantage is the excessive computer time it requires to yield a solution. This is especially true for the multi-machine case. It has been shown that the increase in accuracy obtained by this method compared with the increase in computer time for a series of rotor angle excursions is not justified as comparable accuracy over

a series of swings can be achieved by a simpler model. (38)

On the occurrence of a 3-phase fault the rotor angle does not increase immediately, as is predicted by simple machine models, but in fact has a tendency to decrease before it increases. (87)(43)(41)

This phenomena is termed backswing. It is an effect associated with:

(i) The large individual phase currents produced by the 3-phase fault. (87)

These currents are several times larger than the normal load current and thus the short circuit brings about a considerable increase in the magnetic energy of the generator circuits. This increase in magnetic energy is balanced by a reduction in the kinetic energy of the rotor. Thus an oscillatory component of torque is produced at fundamental frequency which always tends to decelerate the rotor.

(ii) The high rotor transient currents that are induced at the onset of a fault. (41)(43) These currents produce a resistive loss which together with the armature short circuit loss produces a unidirectional retarding torque which opposes the turbine input torque.

Consequently there is less torque available to accelerate the rotor, and in some situations can cause an actual rotor angle backswing. The amount of backswing is found to be very dependent on pre-fault operating conditions, machine parameters and the position of the fault. (41) This effect of rotor backswing is neglected in the majority of machine representations. However this complete model includes this effect. The importance of this backswing is that it gives the power system engineer a longer time in which to clear the fault.

Shackshaft (36) used the full model on an analogue computer simulation but found he had to reduce the amortisseur equivalent resistance by a factor of four to get agreement between test and

calculated results. This reduction in resistance value is to account for skin effects at the surface of the rotor. The effect of this reduction in resistance is verified by Hammons and Winning. (38)

Rogers and Smith (44) used field theory to model eddy current losses within the rotor and produced results slightly more accurate than Shackshaft. This extra accuracy is not justified, except for detailed simulation, as reduction of the amortisseur equivalent resistance is a convenient, valid, method of representing this skin effect.

If a very accurate representation is required the full model should be used, with the refinement of Rogers and Smith, but for most problems its requirements in computer time are too excessive for its increased accuracy.

By using equations (A.21) and (A.27) - (A.32) a model which neglects some of the stator transients is obtained. It is found that the highest frequency component is 5 to 10 times lower than in the full representation (38) and algebraic equations can be used to represent the system components. This results in a larger numerical step length and a corresponding decrease in computer time.

Further simplifications can be listed:

- (i) The rotor angular speed ω is assumed constant and equal to ω_0 during the transient period, i.e. $\omega = 1$
- (ii) Stator transient neglected.
- (iii) Zero subtransient saliency, $x_q'' = x_d''$
- (iv) The gain constants G' and G'' defined in equation (A.21) are set to $G' = 1$, $G'' = 0$ respectively.

With these simplifications a saving in computer time is achieved while the results obtained are comparable with test results. (38)

If now the 3-winding model described by equations (A.36) to (A.39) is considered, noting that damping is not now included, Hammons and Winning⁽³⁸⁾ produce results comparable with the previous two models during the first rotor swing. Future excursions do not compare because of the lack of damping. Shackshaft⁽³⁶⁾ recommends that this model with the armature resistance set to zero and amortisseur effects represented by an equivalent damping coefficient a reasonable model representing the machine should be obtained. This conclusion is also reached by Adkins⁽³⁹⁾ and has been shown to be true by Devotta⁽⁴⁰⁾ where the transient response of a divided-winding-rotor machine is shown both for the full and simplified models. Devotta used the simple model to predict an optimal control scheme for a d.w.r. generator. The resulting controls were applied to the detailed machine model and found to yield good results.

The most simple model can now be discussed where equations (A.36) to (A.39) are used with T_{do}' set equal to infinity, i.e. no flux decrement, and transient saliency neglected i.e. $x_q = x_d'$. With this model reasonable agreement can be obtained during the first swing⁽³⁸⁾ and a second order simplification recommended by Shackshaft⁽³⁶⁾ is the use of this "fixed voltage behind transient reactance" with an equivalent damping coefficient in the equation of motion. A similar model to this has been used by Hughes⁽⁴⁵⁾ when looking at the effect of different feedback parameters to the governor and field regulator.

It was noted that backswing was only important during the first load angle excursion. Dineley and Morris⁽³⁷⁾ have made use of this phenomenon. They suggest the use of the full representation until the first peak of rotor angle is reached. After this the simple model is used but transient saliency is accounted for and damping terms proportional to velocity and square-of-voltage incorporated. A very close approximation

to the full representation is obtained with a substantial reduction in computer time.

Hammons⁽⁴²⁾ has also produced results where the damper windings are represented by two windings on each axis. It is found that this representation produces results only slightly better than the 5 winding model with an increase in the complexity of machine equations and computer time. It is thus not justified.

1.7.5 CONCLUSION

- (i) The full 5 winding model is not justified, especially for multimachine models, when modelling over the complete transient period is required because of the excessive computer time used.
- (ii) By neglecting stator transients results comparable with test results over the transient period are obtained. This model being most economical on computer time when $x_d'' = x_q''$.
- (iii) For multimachine studies the representation using the 3 winding model with a velocity-damping factor produces adequate results.
- (iv) For some studies the simple representation of fixed voltage behind transient reactance with an equivalent coefficient in the mechanical equations of motion produces adequate results.
- (v) The simulation chosen is very problem dependent.
- (vi) The hybrid model of Dineley and Morris⁽³⁷⁾ is commendable but if any design work incorporating control equipment is to be carried out it is advisable to work on one representation.
- (vii) If a simple model can be found that represents the system adequately this is the best model to use for any control design work.

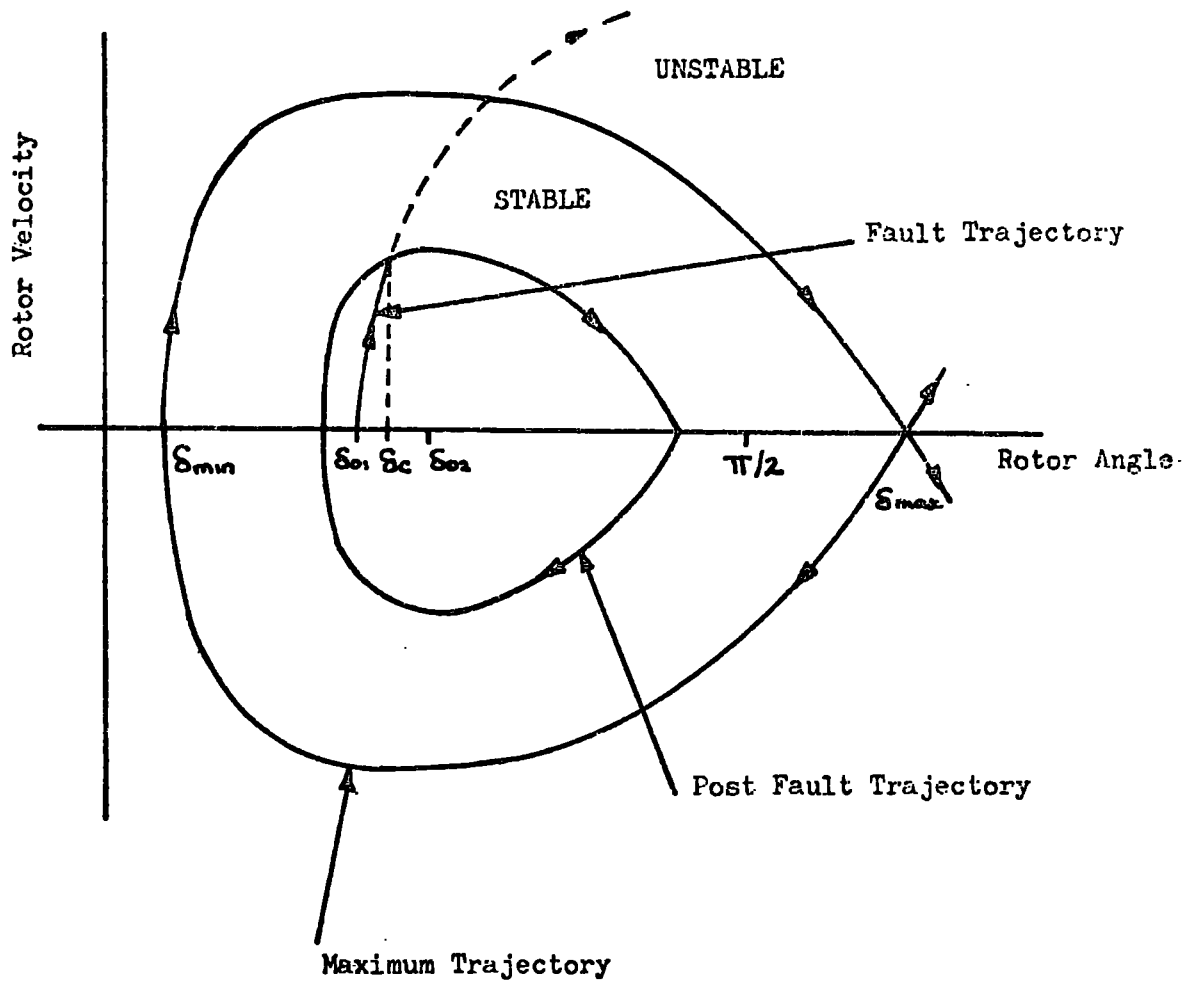


Fig.1.1 Phase Plane Showing Stable and Unstable Regions.
 Examples of Fault and Post Fault Trajectories are Shown.

CHAPTER 2

A NON-LINEAR MULTIMACHINE POWER SYSTEM COMPUTER PROGRAM

2.1 GENERAL PROGRAM SPECIFICATION

The use of digital techniques have become an established method of determining the transient response of power systems. ⁽¹⁸⁾⁽⁶⁾⁽¹¹⁾

The program discussed was written with a view to studying interaction effects in multimachine power systems when different synchronous machine models and system parameters are used. It was also used to investigate the effects of different control schemes.

The synchronous machine models used were based upon Park's 3 winding model. (APPENDIX A).

In general only symmetrical three phase faults will be considered as these are the most severe. ⁽¹²⁾ However by using an equivalent shunt reactance ⁽¹²⁾ in this positive sequence model other types of line disturbance could be accommodated.

Saturation effects are not included for the reasons outlined in section 1.7.3.

2.2 MODELLING TECHNIQUE SYNCHRONOUS MACHINE

The ability to use different synchronous machine models within the program is provided by using a general method of synchronous machine representation outlined by Kimbark. ⁽¹³⁾ Each machine is represented by a variable e.m.f.

$$E_h = E_{hd} + j.E_h q \quad (2.1)$$

in series with the value of modelling reactance X_h . A vector diagram for this model is shown in fig. 2.1. Then in general

$$E_{MOD} = E_T + Z . I_T \quad (2.2)$$

where E_{MOD} is the machine internal modelling voltage.

Applying equation (2.2) to the vector diagram gives

$$E_h = E_T + r.I_T + j.x_h.I_d - x_h.I_q \quad (2.3)$$

and

$$E' = E_T + r.I_T + j.x_d'.I_d - x_q'.I_q \quad (2.4)$$

Capital letters are now used as current and voltages are assumed as slowly changing and so their effective values may be used. This also allows the use of the phasor diagram.

Subtracting (2.3) and (2.4)

$$E_h = E' + j.(x_h - x_d').I_d - (x_h - x_q').I_q \quad (2.5)$$

which in component form yields

$$E_{hd} = E_d' - (x_h - x_q').I_q \quad (2.6)$$

$$E_{hq} = E_q' - (x_h - x_d').I_d$$

By suitable choice of x_h different machines and machine models are made available.

Armature resistance is assumed to be zero in all the models but provision is made in the program to account for it. The load angle in all cases is measured with respect to the quadrature axis.

REP 1

Flux linkages of the rotor circuits are neglected.

Transient saliency is neglected in equation (A.36) and (A.37) by putting $x_q = x_d'$. This gives E' as the reference axis for load angle measurements. However using the modelling equation (2.6) with $x_h = x_d' = x_q'$ and letting x_q take on its full value the same model is obtained but giving the quadrature axis as a reference for load angle measurements. This is a similar model to a round rotor machine with a solid rotor i.e. $x_d' = x_q'$.

Machine damping is not included.

REP 2

As REP 1 but machine damping is included in equation (38)

These two representations provide the classical model of "constant voltage behind transient reactance".

REP 3

Transient saliency is now included but machine damping and flux decrement are assumed negligible. The modelling reactance $x_h = x_q$.

REP 4

As REP 3 but machine damping included.

REP 5

As REP 3 but flux linkages no longer constant.

REP 6

As REP 3 but flux decrement and machine damping included.

2.3 NETWORK PERFORMANCE MODEL

2.3.1 THE MODEL REFERENCE FRAME

The network performance model is used to represent the interconnected network of transmission lines, transformers and other associated equipment. Such a model can be established using either the bus or loop frame of reference. (22)

This program uses the bus frame of reference in the form of the bus admittance matrix with ground as the reference node. This was selected as,

- (i) The bus admittance matrix is easily formed because mutual coupling is not involved.
- (ii) The bus ~~admittance~~^{admittance} matrix is sparse so relatively few elements have to be calculated.

- (iii) Because of the sparsity of the matrix there is a saving in computer time and memory storage as the zero elements within the matrix need not be stored.
- (iv) The bus admittance matrix is easily modified to represent a fault.

2.3.2 BUS BAR REPRESENTATION

In the solution of any power system network it is necessary to represent the bus bars accurately. There are four types.

- (i) Slack bus. This supplies additional real and reactive power for the transmission losses as these are unknown until the final solution is obtained. This is necessary in any load flow program.
- (ii) Infinite bus. This appears to the rest of the system to be a source of voltage constant in phase, magnitude and frequency and not affected by the amount of current drawn from it. It can thus be regarded as a machine having zero impedance and infinite inertia. A large power system often may be regarded as an infinite bus. An infinite bus is accommodated within the program and if required must become bus n of an n bus system. On the inclusion of an infinite bus this also become the slack bus.
- (iii) Voltage controlled bus. The real power and voltage magnitude are fixed.
- (iv) Load bus. The real and reactive powers remain fixed.

The last two buses are refinements to a program and were not included within this program.

The network performance equations are given in Appendix B.

2.3.3 REPRESENTATION OF LOADS

During the transient interval it is necessary to include the system loading conditions within the network performance equations. The

load representation selected was that of static admittance to ground, ⁽⁸⁾⁽¹¹⁾ which is calculated, for bus k , by

$$y_{ko} = \frac{I_{ko}}{E_k} \quad (2.7)$$

This is one of the simplest methods of load representation and strengthens the convergence rate of the Gauss-Seidel iterative process. This process is used in the solution of the non-linear network equations.

2.3.4 SYNCHRONOUS MACHINE CONNECTION

Each machine is connected to some node of the network. To account for this machine connection the elements of the bus admittance matrix are adjusted to accommodate the machine inductances. In the network performance equations new voltages appear to represent the machine internal voltage.

The machines **MUST** be numbered such that machine number 1 is connected node number 1 and becomes node $(n + 1)$ when the data is modified. Similarly machine number 2 is connected to node 2 and becomes node $(n + 2)$, etc. The synchronous machine and load representation is shown in fig. 2.2.

2.3.5 THE INTERCONNECTION OF MACHINE AND NETWORK EQUATIONS

The alternator equations describe each machine separately with reference to its own d, q axis. Consequently it is necessary to transform the machine and network equations into a common reference frame.

A free rotating reference frame at synchronous speed within the space defined by the machines is selected. If necessary this may be adjusted so that one of the machines may be used as the reference.

No voltage transformation is necessary as the network voltage equations are written in the reference frame and the machine voltages are calculated from these. However a current transformation is necessary (see fig. 2.3) and is given as

$$\begin{bmatrix} |I_q'| \\ |I_d| \end{bmatrix} = \begin{bmatrix} \cos \delta & \sin \delta \\ \sin \delta & -\cos \delta \end{bmatrix} * \begin{bmatrix} I_D \\ I_a \end{bmatrix} \quad (2.8)$$

$$\begin{bmatrix} I_d \\ I_q \end{bmatrix} = \begin{bmatrix} \sin \delta & -\cos \delta \\ \cos \delta & \sin \delta \end{bmatrix} * \begin{bmatrix} |I_d| \\ |I_q| \end{bmatrix} \quad (2.9)$$

2.4 DIGITAL PROGRAM SOLUTION METHOD

A description of the subroutines used and flow diagrams are given in APPENDIX D.

The system operating conditions prior to a disturbance are obtained by a load flow solution. The systems generating and loading conditions are used as the inputs. The network performance equations are then modified to accommodate the synchronous machines.

On the occurrence of a fault the bus admittance matrix is modified if necessary and the iterative load flow technique used to obtain the systems new conditions. Depending on the machine model used the machine voltage is either held constant during the iterative process or is updated after each iteration.

The iterative process is carried out during the entire transient period in conjunction with a numerical integration routine to obtain the complete transient response.

2.5 CONTROL EQUIPMENT

2.5.1 ALTERNATOR FIELD EXCITATION REGULATOR

With the developments in the field of solid state electronics the use of fast acting controlled rectifier regulators is becoming increasingly

widespread. (6)(78)

The exciter model available is described by the equations below and shown in fig. 2.4.

$$\dot{y}^* = \frac{y_{fb} - y^*}{T_{fb}} \quad (2.10)$$

$$e_r = V_{ref} \pm y^* \quad (2.11)$$

$$\dot{R}_1 = \frac{K_1 e_r - R_1}{T_1} \quad (2.12)$$

$$x_a = \frac{R_1 - x_e}{T_3} \quad (2.13)$$

$$\dot{x}_e = x_a \quad (2.14)$$

$$E_{fd} = T_2 \cdot x_a + x_e \quad (2.15)$$

The variables x_a and x_e are dummy variables used in representing the rectifier transfer function block.

In some instances it is necessary to compare the action of the static exciter with the older rotating excitation system. The program provides this facility by reducing the exciter model to the first order

$$\frac{E_{fd}}{e_r} = \frac{K_1}{1 + p \cdot T_{ex}} \quad (2.16)$$

and using a small or large time constant to represent the static or rotating exciter respectively.

The value of the ceiling voltages employed is dependant on the type of exciter used. A fixed value being used in the case of the rotating exciter whereas, for economic reasons, the static exciter is usually powered from the machine terminals. (6)(45)

The final block in fig. 2.4 gives the relationship between E_{fd} and the machine voltage. (9) If flux decrement is included in the model then equation A.38 is used with

$$G = \frac{E_{fd_0}}{E_{q_0}} \quad (2.17)$$

with no flux decrement

$$G = \frac{E_{fd0}}{E'_{q0}} \quad (2.18)$$

2.5.2 INPUT POWER REGULATOR

Previous authors⁽¹⁾⁽²⁶⁾⁽²²⁾ have reduced the turbine/boiler model⁽²⁴⁾ to a similar second order model as used in this program (fig.2.5).

The ceiling power limits are given by Stagg and El-Abiad⁽²²⁾ to be zero and the maximum output power of the turbine respectively.

The control system is a model of the turbine valve and with the use of fast valving a time constant of the order 80 - 100 ms would be used.⁽⁵⁾⁽²⁷⁾ The time constant representing the steam system depends on the valving employed and where it is employed.⁽⁵⁾ A value of the order of 0.75s has been suggested⁽²⁷⁾ and used.⁽¹⁾

2.6 NUMERICAL METHODS

2.6.1 ITERATION METHOD

Laughton⁽¹⁶⁾ reviews the iteration methods available and concludes that the use of either Gauss Seidal with acceleration factors or a Newton Raphson iterative method for the solution of the equation set (B.5). The former method was selected for the following reasons:

- (i) The number of arithmetic operations are reduced with the Gauss-Seidal method as the bus admittance matrix is sparse; consequently the time per iteration is small.
- (ii) The Newton-Raphson method converges much faster and requires fewer iterations but the Jacobian matrix has to be calculated at each iteration interval which increases the computer time.

(iii) With systems under 40 buses the methods are comparable ⁽²²⁾ but with larger numbers of buses the Newton-Raphson is more efficient. However as the program was designed to study interaction phenomena the number of busbars will, on the whole, be low.

2.6.2 ITERATION STABILITY

The disadvantage of the Gauss-Seidel method, with or without acceleration factors, is that there is no law guaranteeing convergence. Convergence is helped if ⁽²⁸⁾⁽¹⁶⁾

$$|a_{ii}| \geq \sum_{\substack{j=1 \\ j \neq i}}^n |a_{ij}| \quad (2.19)$$

This is achieved by representing system loads by a static admittance to ground.

2.6.3 INTEGRATION METHODS

Four integration methods are available ⁽¹⁴⁾⁽²²⁾

- (i) Euler.
- (ii) Modified Euler.
- (iii) 4th order Runge-Kutta, fixed step.
- (iv) 4th order Runge-Kutta, variable step.

2.6.4 INTEGRATION INSTABILITIES

Incorrect choice of numerical step length in an integration procedure can cause a mathematical instability. Mathematical unstable regions can be proved for all types of integration method. ⁽¹⁵⁾

Considering Euler's numerical integration method and a differential equation of the form

$$y' = \lambda y \quad (2.20)$$

This system is Lyapunov and Nyquist stable so long as the zeros are in the open left half complex plane.

By Euler's formula⁽¹⁴⁾

$$y_{n+1} = y_n + h \cdot y_n' \quad (2.21)$$

where h is the numerical step length

Substitute (2.20) into (2.21)

$$y_{n+1} = (1 + h \cdot \lambda) \cdot y_n \quad (2.22)$$

If $|1 + h \cdot \lambda| \geq 1$ then the system will be divergent and a mathematical instability will arise even though the system itself is Lyapunov and Nyquist stable.

There is a condition of mathematical stability

$$|1 + h \cdot \lambda| \leq 1 \quad (2.23)$$

shown on the stability chart, fig. 2.6.

The analysis is extended to a set of coupled differential equations

$$y' = [A] \cdot y \quad (2.24)$$

If $\lambda_1, \dots, \lambda_n$ are the eigen-values of this system then the conditions for mathematical stability are⁽¹⁵⁾

$$|1 + h \cdot \lambda_1| \leq 1, |1 + h \cdot \lambda_2| \leq 1, \dots, |1 + h \cdot \lambda_n| \leq 1 \quad (2.25)$$

Consequently the largest λ limits the integration step length.

Extension to non-linear equations is possible where the eigen-values are considered to be continually changing.⁽¹⁵⁾

Mathematical instability can arise in power system analysis due to the step length selected being too large relative to;

(i) The time constants of the system.

(ii) The loop feedback gain.

Including the stator transients in the machine equation set (Appendix A) severely limits the maximum step length that can be taken before a mathematical instability sets in.

2.7 PROGRAM VERIFICATION

A comparative study for the model system of fig. 2.7 was run using REP 6 and the program developed by Preece.⁽⁹⁾⁽²¹⁾ The machine and system data is given in Appendix G. Results compared to within 1% after 6 secs. giving the rotor angle response of fig. 5.15(c).

The program used by Preece was written in Algol and usable only on the type of system of fig. 2.7. In comparison the program discussed here can have any interconnection of buses and machines and relies on an iteration method to provide the new bus voltages at each step. No iteration process is used by Preece.

2.8 CONCLUSION

The program does not provide all the refinements available in power system transient analysis but will allow a detailed investigation into machine interaction. Facilities are available to represent the synchronous machine by different mathematical models.

The main limitations of the program lie in the modelling of the amortisseur windings and the iteration method used. It is suggested that any further refinements to the program should be initiated in these areas.

Neglecting saturation is valid within the context of the program but is a refinement worth consideration as is a more accurate load representation.⁽⁴⁾

The accuracy of the program itself has been verified.

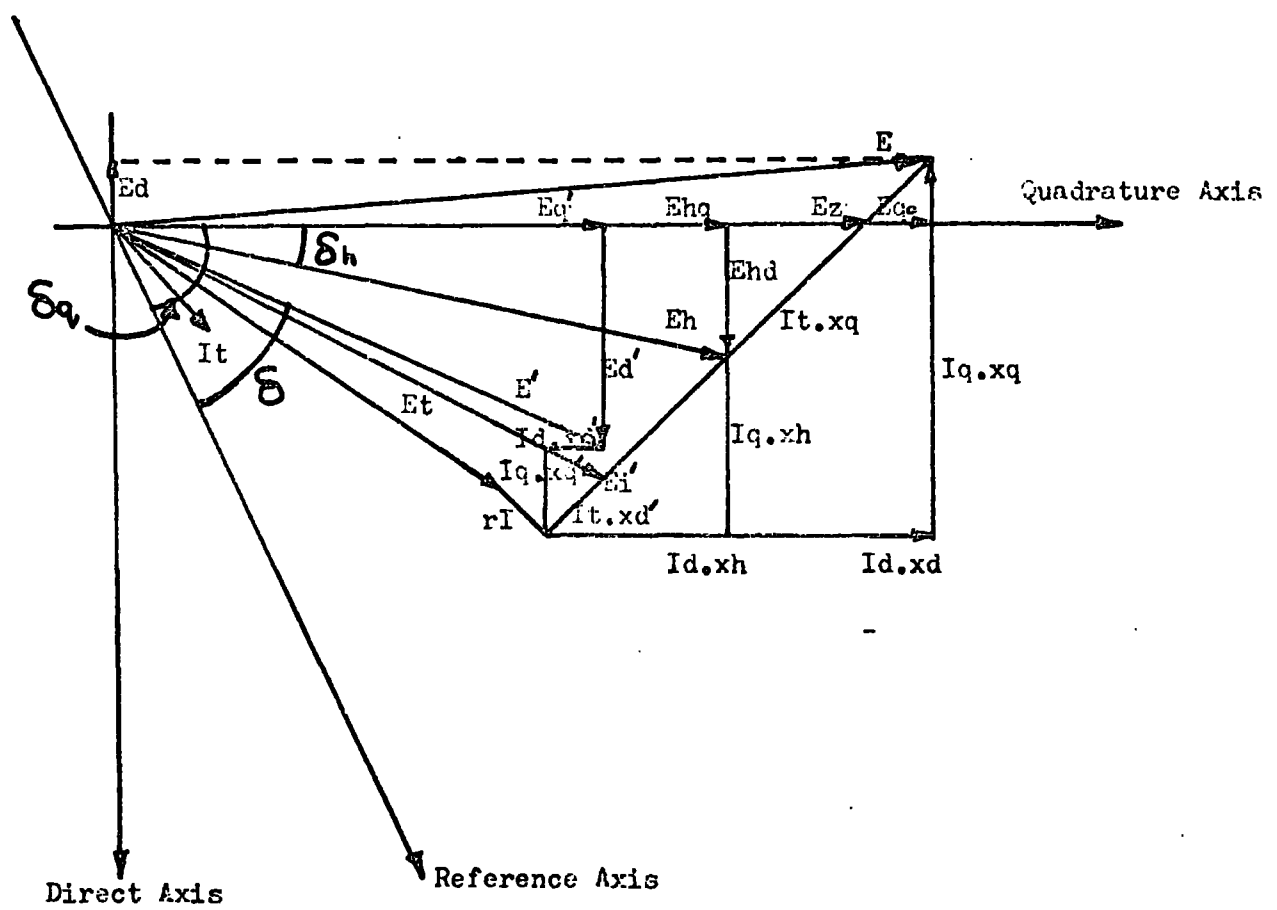


Fig. 2.1 Vector Diagram for the Generalised Machine.

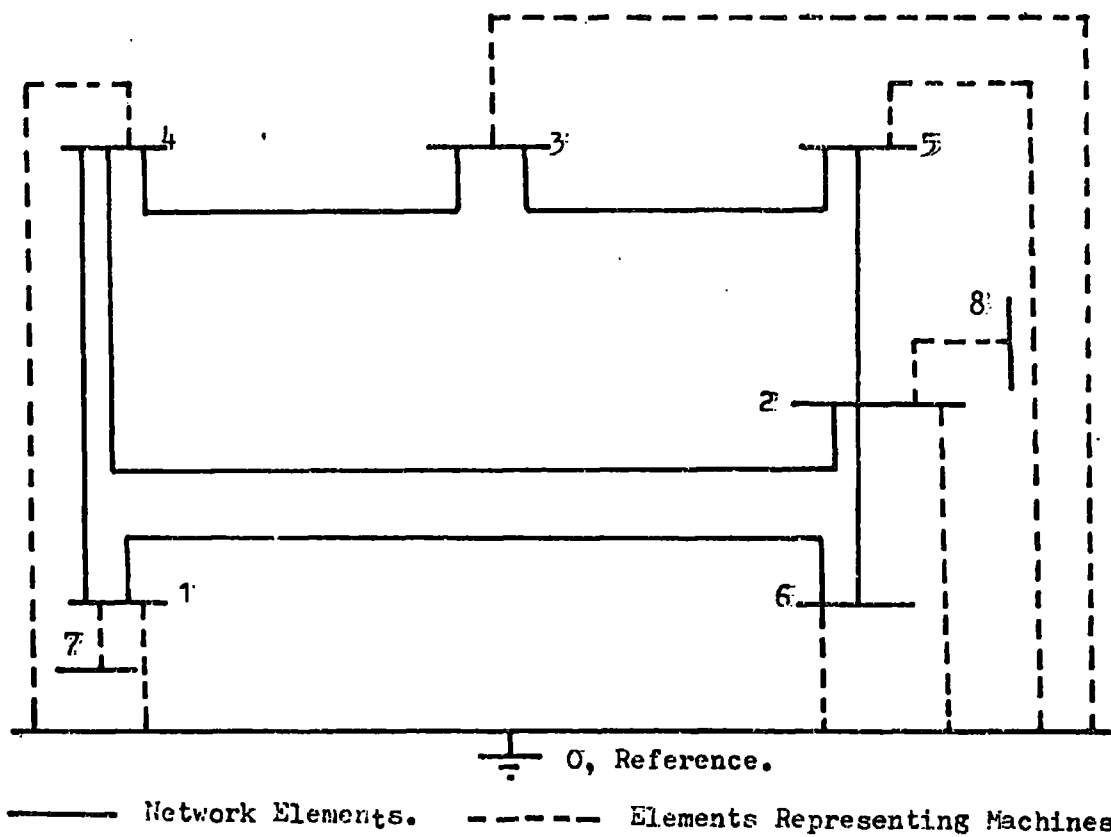


Fig. 2.2 Single Line Diagram of a Power System for Transient Analysis.

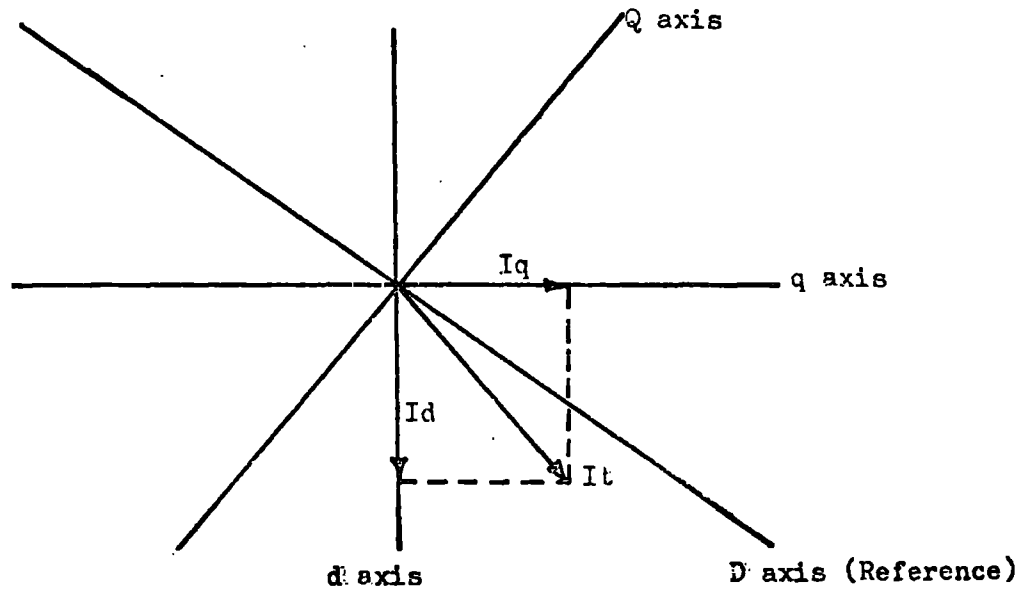


Fig.2.3 Transformation Axis.

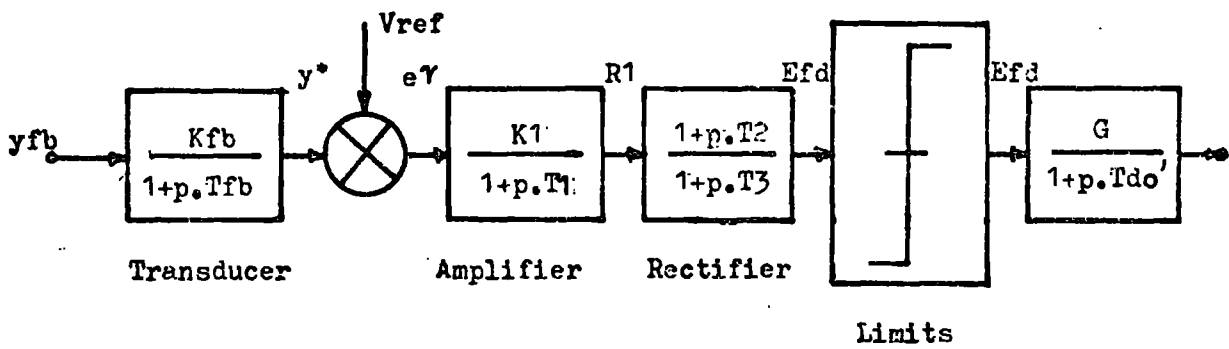


Fig. 2.4 Block Diagram of the Controlled Rectifier Regulator.

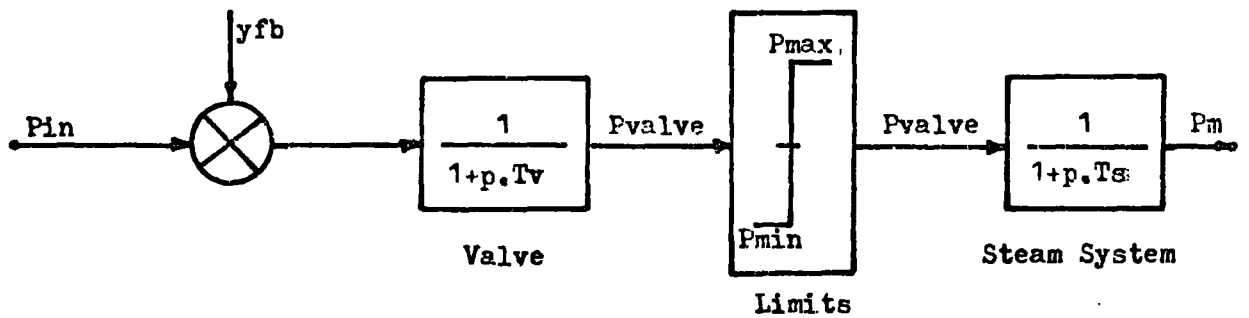


Fig. 2.5 Block Diagram of the Input Power Regulator.

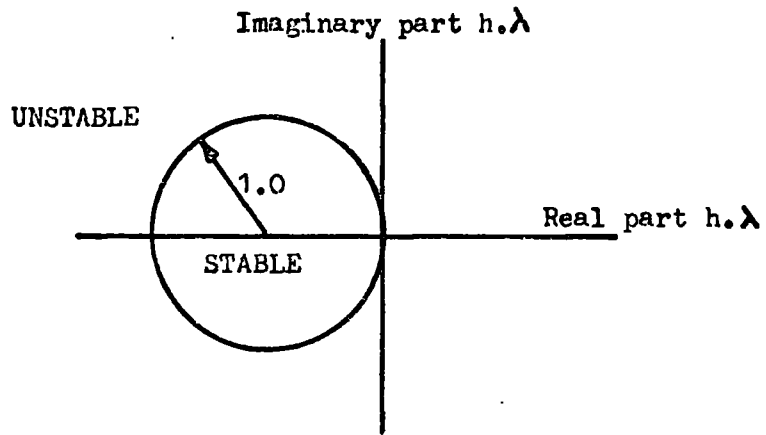


Fig. 2.6 Mathematical Stability Boundary for Euler Integration Method.

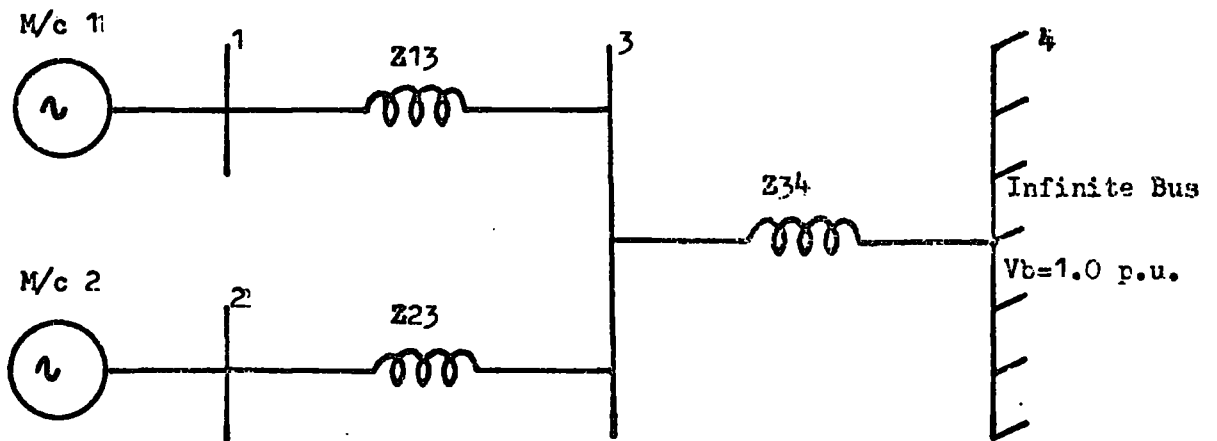


Fig. 2.7 Line Diagram of Power System.

CHAPTER 3

A LINEAR MULTIMACHINE POWER SYSTEM COMPUTER PROGRAM

3.1 GENERAL

The design of a control scheme by Linear Multivariable techniques requires a linearised form of the machine and system equations.

The use of the linear equation set, applied to synchronous machine studies, has become a well established technique both with the use of classical control methods⁽⁴⁸⁾⁽⁵⁰⁾ and more recently with the continued application of optimal control theory.⁽⁴⁷⁾⁽¹⁾⁽⁴⁹⁾⁽⁶¹⁾⁽⁴⁶⁾

The synchronous machine model selected for linearisation was that of constant voltage behind transient reactance with an equivalent damping constant (REP 2). This model was selected as being the simplest model representative of the system transient characteristics.⁽³⁶⁾⁽⁴⁵⁾

Previous authors have used this machine model for the determination of stability boundaries by Lyapunov methods⁽³¹⁾⁽³⁵⁾ and energy methods⁽⁶³⁾⁽⁶⁴⁾ and also for the investigation of control schemes.⁽⁴⁵⁾⁽⁵¹⁾

Regulators are provided within the model to control field excitation and turbine input power.

3.2 THE LINEARISED MACHINE AND NETWORK EQUATIONS

The synchronous machine equations describing REP 2 in APPENDIX A along with the network performance equations, modified for the transient period, are linearised by a first order Taylor expansion. (APPENDIX C) The linearisation being carried out around the systems initial operating points.

The final set of linear equations in Appendix C being

$$\begin{aligned} \dot{x}_k = & \frac{f \cdot \pi}{H_k} \cdot d_k - \begin{bmatrix} \Gamma_{1k} \\ \Gamma_{2k} \end{bmatrix} \begin{bmatrix} x_{2m+k} \\ x_{m+k} \end{bmatrix} - \sum_{\substack{l=1 \\ l \neq k}}^m \begin{bmatrix} \gamma_{1kl} \\ \gamma_{2kl} \end{bmatrix} \begin{bmatrix} x_{2m+l} \\ x_{m+l} \end{bmatrix} \\ & - \frac{K d_k \cdot f \cdot \pi}{H_k} \cdot x_k \end{aligned} \quad (3.1)$$

$$\dot{x}_{2m+k} = \frac{G_k}{T_{d0'k}} \cdot u_k - \frac{1}{T_{d0'k}} \cdot x_{2m+k} \quad (3.2)$$

$$\dot{x}_{m+k} = x_k \quad (3.3)$$

where $x_1, \dots, x_{2m}; x_{2m+1}, \dots, x_{3m}; u_1, \dots, u_{2m}; d_1, \dots, d_{2m}$ are the state variables defined in equation C.35.

This set of first order differential equations is written in the state space form

$$\dot{\underline{x}} = [A] \cdot \underline{x} + [B] \cdot \underline{u} + [D] \cdot \underline{d} \quad (3.4)$$

where A is $n \times n$ plant matrix

B is $n \times m$ Driving matrix (1)

D is $n \times m$ Driving matrix (2)

x is $n \times 1$ vector of State Variables

u is $m \times 1$ vector of inputs (1)

d is $m \times 1$ vector of inputs (2)

and $n = 3m$

which for a two machine system yields

$$\begin{bmatrix} \dot{x}_1 \\ \dot{x}_2 \\ \dot{x}_3 \\ \dot{x}_4 \\ \dot{x}_5 \\ \dot{x}_6 \end{bmatrix} = \begin{bmatrix} \frac{-k_d \cdot f \cdot \pi}{H_1} & 0 & -\Gamma_{21} & -\gamma_{212} & -\Gamma_{11} & -\gamma_{112} \\ 0 & \frac{-k_d \cdot f \cdot \pi}{H_2} & -\gamma_{221} & -\Gamma_{22} & -\gamma_{121} & -\Gamma_{12} \\ 1 & 0 & 0 & 0 & 0 & 0 \\ 0 & 1 & 0 & 0 & 0 & 0 \\ 0 & 0 & 0 & 0 & \frac{1}{T_{d0'1}} & 0 \\ 0 & 0 & 0 & 0 & 0 & \frac{1}{T_{d0'2}} \end{bmatrix} \cdot \begin{bmatrix} x_1 \\ x_2 \\ x_3 \\ x_4 \\ x_5 \\ x_6 \end{bmatrix} + \begin{bmatrix} 0 & 0 \\ 0 & 0 \\ 0 & 0 \\ 0 & 0 \\ \frac{G_1}{T_{d0'1}} & 0 \\ 0 & \frac{G_2}{T_{d0'2}} \end{bmatrix} \cdot \begin{bmatrix} u_1 \\ u_2 \end{bmatrix} + \begin{bmatrix} \frac{f \cdot \pi}{H_1} & 0 \\ 0 & \frac{f \cdot \pi}{H_2} \\ 0 & 0 \\ 0 & 0 \\ 0 & 0 \\ 0 & 0 \end{bmatrix} \cdot \begin{bmatrix} d_1 \\ d_2 \end{bmatrix} \quad (3.5)$$

3.3 REGULATOR MODELLING

The system inputs u_1 to u_m and d_1 to d_m are respectively the field excitation voltage and mechanical input power to the synchronous machines. In general there will be some device regulating the change in these quantities.

Regulators were discussed in section 2.5 and are again used in this program with the inputs to the blocks being the change in the variable relative to its initial steady state value. Previously absolute values were used.

3.4 SOLUTION TECHNIQUE

A description of the subroutines used and flow diagrams is given in APPENDIX E.

The network performance equations are solved using the Load Flow subroutine to determine the initial operating conditions of both the machines and the system. The network equations are then modified for the transient interval and linearised along with the machine equations to obtain equation (3.5). This equation is solved during the transient interval by one of the four integration methods to obtain the complete time response.

3.5 PROGRAM VERIFICATION

With small perturbations the linear and non-linear models correspond. With small deviations the sine wave characteristic of the non-linear equations can be approximated by a linear relationship.

An investigation into the linear and non-linear comparisons is conducted in Chapter 6.

3.6 THE PLANT TRANSFER FUNCTION MATRIX

The transfer function of the system is obtained from equation (3.4), writing

$$p.\underline{x} = A.\underline{x} + B.\underline{u} + D.\underline{d} \quad (3.6)$$

$$\underline{x} = (p.I - A)^{-1}.B.\underline{u} + (p.I - A)^{-1}.D.\underline{d} \quad (3.7)$$

The system outputs are related to the state vectors by the output equation

$$\underline{y} = C.\underline{x} \quad (3.8)$$

where C is $m \times n$ output matrix, then

$$\underline{y} = C.(p.I - A)^{-1}.B.\underline{u} + C.(p.I - A)^{-1}.D.\underline{d} \quad (3.9)$$

There are two transfer functions in equation (3.9) shown diagrammatically in fig. 3.1, which are

$$(i) \quad G(p) = C.(p.I - A)^{-1}.B \quad (3.10)$$

relating the system output and the input vector, \underline{u} of the change in field excitation.

$$(ii) \quad G(p) = C.(p.I - A)^{-1}.D \quad (3.11)$$

relating the system output and the input vector, \underline{d} of the change in mechanical input power.

The possibility of controlling the field excitation and/or the mechanical input power is made available.

3.7 A DEFINITION OF TRANSIENT RESPONSE

The ideal transient response exhibits a quick return to the steady state without excessive excursions of any of the system variables. It is assumed that observation of the instantaneous value of load angle, δ_q , can be used as a measure of the system stability and transient response. Further, it is assumed that if a plot of δ_q is asymptotically stable

a plot of the derivatives of δq will also be asymptotically stable. Consequently the stability and response of a system can be determined by observation of any of these quantities. When load angle, δ , velocity, $\dot{\delta}$, acceleration, $\ddot{\delta}$, or terminal voltage is used as the feedback variable it is also assumed to be the output of the Plant Transfer Function Matrix, $G(p)$.

3.8 THE OUTPUT EQUATION

The values contained within the Output Matrix, C , of equation (3.8) determines the relationship between the system's output, y , and the state vectors, x .

For any "two machines tied to an infinite bus problem" similar to fig. 2.7, with the choice of state variables as in Appendix C, equation C.35, the following output matrices are valid:

(i) Voltage output (See Appendix C) The output matrix is of the form

$$C_{\text{voltage}} = \begin{bmatrix} 0 & 0 & k_{211} & k_{212} & k_{111} & k_{112} \\ 0 & 0 & k_{221} & k_{222} & k_{121} & k_{122} \end{bmatrix} \quad (3.12)$$

(ii) Acceleration output

$$C_{\text{acc}} = \begin{bmatrix} p & 0 & 0 & 0 & 0 & 0 \\ 0 & p & 0 & 0 & 0 & 0 \end{bmatrix} \quad (3.13)$$

(iii) Velocity output

$$C_{\text{vel}} = \begin{bmatrix} 1 & 0 & 0 & 0 & 0 & 0 \\ 0 & 1 & 0 & 0 & 0 & 0 \end{bmatrix} \quad (3.14)$$

or

$$C_{\text{vel}} = \begin{bmatrix} 0 & 0 & p & 0 & 0 & 0 \\ 0 & 0 & 0 & p & 0 & 0 \end{bmatrix} \quad (3.15)$$

(iv) Position output

$$C_{pos} = \begin{bmatrix} 0 & 0 & 1 & 0 & 0 & 0 \\ 0 & 0 & 0 & 1 & 0 & 0 \end{bmatrix} \quad (3.16)$$

Define a matrix

$$S = \begin{bmatrix} P & 0 \\ 0 & P \end{bmatrix} \quad (3.17)$$

and

$$\hat{S} = \begin{bmatrix} 1/P & 0 \\ 0 & 1/P \end{bmatrix}$$

then

$$C_{acc} = S * C_{vel} \quad (3.18)$$

$$C_{vel} = S * C_{pos} \quad (3.19)$$

As the Plant transfer function matrix is of the form

$$G(p) = C \cdot (p.I - A)^{-1} \cdot B \quad (3.20)$$

then

$$G_{acc}(p) = S * G_{vel}(p) \quad (3.21)$$

and

$$\hat{G}_{acc}(p) = \hat{S} * \hat{G}_{vel}(p) \quad (3.22)$$

For the general feedback control system of fig. 4.1

$$H(p) = \frac{G(p) \cdot K(p)}{1 + G(p) \cdot K(p) \cdot F(p)} \quad (3.23)$$

and

$$\hat{H}(p) = \hat{K}(p) \cdot \hat{G}(p) + F(p) \quad (3.24)$$

which for velocity output and $K(p) = I$, the identity matrix, becomes

$$\hat{H}_{vel}(p) = \hat{G}_{vel}(p) + F_{vel}(p) \quad (3.25)$$

multiplying through by \hat{S} yields $\hat{H}_{acc}(p)$

and

$$F_{acc}(p) = \hat{S} * F_{vel}(p) \quad (3.26)$$

3.9 FORMATION OF THE PLANT TRANSFER FUNCTION MATRICES

For a power system model of fig. 2.7 typical numerical values are given in Appendix G.

3.9.1 CONTROL OF TURBINE INPUT POWER

If the regulators are ideal then for acceleration feedback the transfer function matrix $G_{Acc}(p)$ is given by substituting the A and B matrices of equation (3.5) and the relevant C matrix into equation (3.10)

$$G_{Acc}(p) = \frac{\begin{bmatrix} \frac{f \cdot \pi \cdot p [p^3 - a_{22}p^2 - a_{24}p]}{H_1} & , & \frac{f \cdot \pi \cdot p [a_{14}p]}{H_2} \\ \frac{f \cdot \pi \cdot p [a_{23}p]}{H_1} & , & \frac{f \cdot \pi \cdot p [p^3 - a_{11}p^2 - a_{13}p]}{H_2} \end{bmatrix}}{p^4 - (a_{11} + a_{22})p^3 + (a_{22}a_{11} - a_{24} - a_{13})p^2 + (a_{24}a_{11} + a_{13}a_{22})p + (a_{24}a_{13} - a_{14}a_{23})} \quad (3.27)$$

where the a's are the components of the plant matrix A.

Then $G_{VEL}(p)$ is related to $G_{Acc}(p)$ by equation (3.21)

The inverse of equation (3.27) is

$$\hat{G}_{Acc}(p) = \begin{bmatrix} \frac{H_1}{f\pi} \cdot \frac{1}{p^2} (p^2 - a_{11}p - a_{13}), & -\frac{H_1}{f\pi} \cdot \frac{1}{p^2} \cdot a_{14} \\ -\frac{H_2}{f\pi} \cdot \frac{1}{p^2} \cdot a_{23}, & \frac{H_2}{f\pi} \cdot \frac{1}{p^2} \cdot (p^2 - a_{22}p - a_{24}) \end{bmatrix} \quad (3.28)$$

3.9.2 CONTROL OF FIELD EXCITATION

Assuming ideal regulators and acceleration feedback, substitution of the A and D matrices of equation (3.5) and the relevant C matrix into (3.11) yields

$$G_{Acc}(p) =$$

$$\begin{bmatrix} \frac{-p.G_1}{T_{d01}'} \left[\frac{a_{15}p^3 - a_{15}a_{22}p^2 + (a_{14}a_{25} - a_{24}a_{15})p}{p - a_{55}} \right], & \frac{p.G_2}{T_{d02}'} \left[\frac{-a_{16}p^3 + a_{16}a_{22}p^2 + (a_{16}a_{24} - a_{14}a_{26})p}{p - a_{66}} \right] \\ \frac{p.G_1}{T_{d01}'} \left[\frac{-a_{25}p^3 + a_{25}a_{11}p^2 + (a_{13}a_{25} - a_{15}a_{23})p}{p - a_{55}} \right], & \frac{-p.G_2}{T_{d02}'} \left[\frac{a_{26}p^3 - a_{26}a_{11}p^2 + (a_{16}a_{23} - a_{13}a_{26})p}{p - a_{66}} \right] \end{bmatrix}$$

$$p^4 - (a_{11} + a_{22})p^3 + (a_{22}a_{11} - a_{13} - a_{24})p^2 + (a_{24}a_{11} + a_{22}a_{13})p + (a_{13}a_{24} - a_{14}a_{23})$$

(3.29)

giving on inversion

$$\hat{g}_{11} = \frac{-T_{d01}'(p - a_{55})}{p^3 \cdot G_1} \left[\frac{a_{26}p^3 - a_{26}a_{11}p^2 + (a_{16}a_{23} - a_{13}a_{26})p}{a_{15}a_{26} - a_{16}a_{25}} \right]$$

$$\hat{g}_{12} = \frac{-T_{d01}'(p - a_{55})}{p^3 \cdot G_1} \left[\frac{-a_{16}p^3 + a_{16}a_{22}p^2 + (a_{16}a_{24} - a_{14}a_{26})p}{a_{15}a_{26} - a_{16}a_{25}} \right]$$

$$\hat{g}_{21} = \frac{-T_{d02}'(p - a_{66})}{p^3 \cdot G_2} \left[\frac{-a_{25}p^3 + a_{25}a_{11}p^2 + (a_{13}a_{25} - a_{15}a_{23})p}{a_{15}a_{26} - a_{16}a_{25}} \right]$$

$$\hat{g}_{22} = \frac{-T_{d02}'(p - a_{66})}{p^3 \cdot G_2} \left[\frac{a_{15}p^3 - a_{15}a_{22}p^2 + (a_{14}a_{25} - a_{24}a_{15})p}{a_{15}a_{26} - a_{16}a_{25}} \right] \quad (3.30)$$

3.9.3 TRANSFER FUNCTION MATRICES WITH REGULATORS

By pre-multiplying by the transfer function blocks representing the field excitation or input power regulator allows a representation of the control elements to be taken into account in the Plant Transfer function matrix, $G(p)$. Using the second order input power regulator as an example

$$G_{Acc}(p) = \frac{1}{(1+p.T_v)(1+p.T_s)} \cdot G_{Acc}(p) \quad (3.31)$$

$$\text{and } \hat{G}_{Acc}(p) = (1+p.T_v)(1+p.T_s) \cdot \hat{G}_{Acc}(p) \quad (3.32)$$

3.10 CONCLUSION

A linearised model written in the state space form has been produced for a multimachine power system using the initial steady state operating conditions of the system as the linearisation point. The use of REP 2 as the simplest synchronous machine model representative of the system's transient behaviour has been justified.

The use of the state space equation in producing transfer function matrices for the system has been demonstrated.

The main limitation of the linear program is that it is only truly representative of the system over small perturbations. However, using a linear model to produce a control scheme, De Sarkar and Dharma Rao⁽⁶¹⁾ have demonstrated improved response for both small and large disturbances.

The effect of the linear model when subjected to different disturbances is investigated in Chapter 6.

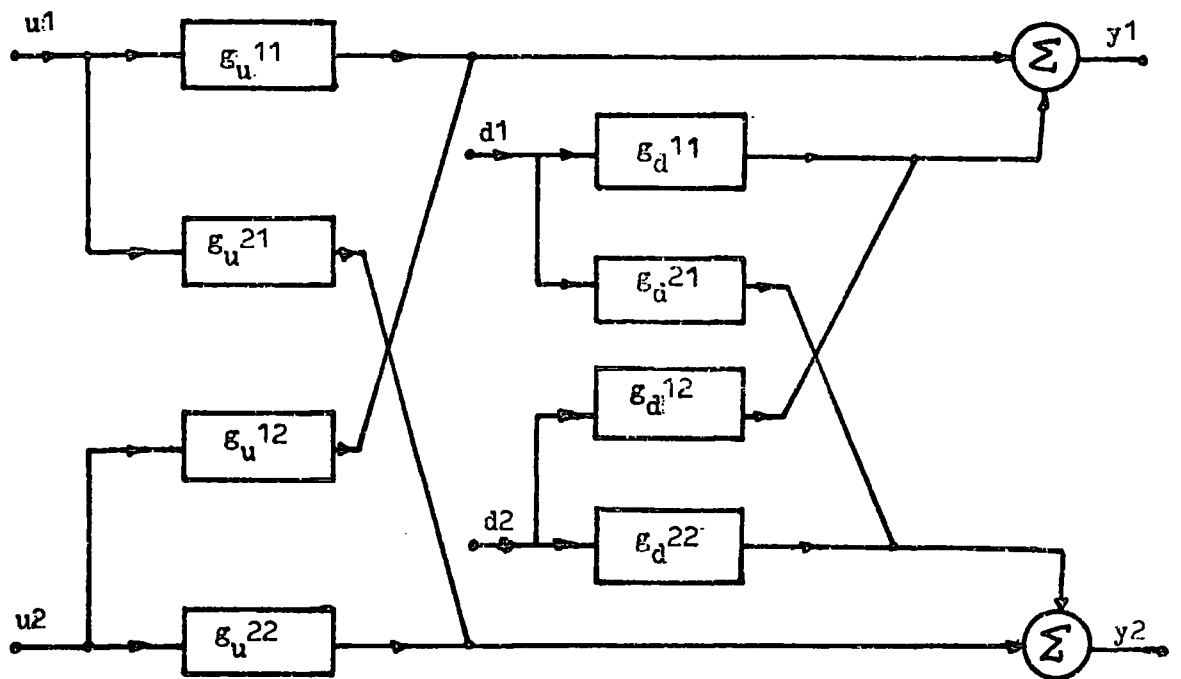


Fig. 3.1 Block Diagram of the Transfer Function Matrices.

CHAPTER 4

LINEAR MULTIVARIABLE CONTROL THEORY

4.1 GENERAL

In any multichannel control problem it is necessary to consider interaction effects between channels in the design technique. (67) This can be achieved by either optimum control methods or Linear Multivariable control methods.

A great deal of work has been carried out on Linear Multivariable Control Theory at Manchester Institute of Science and Technology (65-71) and forms the basis of the control work presented here. Consequently a summary of Linear Multivariable Control Methods is now presented.

4.2 THE CONTROL SYSTEM

Any n^{th} order differential equation describing a system can be represented by a set of n first order simultaneous differential equations of the form (55)

$$\dot{x}_i(t) = f_i(x, u, t) \quad (4.1)$$

which for a linear system is always expressible in the state space form of equation (3.4)

The Plant Transfer function matrix, $G(p)$, forms the basis of the design method and is obtained via equation (3.10).

Some initial definitions concerning the control system of fig. 4.1 are necessary. In fig. 4.1

$h(p)$ = $m \times 1$ matrix of reference input transforms

$e(p)$ = $m \times 1$ matrix of error transforms

$y(p)$ = $m \times 1$ matrix of plant output transforms.

$u(p)$ = $r \times 1$ matrix of plant input transforms

$K(p)$ = $r \times m$ matrix of controller transfer functions

$G(p)$ = $m \times r$ matrix of Plant transfer functions

$F(p)$ = $m \times m$ matrix of feedback transducer transfer functions.

If all the feedback loops are broken at \mathbf{Q} , fig. 4.1, and a signal transform vector $\alpha(p)$ is injected the transform vector of the signal returned at \mathbf{a}^1 is

$$-G(p).K(p).F(p).\alpha(p) \quad (4.2)$$

The difference between injected and returned signals is thus given by

$$[I_m + G(p).K(p).F(p)].\alpha(p) = E(p).\alpha(p) \quad (4.3)$$

where $E(p)$ is defined as the Return Difference Matrix, while the quantity

$$T(p) = G(p).K(p).F(p) \quad (4.4)$$

is defined as the Return-ratio Matrix. This gives

$$E(p) = I_m + T(p) \quad (4.5)$$

The closed loop transfer function matrix of fig. 4.1 is

$$H(p) = [I_m + G(p).K(p).F(p)]^{-1}.G(p).K(p) \quad (4.6)$$

so that

$$H(p) = E^{-1}(p).Q(p) \quad (4.7)$$

where

$$Q(p) = G(p).K(p) \quad (4.8)$$

and is the open loop transfer function matrix.

4.3 VECTOR FEEDBACK STABILITY CRITERIA

4.3.1 GENERAL STABILITY DEFINITIONS

Let $|G(p)|$ and $|H(p)|$ be the determinants of $G(p)$ and $H(p)$, in fig. 4.1 with $k(p) = I_m$, respectively then if⁽⁷⁰⁾

$$|G(p)| = \frac{\phi_1(p)}{\phi_0(p)} \quad (4.9)$$

$$|H(p)| = \frac{\phi_1(p)}{\phi_2(p)} \quad (4.10)$$

and

$$\frac{|G(p)|}{|H(p)|} = \frac{\phi_2(p)}{\phi_0(p)} \quad (4.11)$$

where,

$\phi_0(p)$ is the open-loop-system characteristic polynomial and $\phi_2(p)$ is the closed-loop-system characteristic polynomial.

From equation (3.10)

$$G(p) = C.(pI - A)^{-1}. B \quad (3.10)$$

$$= \frac{C. [\text{adj}(pI - A)]. B}{|pI - A|} \quad (4.12)$$

then $|G(p)|$ has,

$$\phi_0(p) = |pI - A| \quad (4.13)$$

The open loop system is stable if and only if all the zeros of $\phi_0(p)$ lie in the open left half complex plane. Similarly the closed loop system is stable if and only if all the zeros of $\phi_2(p)$ lie in the open left half complex plane.

For design purposes it is easier to work in terms of the control systems transfer function matrices of section 4.2 than in terms of $\phi(p)$. From equation (4.7), with $K(p) = I$,

$$H(p) = E^{-1}(p). G(p) \quad (4.14)$$

taking determinants

$$|H(p)| = \frac{|G(p)|}{|E(p)|} \quad (4.15)$$

or

$$|E(p)| = \frac{|G(p)|}{|H(p)|} \quad (4.16)$$

and from equation (4.11) the determinant of the Return Difference Matrix $|E(p)|$ can be written

$$|E(p)| = \frac{\Phi_2(p)}{\Phi_0(p)} \quad (4.17)$$

When working in terms of the system's transfer function matrices it is necessary to recognise that cancellation may occur in equations (4.11) and (4.17). To ensure that the cancelled poles are not unstable terms it is assumed that the open-loop system is asymptotically stable. At this stage it is necessary to define a contour, D_c , in the complex plane, in the usual Nyquist sense, to allow further analysis of system stability.

Let D_c be a contour in the complex plane consisting of the imaginary axis from $-j\alpha$ to $+j\alpha$ and a semi-circle centred on the origin of radius α in the right half plane. Let α be large enough to ensure that every zero and pole of $|G(p)|$ and $|H(p)|$ in the open right half plane lie within D_c . Further let D be indented into the left half plane to avoid any poles or zeros of $|G(p)|$ or $|H(p)|$ that lie on the imaginary axis between $-j\alpha$ and $+j\alpha$. The indentations are assumed to be small enough to avoid any pole or zero in the open left half plane.

4.3.2 STABILITY IN TERMS OF THE RETURN DIFFERENCE MATRIX

From equation (4.17) with the open-loop system stable the closed-loop characteristic polynomial will not vanish in the closed right half complex plane if and only if $|E(p)|$ does not vanish in the closed right-half complex plane.

If D_c maps into a closed curve Γ in the complex plane under the mapping of $|E(p)|$ then the system is closed loop stable if no point within D_c maps onto the origin of the complex plane under the mapping $|E(p)|$.

The system is thus closed loop stable if Γ does not enclose the origin.

If $|E(p)| \rightarrow 1$ as $|p| \rightarrow \infty$, then α can be taken as arbitrarily large and Γ can be referred to as the locus $|E(j\omega)|$.

This gives a Nyquist type stability criterion for the multiloop system with the point $(0,0)$ as the critical point.

If the eigen-values of $E(p)$ are $\rho_i(p), i=1,2,\dots,m$ then

$$|E(p)| = \prod_{i=1}^m \rho_i(p) \quad (4.18)$$

$|E(p)|$ will not vanish for any p enclosed by D_c if and only if none of $\rho_i(p), i=1,2,\dots,m$ vanish for any p enclosed by D_c . If D_c maps in Δ_i under $\rho_i(p), i=1,2,\dots,m$ then Γ will not enclose the origin of the complex plane if and only if none of Δ_i enclose the origin of the complex plane. The following statement of stability holds -

"The system is closed-loop stable if and only if all the eigen-value loci $\rho_i(j\omega)$ for $i=1,\dots,m$ satisfy the Nyquist criteria with the critical point as $(0,0)$."

By equation (4.5) and the eigen value shift theorem

$$\rho_i(p) = 1 + \nu_i(p) \quad (4.19)$$

where $\nu_i(p), i=1,\dots,m$ are the eigen-values of $T(p)$ then a similar statement of stability holds as above the critical point now being $(-1,0)$.

4.3.3 AN INDIRECT STATEMENT OF STABILITY IN TERMS OF THE RETURN DIFFERENCE MATRIX

Gershgorin's theorem states ⁽⁷⁰⁾ that the eigen-values of any matrix $E(p)$ are contained within a union of discs having centres

$$e_{ii}(p), i=1,2,\dots,m$$

and radii

$$\sum_{\substack{j=1 \\ j \neq i}}^m |e_{ij}(p)|, i=1,2,\dots,m \quad (4.20)$$

The mapping of D_c under the particular element $e_{ii}(j\omega)$, the Gershgorin disc set generated ensures that every eigen-value locus $p_i(j\omega)$ lies within the generated Gershgorin disc set. If

$$|e_{ii}(p)| > \sum_{\substack{j=1 \\ j \neq i}}^m |e_{ij}(p)| \quad (4.21)$$

then the system is stable with all feedback loops closed if none of

Γ_i , $i=1,2,\dots,m$ enclose the origin of the complex plane, where D_c maps into Γ_i under $e_{ii}(p)$, $i=1,2,\dots,m$.

Since

$$e_{ii}(p) = 1 + t_{ii}(p), \quad i=1,2,\dots,m \quad (4.22)$$

and

$$e_{ij}(p) = t_{ij}(p), \quad i=1,2,\dots,m \quad (4.23)$$

then a similar statement of stability can be made with $t_{ii}(j\omega)$, $i=1,2,\dots,m$ satisfying the Nyquist stability criterion with critical point at $(-1,0)$, then the system is stable with all loops closed.

4.3.4 STABILITY IN TERMS OF OPEN LOOP AND CLOSED LOOP TRANSFER FUNCTION MATRICES

Working in terms of $Q(p)$ and $H(p)$ make it more convenient to relate open and closed loop responses. Further $H(p)$ is not a simple function of $G(p)$, $K(p)$ and $F(p)$ and thus if $Q^{-1}(p)$ exists it is more convenient to use the inverse form, thus inverting equation (4.6)

$$\hat{H}(p) = F(p) + \hat{Q}(p) \quad (4.24)$$

working with these transfer function matrices Rosenbrock⁽⁷⁰⁾ has proved the following stability theorems:-

Theorem 1

Let the open loop system be asymptotically stable. Let $|\hat{Q}(p)|$ map D_c into $\hat{\Gamma}_o$, and $|\hat{H}(p)|$ map D_c into $\hat{\Gamma}_c$. Then the closed

loop system is stable if and only if $\hat{\Gamma}_0$, $\hat{\Gamma}_c$ encircle the origin the same number of times.

Theorem 2

Define,

$$d_i(p) = \sum_{\substack{j=1 \\ j \neq i}}^m |q_{ij}(p)| \quad (4.25)$$

$$\delta_i(p) = \sum_{\substack{j=1 \\ j \neq i}}^m |q_{ji}(p)|$$

Let $|Q(p)|$ map D_c into Γ and $q_{ii}(p)$ map D_c into Γ_i .

Let Γ encircle the origin N times and Γ_i encircle the origin N_i times, then;

For all p on D_c , let $|q_{ii}(p)| - d_i(p) > 0$
(resp. $|q_{ii}(p)| - \delta_i(p) > 0$), $i = 1, 2, \dots, m$.

Then

$$N = N_1 + N_2 + \dots + N_m$$

Theorem 3

Let D_c be mapped by $|\hat{Q}(p)|$ into $\hat{\Gamma}_0$, by $|\hat{H}(p)|$ into $\hat{\Gamma}_c$, by $\hat{q}_{ii}(p)$ into $\hat{\Gamma}_{0i}$ and by $h_{ii}(p)$ into $\hat{\Gamma}_{ci}$. Let the number of encirclements of the origin by $\hat{\Gamma}_0$ be N_0 , by $\hat{\Gamma}_c$ be N_c , by $\hat{\Gamma}_{0i}$ be N_{0i} and by $\hat{\Gamma}_{ci}$ be N_{ci} .

Define

$$d_i(p) = \sum_{\substack{j=1 \\ j \neq i}}^m |\hat{q}_{ij}(p) + f_{ij}(p)| \quad (4.26)$$

$$\delta_i(p) = \sum_{\substack{j=1 \\ j \neq i}}^m |\hat{q}_{ji}(p) + f_{ji}(p)|$$

Then;

Let the open loop system be asymptotically stable and let $|G(p)|$ have no zero in the closed right half-plane.

Let $|f_{ii}(p) - \hat{q}_{ii}(p)| - d_i(p) > 0$,

(resp. $|f_{ii}(p) + \hat{q}_{ii}(p)| - \delta_i(p) > 0$), $i=1, 2, \dots, m$.

Then the closed-loop system is asymptotically stable if and only if

$$\sum_{i=1}^m N_{ci} = 0 \quad (4.27)$$

Equation (4.27) may be replaced by

$$N_{ci} = 0, \quad i=1, 2, \dots, m. \quad (4.28)$$

This is the usual inverse Nyquist criterion applied separately to each $\hat{q}_{ii}(p)$

Theorem 4

Let the open loop system be asymptotically stable. Let

$$(i) \quad |\hat{q}_{ii}(p)| - \sum_{\substack{j=1 \\ j \neq i}}^m |\hat{q}_{ij}(p)| > 0, \quad (\text{resp. } |\hat{q}_{ii}(p)| - \sum_{\substack{j=1 \\ j \neq i}}^m |\hat{q}_{ji}(p)| > 0)$$

$$(ii) \quad |f_{ii}(p) + \hat{q}_{ii}(p)| - d_i(p) > 0, \quad (\text{resp. } |f_{ii}(p) + \hat{q}_{ii}(p)| - \delta_i(p) > 0)$$

then the closed loop system is asymptotically stable if and only if

$$\sum_{i=1}^m N_{ci} = \sum_{i=1}^m N_{oi} \quad (4.29)$$

Equation (4.29) may be replaced by

$$N_{ci} = N_{oi}, \quad i=1, 2, \dots, m \quad (4.30)$$

This is the usual inverse Nyquist criterion applied separately to each $\hat{q}_{ii}(p)$.

If the diagonal element of $F(p)$ are $f_{ii} = k_i$ then

equations (4.28) and (4.30) use the point $(-k_i, 0)$ as the critical point.

4.4 APPLICATION OF THE STABILITY CRITERIA

For each discrete value on the D_c contour $\hat{q}_{ii}(p)$ is evaluated and a circle of radius $d_i(p)$ (resp. $\delta_i(p)$) is drawn centred on $q_{ii}(p)$. The line locus of $\hat{q}_{ii}(p)$ now changes to that of an envelope. By Gershgorin's⁽⁷⁰⁾ Theorem this envelope contains the critical locus. However this union of d-circles does not give the exact location of the locus but does contain it. The usual Nyquist stability criterion is applied to this envelope.

If the critical point given by $(-k_i, 0)$ is outside this envelope and in the correct position as given by the Nyquist criteria, stability would be guaranteed and the system said to be diagonal dominant for this corresponding gain, k_i . If the envelopes do not touch or cut the negative real axis between the origin and the points $-k_i$ the stability of the multivariable system is determined by the Nyquist stability criteria.

The transfer function that a single loop controller must be designed for is $\hat{p}_i(p)$ where

$$\hat{p}_i(p) = \hat{h}_{ii}(p) - k_i(p) \quad (4.31)$$

This is the transfer function seen in the i^{th} loop when this is open and all other loops are closed. Ostrowski's Theorem says that this $\hat{p}_i(p)$ is contained within the envelope swept out by the circles centred on $\hat{q}_{ii}(p)$ and that this remains true for all values of gains k_j in each loop j , between zero and k_j . Furthermore provided $\hat{Q}(p)$ and $\hat{H}(p)$ are dominant this same theorem narrows the band and gives circles $\phi_i(p) \cdot d_i(p)$ where

$$\phi_i(p) = \text{Max}_{j \neq i} \frac{d_j(p)}{|k_j + \hat{q}_{jj}(p)|} \quad (4.32)$$

$$\text{If } |\hat{q}_{ii}(p)| \leq \sum_{\substack{j=1 \\ j \neq i}}^n |\hat{q}_{ij}(p)|$$

then the system may be made dominant with respect to a certain feedback gain in the i^{th} loop and the above criteria applied.^(69A)

Before applying the ϕ circles stability of the system must first be determined via the d-circles.

4.5 DIGITAL COMPUTATION OF THE INVERSE NYQUIST DIAGRAMS

The prediction of the I.N. diagrams for each element, \hat{q}_{ii} of a matrix is a tedious longhand process but one that ideally lends itself to a computer solution.

A program was written (Appendix F) that will calculate $G(p)$ from the state space equations or allow it to be specified directly in a transfer function form.

$Q(p)$ and $\hat{Q}(p)$ are then calculated where

$$\hat{Q}(p) = \hat{K}(p) \cdot \hat{G}(p) \cdot \hat{L}(p) \quad (4.33)$$

and $K(p)$ and $G(p)$ take on their usual forms and $L(p)$ is a post-compensator matrix.

The I.N. diagram for each element $\hat{q}_{ii}(p)$ is then plotted on a line printer. The magnitude of the d and S circles are calculated and can be added to the I.N. plots if required.

4.6 DESIGN OF NON-INTERACTIVE CONTROLLERS

The aim of designing non-interactive controllers is to make the interaction between channels negligible, i.e. to obtain a diagonal dominant condition. This condition of diagonal dominance may be achieved by the addition of control elements into either the pre - or post - compensator matrices or into the feedback matrix, $F(p)$.

4.6.1 CONTROLLER DESIGN BY MATRIX DIVISION

The feedback matrix $F(p)$ is assumed diagonal. Control elements are added into the pre-compensator matrix $K(p)$ by assuming a diagonal form of $Q(p)$, then

$$K(p) = G^{-1}(p) \cdot Q(p) \quad (4.34)$$

It follows that $H(p)$ is diagonal.

The danger of this method is that much of the design freedom can be used up in choosing the elements of $K(p)$, thus leaving little room for compensation. (68)

4.6.2 COMPENSATION IN THE FEEDBACK MATRIX, $F(p)$

Frequency dependent terms may be added into the off-diagonal elements of $F(j\omega)$ to cancel directly with the off-diagonal elements of $Q(j\omega)$. (equation 4.24).

Such methods can introduce phase advance and must be closely controlled.

4.6.3 ROSENBRACK'S INVERSE NYQUIST ARRAY DESIGN METHOD

The pre-compensator matrix $K(p)$ is synthesised in three successive stages. (65)(66)

$$K(p) = K_a \cdot K_b(p) \cdot K_c(p) \quad (4.35)$$

where,

K_a is a permutation matrix representing a preliminary renumbering of the inputs to $G(p)$.

$K_b(p)$ represents a sequence of elementary row and column operations so as to make the matrix diagonal dominant.

$K_c(p)$ a diagonal matrix which synthesises the m principle control loops.

Having selected K_a , $K_b(p)$ is chosen so as to make $\hat{Q}(p)$ diagonal dominant. The transient response is now shaped in the m principle loops by addition of control elements into the diagonal matrix $K_c(p)$.

4.6.4 DISCUSSION

Control schemes may also be designed by using these design methods in conjunction with each other. The methods outlined above have been used in this work; other design methods have been summarised by MacFarlane in reference (68).

4.7 CONCLUSION

The theory and some controller design methods for use in linear multivariable control problems have been outlined.

A digital program to compute the Inverse Nyquist loci was written. This program does not completely automise the process but eliminates the majority of the tedious longhand calculations. The program is easily converted to the advantageous graphical display output medium if it is available.

A comprehensive suite of programs using graphical display equipment has previously been written^(69B) by researchers at U.M.I.S.T.

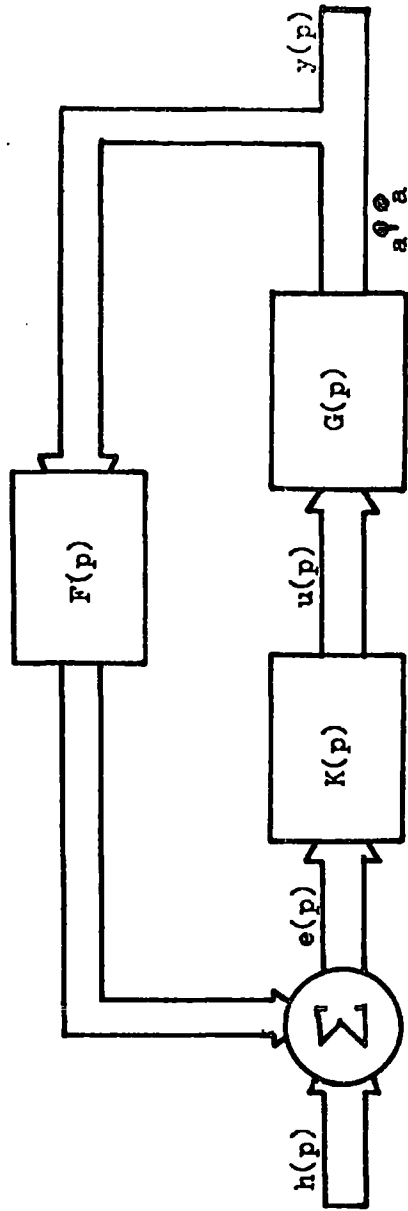


Fig. 4.1 The Basic Control System.

CHAPTER 5

THE DYNAMIC INTERACTION OF SYNCHRONOUS MACHINES

5.1 INTRODUCTION

In determining the transient stability limit of large electrical power systems it is common practice to lump together synchronous machines in the same physical vicinity, such as in an individual power station, and use an equivalent machine to represent this group. The main advantage of this simplification is a large saving in computer time. However Dineley and Morris⁽⁵⁷⁾ have shown that the flow of synchronising power between electrically close-coupled machines of varying inertias, can lead to multiwing instabilities. Under such conditions representation by an equivalent machine can lead to inaccurate results.

A saving on computer time can be made by using the simplest machine model representative of the system's dynamics. The model of "constant voltage behind transient reactance with an equivalent damping constant" has been suggested.⁽³⁶⁾

If such simple models are to be used then their behaviour in a multimachine system relative to the more complete models must be understood. This and the study of interaction phenomena are the intentions of this Chapter.

5.2 CONTROL EQUIPMENT

Modelling of the associated control equipment can hide the effects produced by different machine models. Consequently both excitation voltage and input power to the machine are assumed constant during the study interval.

5.3 TRANSMISSION SYSTEMS STUDIED

The network configurations of figs. 2.7 and 5.1 are used. Both networks, could, if required, be transformed into the other by the non-linear $\nabla-\lambda$ transform.⁽⁷⁴⁾ The ∇ configuration of fig. 5.1 has the advantage over the λ network, even though the latter is the most likely to be found in a practical system,⁽²¹⁾⁽⁵⁷⁾ in that it allows an easy measure of the power transferred between the machines.

5.4 A QUALITATIVE ASSESSMENT OF PARAMETER VARIATION ON THE OSCILLATION FREQUENCY

The flow of synchronising power between machines is dependent on the frequency at which the machine load angles oscillate. Power will flow from machine one to machine two when $\delta_1 > \delta_2$ and vice versa. Section 5.5 shows that a small change in the oscillation frequency can induce a critical condition within the system such that there is an adverse power flow causing instability. Conversely a small change in oscillation frequency could offset this critical condition.

The oscillation frequency of the machine is a function of the machine and system parameters and can be calculated for small perturbations using a first order Taylor expansion.

If a single machine tied to an infinite busbar is considered and, using REP 2, the equation of motion is

$$H \cdot \frac{d^2\delta}{dt^2} + Kd \cdot \frac{d\delta}{dt} = P_m - P_e \cdot \sin \delta \quad (5.1)$$

$$P_e = \frac{E' \cdot V_b}{X} \quad \text{-----} \quad \text{Maximum electrical power output}$$

X ----- Machine and line combined impedance.

Linearising equation (5.1) and assuming only variations in mechanical power and load angle, then

$$H \cdot \Delta \ddot{\delta} + K_d \cdot \Delta \dot{\delta} + P_e \cdot \cos \delta_0 \cdot \Delta \delta = \Delta P_m \quad (5.2)$$

where Δ represents a small change.

Initially the rotor of the machine is stationary with respect to the rotating reference frame, then

$$\begin{aligned} \Delta \ddot{\delta} &= \ddot{\delta} - \ddot{\delta}_0 = \ddot{\delta} \\ \Delta \dot{\delta} &= \dot{\delta} - \dot{\delta}_0 = \dot{\delta} \\ \Delta \delta &= \delta - \delta_0 = x \end{aligned} \quad (5.3)$$

Let

$$P_e \cdot \cos \delta_0 = P_e'$$

Substituting equation (5.3) into (5.2) and introducing the Laplace operator, yields

$$\frac{x}{\Delta P_m} = \frac{1}{H \cdot p^2 + K_d \cdot p + P_e'} \quad (5.4)$$

The poles of equation (5.4) are

$$p_1, p_2 = -\frac{K_d}{2H} \pm j \sqrt{\frac{P_e'}{H} - \frac{K_d^2}{4H^2}} \quad (5.5)$$

The oscillation frequency is given by the imaginary part of equation (5.5) as

$$f = \frac{1}{2\pi} \sqrt{\frac{P_e'}{H} - \frac{K_d^2}{4H^2}} \quad (5.6)$$

and is dependent on all the system parameters, especially the inertia constant, H.

For the non-linear system of equation (5.1) the oscillation frequency is a function of the system parameters such that

$$f = g(H, K_d, E', V_B, X, t) \quad (5.7)$$

Because of the interconnection between machines in a multimachine system the oscillation frequency of any one machine becomes a function of

all machine and system parameters. Changing a parameter in one machine would affect the oscillation frequency of the others.

This change in frequency is discussed by Dineley and Morris⁽⁵⁷⁾ when a change in inertia constant is made. The same effect will be prominent in later sections.

5.5 INTERACTION PHENOMENA - A GENERAL DESCRIPTION

Electrical power is transferred between synchronous machines in a direction determined by their respective load angles. The transfer of electrical power is explained by reference to fig. 5.2.

Power is transferred to an infinite bus from the synchronous machines when their load angles are greater than zero, i.e. they act as generators. If any load angle falls below zero then that machine will be motoring and electrical power flows from the infinite source to that machine - point (c).

A similar situation arises when electrical power is transferred between actual machines. The power transfer occurs when the load angles of the respective machines differ and flows from the machine with the higher load angle to that with the lower.

The actual power output of a machine depends upon its position on the operating locus at any instant. As the magnitude of the rotor angles initially increase the power output from the machines will also increase until the peak of the operating locus is reached and then it will decrease. Consequently in certain circumstances a machine having a much larger load angle than the other can be developing less power.

e.g. suppose

$$\begin{aligned} \delta_1 &> \delta_2 \\ \delta_2 &< \alpha \\ \alpha &> (180 - \delta_1) < \delta_2 \end{aligned} \quad (5.8)$$

where α° is the peak of the operating locus, then power will transfer from

machine 1 to machine 2 yet machine 2 will be developing more power output. This is demonstrated by point (a) fig. 5.2.

The first reverse load angle excursion of machine 2 - point (b) - is limited. This is associated with the power flows at bus 2 which are:-

- (i) Power being transferred from bus 1.
- (ii) Power being transferred from bus 2 to the infinite source.

The power transfer from bus 1 reduces the loading condition on machine 2 and produces a reduction in the terminal power. Consequently the power balance between mechanical input and electrical output power is upset. A situation is created whereby the machine has a tendency to accelerate to accommodate this excess power. This tendency to accelerate limits the reverse load angle swing and, in this case, produces a subsequent increase in load angle.

If these power flow conditions arise when both machines are accelerating then a substantial increase in load angle can result - point (d) - which can ultimately cause a multiswing instability, fig.5.3(a). This critical condition has been related to the oscillation frequencies of the respective load angles - section 5.4. By increasing the mechanical input power to machine 2 to 0.92 p.u. and thus changing rotor angle oscillation frequency slightly the system is rendered stable - fig. 5.3(b).

These critical conditions are generally associated with the machine of lighter inertia as the accelerating power is inversely proportional to inertia constant - equation (1.1).

5.6 SYNCHRONOUS MACHINE MODELS - THE EFFECT OF NEGLECTING TRANSIENT SALIENCY

By including transient saliency an increase in the estimate of the transient stability limit is obtained - REP 1 and REP 3 in fig. 5.4. Transient saliency introduces a second harmonic term dependent on load

angle into the operating locus⁽¹³⁾ which is responsible for the increase in stability limit.

Using REP 1 and REP 3 multiswing instability was obtained with similar machine and system parameters. The asymmetry being introduced into the system by the unsymmetrical 3ϕ fault. By changing the inertia constants to values of 6 and $3KJ/KVA$ respectively the asymmetry within the system is exaggerated and multiswing instability readily produced - fig. 5.3(a) and 5.9.

The effect of the coupling impedance on the transient stability limit depends on the inertia constant used, fig. 5.5 and 5.6. With all inertia combinations the stability limit initially increases as the coupling impedance decreases. However as the machines become more electrically close coupled inertia effects predominate.

These differences in the stability limit are associated with the ability of the machines to absorb the excess fault energy without producing a Lyapunov instability. As the inertia increases the machines can accommodate more kinetic energy without producing this instability and a corresponding increase in the stability limit results.

In a remote system the majority of the fault energy has to be accommodated by the electrically nearest machine. If the inertia of this machine is small then the stability limit obtained is less than if the machine had a large inertia - (b), (c), (a). If there is a possibility of accommodating some of this excess energy in another part of the system the stability limit would also increase. Another machine, particularly one of heavier inertia, and a low coupling impedance, provides a convenient means of absorbing and transmitting this excess energy - curve (b). This effect is also demonstrated by machines of similar inertias but to a lesser degree - curve (c).

When the fault is nearest the heavy machine there is a tendency for the stability limit to reach a maximum at one value of coupling impedance - demonstrated by curve (a) in figs. 5.5 and 5.6 - i.e. there is an optimum coupling value. The initial increase in the stability limit, with decrease in coupling impedance, is caused by the lighter machine absorbing some of the fault energy. During this period the load angle of the heavy machine is always greater than the lighter machine - fig. 5.10(a). A further decrease in coupling impedance results in the fault energy seen by the light machine being of such magnitude that it accelerates quicker than the heavy machine - fig. 5.10(c). The heavy machine now has to try and absorb both the fault energy and the energy transferred from the lighter machine. A decrease in the stability limit results - curve (a). The optimum coupling impedance is obtained when the two machines' rotor angles rise at the same rate - fig. 5.10(b).

At low values of coupling impedance the two generators tend to appear as being attached to the same busbar. An equivalent machine representation would give a stability limit - curves (f) in figs. 5.6 and 5.7 - that all the inertia combinations would tend to at low coupling impedances. By comparing curve (f) and the stability limit produced by the other inertia combinations the errors that could be introduced by indiscriminantly lumping together synchronous machines and using an equivalent machine model is apparent. (57)

The scatter of the points in fig. 5.5 and 5.6 is the tendency of REP 1 and REP 3 to produce multiswing instabilities. To reduce the computer time a numerical step length of 0.01 was used. Consequently the accuracy in the critical clearing time is $\pm 0.01s$. This accounts for the difference between curves (c) and (f1) and (c) and (f2) at low coupling impedances in fig. 5.6.

5.7 MULTISWING AND FIRST SWING INSTABILITY

The general approach used to predict the stability of large power systems is to observe the computed load angle response of those machines nearest the fault. This computation lasts for a time period slightly in excess of that required for the first rotor angle swing. If these load angle responses do not show a Lyapunov instability the system is assumed stable under test fault conditions.

For some machine combinations instability may not arise until after the first load angle swing. The error introduced into the stability limit by using the first swing criteria over the actual stability limit can be of the order of 5% - fig. 5.5 curves (a) and (am) - giving a wrong impression of system security.

Multiswing instability is also predicted by REP 6⁽⁵⁷⁾⁽²¹⁾ - section 5.9.

5.8 THE EFFECT OF DAMPING CONSTANTS ON DYNAMIC INTERACTION

Introducing a damping term into the machine equations reduces the energy available to accelerate the machine. The system becomes positively damped - fig. 5.11 - and the stability limit for all values of coupling impedance increases - curves (d) and (e) in figs. 5.6 and 5.7.

Consider the 3ϕ fault nearest the heavy machine and unsymmetrical machine damping. An increase in the damping factor of the heavy machine only, in a remote system, produces a greater stability limit than increasing the damping on only the lighter machine - curves (g) and (h), fig. 5.8. This is due to the system being remote and the damping term helping to reduce the fault energy.

Reducing the coupling impedance increases the stability limit until the optimum coupling value is attained. This is more pronounced

when only the heavy machine is damped - curve (h), fig. 5.8. Damping only the lighter machine reduces its acceleration so that at low coupling impedances δ_2 is not very much greater than δ_1 and the transfer of power to the heavy machine is small causing little change in the stability limit - curve (g). Damping the heavy machine produces the opposite effect.

It is concluded that by changing the damping constant of an individual machine the optimum increase in the transient stability limit may not always result. Willems⁽⁷³⁾ in his work on Lyapunov methods found that increasing the system damping did not necessarily increase the overall stability region. Model systems demonstrating this effect have been discussed.⁽⁵⁸⁾⁽⁵⁹⁾

5.9 THE EFFECT OF FLUX DECREMENT ON THE TRANSIENT INTERACTION

Incorporating flux decay effects into the model reduces the stability limit with respect to REP 3 - fig. 5.4. The 3ϕ fault causes a reduction in the flux linkages of the rotor circuits and consequently less energy is required to push the machine into the Lyapunov unstable region. The stability boundary obtained for REP 5 was given by first swing instability, the decrease in flux linkages causing an increase in first load angle maximum as compared with REP 3.

A general response is shown in fig. 5.12. The first reverse load angle swings are reduced as the decrease in the flux linkages during the fault period have not had time to recover. The subsequent load angle oscillations are positively damped due to the change in flux linkage.

For reasons outlined in section (5.8) addition of a damping constant increases the stability limit - curves (e) and (d) fig. 5.7 - while the effect of the optimum coupling impedance is substantiated.

The presence of multiswing instabilities has been associated with certain power flow conditions. The addition of flux decrement allows for the decay of the transient operating locus to that of the steady state locus. This effect in itself can cause multiswing instability.

For a single machine, infinite bus system the two operating curves are given by Kimbark⁽¹³⁾ as

$$P_{\text{STEADY}} = \frac{E_q \cdot V_B \cdot \sin \delta}{x_d} + \frac{V_B^2 \cdot (x_d - x_q) \cdot \sin(2\delta)}{2 \cdot x_d \cdot x_q} \quad (5.10)$$

$$P_{\text{TRANSIENT}} = \frac{E_q' \cdot V_B \cdot \sin \delta}{x_d'} - \frac{V_B^2 \cdot (x_q - x_d') \cdot \sin(2\delta)}{2 \cdot x_d' \cdot x_q} \quad (5.11)$$

Sketch graphs of these are shown in fig. 5.13 where the peak on the transient loci is greater than 90° whereas in the steady state this peak value is less than 90° .

During the dynamic response the operating curve decays from the transient condition towards that of the steady state. If during this dynamic interval powerflow conditions are such as to keep the rotor angles high, at around 90° , then as the operating curve decays towards the steady state it is possible for the operating point to be on the unstable right hand side of the steady state loci. This will cause the machines to accelerate out of the Lyapunov stable region. This change in operating locus is demonstrated in fig. 5.14 for the power system of fig. 2.7 where the terminal power of machine 2 is plotted against rotor angle each time certain fixed values of rotor angle are reached. A straightforward decay between the operating curves is not obtained because of the power transfer between machines. Fig. 5.15(c) shows the corresponding rotor angle response.

Further examples of this multiswing instability are shown in fig. 5.15(a) and (b) where the damping constant is varied. The results

are similar to those produced by Dineley and Morris⁽⁵⁷⁾ and Preece⁽²¹⁾ to demonstrate multiswing instability.

The rate at which the flux linkages vary is governed by the value of the field open circuit time constant, T_{do}' . If this is large then the positive damping effect associated with the flux decay is lost but the maximum size of rotor angle swing during the first oscillation is reduced. The decay time from one operating locus to the other is also increased diminishing the flux decrement effect on multiswing instability. Removal of the positive damping by the increase in T_{do}' renders the critical flow conditions of section 5.5 more likely to produce, not only an increase in a future load angle swing, but possibly a multiswing instability.

5.10 CONCLUSION

In the preceding sections the effect of different machine representations on the dynamic interaction within multimachine power systems has been discussed.

It has been demonstrated that:-

- (i) Varying system and machine parameters affect the overall stability of the system.
- (ii) Indiscriminately increasing damping on a machine does not guarantee the best increase in overall stability level.
- (iii) For some system conditions there is an optimum value of impedance between the machines to produce the maximum system stability.
- (iv) Dynamic interaction effects can produce an increase in the size of a load angle excursion. At the limit this excursion can result in a multiswing instability in the Lyapunov sense.
- (v) Flux decrement adds positive damping to a system in so much as it tends to decrease the overall oscillation size.

- (vi) Flux decrement increases the first load angle excursion.
- (vii) For a salient pole machine flux decrement can cause multising instability as it allows for the decay of one operating locus to another.
- (viii) If there is any possibility of a multising instability arising within a system a study time of at least 6 secs. should be used. This conclusion was also reached by Dineley and Morris⁽⁵⁷⁾
- (ix) Because of (iv) a method of removing harmful interaction should be investigated, providing it does not reduce the overall system stability level.
- (x) A control scheme of the nature outlined in (ix) should be practical and readily implemented.

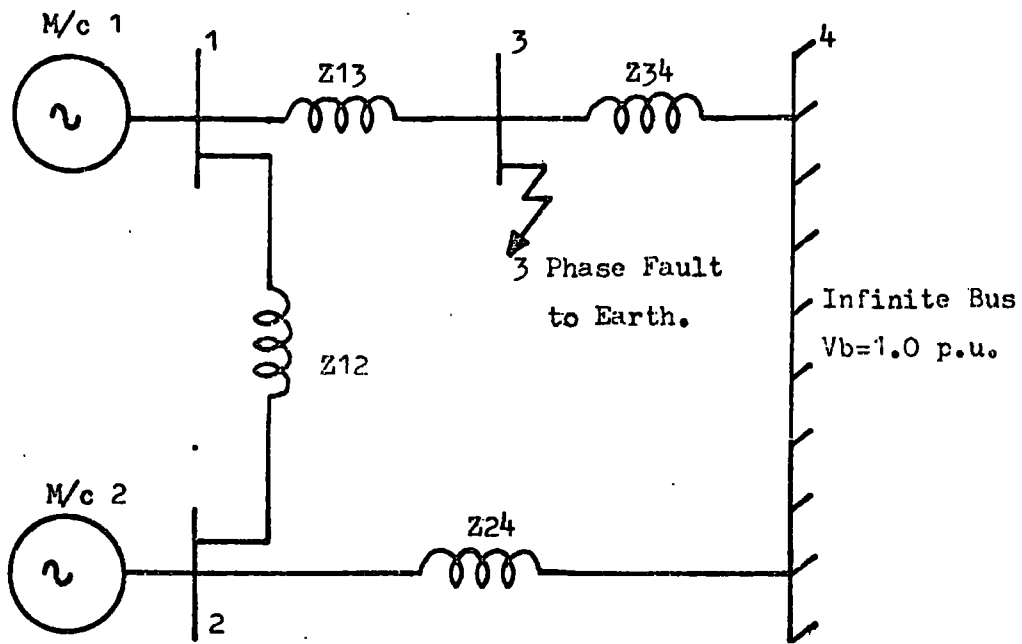


Fig. 5.1 Line Diagram of a Model Power System.

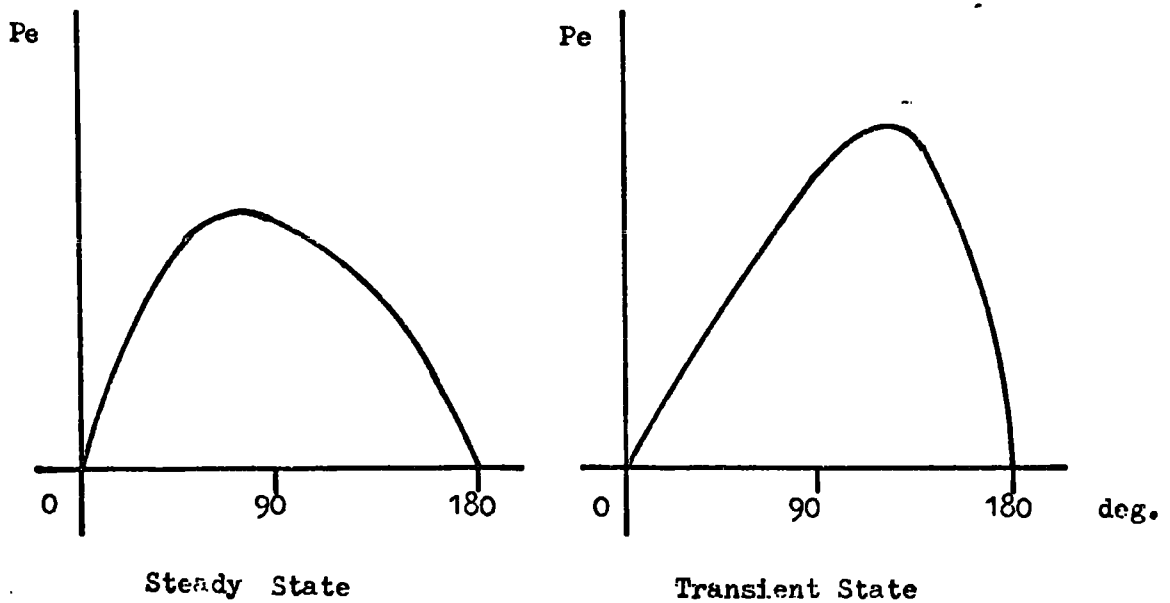


Fig. 5.13 Power Angle Operating Curves for a Salient Pole Synchronous Machine.

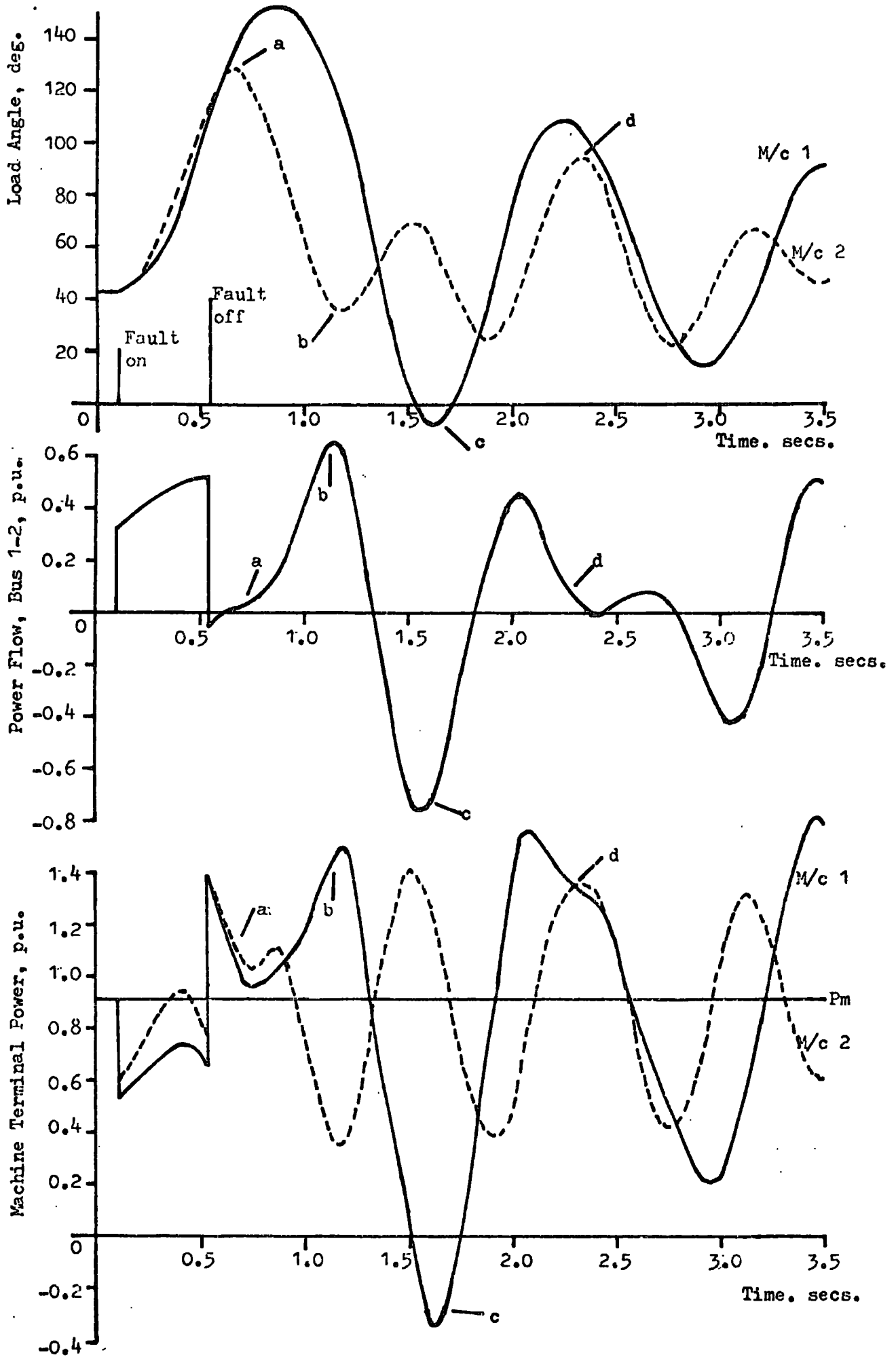
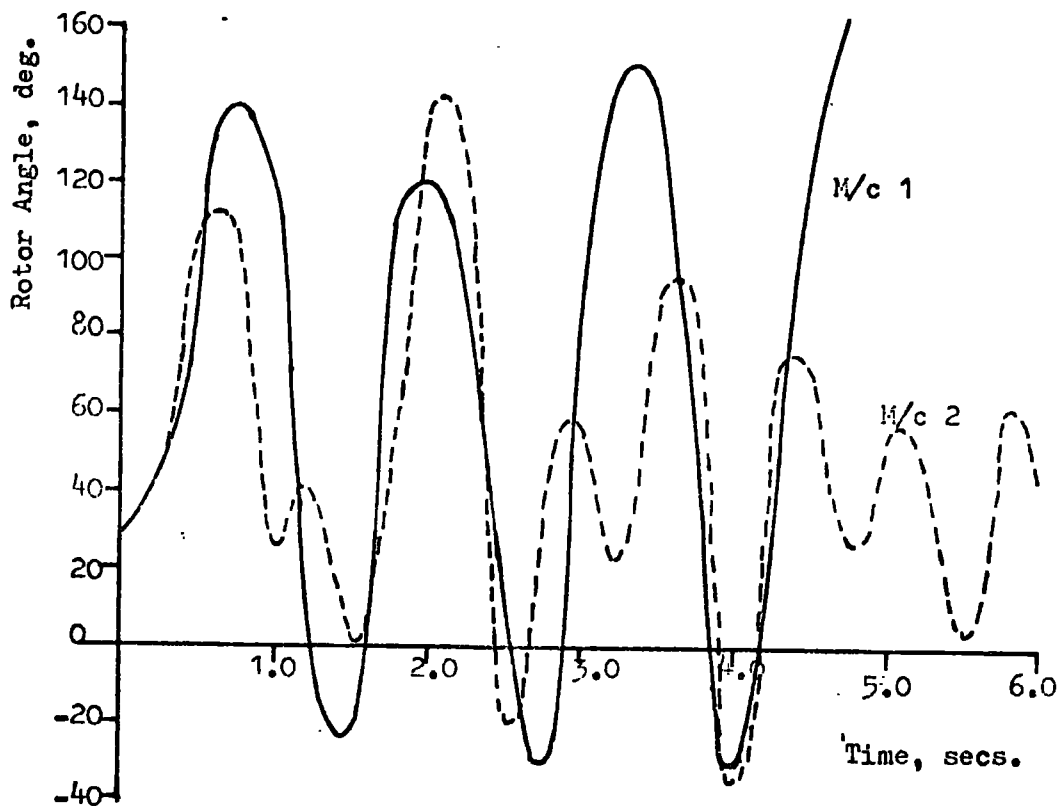
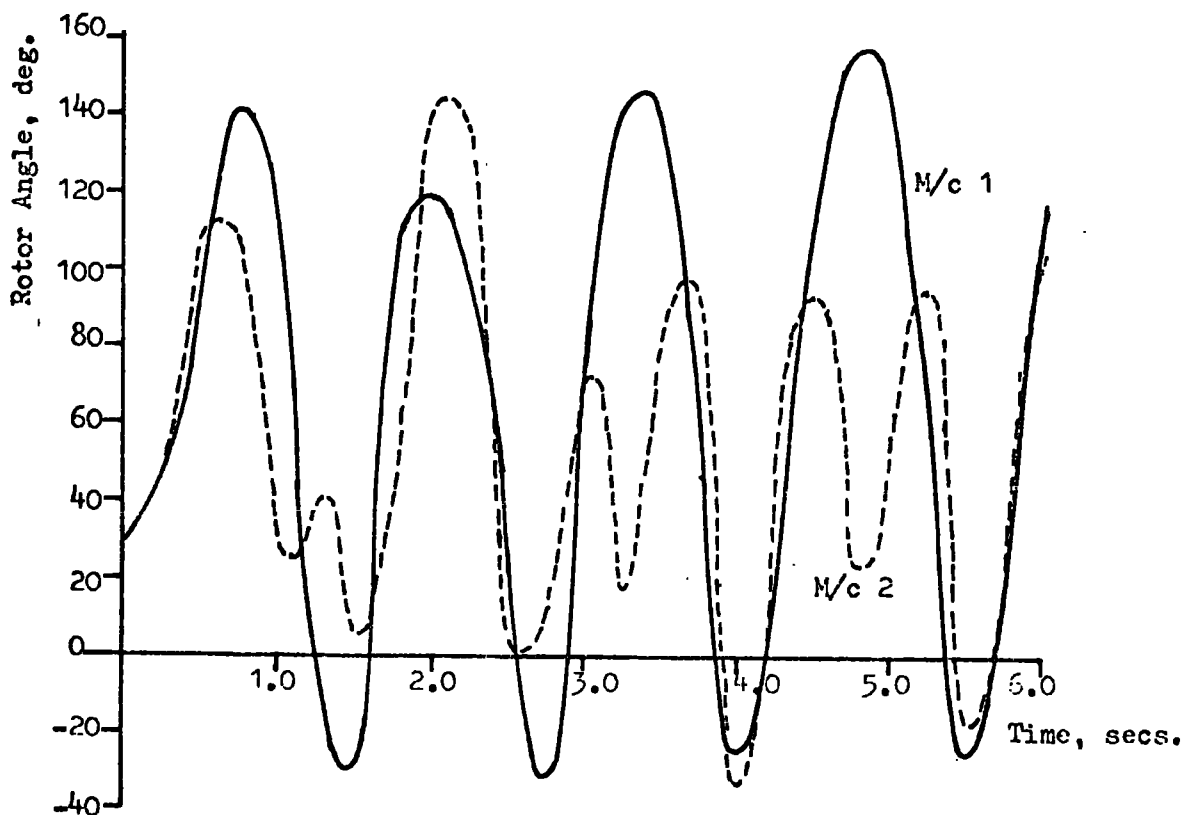


Fig.5.2 Time Responses for REP 6 using the Model System Fig.5.1, Data Appendix G, $Z_{12}=0.04$ p.u., $H_1=6$ KJ/KVA, $H_2=3$ KJ/KVA, $K_{d1}=K_{d2}=0.01$, $T_{fc}=0.43$ secs.



(a) $P_{m1}=P_{m2}=0.915$ p.u.



(b) $P_{m1}=0.915$ p.u., $P_{m2}=0.92$ p.u.

Fig. 5.3 Rotor Angle Response for REP 1 using Model System of Fig. 5.1
 Data Appendix G and $H_1=6$ KJ/KVA, $H_2=3$ KJ/KVA, $Z_{12}=0.02$ p.u.,
 $T_{fc}=0.4$ s.

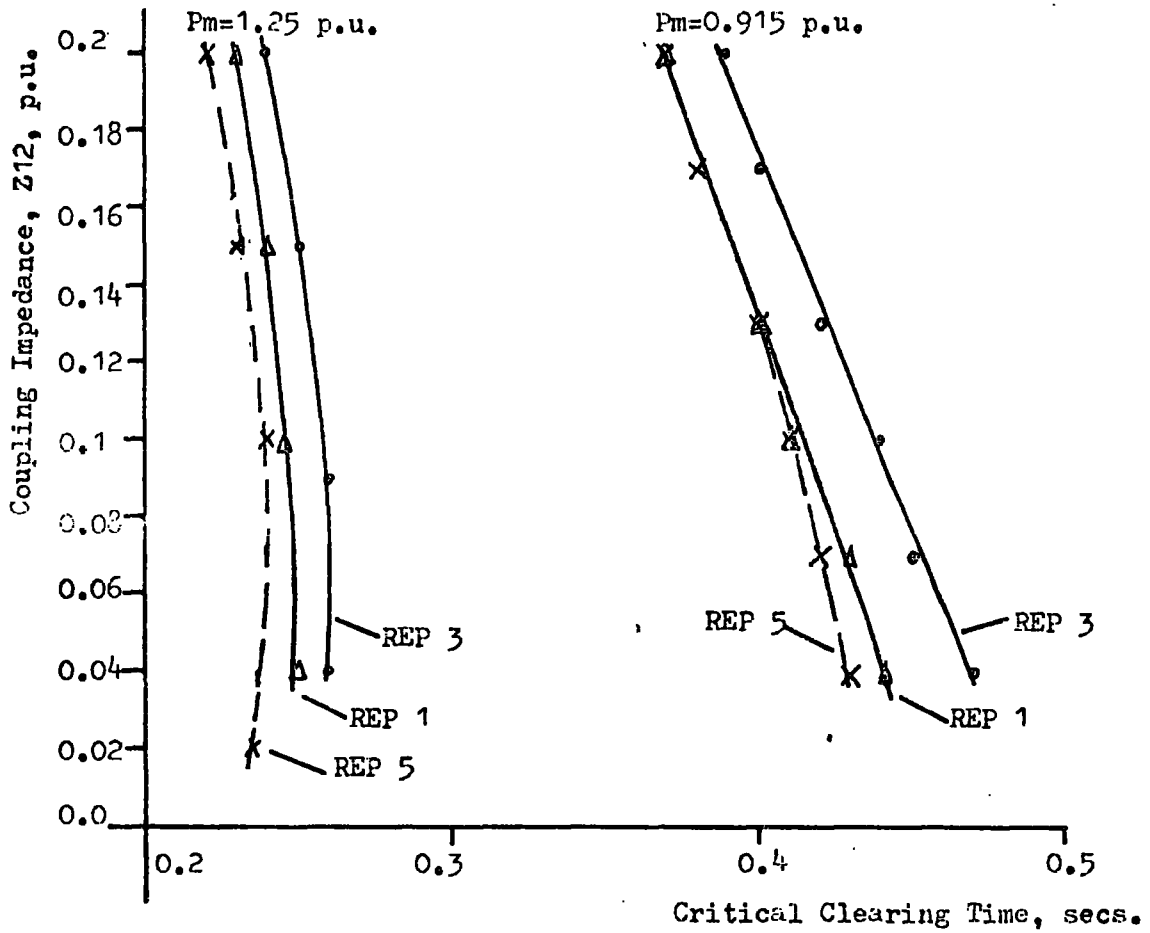


Fig. 5.4 The Effect of Machine Representation on the System Stability Limit. Model System Fig. 5.1 Data Appendix G and $H_1=H_2=5.0$ KJ/KVA.

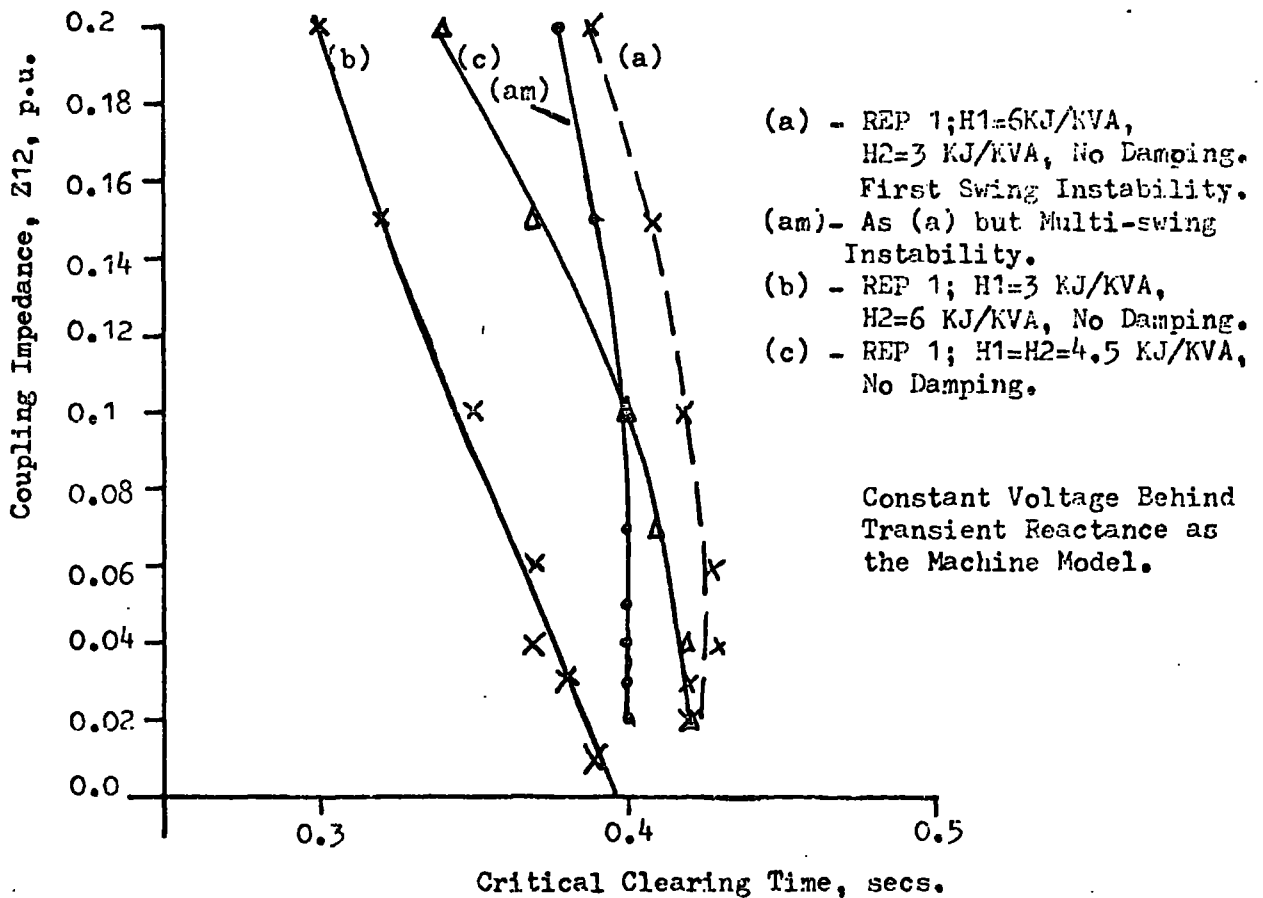


Fig. 5.5 The Effect of Inertia Change on System Stability. Model System Fig. 5.1 Data Appendix G.

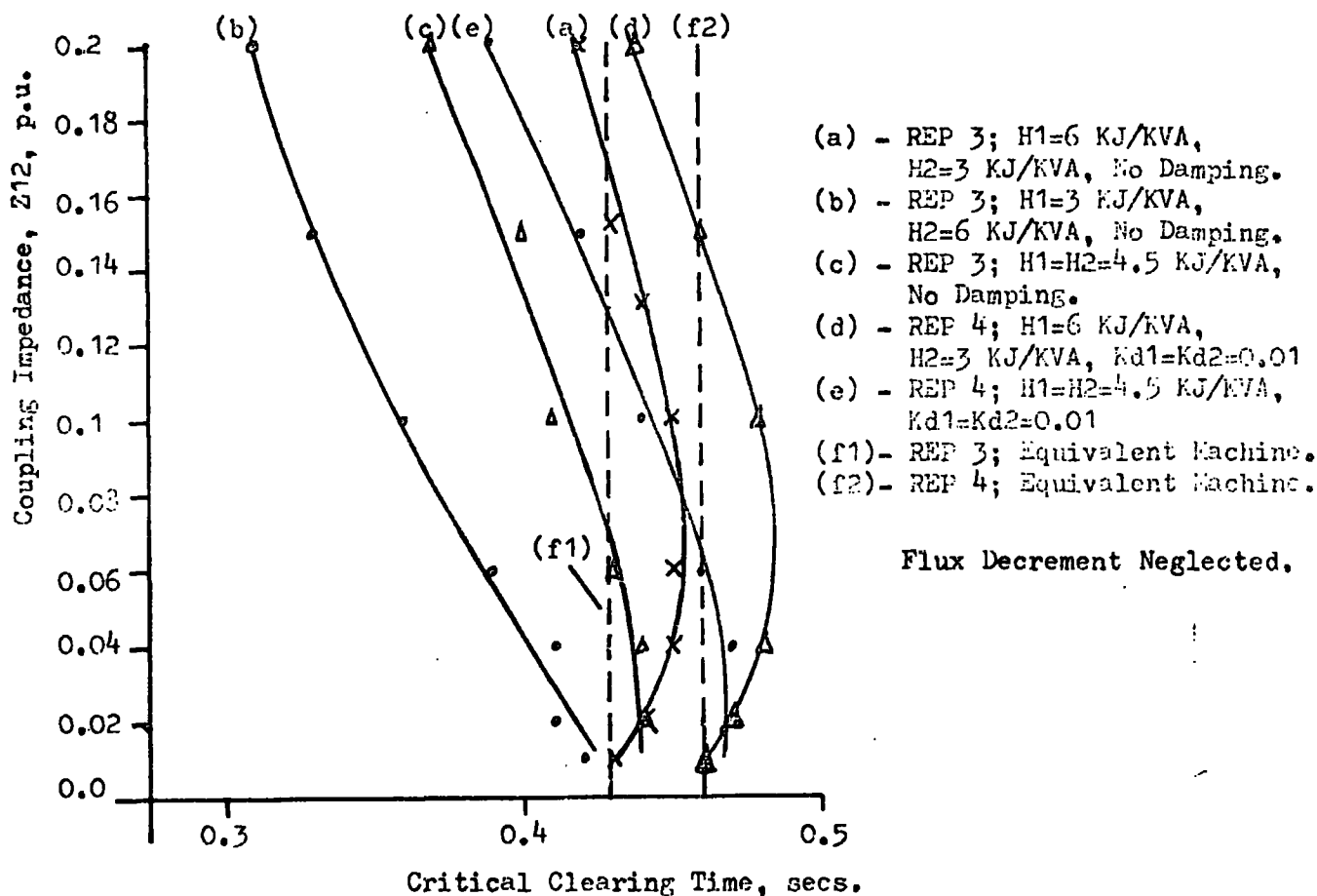


Fig. 5.6 The Effect of Inertia Change and Damping Constant On System Stability. Model System Fig. 5.1 Data Appendix G.

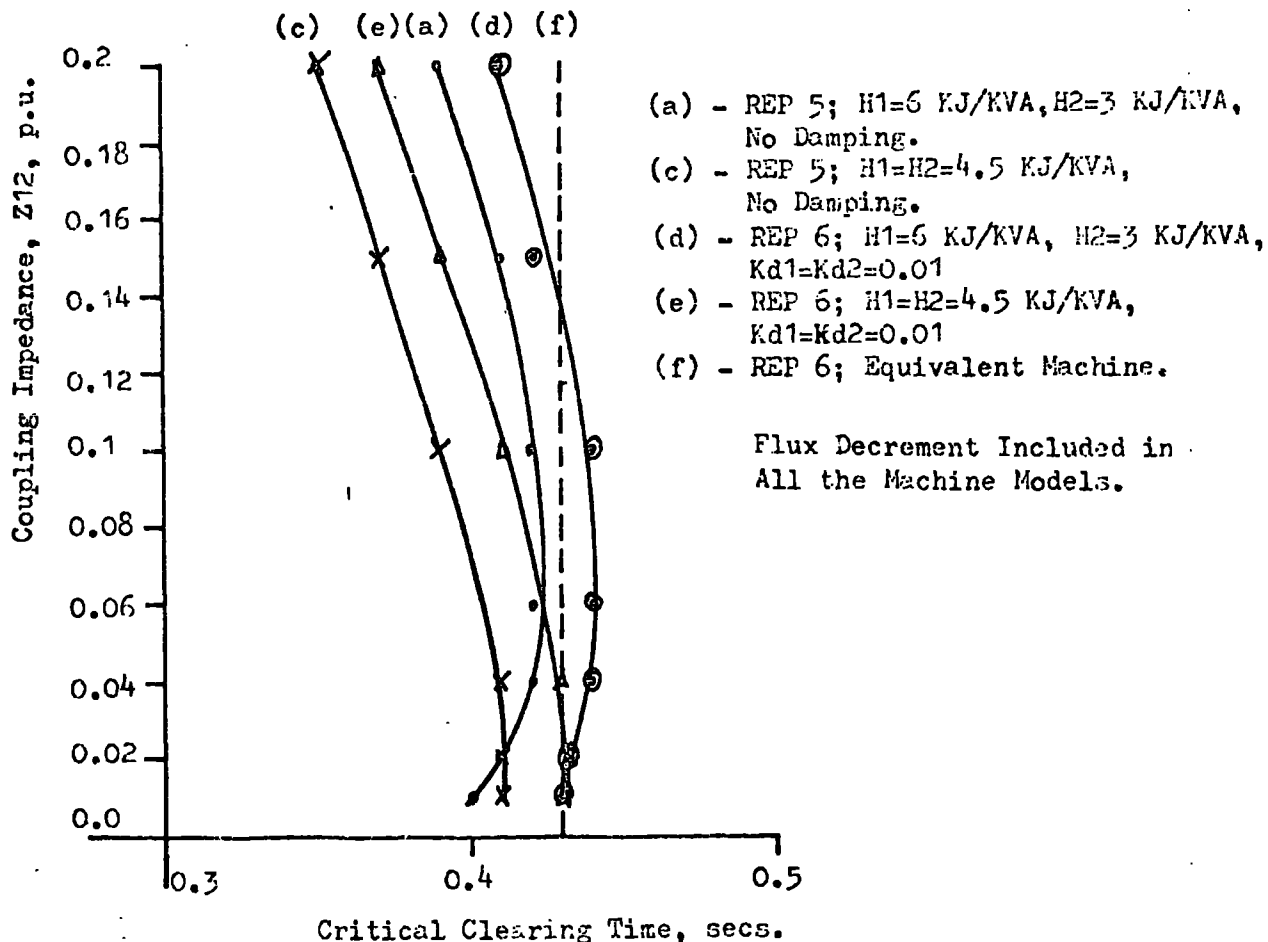


Fig. 5.7 The Effect of Inertia Change on System Stability. Model System Fig. 5.1 Data Appendix G.

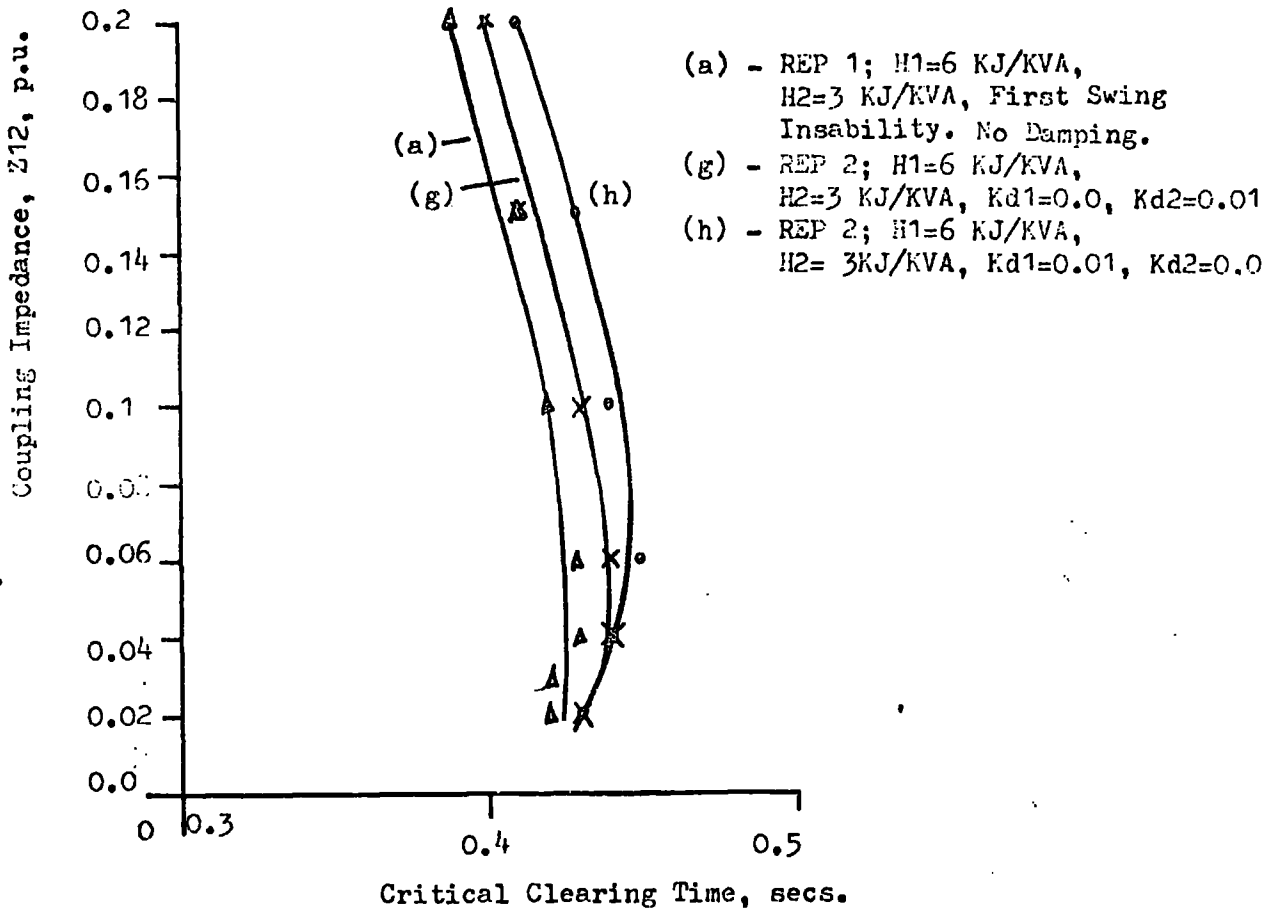


Fig. 5.8 The Effect of Damping Constant on System Stability.
 Model System Fig. 5.1 Data Appendix G.

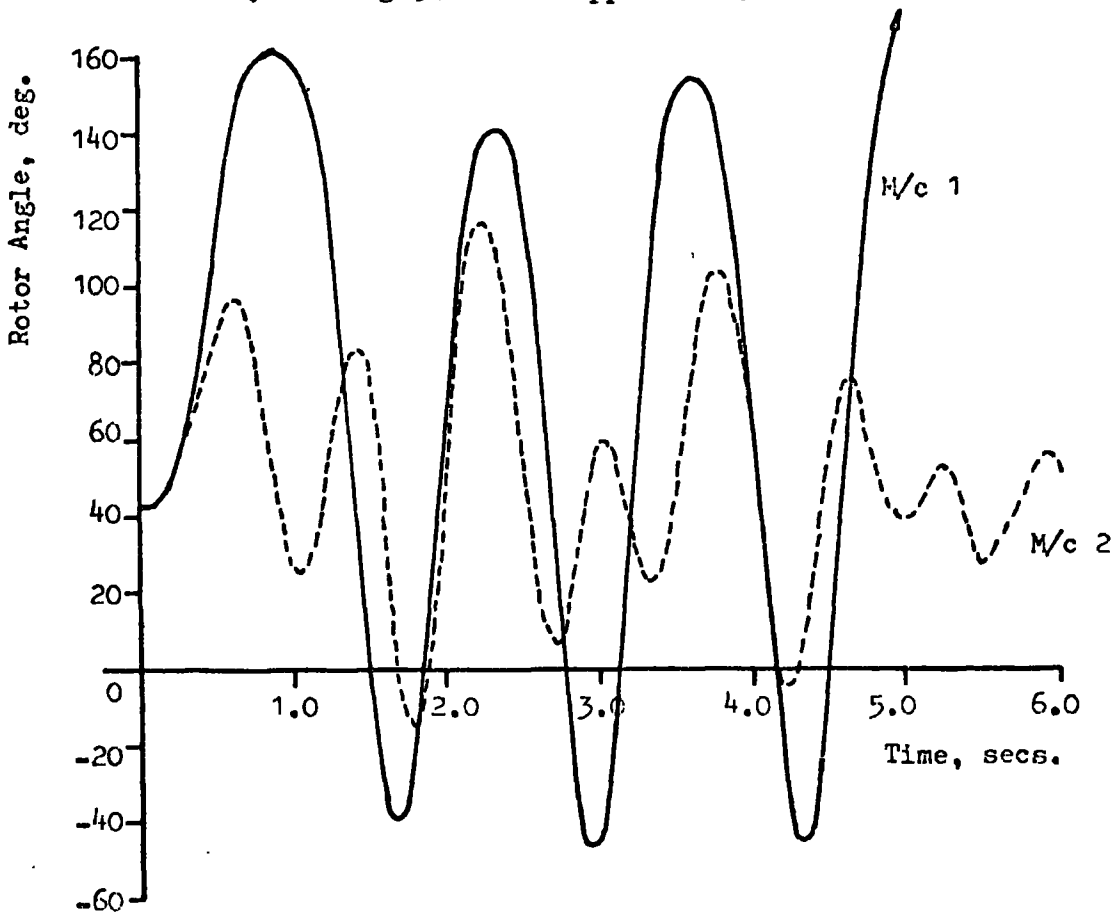
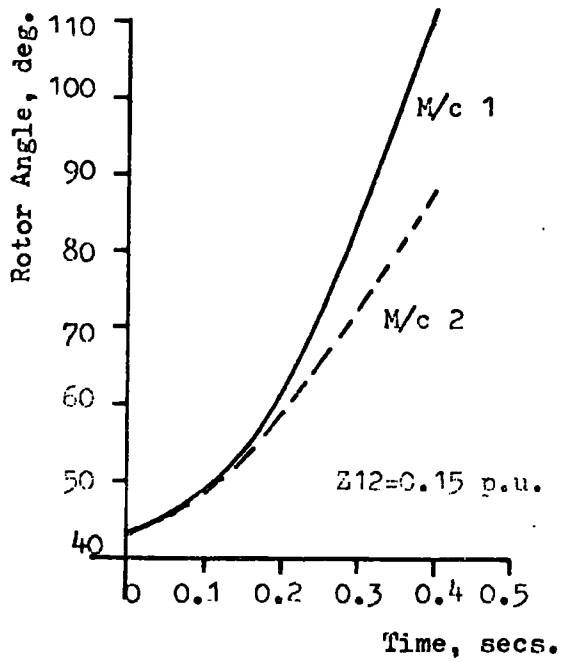
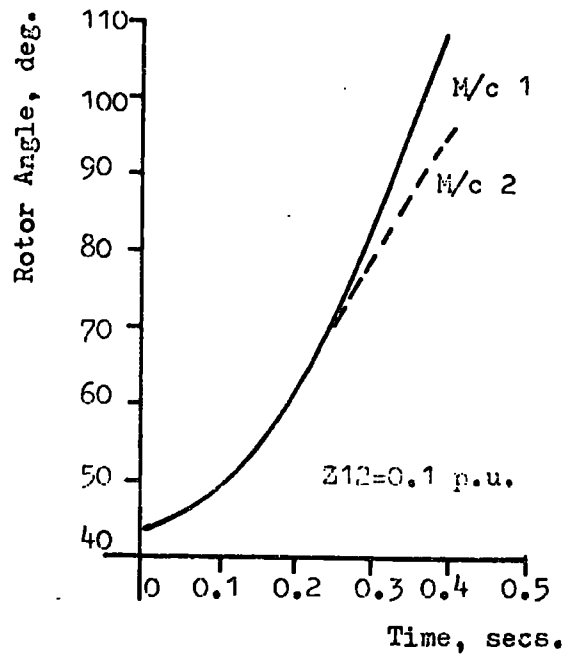


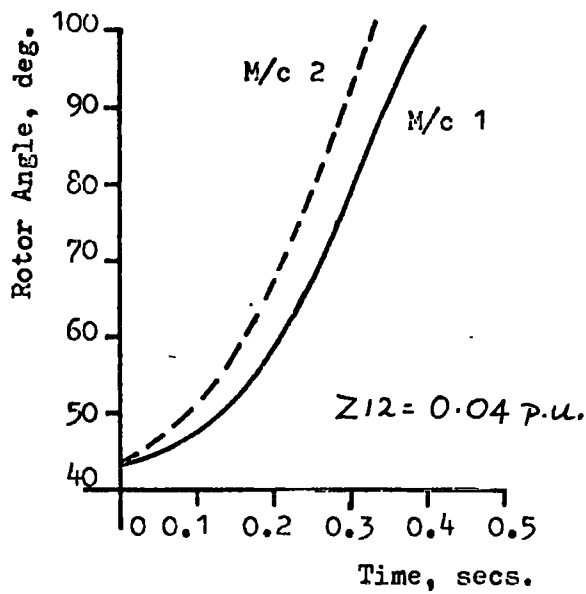
Fig. 5.9 Rotor Angle Response for REP 3 using the Model System of Fig. 5.1
 Data Appendix G and $H_1=6$ KJ/KVA, $H_2=3$ KJ/KVA, $Z_{12}=0.15$ p.u., $T_{fc}=0.43$ s.



(a)



(b)



(c)

Fig. 5.10 Rotor Angle responses for REP 3 using Model System Fig. 5.1
Data Appendix G and $H_1 = 6$ KJ/KVA, $H_2 = 3$ KJ/KVA, $T_{fc} = 0.42$ s.

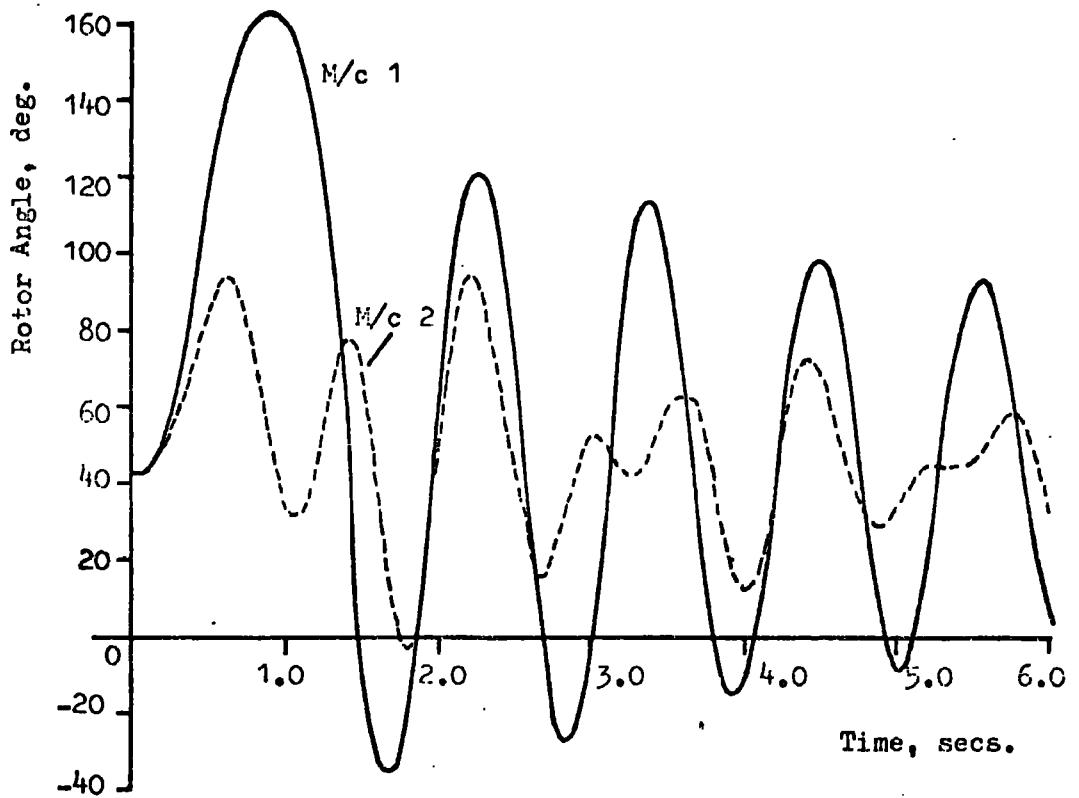


Fig. 5.11 Rotor Angle Response for REP 4 using Model System Fig. 5.1
 Data Appendix G and $H_1=6$ KJ/KVA, $H_2=3$ KJ/KVA, $Z_{12}=0.15$ p.u.,
 $K_{d1}=K_{d2}=0.01$, $T_{fc}=0.45$ s.

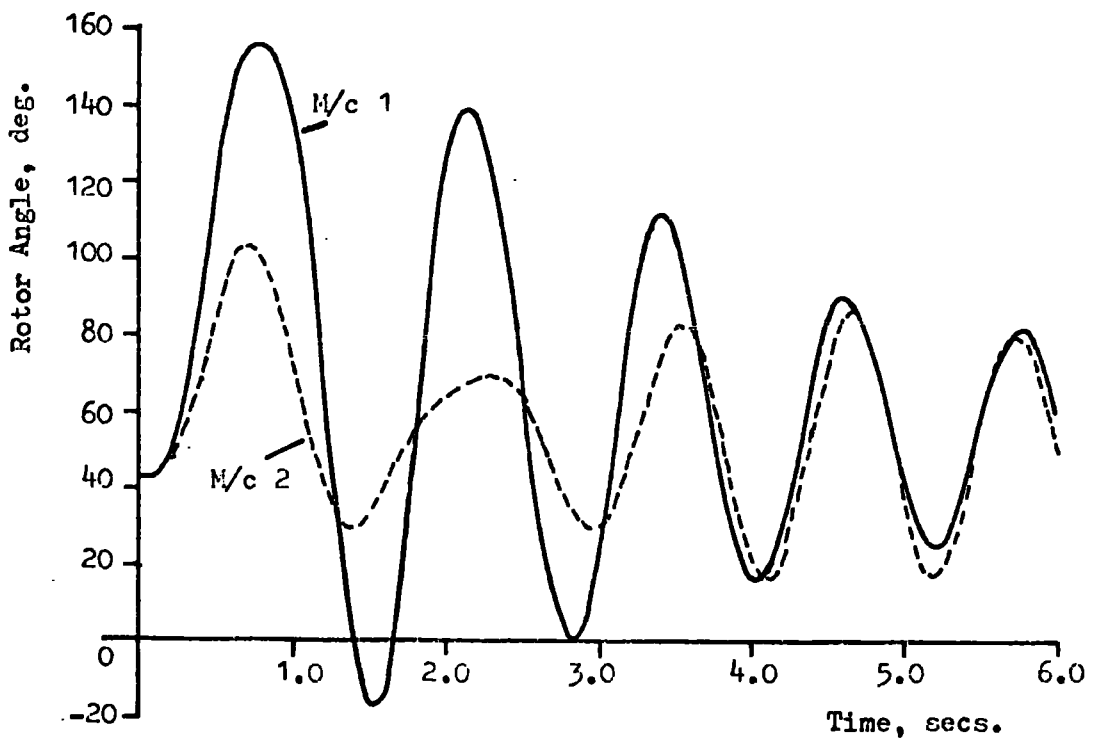


Fig. 5.12 Rotor Angle Response for REP 5 using Model System Fig. 5.1
 Data Appendix G and $H_1=H_2=5.0$ KJ/KVA, $Z_{12}=0.1$ p.u., $T_{fc}=0.4$ s.

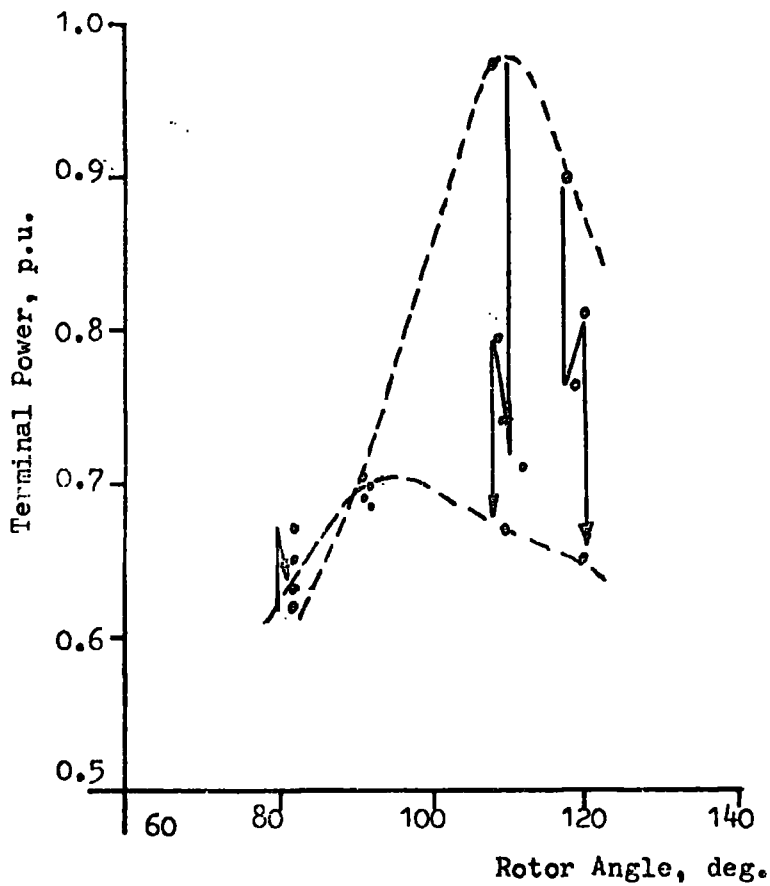


Fig. 5.14 Terminal Power Against Rotor Angle for Machine 2 Showing The Decay from the Transient to the Steady State Operating Loci.

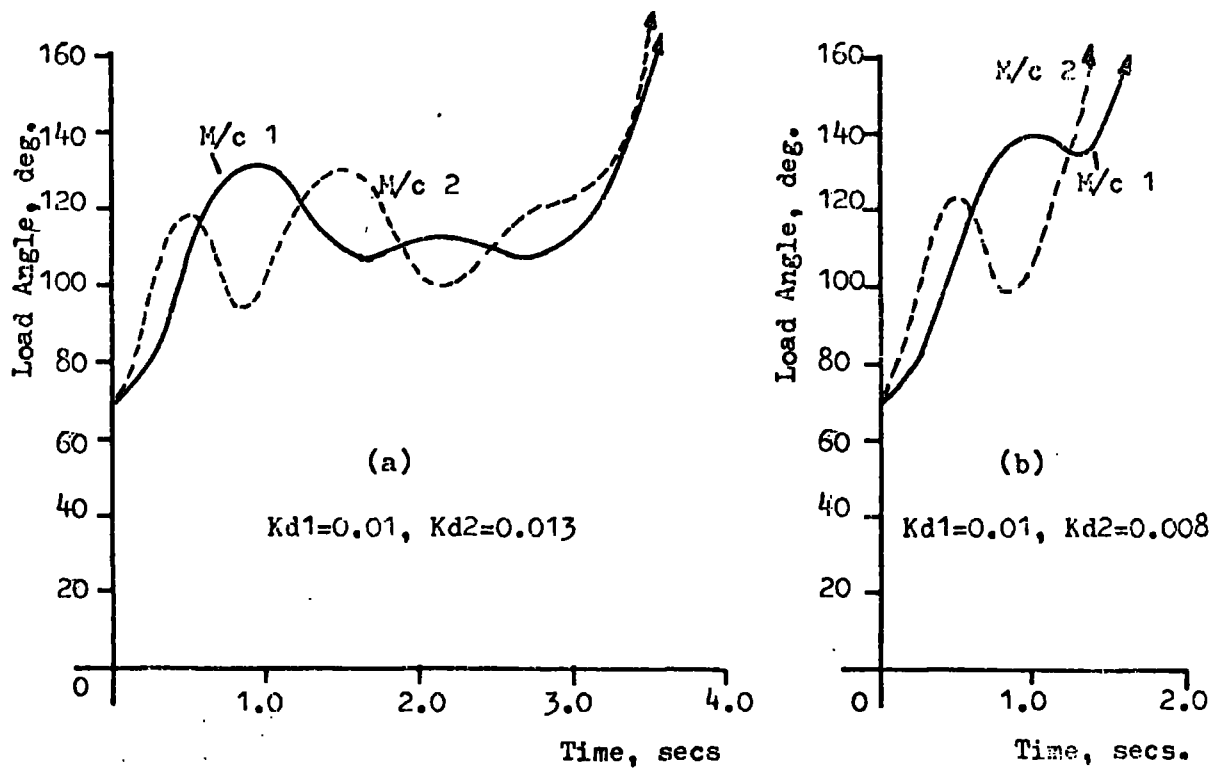


Fig. 5.15 Load Angle Responses for REP 6 using Model Fig. 2.7

Data Appendix G and $H1=6$ KJ/KVA, $H2=2$ KJ/KVA, $Tfc=0.1s$.

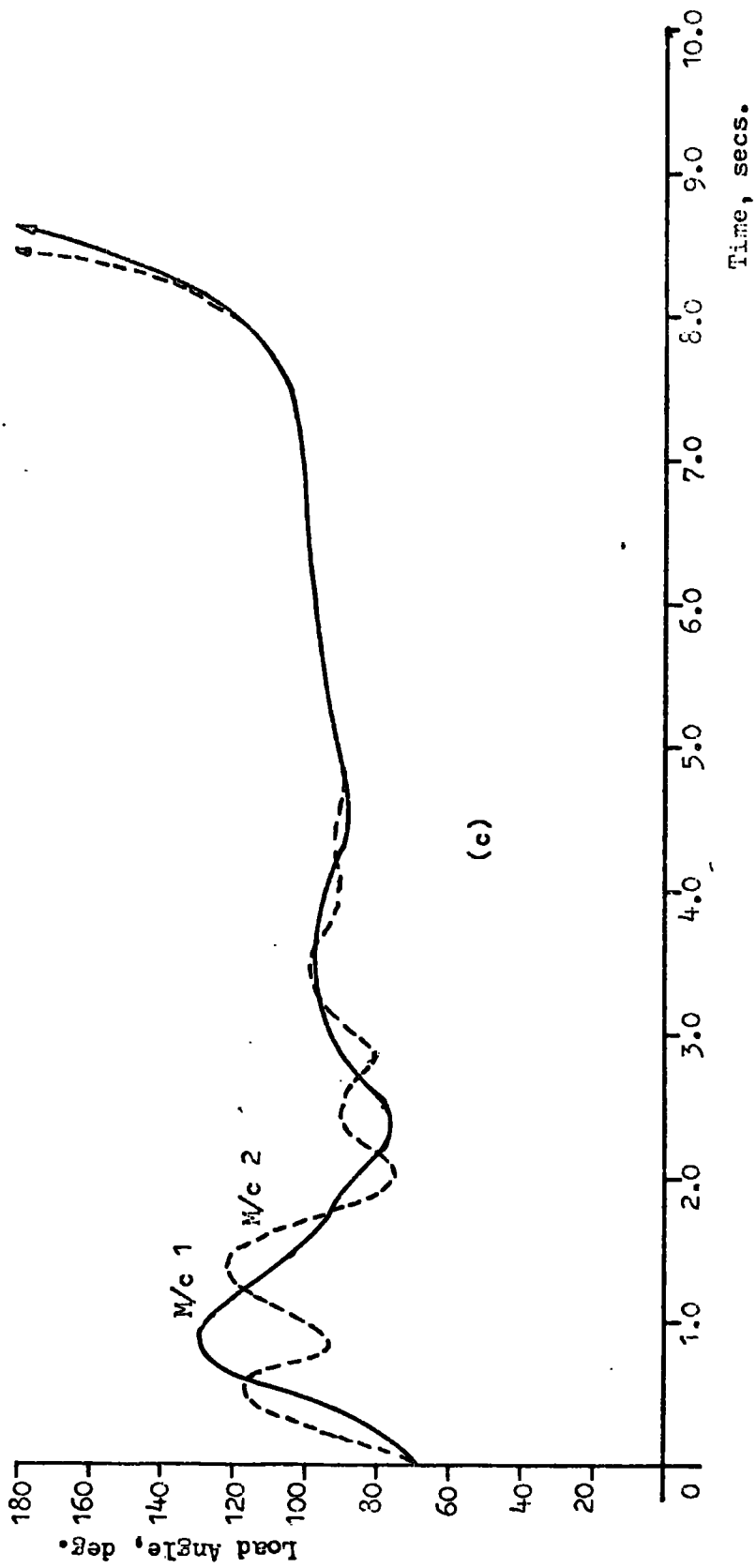


Fig. 5.15(c) Load Angle Response for REP 6 using Model Fig.2.7 Data Appendix G and $H1=6 \text{ KJ/KVA}$,

$H2=2 \text{ KJ/KVA}$, $T_{d0}'=4.58\text{s}$, $K_{d1}=0.01$, $K_{d2}=0.015$, $T_{fc}=0.1\text{s}$.

CHAPTER 6

A TRANSIENT CONTROL SCHEME BY IMPEDANCE SWITCHING

6.1 GENERAL

Chapter 5 demonstrated how machine interaction can produce adverse load angle excursions, leading ultimately to possible multiswing instability. This chapter, along with chapters 7, 8 and 9, demonstrates methods by which this interaction can be removed or at least reduced. It will be shown that reducing interaction increases the systems transient stability limit.

Because the design is carried out on a set of linear equations the controller when applied to the practical non-linear set will not yield the same results. It is therefore necessary to understand the cause, and the effect, of the differences between the linear and non-linear equations.

6.2 A COMPARISON BETWEEN THE LINEAR/NON-LINEAR EQUATIONS

6.2.1 THE EFFECT OF THE INITIAL CONDITIONS

The initial steady state operating conditions of a multimachine power system are determined by the system loading and the network parameters.

For REP 2 the operating locus is that of a sine curve.⁽¹³⁾ As the initial load angles, δ_{0i} increase the operating range over which the sine curve can be approximated by a straight line decreases. For example, a step change on the input power to machine 2 in fig. 5.1 causes a first load angle excursion of machine 2 of approximately 20° . With $\delta_{0,2} = 30.5^\circ$ the difference between the models was 0.55° while with $\delta_{0,2} = 65^\circ$ it was 1.59° .

6.2.2 THE EFFECT OF FAULT CONDITIONS

The comparison between the linear and non-linear models depends on the fault size and its duration. The linear model is only truly

representative of the non-linear system over a limited range. Increasing either the fault size or duration produces a greater discrepancy between the two models - fig. 6.1. Increasing the fault size still further produces a Lyapunov instability in the non-linear model while the linear model remains stable - fig. 6.2. The linear model gives no indication of instability in the Lyapunov sense but will indicate stability of the operating point. It also allows a Nyquist assessment of stability for different feedback arrangements.

Consider fig. 6.3 and a step change on the input power from P_{i_1} to P_{i_2} and then back to P_{i_1} . If $P_{i_2} \gg P_{i_1}$ then there will be a substantial amount of fault energy available to accelerate the rotor which results in a rapid machine response. Because of the large amount of accelerating power available the different gradients of the linear and non-linear operating curves have little effect on the time response and a good comparison is achieved - fig. 6.4. If P_{i_2} is only slightly greater than P_{i_1} then the associated fault energy is small and the response of the machine is not so rapid. The gradient differences between the two operating curves now affect the response - fig. 6.5. To produce a similar first load angle oscillation to fig. 6.4 a larger fault clearing time is required.

A disturbance associated with a large clearing time does not give such a good comparison as the disturbance of short duration required to give similar first rotor angle swings.

Extending this to the case where a disturbance is applied and not removed - fig. 6.15 - the comparison between models is very poor. This is mainly attributed to the linear model being designed to operate round the initial steady state operating points and the final operating conditions being different.

6.2.3 CONCLUSION

It is concluded from the previous discussion that:

- (i) If δ_{oi} is small, preferably less than 60° , a larger oscillation range in which the models are comparable is obtained. In most practical systems the operating angles of the machines are in excess of 60° . However for small disturbances the comparison range is still sufficient to produce a control scheme. For large disturbances drastic action is required to limit acceleration into the Lyapunov unstable region. This is available to a degree in the multivariable design technique by a change in the feedback gain (Chapter 8).
- (ii) The best comparison is achieved over small deviations. For a similar, relatively large, load angle excursion the comparison deteriorates as the disturbance size decreases and clearing time increases.

6.3 A SWITCHED SERIES IMPEDANCE CONTROL SCHEME

In Chapter 5 the effect of line impedance on the stability limit was seen to be a significant factor. Previous authors⁽⁷⁵⁾⁽⁸¹⁾⁽⁸⁴⁾⁽⁵¹⁻⁵³⁾ have demonstrated the power of switched capacitance control schemes. A system similar to that used by Gless⁽³¹⁾ - fig. 6.6 - was investigated to discover a control scheme based on impedance switching working from only the linear equation set.

A damping term was included in the machine equations as previous work by the author and Preece⁽⁶⁰⁾ showed a tendency of the non-linear controlled model to produce self-induced oscillations. This was attributed to:

- (i) The machine equations being undamped.
- (ii) The discrepancy of using a controller designed on a linear equation set on the non-linear model.

Including the damping term removed any tendency towards self-induced oscillation.

6.4 DERIVATION OF THE LINEAR EQUATIONS

Using REP 2 and assuming no change in field excitation voltage or mechanical input power the non-linear equations describing fig. 6.6 are

$$\begin{aligned} H_1 \cdot \ddot{\delta}_1 &= P_{M1} - V_1 V_2 Y_{12} \sin(\delta_1 - \delta_2) - V_1 V_3 Y_{13} \sin \delta_1 - K d_1 \dot{\delta}_1 \\ H_2 \cdot \ddot{\delta}_2 &= P_{M2} - V_2 V_1 Y_{21} \sin(\delta_2 - \delta_1) - V_2 V_3 Y_{23} \sin \delta_2 - K d_2 \dot{\delta}_2 \end{aligned} \quad (6.1)$$

The rotor angles are measured with respect to the infinite bus while impedances represent the total impedance between machines.

Linearising the equations by a first order Taylor expansion and introducing the state variables, x

$$\begin{aligned} x_1 &= \delta_1 - \delta_{10} = \Delta \delta_1 \\ x_2 &= \delta_2 - \delta_{20} = \Delta \delta_2 \\ x_{12} &= x_1 - x_2 = \delta_1 - \delta_{10} - \delta_2 + \delta_{20} \\ &= \delta_{12} - \delta_{120} = \Delta \delta_{12} \\ x_3 &= \dot{x}_1 \\ x_4 &= \dot{x}_2 \end{aligned} \quad (6.2)$$

yields

$$\begin{aligned} H_1 \cdot \dot{x}_3 &= -b_{12} x_{12} - C_{12} \Delta Y_{12} - C_{13} \Delta Y_{13} - b_{13} x_1 - K d_1 \dot{x}_1 \\ H_2 \cdot \dot{x}_4 &= -b_{21} x_{21} - C_{21} \Delta Y_{12} - C_{23} \Delta Y_{23} - b_{23} x_2 - K d_2 \dot{x}_2 \end{aligned} \quad (6.3)$$

where

$$\begin{aligned} b_{ij} &= V_i V_j Y_{ij} \cos \delta_{ij0} \\ c_{ij} &= V_i V_j Y_{ij} \sin \delta_{ij0} \end{aligned} \quad \begin{matrix} i=1,2,3; j=1,2,3 \\ i \neq j \end{matrix} \quad (6.4)$$

Note;

$$\delta_{i30} = \delta_{i0} \quad \text{as} \quad \delta_3 = 0^\circ$$

$\Delta Y_{12}, \Delta Y_{13}, \Delta Y_{23}$ represent the impedance changes and combine to give the inputs

$$\begin{aligned} u_1 &= -C_{12} \cdot \Delta Y_{12} - C_{13} \cdot \Delta Y_{13} \\ u_2 &= -C_{21} \cdot \Delta Y_{12} - C_{23} \cdot \Delta Y_{23} \end{aligned} \quad (6.5)$$

Substituting into (6.3)

$$\begin{aligned} H_1 \cdot \dot{x}_3 + (b_{12} + b_{13})x_1 - b_{12}x_2 + kd_1x_3 &= u_1 \\ H_2 \cdot \dot{x}_4 + (b_{21} + b_{23})x_2 - b_{21}x_1 + kd_2x_4 &= u_2 \end{aligned} \quad (6.6)$$

Writing in the state space form of (3.4)

$$\begin{bmatrix} \dot{x}_1 \\ \dot{x}_2 \\ \dot{x}_3 \\ \dot{x}_4 \end{bmatrix} = \begin{bmatrix} 0 & 0 & 1 & 0 \\ 0 & 0 & 0 & 1 \\ -\frac{(b_{12}+b_{13})}{H_1} & \frac{b_{12}}{H_1} & -\frac{kd_1}{H_1} & 0 \\ \frac{b_{21}}{H_2} & -\frac{(b_{21}+b_{23})}{H_2} & 0 & -\frac{kd_2}{H_2} \end{bmatrix} * \begin{bmatrix} x_1 \\ x_2 \\ x_3 \\ x_4 \end{bmatrix} + \begin{bmatrix} 0 & 0 \\ 0 & 0 \\ \frac{1}{H_1} & 0 \\ 0 & \frac{1}{H_2} \end{bmatrix} * \begin{bmatrix} u_1 \\ u_2 \end{bmatrix} \quad (6.7)$$

Define the systems outputs as

$$\begin{aligned} y_1 &= \Delta \delta_1 \\ y_2 &= \Delta \delta_2 \end{aligned} \quad (6.8)$$

then the output equation is

$$\begin{bmatrix} y_1 \\ y_2 \end{bmatrix} = \begin{bmatrix} 1 & 0 & 0 & 0 \\ 0 & 1 & 0 & 0 \end{bmatrix} * \begin{bmatrix} x_1 \\ x_2 \\ x_3 \\ x_4 \end{bmatrix} \quad (6.9)$$

The Plant transfer function matrix $G(p)$ is derived as

$$G(p) = \frac{1}{\alpha} \begin{bmatrix} H_2 p^2 + kd_2 p + (b_{21} + b_{23}), & b_{12} \\ b_{21}, & H_1 p^2 + kd_1 p + (b_{12} + b_{13}) \end{bmatrix} \quad (6.10)$$

where

$$\begin{aligned} \alpha &= (H_1 p^2 + kd_1 p + (b_{12} + b_{13})) (H_2 p^2 + kd_2 p + (b_{21} + b_{23})) \\ &\quad - b_{12} \cdot b_{21} \end{aligned} \quad (6.11)$$

This forms the basic equation for the design process.

6.5 COMPENSATOR DESIGN

The design method of section 4.6.1 was used. By observation of $G(p)$, $Q(p)$ is assumed to have the form

$$Q(p) = \begin{bmatrix} \frac{1}{A.p^2 + B.p + D} & 0 \\ 0 & \frac{1}{E.p^2 + F.p + G} \end{bmatrix} \quad (6.12)$$

which yields

$$K(p) = \begin{bmatrix} \frac{H_1.p^2 + (b_{12} + b_{13}) + Kd_1.p}{A.p^2 + B.p + D} & , & \frac{-b_{12}}{E.p^2 + F.p + G} \\ \frac{-b_{21}}{A.p^2 + B.p + D} & , & \frac{H_2.p^2 + (b_{21} + b_{23}) + Kd_2.p}{E.p^2 + F.p + G} \end{bmatrix} \quad (6.13)$$

The general diagonal properties of $G(p)$ are retained if

$$\begin{aligned} A &= H_1, & B &= Kd_1, & D &= (b_{12} + b_{13}) \\ E &= H_2, & F &= Kd_2, & G &= (b_{21} + b_{23}) \end{aligned} \quad (6.14)$$

then

$$K(p) = \begin{bmatrix} 1 \cdot 0 & \frac{-b_{12}}{H_2.p^2 + Kd_2.p + (b_{21} + b_{23})} \\ \frac{-b_{21}}{H_1.p^2 + Kd_1.p + (b_{12} + b_{13})} & 1 \cdot 0 \end{bmatrix} \quad (6.15)$$

and

$$Q(p) = \begin{bmatrix} \frac{1}{H_1.p^2 + Kd_1.p + (b_{12} + b_{13})} & 0 \\ 0 & \frac{1}{H_2.p^2 + Kd_2.p + (b_{21} + b_{23})} \end{bmatrix} \quad (6.16)$$

A block diagram of the system is illustrated in fig. 6.7.

The effect of this compensator on the linear, non-linear models was investigated using an I.B.M. Application Program - Continuous System Modelling Program, C.S.M.P.⁽⁸³⁾

6.6 STABILITY

For the uncontrolled system

$$|pI - A| = \frac{1}{H_1 H_2} \alpha$$

$$\begin{aligned} \text{where } \alpha = & (H_1 H_2 p^4 + p^3 (H_1 K_{d2} + H_2 K_{d1}) + p^2 (H_1 (b_{21} + b_{23}) \\ & + K_{d1} K_{d2} + H_2 (b_{12} + b_{13})) + p (K_{d1} (b_{21} + b_{23}) + K_{d2} (b_{12} + b_{13})) \\ & + (b_{12} + b_{13})(b_{21} + b_{23}) - b_{12} b_{21}) \end{aligned} \quad (6.17)$$

Substituting in the numerical values of fig. 6.6 gives zeros at

$$\begin{aligned} p_{1,2} &= -0.1083 \pm j 1.6372 \\ p_{3,4} &= -0.0792 \pm j 0.7814 \end{aligned} \quad (6.18)$$

With the controller added the zeros are given by the roots of the denominators of $q_{11}(p)$ and $q_{22}(p)$ which give,

for $q_{11}(p)$

$$p_{1,2} = -0.125 \pm j 1.458 \quad (6.19)$$

and for $q_{22}(p)$

$$p_{3,4} = -0.0625 \pm j 1.08$$

Both systems are thus stable.

6.7 FAULT CONDITIONS

One of the double circuit transmission lines in line 1-3 of fig. 6.6 was tripped out, for a set fault period, by opening the circuit breakers at each end of the line. The load angle response for the uncontrolled system - fig. 6.8 - shows the interaction present within the system.

In equation (6.5) the input quantities to $G(p)$ are

$$\begin{aligned} u_1 &= f_1(\Delta Y_{12}, \Delta Y_{13}) \\ u_2 &= f_2(\Delta Y_{12}, \Delta Y_{23}) \end{aligned} \quad (6.20)$$

To eliminate the dependence of both u_1 and u_2 on ΔY_{12} , Y_{12} is assumed constant. Any control is exerted on the system via Y_{13} or Y_{23} . The line outage on Z_{13} is applied as a step input to u_1 .

6.8 APPLICATION OF THE CONTROL MATRIX

Applying the control scheme to the linear model the two machines are completely decoupled while for the non-linear model interaction is substantially reduced - fig. 6.9. The oscillations of machine 2 are caused by a transfer of power from machine 1. The control scheme works by adjusting the impedance, Z_{23} , (shown dotted in fig. 6.9) to counteract this power transfer, thus keeping the accelerating power of machine 2 at a minimum.

Reducing the impedance value, Z_{23} , immediately at the onset of the disturbance allows an easy transfer of excess fault energy to the infinite bus. A reduction in the first load angle maximum of machine 1 results. This reduction in Z_{23} is equivalent to inserting a capacitance on fault occurrence as has been suggested by other authors. (51-53)(75)(81)(84)

The control scheme suggests a reduction of Z_{23} on each forward oscillation of machine 1. This is equivalent to inserting a variable capacitance into line 2-3. Similarly introducing a variable inductance on the reverse swing would increase this impedance. The practical control system is shown in fig. 6.10.

The control unit would be operated by fault relaying indicators to activate an input to the control unit proportional to the fault size. The output of the unit would then control the magnitude of the capacitive and inductive elements of fig. 6.10.

6.9 IMPLEMENTATION OF A SWITCHED CONTROL UNIT

The control scheme outlined in the previous section is practically unrealistic, but using series capacitance and inductance of fixed values and predetermined switching instants it becomes a practical proposition.

The results of such a control scheme are shown in fig. 6.11 where the size of the capacitive and inductive elements are taken as the maximum and minimum of those obtained for Z_{23} in fig. 6.9. The switching instants are computed by the control unit, the output of which is proportional to the decaying sinusoid, CY_{23} in fig. 6.9. The switching function used is of the form:-

$$\begin{aligned} \frac{Y_{23P} + Y_{23I}}{2} < u_2' < \frac{Y_{23C} + Y_{23P}}{2}, \quad Y_{23} = Y_{23P} \\ u_2' < \frac{Y_{23P} + Y_{23I}}{2}, \quad Y_{23} = Y_{23I} \\ u_2' > \frac{Y_{23P} + Y_{23C}}{2}, \quad Y_{23} = Y_{23C} \end{aligned} \quad (6.21)$$

where,

- u_2' - instantaneous output of the controller
- Y_{23P} - pre-fault value of Y_{23}
- Y_{23C} - maximum value of Y_{23} - point B on fig. 6.9.
- Y_{23I} - minimum value of Y_{23} - point C on fig. 6.9.

Good interaction removal is obtained until after the third rotor swing when there is no control acting. However the rotor angles have been brought to a position very near their final equilibrium point.

6.10 CONTROLLED CAPACITOR INSERTION

Because of arcing difficulties the inductance was removed from the control scheme and capacitance switching alone used - fig. 6.12. The switching function used is of the form

$$\begin{aligned} u_2' < \frac{Y_{23C} + Y_{23P}}{2}, \quad Y_{23} = Y_{23P} \\ u_2' > \frac{Y_{23C} + Y_{23P}}{2}, \quad Y_{23} = Y_{23C} \end{aligned} \quad (6.22)$$

By neglecting the inductance in the control scheme the effect of reducing the accelerating power of machine 2 on reverse load angle swings has been

removed. Interaction is removed to a lesser degree than in fig. 6.11, with the first reverse swing - point (c) - of machine 2 producing a 10° oscillation.

As capacitance is inserted during the fault the first load angle maximum of machine 1 is still reduced as compared with the uncontrolled case - fig. 6.8.

6.11 LARGE DISTURBANCES

By increasing the size of the line outage in the double circuit transmission line 1-3 large rotor angle oscillations are obtained - fig. 6.13. Implementing the control scheme of section (6.9) a substantial amount of interaction is removed - fig. 6.14 - until later excursions when control ceases to exist. However these later excursions have been reduced.

By not reclosing on line 1-3 the discrepancies discussed in section 6.2.2 result in a poor comparison between the models - fig. 6.15 (a) and (b). Implementing the continuous controller - section 6.8 - produces a drastic reduction in the first load angle maximum of machine 1 along with substantial interaction removal - fig. 6.15(c).

The reduction in the first load angle maximum is apparent in all the control schemes and is attributed to the capacitor insertion on fault occurrence.

6.12 CONTROLLER VERSATILITY

The continuous controller of section (6.8) is used with the loading conditions on fig. 6.6 increased to give initial load angles of $\delta_{10} = \delta_{20} = 60^\circ$ - fig. 6.16. As a comparison the results obtained by applying the continuous controller designed for the new loading conditions are reproduced - fig. 6.17.

The capacitance inserted by the 30° , 40° design in fig. 6.16 is larger than that necessary to remove interaction at the new initial loading conditions. During the first load angle swings power transfer to the infinite bus easier resulting in a decrease in first load angle excursions - point (A). As the optimum insertion is not continuously used future excursions are not so positively damped and interaction effects are more apparent than in fig. 6.17. However a substantial amount of interaction is removed as compared with the uncontrolled case - fig. 6.18.

6.13 PRACTICAL DIFFICULTIES INVOLVED WITH IMPEDANCE SWITCHING

The practicalities of implementing the control scheme are outlined and must be considered in conjunction with the computer aided design.

- (i) When the circuit breakers are operating with a capacitor across the contacts both arcing and recovery voltage are minimised, however, if switched inductors are also used problems of arcing will be introduced.
- (ii) The capacitor/inductors themselves need only have a few seconds rating and are thus less expensive than conventional continuous duty series elements.⁽⁵¹⁾
- (iii) Due to (ii) a lot of switching operations are inadvisable. The switched control scheme of section 6.9 and 6.10 provides for this limited amount of switching.
- (iv) If the capacitor is in series with a very lightly loaded transformer large distorted exciting currents may result.⁽⁷⁷⁾
- (v) As the ratio R/X for a transmission line increases there is a tendency for the machine to hunt.⁽⁷⁷⁾ Capacitor insertion decreases X and hence increases the ratio.

- (vi) Insertion of a large series capacitor at a large angle in the system swing can cause large subharmonic line and ground currents. (86)

6.14 CONCLUSIONS

The design scheme reduces interaction and increases the positive damping within the system. Insertion of larger switched capacitances would further reduce first load angle swings but could render the system more susceptible to interaction than when the "optimum" capacitance value is used. However the advantage of the increased first load angle reduction could be achieved without affecting the non-interacting properties but would require variable capacitor/inductor insertion in both lines 1-3 and 2-3. The feedback of one of the machine output variables to control the instantaneous value of the impedance would be required.

This is a theoretical ideal and not a practical possibility when considering impedance control. However if continuously operating control elements such as field excitation and/or input power control are available a control scheme similar to that outlined above is possible. This is discussed in Chapter 7, 8 and 9.

Considering switched impedance control the size of the control capacitor/inductor is dependent on both the fault size and the initial operating conditions. Consequently it is economically unrealistic to use the optimum control value for each fault occurrence. By using some form of continuous control e.g. fast valving or field excitation control these problems, along with some of the practical difficulties can be overcome.

Control units regulating field excitation and/or mechanical input power already exist to some degree on synchronous machines and operate at lower power levels relative to those used in impedance switching. Consequently lower implementation costs are envisaged.

The use of these control units in producing non-interactive control schemes are discussed in the following Chapters.

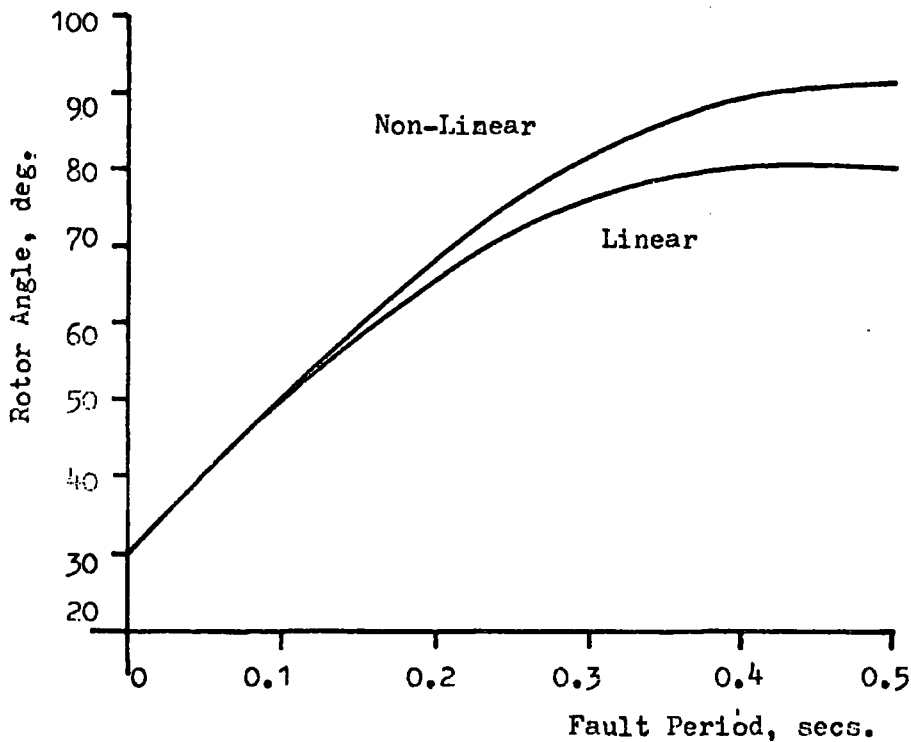


Fig.6.1 The Effect of Increasing the Fault Period on the Non-Linear, Linear Discrepancy in the First Rotor Angle Maximum of Machine 2. Model System Fig.5.1, Data Appendix G and $H_1=H_2=5.0$ KJ/KVA, $Z_{12}=0.04$ p.u. $K_{d1}=K_{d2}=0.0$, $P_{m1}=P_{m2}=0.915$ p.u., Fault $P_{m2}=P_{m2} \cdot 2.0$ p.u.

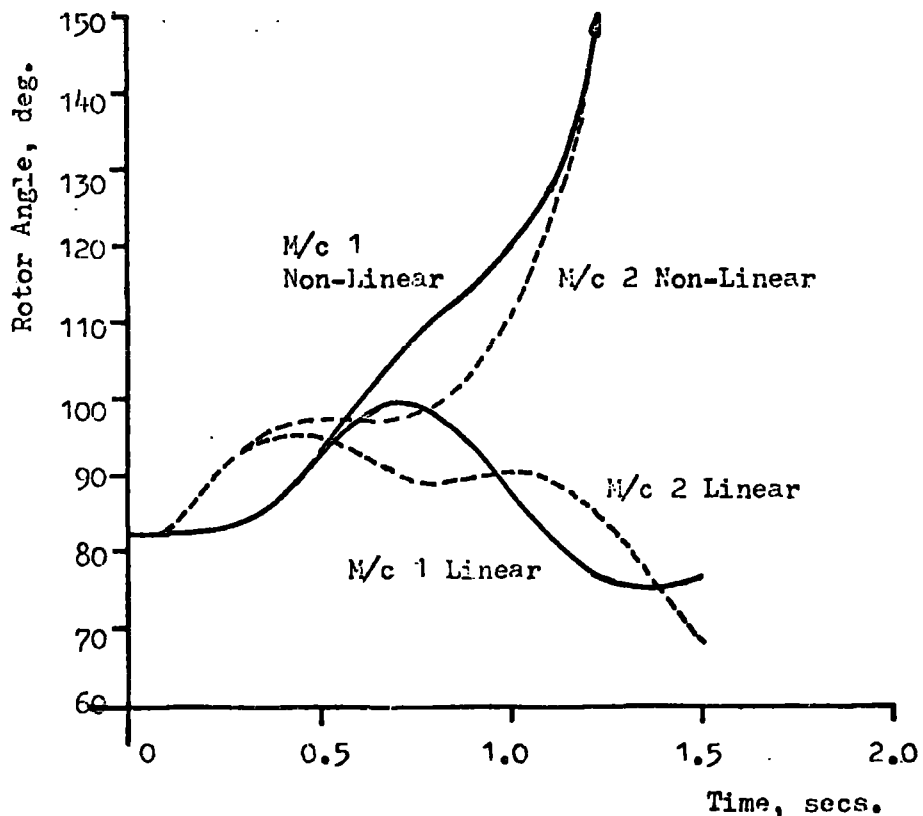


Fig.6.2 Linear/Non-Linear Rotor Angle Response Using Model System Fig.5.1 Data Appendix G and $H_1=H_2=5.0$ KJ/KVA, $Z_{12}=0.04$ p.u. $K_{d1}=K_{d2}=0.0$, $P_{m1}=P_{m2}=2.0$ p.u., Fault $P_{m2}=P_{m2} \cdot 2.0$, $T_{fc}=0.02$ s.

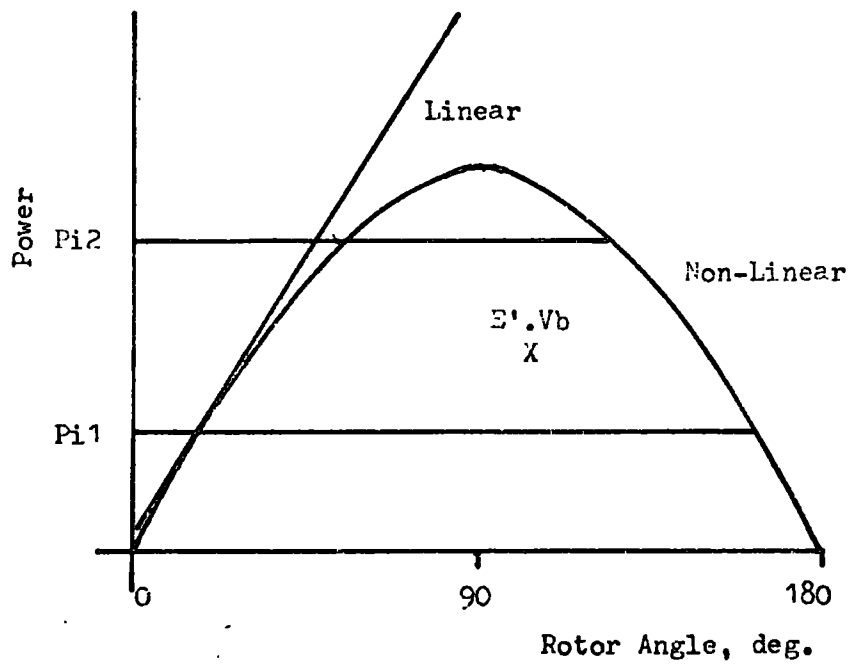


Fig. 6.3 Operating Curve For a Synchronous Machine using REP 1 and REP 2.

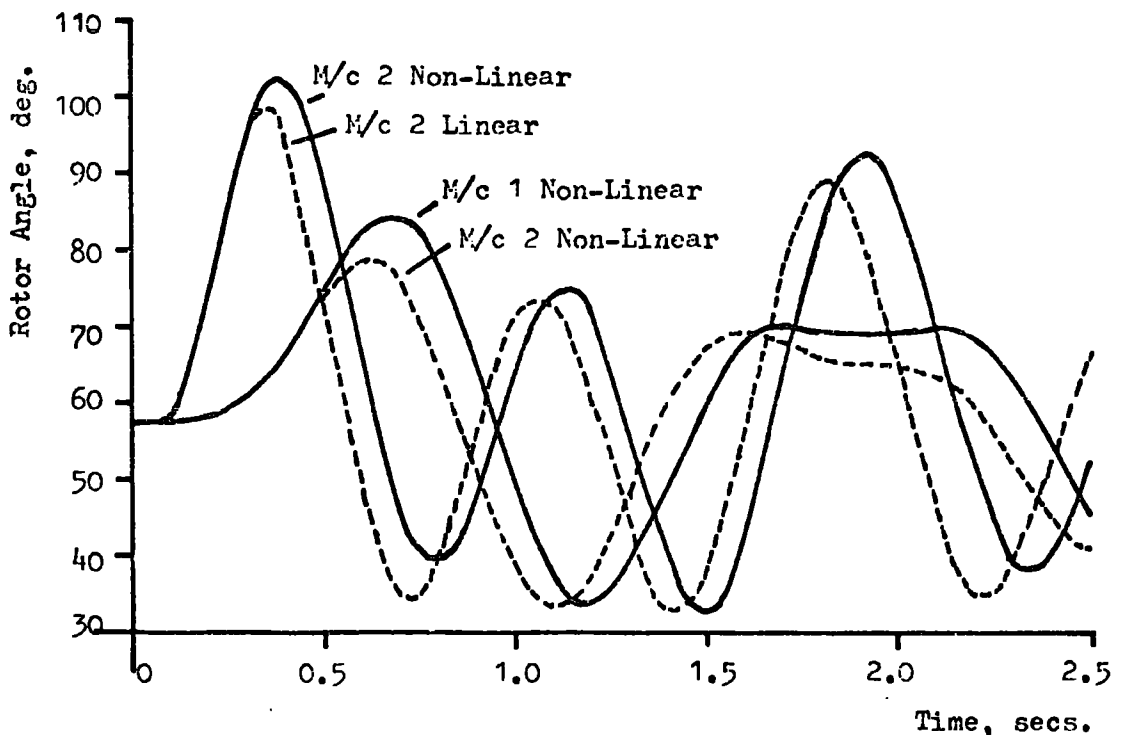


Fig. 6.4 Linear/Non-Linear Rotor Angle Response Using Model System Fig. 2.7
 Data Appendix GG and $H_1=6$ KJ/KVA, $H_2=3$ KJ/KVA, $Z_{34}=0.24$ p.u., $K_{d1}=K_{d2}=0.01$
 $P_{m1}=P_{m2}=0.7$ p.u., Fault $P_{m2}=2.1$ p.u., $T_{fc}=0.08$ secs.

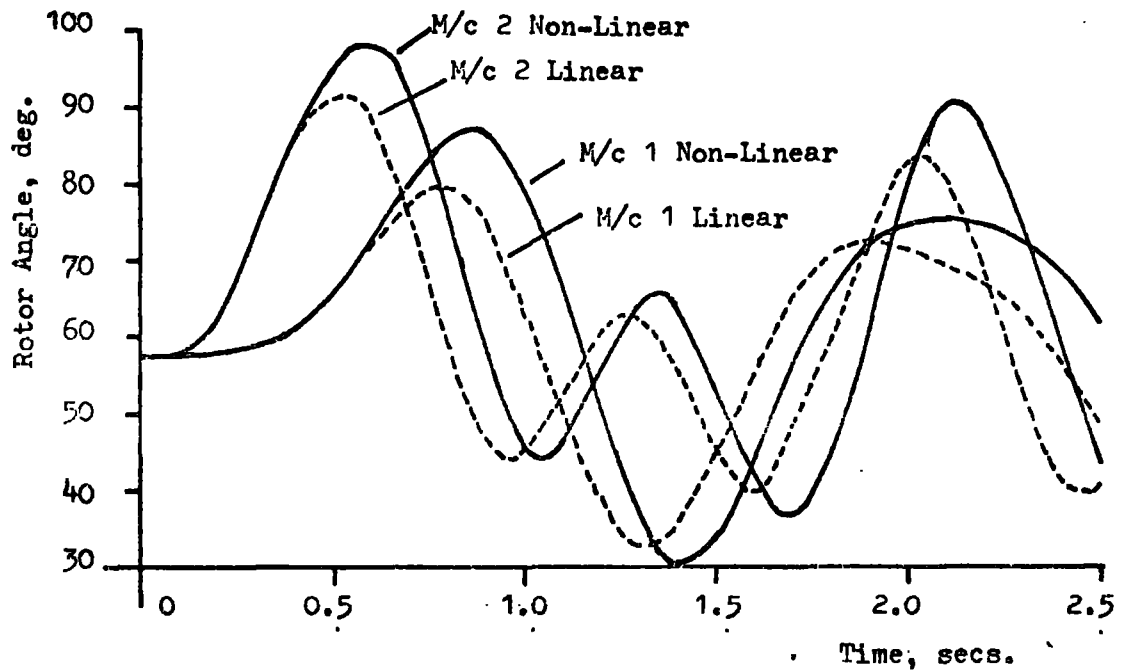


Fig. 6.5 Linear/Non-Linear Rotor Angle Response Using Model System
 Fig. 2.7, Data Appendix G and $H_1=6$ KJ/KVA, $H_2=3$ KJ/KVA,
 $Z_{34}=0.24$ p.u., $K_{d1}=K_{d2}=0.01$, $P_{m1}=P_{m2}=0.7$ p.u., During
 Fault $P_{m2}=1.05$ p.u., $T_{fc}=0.5$ secs.

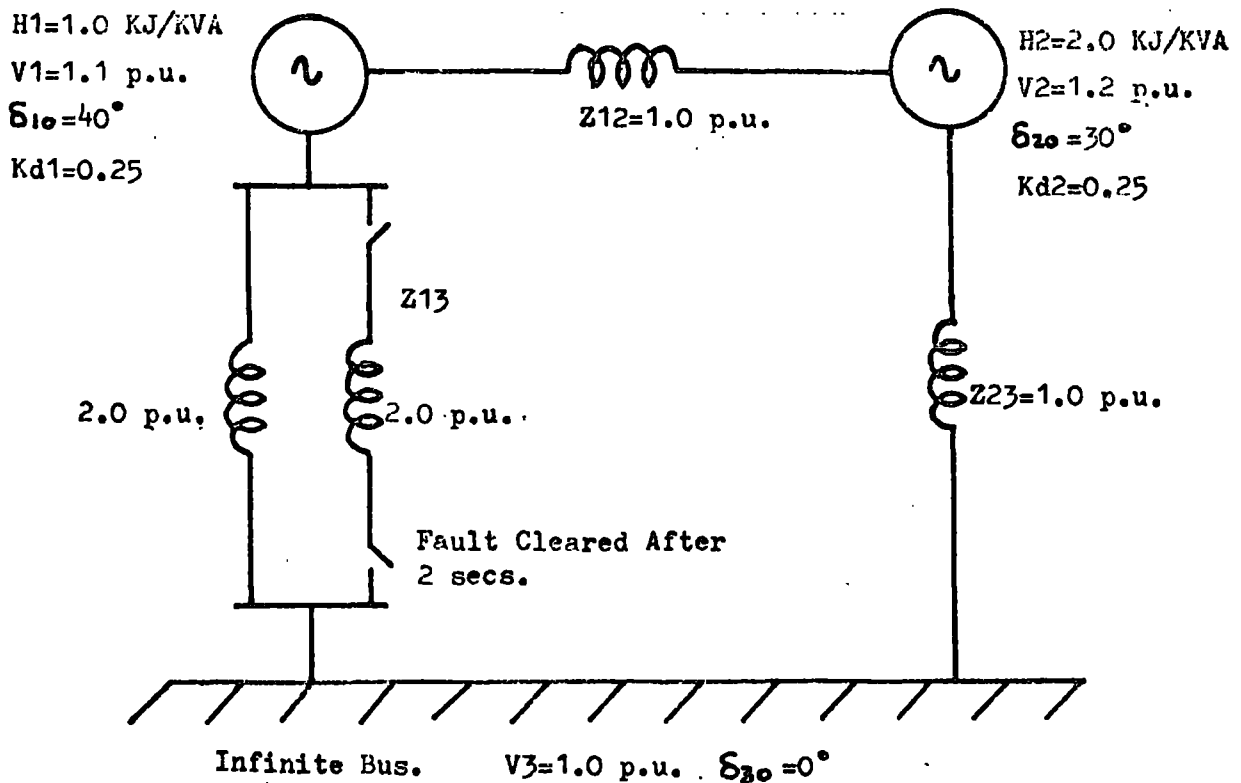


Fig. 6.6 Line Diagram of Model Power System.

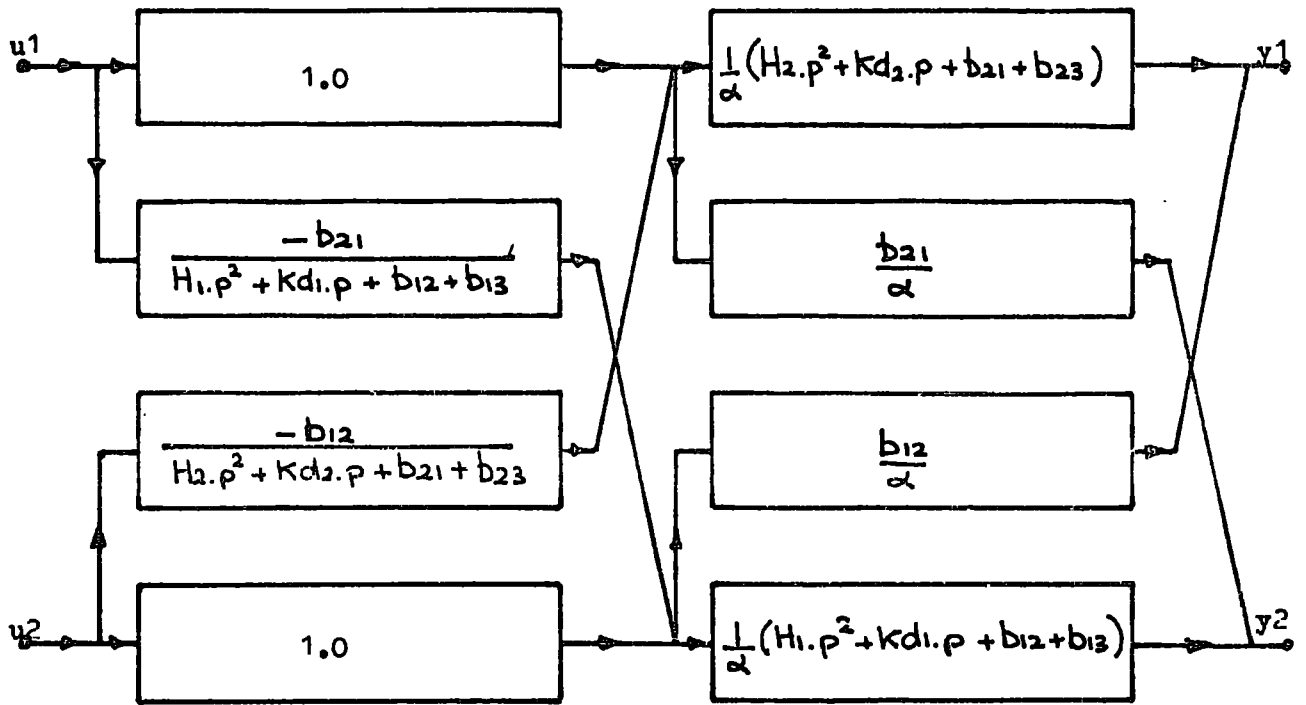


Fig. 6.7 Block Diagram Of The Control Unit And Linearised Machine System.

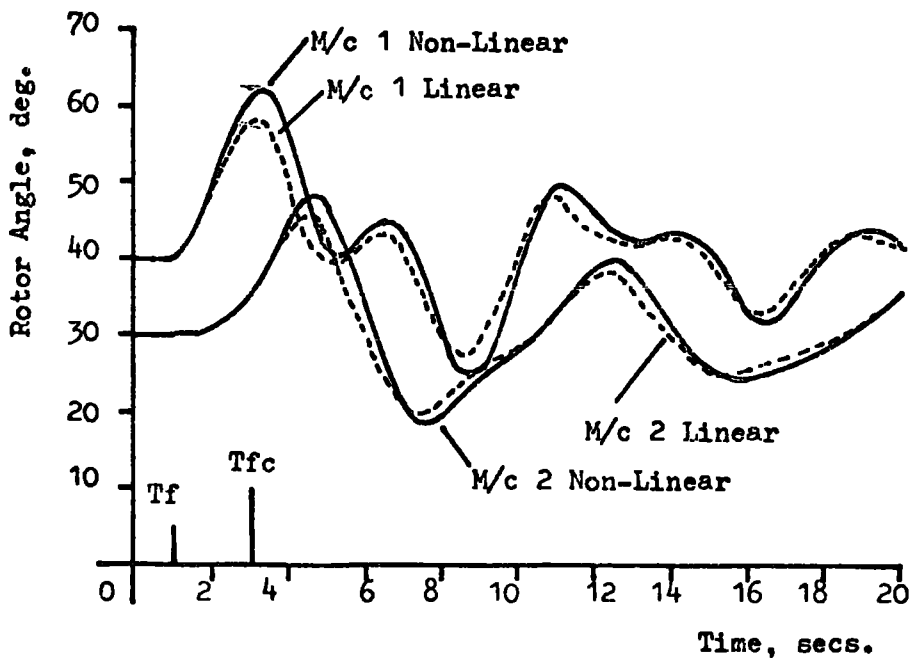
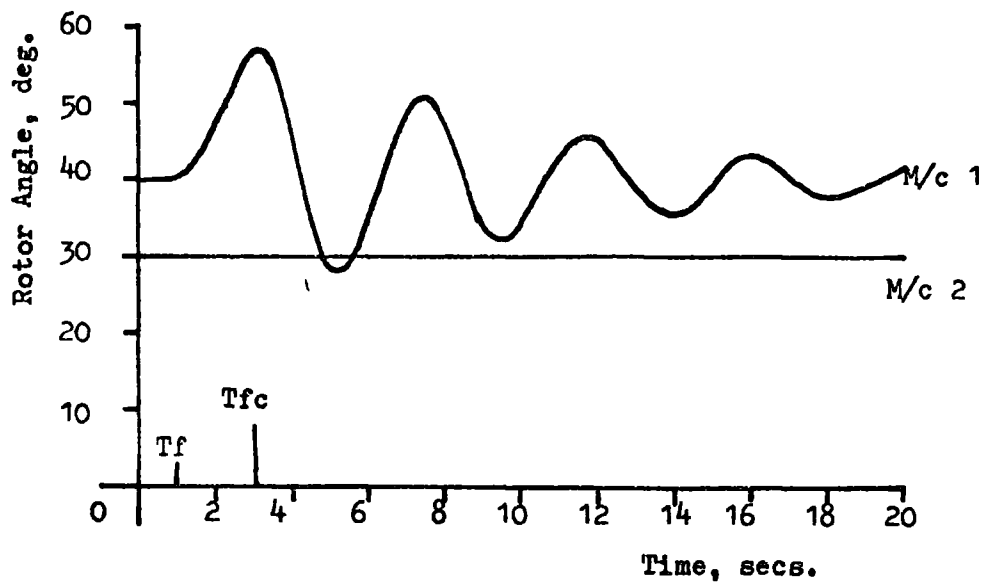
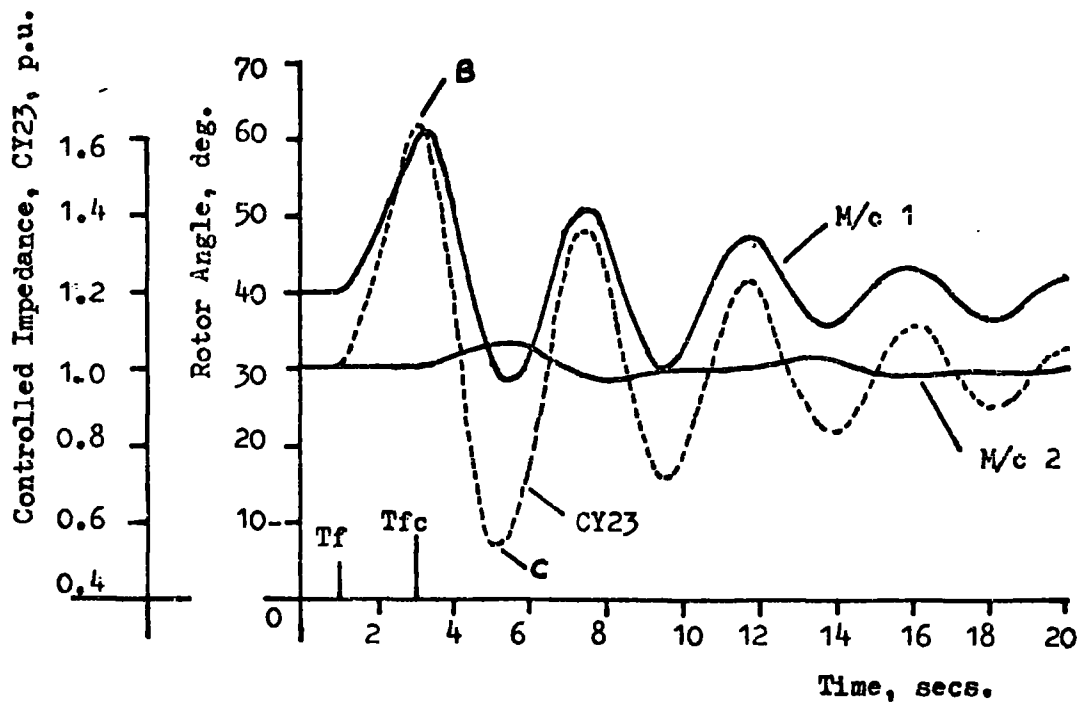


Fig. 6.8 Rotor Angle Response of the Uncontrolled Power System of Fig 6.6.



(a) Rotor Angle Response of Linearised System.



(b) Rotor Angle Response of The Non-Linear System.

Fig. 6.9 Rotor Angle Response of the Power System of Fig. 6.6 With Continuous Control of The Impedance Z23.

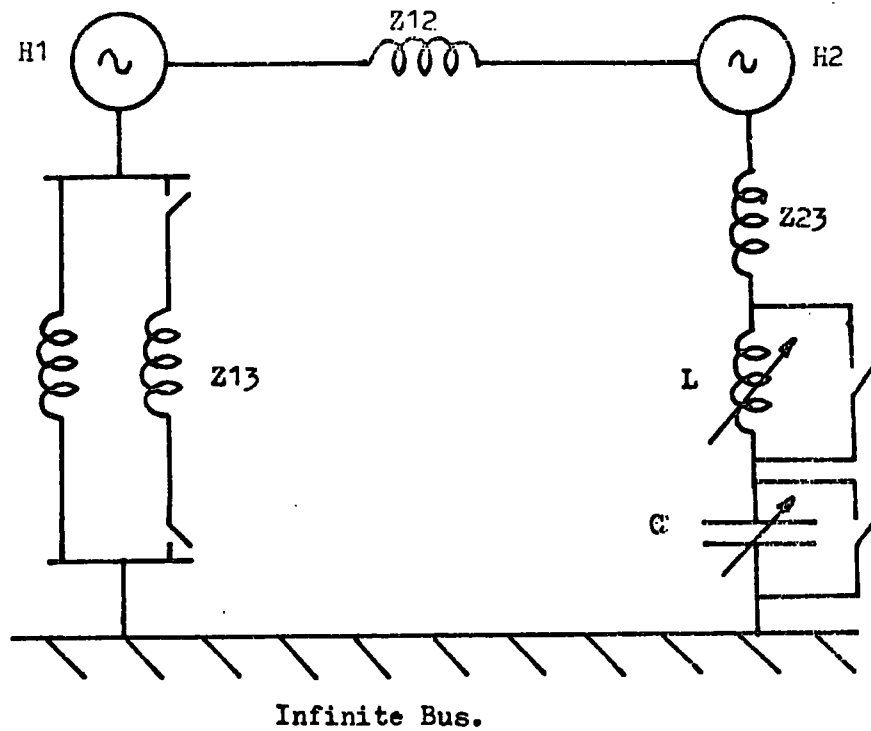


Fig. 6.10 Line Diagram of the Model Power System Including the Control Capacitance and Inductance in Line 2-3.

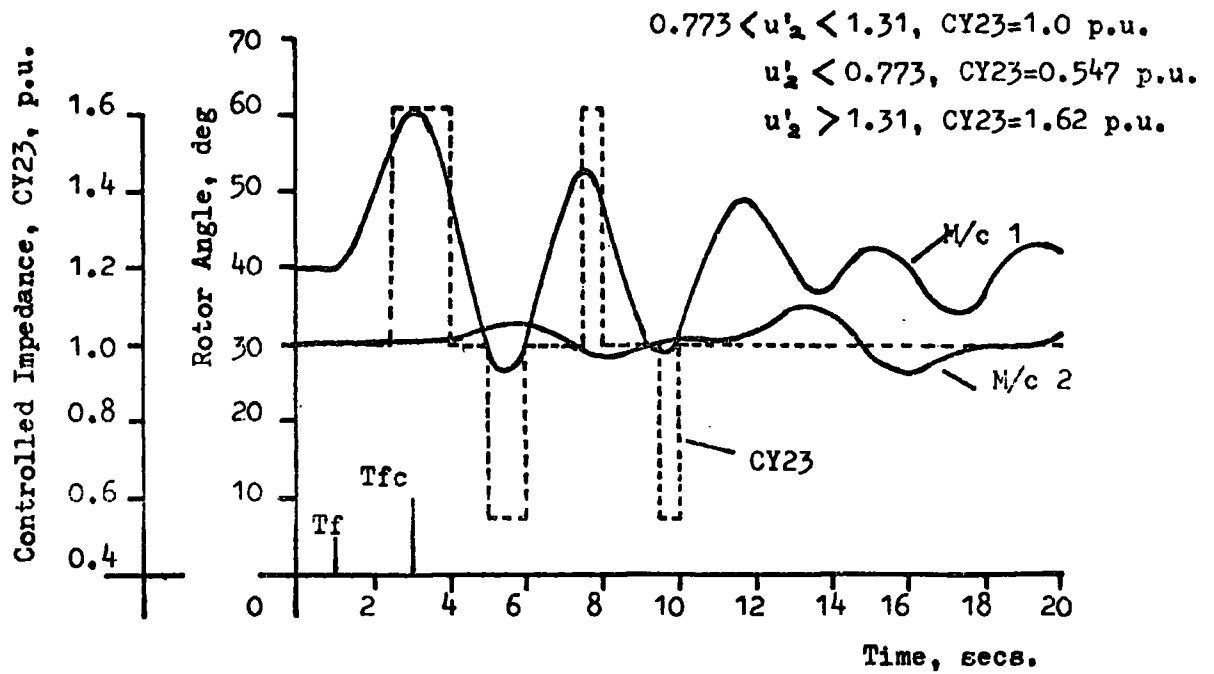


Fig. 6.11 Non-Linear Rotor Angle Response of the Power System of Fig. 6.6 Using Switched Capacitance and Inductance Control.

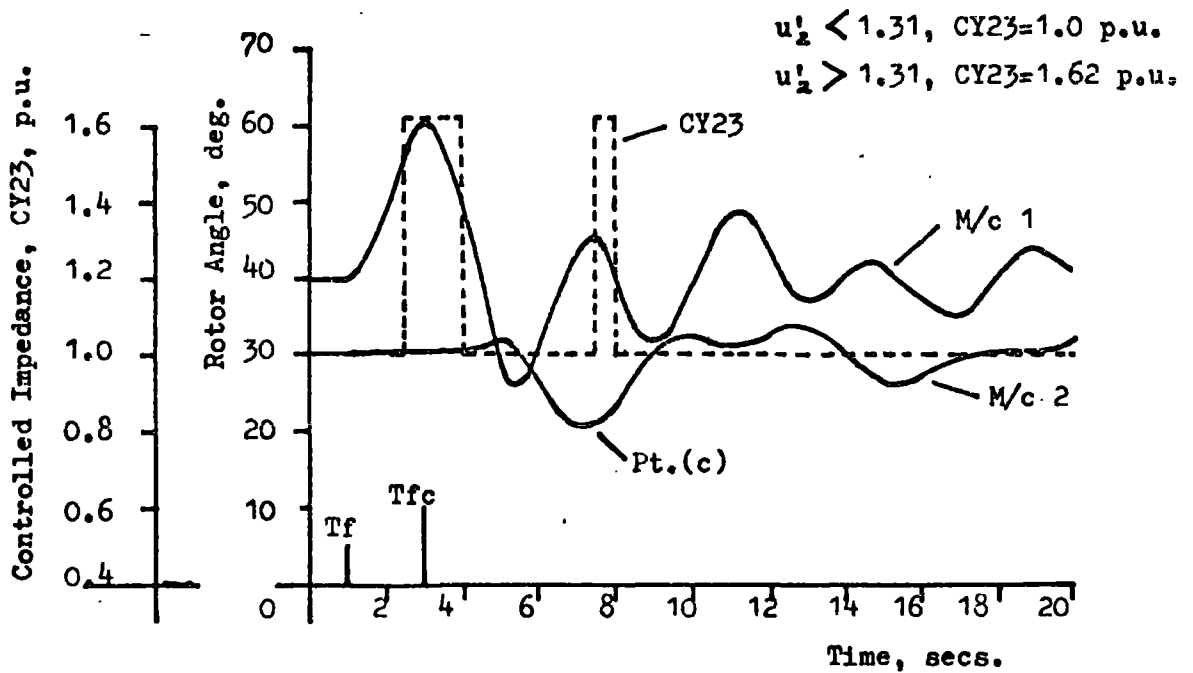


Fig. 6.12 Non-Linear Rotor Angle Response for the Power System of Fig. 6.6 Using Switched Capacitance Control.

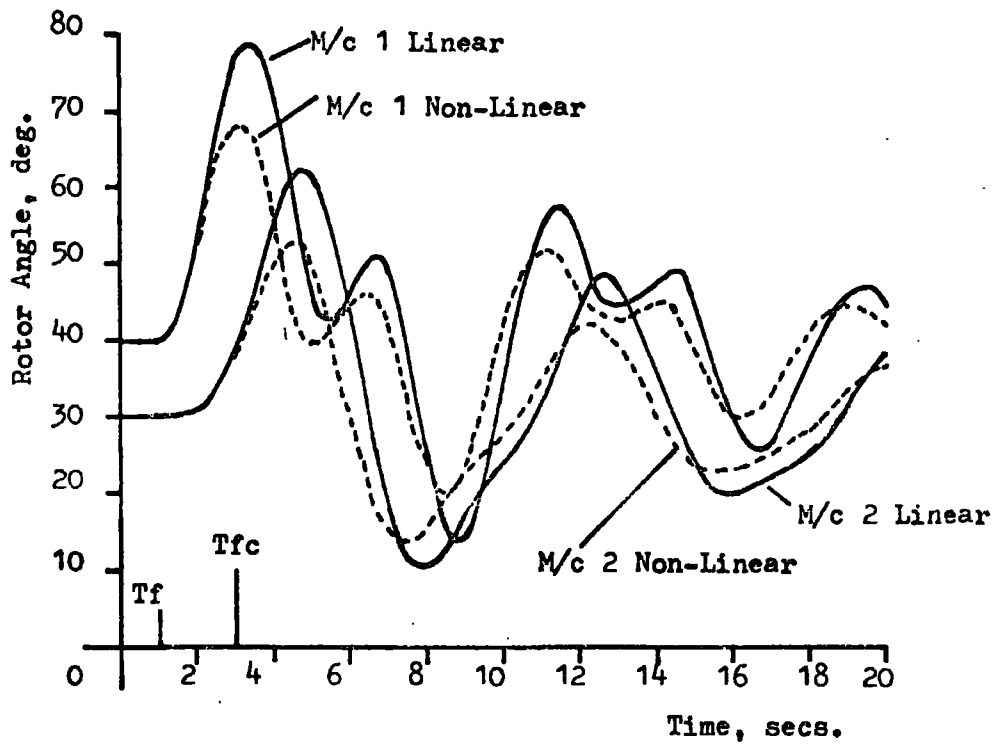


Fig. 6.13 Rotor Angle Response for the Uncontrolled Power System of Fig. 6.6 with Pre-Fault $Z_{13}=1.0$ p.u., Fault $Z_{13}=5.0$ p.u., Post-Fault $Z_{13}=1.0$ p.u.

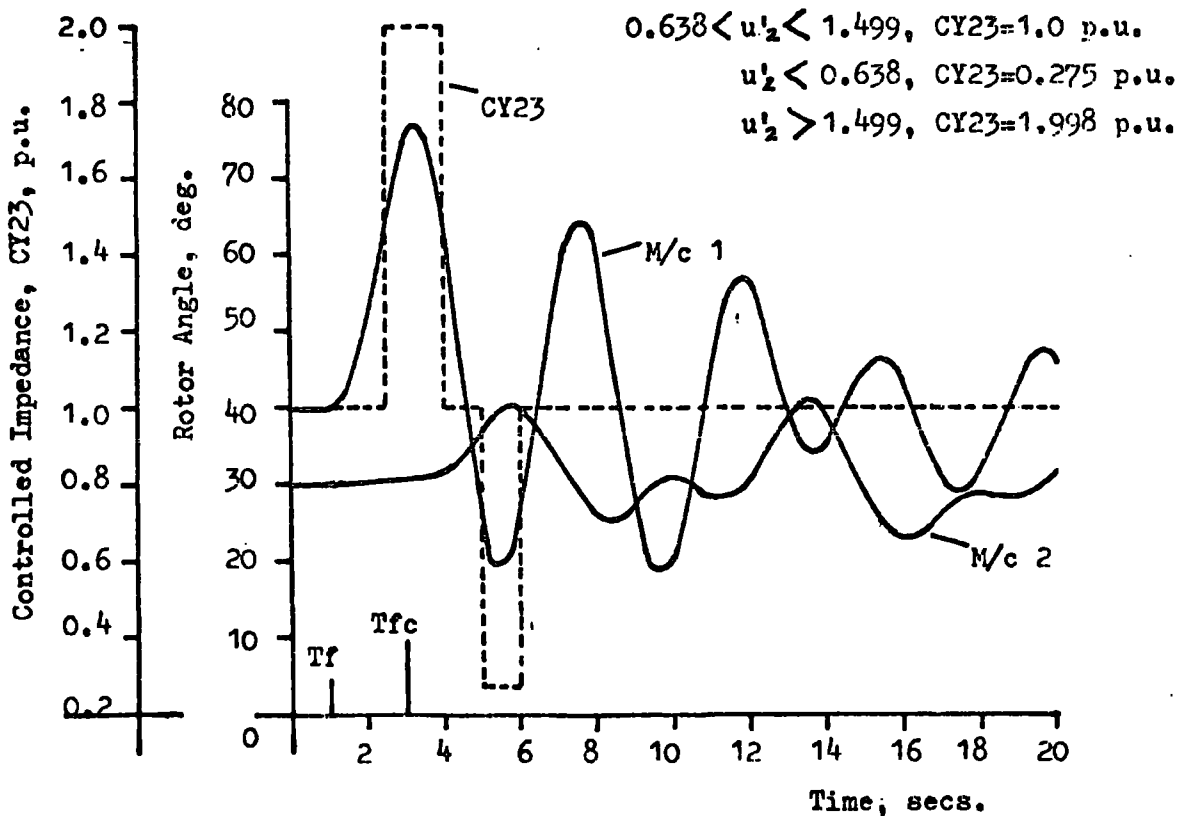


Fig. 6.14 Non-Linear Rotor Angle Response for the Power System of Fig 6.6 Using Switched Capacitance and Inductance Control. During the Fault $Z_{13}=5.0$ p.u.

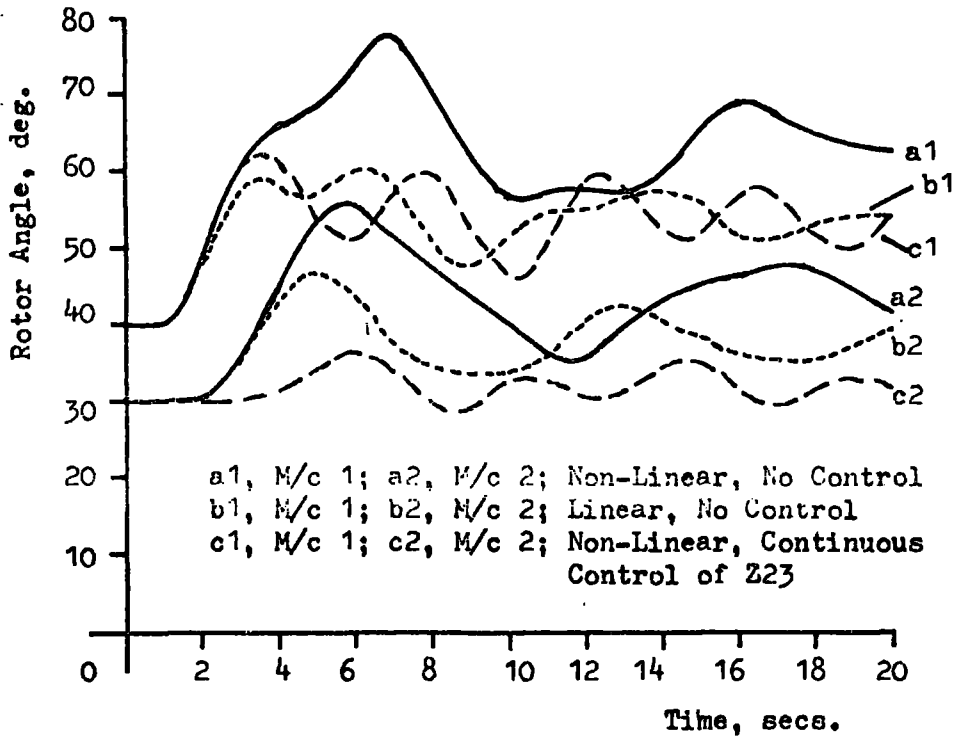


Fig. 6.15 Rotor Angle Time Response for Model System Fig. 6.6 With Unsuccessful Reclosure.

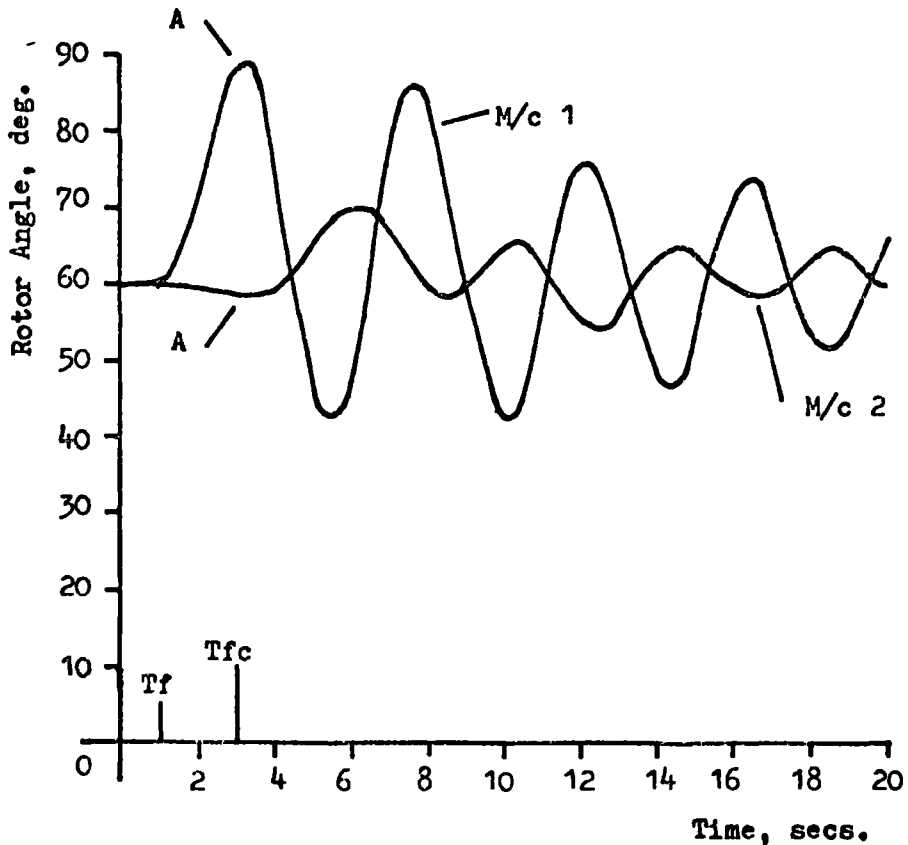


Fig. 6.16 Rotor Angle Time Response for Model System Fig. 6.6 with Higher Initial Loading Conditions. Continuous Control of Z23 and Controller Designed at $\delta_{01}=40^\circ$, $\delta_{02}=30$

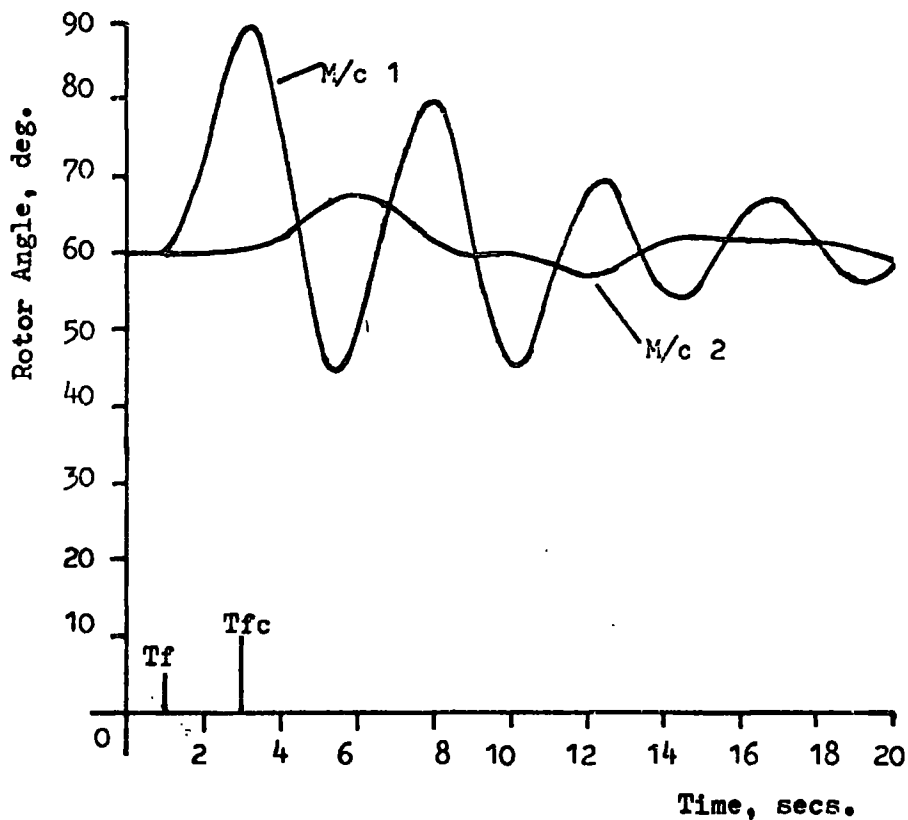


Fig. 6.17 Rotor Angle Time Response for Model System of Fig 6.6 with Higher Initial Loading Conditions. Continuous Control of Z23 and Controller Designed at $\delta_{01} = \delta_{02} = 60$.

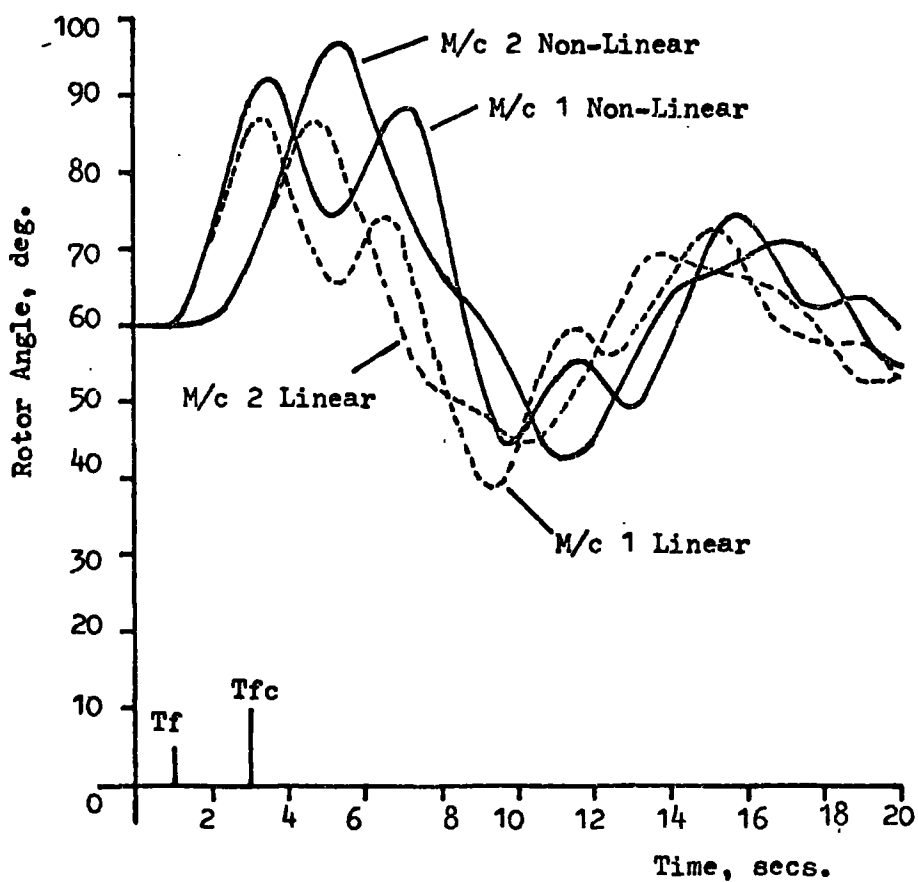


Fig. 6.18 Rotor Angle Time Response for Model System Fig. 6.6 with Higher Initial Loading Conditions. No Control.

CHAPTER 7

A NON-INTERACTIVE CONTROL SCHEME - SMALL PERTURBATION STUDY

7.1 GENERAL

The control units regulating field excitation and/or mechanical input power are used to produce a non-interacting group control scheme. These same units are then further used, in a more conventional mode, to improve the system response. Should there be a failure in the group control the regulators would be operative in their conventional mode. It is therefore necessary to investigate the effect of these units in a multimachine power system before implementation of the non-interactive control scheme. It also provides a comparison by which the performance of the group control can be judged.

Nyquist methods have been used previously by Aldred and Shackshaft⁽⁴⁸⁾ to investigate the effect of excitation control on stability, while in a similar study Concordia⁽⁵⁰⁾ used Routh-Hurwitz criteria. More recently Laughton⁽⁴⁷⁾ has applied state space methods. The approach taken here is similar to both that of Laughton and Aldred/Shackshaft in that the problem is attacked via the state space equations and the extended form of Nyquist's criteria, as discussed in Chapter 4. One of the advantages of the Nyquist method is that it gives an indication of both stability and the form of response obtained.

7.2 SYSTEM DISTURBANCES

The model system under investigation is that of fig. 2.7. The numerical values of the Plant Matrix and Driving Matrices are given in Appendix H.

For these small perturbation studies either

- (i) A step change is made to the turbine input power to investigate the effect of the input power regulator.

(ii) To investigate the exciter a step change is applied to the exciter reference voltage.

(iii) A three phase fault is applied to the machine terminals.

All disturbances were removed after a set time period.

7.3 THE REMOVAL OF INTERACTION EFFECTS BY TURBINE FAST VALVING

7.3.1 THE DESIGN SCHEME

The Plant transfer function matrix, $G(p)$, is diagonalised by compensating for interaction in the off-diagonal elements of the feedback matrix, $F(p)$. The values used in $f_{ij}(p)$ being dependent on the regulator model and not on the type of feedback used. A block diagram demonstrating this type of compensation is shown in fig. 7.1. The diagonal terms, $f_{ii}(p)$ in $F(p)$ are used to improve the individual responses by standard feedback methods once the interaction has been removed.

If the regulator is ideal i.e. $T_v = T_s = 0 \cdot 0$ in fig. 2.5 then the transfer function $\hat{G}_{VEL}(p)$ is obtained from equations (3.22) and

$$(3.28) \quad \hat{G}_{VEL}(p) = \begin{bmatrix} \frac{H_1 \cdot (p - a_{11} - \frac{a_{13}}{p})}{f \cdot \pi} & -\frac{H_1 \cdot a_{14}}{f \cdot \pi \cdot p} \\ -\frac{H_2 \cdot a_{23}}{f \cdot \pi \cdot p} & \frac{H_2 \cdot (p - a_{22} - \frac{a_{24}}{p})}{f \cdot \pi} \end{bmatrix} \quad (7.1)$$

If input one is required to control output one and similarly input two to control output two

$$K_a = \begin{bmatrix} 1 & 0 \\ 0 & 1 \end{bmatrix} \quad (7.2)$$

$$\text{then} \quad \hat{Q}_{VEL}(p) = \hat{G}_{VEL}(p) \cdot K_a \quad (7.3)$$

and by equation (3.24)

$$\hat{H}_{VEL}(p) = F_{VEL}(p) + \hat{Q}_{VEL}(p) \quad (7.4)$$

$\hat{H}_{VEL}(p)$ will be diagonal if $F_{VEL}(p)$ becomes

$$F_{VEL}(p) = \begin{bmatrix} 0 & , & \frac{H_1 \cdot a_{14}}{f \cdot \pi \cdot p} \\ \frac{H_2 \cdot a_{23}}{f \cdot \pi \cdot p} & , & 0 \end{bmatrix} \quad (7.5)$$

Interaction is removed by feeding across the machines a signal proportional to the instantaneous value of load angle.

Now

$$\hat{H}_{VEL}(p) = \begin{bmatrix} \frac{H_1 \cdot (p - a_{11} - \frac{a_{13}}{p})}{f \cdot \pi} & 0 \\ 0 & \frac{H_2 \cdot (p - a_{22} - \frac{a_{24}}{p})}{f \cdot \pi} \end{bmatrix} \quad (7.6)$$

which on inverting gives

$$H_{VEL}(p) = \begin{bmatrix} \frac{f \cdot \pi}{H_1} \left(\frac{p}{p^2 - a_{11} \cdot p - a_{13}} \right) & 0 \\ 0 & \frac{f \cdot \pi}{H_2} \left(\frac{p}{p^2 - a_{22} \cdot p - a_{24}} \right) \end{bmatrix} \quad (7.7)$$

Two individual second order systems result. Their response can be shaped by altering the feedback gain round each individual machine i.e. changing $f_{u_i}(p)$ to k_{fbi} .

If the regulator models for each machine within the system are similar then $G(p)$ becomes

$$G(p) = \frac{k_p}{(1 + p \cdot T_v)(1 + p \cdot T_s)} \cdot G(p) \quad (7.8)$$

and

$$\hat{G}(p) = \frac{(1 + p \cdot T_v)(1 + p \cdot T_s)}{k_p} \cdot \hat{G}(p) \quad (7.9)$$

Multiplying equation (7.4) through by the regulator transfer function model yields for $F(p)$

$$F(p) = \frac{(1 + p \cdot T_v)(1 + p \cdot T_s)}{k_p} \cdot F(p) \quad (7.10)$$

Thus for acceleration feedback and a second order regulator

$$F_{ACC}(p) = \hat{S} * F_{VEL}(p) \quad (3.26)$$

then

$$F_{Acc}(p) = \begin{bmatrix} Kfb_1, \frac{H_1 \cdot a_{14}}{f \cdot \pi \cdot k_p \cdot p^2} + \frac{H_1 \cdot (Ts+Tv) \cdot a_{14}}{f \cdot \pi \cdot k_p \cdot p} + \frac{Ts \cdot Tv \cdot H_1 \cdot a_{14}}{f \cdot \pi \cdot k_p} \\ \frac{H_2 \cdot a_{23}}{f \cdot \pi \cdot k_p \cdot p^2} + \frac{H_2 \cdot (Ts+Tv) \cdot a_{23}}{f \cdot \pi \cdot k_p \cdot p} + \frac{Ts \cdot Tv \cdot H_2 \cdot a_{23}}{f \cdot \pi \cdot k_p}, 0 \end{bmatrix} \quad (7.11)$$

and interaction is removed by cross feedback of rotor velocity, $p\delta$, rotor acceleration, $p^2\delta$, and rotor position. This is shown in block diagram form in fig. 7.2(a).

The same cross-feedback terms are required for velocity feedback.

7.3.2 STABILITY AND CONTROL

The stability of the open loop system is determined from the open-loop characteristic polynomial, $|pI-A|$ (Section 4.3)

$$\begin{aligned} |pI-A| &= (p^4 - (a_{11}+a_{22})p^3 + (a_{22}a_{11} - a_{24} - a_{13})p^2 \\ &\quad + (a_{24}a_{11} + a_{13}a_{22})p + (a_{24}a_{13} - a_{14}a_{23})) \\ &\quad * (p - a_{55})(p - a_{66}) \end{aligned} \quad (7.12)$$

Substituting from Appendix H yields

$$\begin{aligned} |pI-A| &= (p^4 + 0.785p^3 + 93.51p^2 + 32.6p + 1609.8) \\ &\quad * (p + 0.218)^2 \end{aligned} \quad (7.13)$$

giving zeros at

$$\begin{aligned} p_{1,2} &= -0.218 \\ p_{3,4} &= -0.154 \pm j \cdot 4.775 \\ p_{5,6} &= -0.239 \pm j \cdot 8.396 \end{aligned} \quad (7.14)$$

which are all stable.

Transfer functions of the form

$$\frac{K}{1 + p \cdot T_k} \quad (7.15)$$

are used to represent control elements. Further zeros at the point $-1/T_k$ are introduced, and as T_k is a positive time constant the zero is stable.

The presence of zeros in the positive right-half-plane of $\det G(p)$ introduces non-minimum phase transference and possible closed loop control difficulties. ⁽⁶⁷⁾ For the present problem $G_{ACC}(p)$ is given by equation (3.27) and substituting the numerical values of Appendix H the zeros of $\det G_{ACC}(p)$ are

$$\begin{aligned} p_{1,2,3,4} &= 0.0 \\ p_{5,6} &= -0.154 \pm 4.775j \\ p_{7,8} &= -0.239 \pm 8.396j \end{aligned} \quad (7.16)$$

which all lie in the left-half complex plane and the problem of non-minimum phase does not exist. For velocity feedback two of the zeros at 0.0 disappear.

Once interaction has been removed stability is assessed by either,

- (i) The I.N. diagram - the critical point being taken as 0.0 as the feedback gains, K_{F_i} , are zero.
- (ii) By observation of the poles of the diagonal elements of $Q(p)$.

7.4 THE REMOVAL OF INTERACTION EFFECTS BY EXCITATION METHODS

7.4.1 THE DESIGN SCHEME

If the excitation system is assumed ideal with no time lags the plant transfer function matrix $\hat{G}_{ACC}(p)$ is given by equation (3.30).

Substituting the numerical values of Appendix H into this equation gives

$$\hat{G}_{ACC}(p) = K_N \begin{bmatrix} -55.44p^2 - 14.51p - 1644.26, & -3.17p^2 - 1.66p + 512.27 \\ 6.34p^2 - 1.66p + 512.27, & -27.72p^2 - 14.51p - 1644.26 \end{bmatrix} \quad (7.19)$$

where

$$K_N = \frac{-(p + 0.218)}{251.77p^2}$$

The control equipment is modelled by a first order lag with a time constant of 0.03 or 0.5s depending whether a static or rotating exciter is used. This time constant will influence the magnitude of the off-diagonal terms in $F(p)$.

The design used is a hybrid of the methods in section 4.6.

Again it is required to control output 1 by input 1 and output 2 by input 2. Then

$$K_a = \begin{bmatrix} 1 & 0 \\ 0 & 1 \end{bmatrix} \quad (7.20)$$

The terms \hat{g}_{11} , \hat{g}_{21} and \hat{g}_{22} , \hat{g}_{12} bear the same constant relationship to each other

$$\text{i.e.} \quad \frac{6.23}{55.44} = \frac{1.65}{14.514} = 0.1143 \quad (7.21)$$

then let

$$\hat{K}_b = \begin{bmatrix} 1.0 & , & -0.1143 \\ -0.1143 & , & 1.0 \end{bmatrix} \quad (7.22)$$

$$\text{and} \quad \hat{Q}(p) = \hat{K}_a \cdot \hat{K}_b \cdot \hat{G}(p) \quad (7.23)$$

giving

$$\hat{Q}_{Acc}(p) = K_N \begin{bmatrix} -54.72p^2 - 14.32p - 1702.81 & , & 700.21 \\ 700.21 & , & -27.36p^2 - 14.32p - 1702.81 \end{bmatrix} \quad (7.24)$$

If now compensation is made in $F(p)$ in a similar manner as equation (7.4), with

$$F_{Acc}(p) = \begin{bmatrix} 0 & , & \frac{2.78}{p} + \frac{0.606}{p^2} \\ \frac{2.78}{p} + \frac{0.606}{p^2} & , & 0 \end{bmatrix} \quad (7.25)$$

interaction is completely removed.

When the exciter is modelled

$$\hat{Q}(p) = K_N \cdot \frac{(1 + p.T_{ex})}{K_{ex}} \cdot \hat{Q}(p) \quad (7.26)$$

which modifies

$$F(p) = \frac{(1 + p.T_{ex})}{K_{ex}} \cdot F(p) \quad (7.27)$$

Cross feedback of velocity, position and acceleration removes the interaction. These values change depending whether a static or rotating exciter is used

For the static system $f_{ij}(p)$ is

$$\left. \begin{array}{l} 2.799 * \text{velocity} \\ 0.606 * \text{position} \\ 0.083 * \text{acceleration} \end{array} \right\}$$

while for the rotating system is

$$\left. \begin{array}{l} 3.084 * \text{velocity} \\ 0.606 * \text{position} \\ 1.391 * \text{acceleration} \end{array} \right\}$$

(7.28)

A block diagram of this control method is shown in fig. 7.2(b)

For velocity feedback the same control scheme unfolds with

$$F_{VEL}(p) = S * F_{ACC}(p) \quad (7.29)$$

7.4.2 CONTROLLABILITY

The open-loop system has been shown to be stable - section 7.3.2.

The non-minimum phase transference is checked by finding, for acceleration feedback,

$$\det G(p) = p^4 \cdot G_1 \cdot G_2 \cdot A \cdot (a_{15} \cdot a_{26} - a_{16} \cdot a_{25}) \quad (7.30)$$

$$\text{where } A = p^4 - (a_{11} + a_{22})p^3 + (a_{22} \cdot a_{11} - a_{13} - a_{24}) \cdot p^2 + (a_{24} \cdot a_{11} + a_{22} \cdot a_{13}) \cdot p + (a_{13} \cdot a_{24} - a_{14} \cdot a_{23})$$

The roots of A were found in section 7.3.2 and are now modified by the factor,

$$G_1 \cdot G_2 \cdot (a_{15} \cdot a_{26} - a_{16} \cdot a_{25})$$

G_1 and G_2 are positive and the term

$$(a_{15} \cdot a_{26} - a_{16} \cdot a_{25}) = 1511, \quad \text{which is also positive.}$$

The zeros are all in the left-half-complex-plane and non-minimum phase does not exist.

7.5 A MEASURE OF DAMPING

In interactive systems it is very difficult to measure the amount of damping, positive or negative, introduced by different feedback arrangements. Oscillation frequency was shown to be very parameter dependent in section 5.4. Consequently any change in the feedback gain alters the oscillation frequency and interaction between channels. In general the majority of feedback arrangements tend to reduce the first load angle excursion. This also disguises the damping effect.

For small perturbations a measure of the damping was obtained by averaging successive load angle maximums and then normalising by dividing by the first load angle maximum. For any Nyquist unstable system the normalised damping measure will be greater than one. If stable it will be less than one and, in general, as the amount of positive damping increases the damping measure will decrease.

Because of interaction effects the graphs are used to demonstrate the general trend of damping introduced by different feedback gains for ONE specific feedback arrangement. They should NOT be used as an exact, quantitative, measure of the amount of damping introduced by the different feedback arrangements.

7.6 FAST VALVING - THE EFFECT OF REGULATOR MODELS

7.6.1 GENERAL

Because of time delays within the regulator it is impossible to have direct control over the mechanical power input to the machine. These time delays are associated with the transducers, valve operating gear and the steam system. The effect of these lags is investigated in terms of the Inverse Nyquist diagrams.

Position feedback is not considered as it has previously been shown to be a poor choice of feedback signal. ⁽³⁴⁾

7.6.2 DIRECT CONTROL OF TURBINE POWER INPUT

Direct manipulation of P_M would produce strong control. This is possible if the time constants of the valve gear and steam system are assumed to be ideally zero

$$\text{i.e. } T_V = 0.0$$

$$T_S = 0.0$$

$$\text{Limits} = \pm \infty \quad \text{in fig. 2.5.}$$

Equation (1.1) suggests that feeding back a signal proportional to the instantaneous difference between P_M and P_E should produce strong control. However because of the ideal regulator model a numerical instability results. This numerical instability is removed by feeding back a signal proportional to shaft velocity, $\dot{\delta}$. For this feedback arrangement the I.N. plots, complete with d-circles are shown in fig. 7.3. The d-circles enclose the origin, which was shown stable in section 7.3.2, while rotor angle time responses showed a stable system for values of feedback gain enclosed by the union of d-circles, as exemplified by curves (a) in fig. 7.4. Stability can now be guaranteed for all feedback gains.

Substituting the numerical values of Appendix H into equation (7.5) yields a feedback matrix

$$F_{VEL}(p) = \begin{bmatrix} kfb_1, & \frac{0.489}{p} \\ \frac{0.489}{p}, & kfb_2 \end{bmatrix} \quad (7.31)$$

which is equivalent to the connection of link (c) in fig. 7.2(a).

Implementing this feedback arrangement removes interaction from within the system as demonstrated by fig. 7.4, curve (b). The diagonal terms of $\hat{H}_{VEL}(p)$ are identical to those in $\hat{G}_{VEL}(p)$ and the I.N. plots are those of fig. 7.3 without the d-circles.

With this regulator model the diagonal terms in the plant transfer function matrices are second order and changing the magnitude of the diagonal terms, K_{fb_i} , in $F_{VEL}(p)$ is equivalent to varying the damping constant, k_d , in the machine equations of Appendix A. As the damping constant, k_d , is included in $G_{VEL}(p)$ the I.N. locus of fig. 7.3 is to the right of the imaginary axis. This shift being 0.01, corresponding to the value of the damping factor used. In the work by Aldred and Shackshaft⁽⁴⁸⁾ k_d was not included in $G(p)$ and a direct study of its effect on system stability obtained.

Increasing the feedback gain, K_{fb_i} , increases the distance between the critical point and the I.N. locus. The system becomes more positively damped with a corresponding decrease in the first load angle maximum.

7.6.3 REGULATOR MODELLED BY A FIRST ORDER LAG

A time constant of 0.75s is introduced to represent the steam system while the electro-hydraulic valve is assumed ideal

$$\text{i.e. } T_v = 0.0$$

$$T_s = 0.75s$$

$$\text{Limits} = \pm \infty$$

$$K_p = 1.0$$

fig. 2.5

The feedback matrix to remove interaction now becomes

$$F_{VEL}(p) = \begin{bmatrix} K_{fb_1} & \frac{0.489}{p} + 0.367 \\ \frac{0.489}{p} + 0.367 & K_{fb_2} \end{bmatrix} \quad (7.32)$$

i.e. feedback across machines of

$$\begin{array}{ll} 0.489 & \times \text{ position} \\ 0.367 & \times \text{ velocity} \end{array}$$

which corresponds to the connection of links (b) and (c) in fig. 7.2(a).

The I.N. plots for both velocity and acceleration feedback are shown in fig. 7.5 and 7.6 respectively with the origin stable in both cases. The effect of the non-interactive control unit is to remove the d-circles from the diagrams.

When interaction is present stability cannot be guaranteed in the case of velocity feedback until feedback gains in excess of 3.0 for machine 2 and 2.5 for machine 1 are used. However rotor angle time responses demonstrated asymptotic stability within this region showing the system was Nyquist stable at all velocity feedback gains.

By observation of the I.N. diagrams of fig. 7.5 and 7.6 increasing either the velocity or acceleration feedback gain increases the positive damping within the system and reduces first load angle excursion; two important factors of a good control scheme. For similar feedback gains this effect is more prominent for acceleration feedback as,

- (i) The critical point is nearer the I.N. locus with velocity feedback than with acceleration feedback.
- (ii) With a signal proportional to $\ddot{\delta}$ a full forcing signal proportional to the instantaneous difference between P_M and P_L is continually applied to the input of the regulator.

With interaction present and high acceleration feedback gains, $k_{fb_i} > 3.0$, stability cannot be guaranteed from the I.N. diagram. This causes no problems as with feedback gains of this magnitude the system would be excessively overdamped.

7.6.4 SECOND ORDER REGULATOR

Modelling the steam system and the electrohydraulic valves produces the most realistic model,

$$T_v = 0.08s$$

$$T_s = 0.75s$$

$$k_p = 1.0$$

$$\text{Limits} = \pm \infty$$

in fig. 2.5

Such a system is decoupled if a feedback matrix

$$F_{VEL}(p) = \begin{bmatrix} Kfb_1, & \frac{0.489 + 0.029p + 0.406}{p} \\ \frac{0.489 + 0.029p + 0.406}{p}, & kfb_2 \end{bmatrix} \quad (7.33)$$

feeding back across the machines

0.489 x position

0.029 x acceleration

0.406 x velocity

corresponding to the connection of links (a) (b) and (c) in fig. 7.2(a).

The I.N. plots of fig. 7.7 show that velocity feedback gain is limited in that an excessive gain will produce self-induced oscillations ultimately leading to Nyquist instability. This is demonstrated for a feedback gain of $Kfb_i = 0.6$ by rotor angle response of fig. 7.11. If interaction effects are removed the position of the critical point is defined exactly from the I.N. plots of fig. 7.7 which for this system is 0.25 for \hat{Q}_{11} and 0.22 for \hat{Q}_{22} .

The tendency towards self-induced oscillation with high velocity feedback gains is further emphasised by fig. 7.10(a) where the effect of velocity feedback is to reduce the positive damping within the system. The large changes in gradient of curve a_2 in fig. 7.10(a) suggest that it is machines of small inertia constant that are more significantly affected by the velocity feedback gain and more prone to self-induced oscillations. In earlier work Dineley and Kennedy⁽³⁴⁾ demonstrated the introduction of positive damping at low feedback gains but obtained self-induced oscillations at higher feedback values, especially when the machine inertia was small. It is concluded that the damping attributed to velocity feedback is system dependent.

One of the advantages of velocity feedback is its ability to reduce first load angle excursions with increasing feedback gain, as

demonstrated by fig. 7.9 curve (a). Curve (c) shows that if interaction is removed a further reduction in first load angle maximum results. This is due to the movement of machine one being kept to a minimum by the control unit. The value $(\delta_2 - \delta_1)$ is now greater than when interaction was present allowing a larger flow of synchronising power to machine one producing a corresponding reduction in the first load angle maximum of machine 2. The build up of power at the terminals of machine 1 is counteracted by a change of input conditions to this machine as directed by the cross-feedback. The balance of electrical to mechanical power is maintained in machine 1 ensuring minimum movement of this machine.

Observation of the I.N. plots of fig. 7.8 produced for acceleration feedback suggests that acceleration feedback would both reduce first rotor angle excursions and enhance the positive damping within the system. This reduction in first load angle maximum is demonstrated for the study system by curves (e) and (f) in fig. 7.9 and for similar reasons as outlined above, when dealing with velocity feedback, removing interaction further reduces first load angle excursions as shown by curve (c) in fig. 7.9. Fig. 7.10(b) demonstrates the increase in positive damping with increasing gain while the rotor angle time response of fig. 7.11(c) exhibits near optimum damping with a feedback gain of $K_{fb,1,2} = 0.05$. Increasing the feedback gain would overdamp the system.

From this discussion it is apparent that acceleration feedback produces more powerful control than rotor velocity, a conclusion also reached by Dineley and Kennedy.⁽³⁴⁾

7.7 STABILISATION OF VELOCITY FEEDBACK WITH AN ADDITIONAL ACCELERATION TERM

Dineley and Kennedy⁽³⁴⁾ suggest that the self-induced oscillations produced by the velocity feedback can be reduced if an acceleration signal

is used to stabilise the velocity term. This is demonstrated for small perturbations in fig. 7.10(c) where the critical gain of $kfb = 0.25$ in fig. 7.10(a) has been increased to 1.0. Further, the previous unstable rotor angle response of fig. 7.11(b) is now stable, fig. 7.11(d), and self-induced oscillations do not cause instability until a velocity feedback gain in excess of 1.0 is reached.

The combined feedback signal produces large reductions in first load angle excursions, fig. 7.9 curves (b) and (d), without overdamping the system, which would occur with high acceleration feedback gains. Again the effect of the non-interactive control unit is to reduce the first load angle maximum of machine 2, fig. 7.9 curve (d2). A similar improved control signal is suggested by Hughes⁽⁴⁵⁾ when velocity governing with phase advance is used to produce a more acceptable response.

The stabilising effect of acceleration feedback can be further studied for the non-interactive system by I.N. plots. The stabilizing effect of an acceleration term on velocity is shown in fig. 7.12 where the critical point increases as the acceleration feedback gain increases. The higher series of critical points for the heavier machine in fig. 7.12 indicates the susceptibility of machines of small inertia constant to self-induced oscillations. The critical velocity feedback gain increases not only with acceleration feedback gain but also with initial load angle as indicated by fig. 7.13. Thus, the initial load angle exerts a certain stabilizing effect on the velocity feedback.

If system stability is defined as the point at which one channel within that system displays an unstable condition then, in the case of velocity feedback, it is the lighter machine that sets this limit; a result in agreement with Dineley and Kennedy.⁽³⁴⁾

7.8 THE REMOVAL OF INTERACTION ON 3 ϕ FAULTS OF SHORT DURATION

7.8.1 GENERAL

The control method was designed to be non-interactive when subjected to a disturbance at the machine inputs. The effect of using the non-interactive control unit when the disturbance takes the form of a three phase fault at the machine terminals is investigated.

With this type of fault a disturbance will be felt by both machines and will appear as though two disturbances have been applied, one to each channel, simultaneously as indicated by fig. 7.14.

The second order regulator model with an acceleration damping signal is used. The fault being applied at the terminals of machine two for 0.05s, when it is cleared and the system resumes its initial conditions.

7.8.2 THE BENEFIT OF INTERACTION REMOVAL

When interaction is present the synchronising power flowing from machine 2 after reclosure "drags" machine 1 into higher load angle swings, fig. 7.15, curves (a1) and (b1). Removing interaction counteracts this flow of synchronising power by adjusting the machine input power in a determined manner as shown in fig. 7.17 and 7.18 by curves (c) and (d). The disturbance now causing machine 1 to accelerate at all is that of fig. 7.14(b).

An acceleration feedback signal tends to remove the valve closing signal on fault removal, as shown by curves (b2) and (d2) in fig. 7.17. As the fault period is small the power limits do not play an important role, provided the acceleration feedback gain is not exceptionally high. P_m is held lower than its steady state value until the rotor angle reaches its maximum value as indicated by point X in fig. 7.18(b). Section 8.2 demonstrates that if P_m is substantially greater than its steady state value, while the rotor angle is increasing, the first load angle maximum will increase.

As the fault is applied at the terminals of machine 2 the largest feedback signals are derived from this machine. Where interaction is removed there is little change in the input signal to machine 2, relative to the interactive study, and only a small decrease in first rotor angle maximum results. In comparison the change in the feedback signal to machine 1 is large, due to cross feedback from machine 2, resulting in the large decrease in first load angle. This is demonstrated by curves (b2) and (d2) in fig. 7.15, 7.17 and 7.18.

Implementation of the non-interactive control unit with an acceleration feedback gain of 0.07 produces near optimum response, curves (d) fig. 7.15. Comparing curves (b) and (d) in fig. 7.18 shows that the penalty paid for this improved control is a greater change in the input power to machine 1 than when interaction was present. However as discussed above the input power deviation of machine 2 remains approximately the same.

A good control system should provide rapid voltage recovery on fault clearance, to ensure that induction motor loads do not stall, as well as the good system damping and reduction in first load angle.⁽⁴⁵⁾ The good voltage recovery produced by the non-interactive control unit is shown in fig. 7.16 where curve (d) corresponds to the near optimum response of curve (d), fig. 7.15.

As input power is being varied to both machines the author feels that the additional variation attributed to the non-interactive control unit is justified when considering the improved response that is obtained as indicated by curves (d) in figs. 7.15 to 7.18.

A similar set of results was obtained when the fault was applied at the terminals of the heavier machine.

7.9 EXCITATION CONTROL

7.9.1 GENERAL

Regulators used to control the alternator field excitation are either the older rotating exciter⁽¹³⁾ or the more modern static excitation system.⁽⁶⁾ The effect of both these exciters on system stability and response are investigated when subjected to different feedback signals.

The alternator field regulator model discussed in section 2.5 is reduced to the first order

i.e.

$$\frac{K_1}{1 + p.T_{ex}} \quad (7.34)$$

The value of the time constant being adjusted to

$$\begin{aligned} T_{ex} &= 0.03s, & \text{static exciter} \\ T_{ex} &= 0.5s, & \text{rotating exciter} \end{aligned}$$

while a gain value for $K_1 = 10.0$ is used.

When interaction is removed the exciter reference voltage, V_{ref} , is not the input to the control unit, see fig. 7.21. Consequently any change in V_{ref} causes a small disturbance in both machines as shown in fig. 7.30(b). However if the input step was applied as in fig. 7.21(b) interaction would be removed, fig. 7.30(a). The latter disturbance is not used as the former is the more practical of the two.

As the disturbance imposed is small excitation limits do not play an important role. Their effect on large disturbances is discussed in Chapter 8.

7.9.2 VOLTAGE FEEDBACK

Historically the control of field excitation was developed to maintain internal power factor angle and terminal voltage at pre-set levels during steady state operation. This was achieved by feeding back a signal proportional to the magnitude of terminal voltage to a rotating exciter.

Not only did this form of control improve steady state operation but was also found to assist system stability during the transient interval.

I.N. plots for both rotating and static excitation systems are shown in figs. 7.19 and 7.20 respectively for a change in exciter reference voltage. The band so produced is extremely divergent with d-circles at higher frequencies overlapping the smaller d-circles and enclosing the origin. This makes any assessment of the critical feedback gain from the I.N. plot difficult. With experience gained from previous analysis and knowing the stability of the origin (section 7.3.2) self-induced oscillations would be expected as the feedback gain was increased ultimately leading to instability. This was verified by computing rotor angle time responses at different feedback gains. Further the onset of this self-induced instability is demonstrated in the damping curves of fig. 7.24(a) by point X where feedback gains in excess of $K_{fb_{1,2}} = 1.0$ produce Nyquist instability. As previously stated d-circles do not allow an accurate assessment of the critical gain values from the I.N. plots. However by plotting $\det T(p)$ (Section 4.3.2) for different feedback gains an accurate assessment of stability is achieved. Fig. 7.22 shows plots of $\det T(p)$ for this system and with feedback gains greater than $K_{fb_{1,2}} = 1.0$ the origin is enclosed and the system is unstable. This agrees with fig. 7.24(a).

The main locus, i.e. the locus of the centres of the d-circles, on the I.N. plots of figs. 7.19 and 7.20 indicate a higher stability margin for the rotating exciter than for the static. An effect first suggested by Aldred/Shackshaft in 1960.⁽⁴⁸⁾ This same effect has caused other authors to look for supplementary feedback signals.⁽⁶⁾⁽⁷⁸⁾⁽⁷⁹⁾ Because of the low time constant of the static exciter the phase of response to terminal voltage can be sufficiently advanced to cancel the positive

damping effect produced by the field time constant. ⁽⁷⁹⁾ However increasing the feedback gain, K_{fb} , continually reduces first load angle excursions, as demonstrated by curves (a) and (b) in fig. 7.23, but has to be limited because of the improper phasing and resulting Nyquist instability.

Implementing the non-interactive control unit reduces the movement of the indirectly disturbed machine(s) to a minimum as seen in fig. 7.30. However there is no significant further reduction in the first load angle maximum of the disturbed machine; curves (a2) and (b2) in fig. 7.23 show no appreciable difference. This effect is found with all feedback signals to the exciter and is attributed to the large field open circuit time constant, T_{do}' . Removing interaction changes the magnitude of the feedback signal to the exciter, but because of the magnitude of T_{do}' the effect of the interaction removal has little influence on the first load angle excursion of the disturbed machine.

7.9.3 VELOCITY FEEDBACK

One method of stabilising voltage feedback to the static exciter is to incorporate a signal proportional to slip frequency. ⁽⁶⁾⁽⁷⁹⁾ I.N. plots using rotor velocity as the feedback signal are shown for the system with and without interaction in fig. 7.25 and 7.26. In all cases the amount of velocity feedback is limited. Previous authors ⁽⁶⁾⁽⁷⁹⁾ have shown that using $\dot{\delta}$ as the feedback signal either positive or negative damping can be introduced depending on the relative gains and time constants. For this system incorporating a static exciter the time constants are such that there is a tendency to reduce the positive damping at all feedback gains, fig. 7.24(B). The presence of self-induced oscillations is more prominent on the lighter machine as indicated by the steeper gradient of curves (a2) and (b2) relative to (a1) in fig. 7.24(B). However increasing the velocity feedback gain continually decreases first load angle maximums, fig. 7.23, curves (c) and (d).

For clarity consider the non-interactive I.N. plots of figs. 7.25 and 7.26. The critical velocity feedback gain required to induce oscillations is similar in both static and rotating excitation systems for the lighter machine, $\hat{q}_{22}(p)$ giving a gain limit of approximately 2.0 in both cases. Reducing the exciter time constant increases the critical feedback gain for the heavier machine from 0.9 with the rotating exciter to 3.0 with the static system. These limits being obtained from $\hat{q}_{11}(p)$.

With the static exciter, increasing the inertia constant reduces the speed of response to the field forcing. This limits the tendency to overcorrect and produce self-induced oscillations. If the time constant of the exciter is increased, as is the case with a rotating exciter, the strength of the field forcing is reduced and with the large response time of the heavy machine improper phasing results causing Nyquist instability. Lowering the machine inertia with the rotating exciter the response to any field forcing is more rapid and counteracts the low forcing.

From this discussion it is concluded that a greater stability level is obtained with the rotating exciter when machines of low inertia constant are used. It also provides a greater stability level with light machines than the static exciter. Conversely a static exciter operating on a system with large inertia machines is less susceptible to self-induced oscillations than if rotating exciters are used.

These two effects correspond. Fig. 7.27 shows block diagrams of the two excitation systems with arrangement (i) in both cases producing the greater stability level. As a linear design was used superposition could be applied. Rearranging the blocks of fig. 7.27(a) so that the first and last are interchanged arrangement (i) in fig. 7.27(a) and (b) are now similar. These results also correspond with those obtained in section 7.6.4

where with fast valving it was found that the lighter machine was more susceptible to self-induced oscillations.

7.9.4 ACCELERATION FEEDBACK

Previous authors⁽⁸⁰⁾⁽⁴⁵⁾⁽⁷⁸⁾⁽⁷⁾ have shown that control is improved by including a term proportional to rotor acceleration in the control signal. With acceleration feedback to the machines in the study system the I.N. plots shown in figs. 7.28 and 7.29 result. When interaction is present the feedback gains included by the union of discs in fig. 7.28 were found to be asymptotically stable by time response results while the stability of the origin was demonstrated in section 7.3.2. Stability can now be guaranteed for all acceleration feedback gains.

The I.N. diagrams show that by increasing the feedback gain the amount of positive damping introduced also increases. Because of the nearness of the locus to the critical point this effect is more prominent in the static exciter. This damping effect is further demonstrated by fig. 7.24(c). Also as the feedback gain increases the first load angle excursion is reduced, fig. 7.23 curves (e) and (f). However as with acceleration feedback to the input power regulator the feedback gain has to be limited or an overdamped response results.

The use of an acceleration feedback signal produces strong control.

7.10 CONCLUSION

The work discussed in this chapter proposed various control methods based on linear multivariable control theory. These control methods were then applied to the system when it was subjected to small perturbations. As these perturbations were small both the transmission system and the

synchronous machines can be accurately represented by a linear model. This then allows the performance of the control method to be assessed from the Nyquist diagram.

The early stages of the work in developing a model to represent the input power regulator demonstrated that this had to be represented by a second order model or else an unstable response could be predicted stable. This was demonstrated when considering velocity governing as the first order model showed the system to be stable at any value of velocity feedback gain. This is untrue as was shown by Dineley and Kennedy⁽³⁴⁾ and results comparable with theirs were not obtained until the second order model was evolved.

The field excitation regulator was also second order.

Feedback of a velocity term to either of these two regulators, when interaction was present or not, showed a reduction in the first rotor angle swings but tends to produce self-induced oscillations as the feedback gain is increased ultimately leading to instability. However if a signal proportional to rotor acceleration is used as the control signal any tendency towards instability is removed while still reducing first rotor angle swings. This control signal also has the advantage of introducing strong positive damping into the system but has to be limited as it can produce a very heavily damped response culminating in a slow recovery of terminal voltage. As one of the aims of any control system is to retain good recovery of terminal voltage this is clearly a limitation on the control system. However with a correctly selected value of acceleration feedback gain section 7.8 demonstrated how good voltage recovery could be achieved by input power control.

The introduction of positive damping by acceleration feedback to the exciter was more pronounced with the static exciter than the rotating

exciter because of the lower time constant employed.

An improved control scheme was obtained by using both an acceleration term and a velocity term in the control signal to the power regulator. The acceleration term stabilises the velocity signal and hence allows a greater first rotor angle reduction while the system does not become overdamped.

Investigations on the exciter demonstrated that the feedback of terminal voltage also reduces first rotor angle swings but has to be limited as it tends to produce instability as the feedback gain is increased. However different authors⁽⁴⁵⁾⁽⁹⁾ have shown that this can be stabilised, in the same way as the velocity signal, by incorporating supplementary signals describing the machines state into the feedback signal.

These conclusions equally apply both to the system with interaction present or when interaction is removed but when interaction is removed an accurate assessment of the system's feedback limitations is available from the I.N. diagrams.

The effect of interaction removal is paramount in this work and one of the advantages of the non-interactive controller in producing improved terminal voltage recovery is demonstrated in section 7.8 in connection with input power control. Another advantage of this form of control is that only one machine is significantly affected by the disturbance. The transfer of synchronising power between the machines producing the relative movement is counteracted by altering either the mechanical input torque or the electromagnetic torque on the machine. This does not imply an increase in the rotor angle swings of the faulted machine. As the synchronising power is transferred between the machines it is accommodated in the usual form of kinetic energy but this change in energy is balanced

by either a change in input power or electromagnetic power depending on the regulator used. This keeps the energy balance within the machine.

Further by constraining the movement of the undisturbed machine the instantaneous difference in rotor angles is increased allowing more power to be transferred. This leads to a further reduction in first rotor angle swings.

Because of the large field open circuit time constant of the machine this is more pronounced when the control is applied to the input power regulator than field excitation.

Continuous control of input power both when interaction is present or not has been shown to produce stronger control action than excitation control both in its control of terminal voltage, first rotor angle reduction and the positive damping it introduces into the system. This is further emphasised in the following chapter.

Present technology does not allow continuous operation of electro-hydraulic valves because of the high hydraulic pressures required for valve opening but is foreseen in the near future.⁽⁸²⁾ At the present time systems that allow 5 strokings are available and future development will produce continuous valve operation.

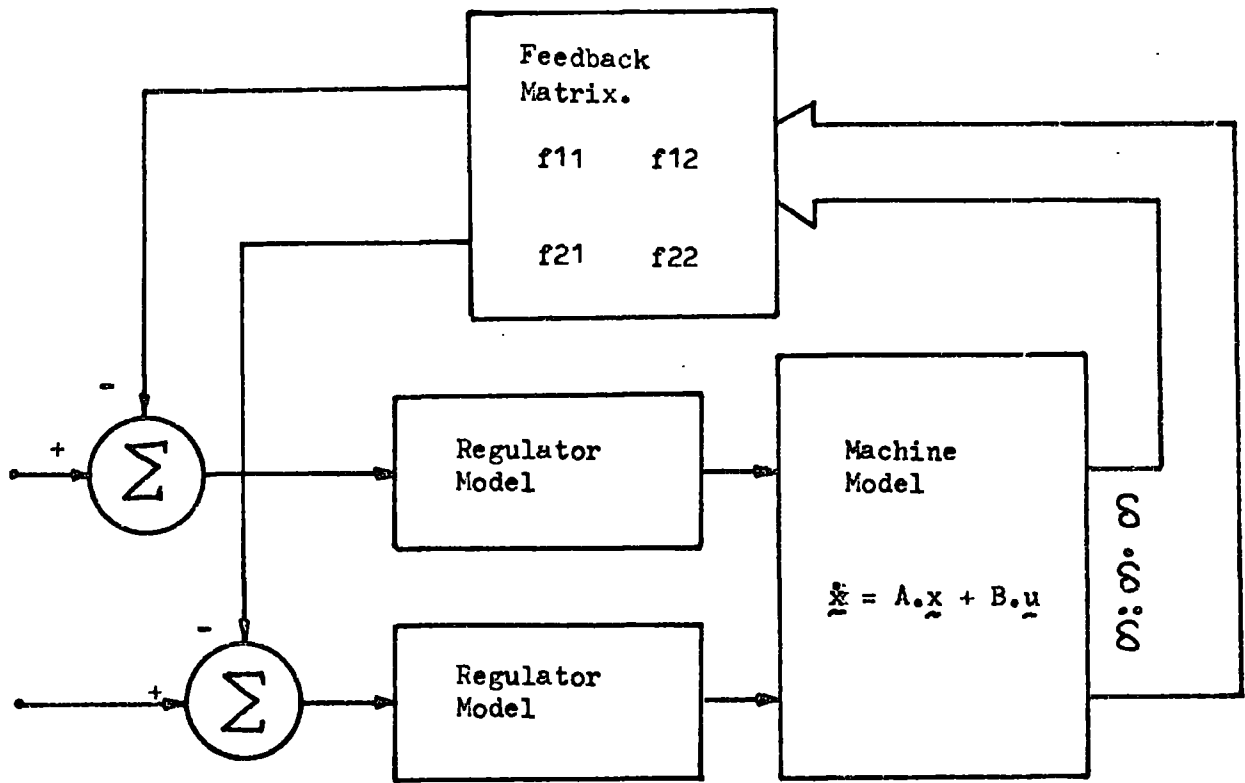
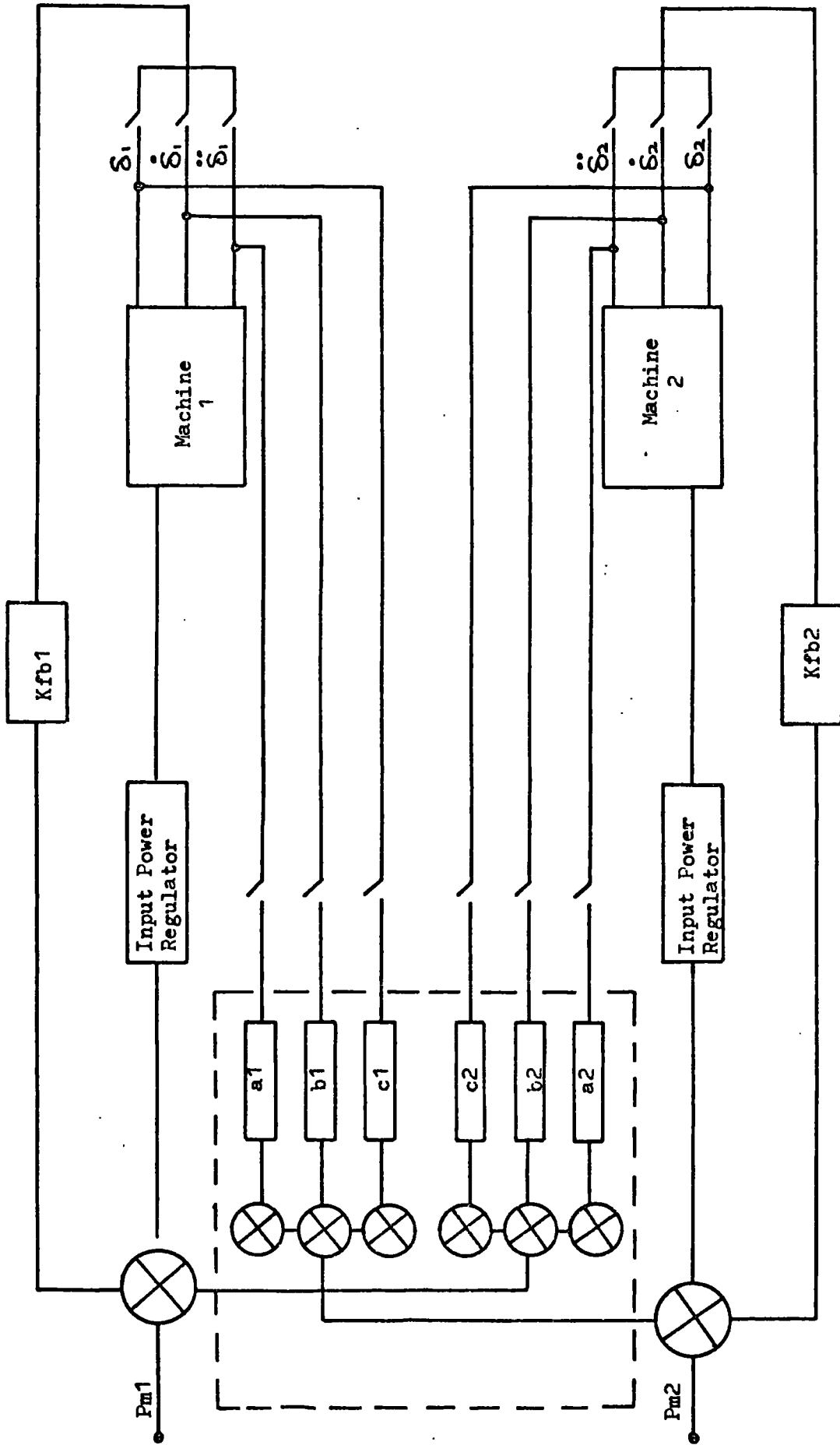
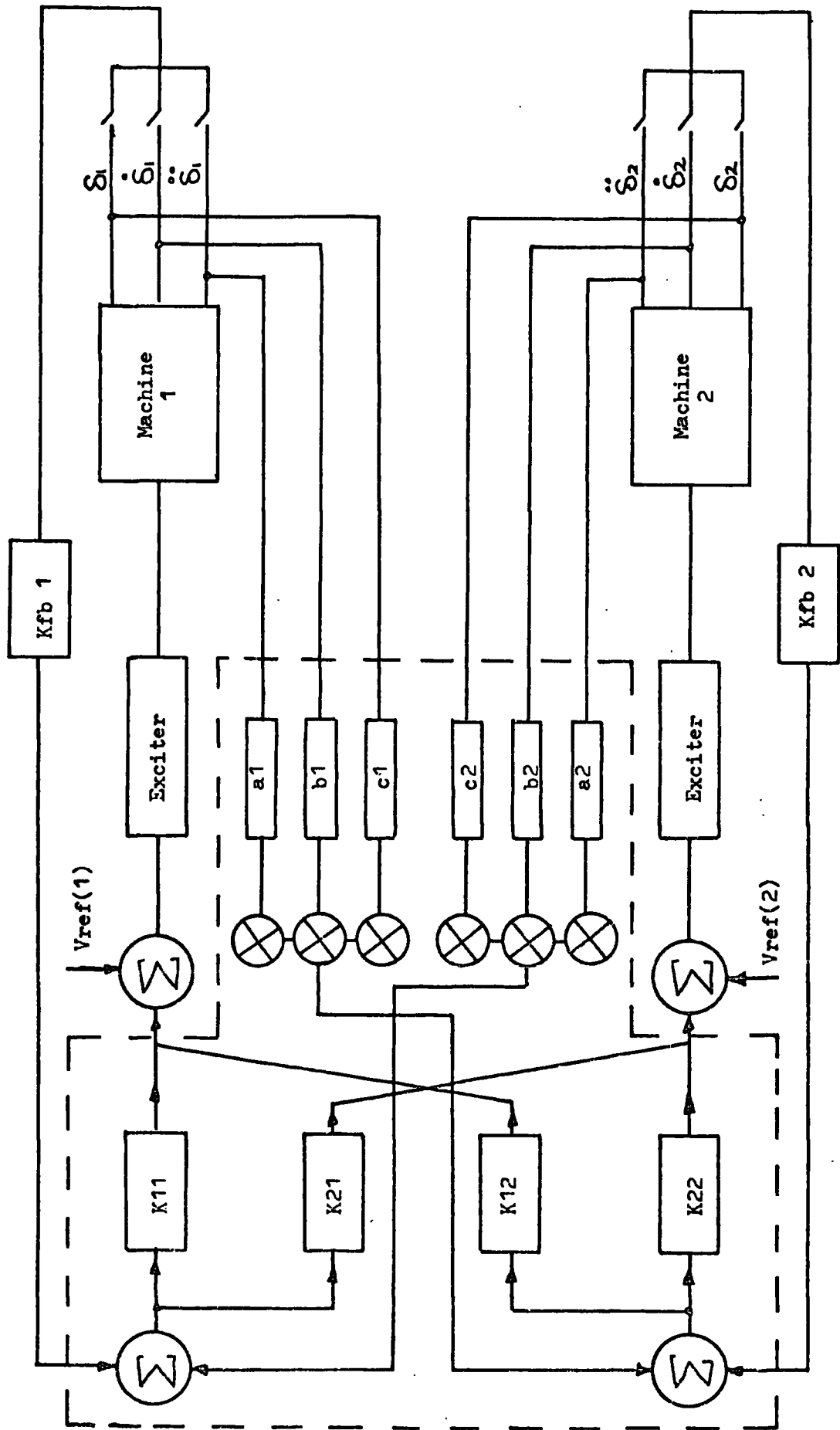


FIG. 7.1 Block Diagram of a Non-Interacting Control System For Two Synchronous Machines.



Block Diagram of the Non-Interactive Control Method Applied to Input Power Control

Fig. 7.2(a)



Block Diagram of the Non-Interactive Control Method Applied to Excitation Control

Fig. 7.2(b)

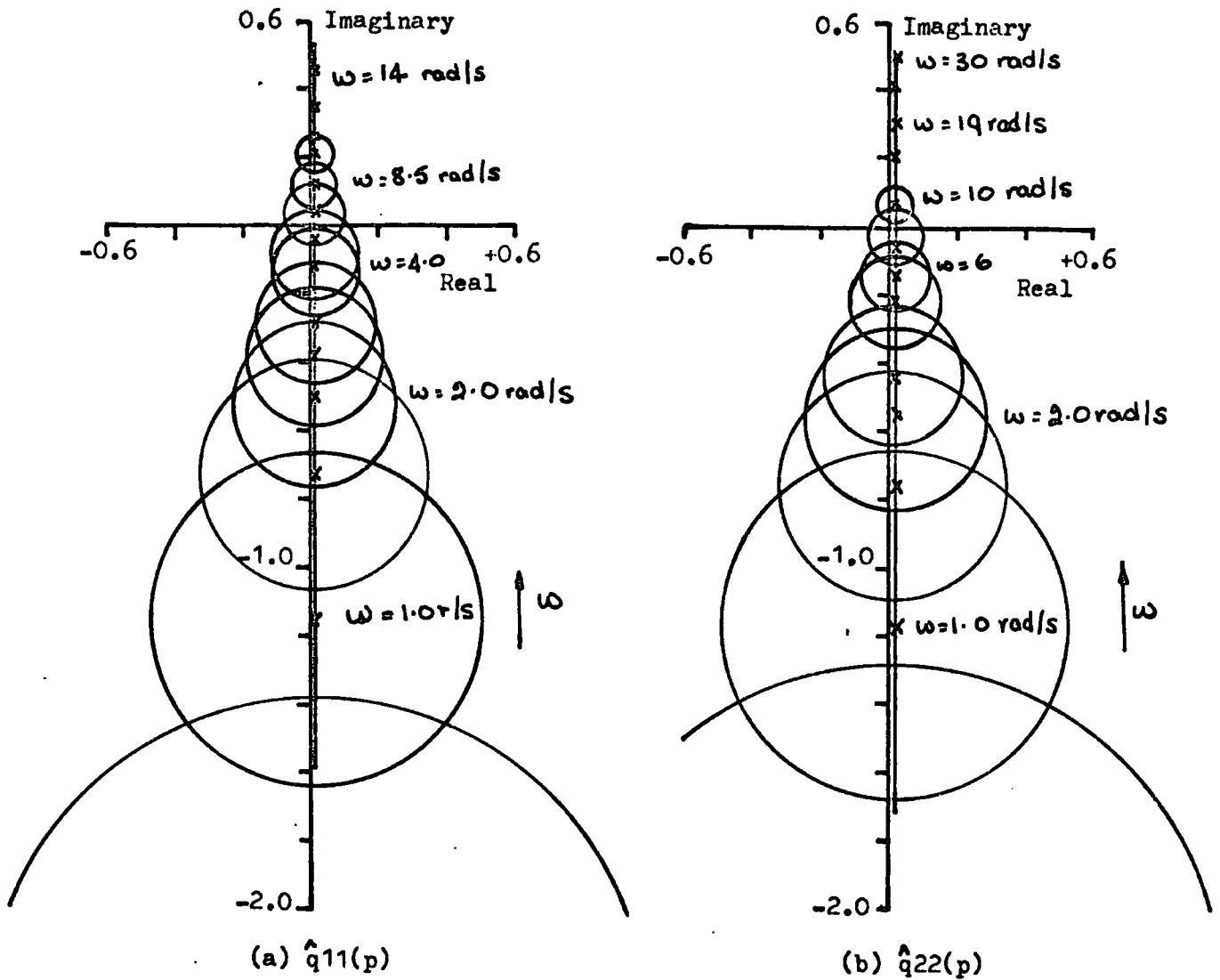


Fig. 7.3 Inverse Nyquist Plots with d-Circles for Input Power Control with Velocity Feedback. Direct Control of Pm Assumed.

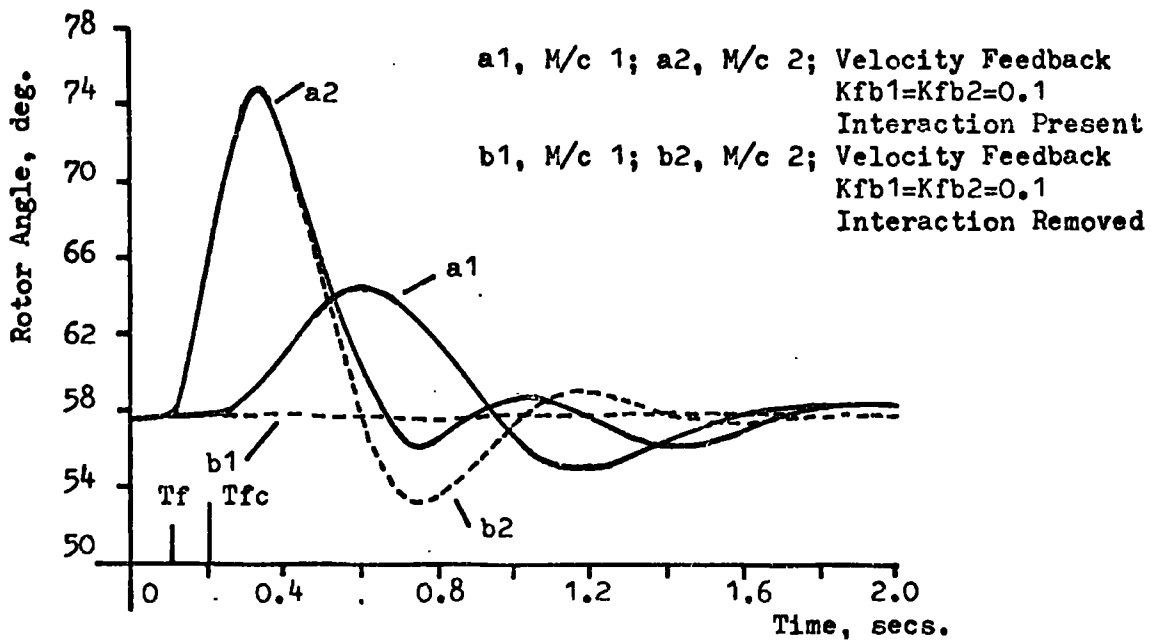
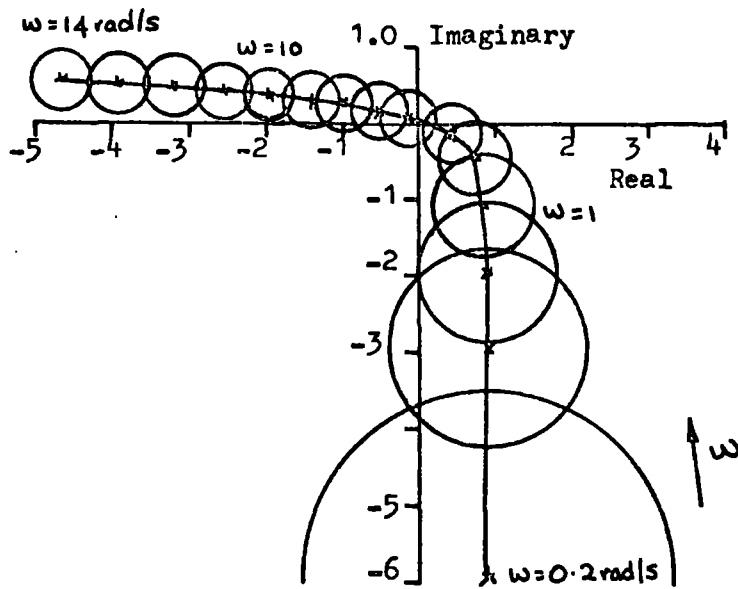
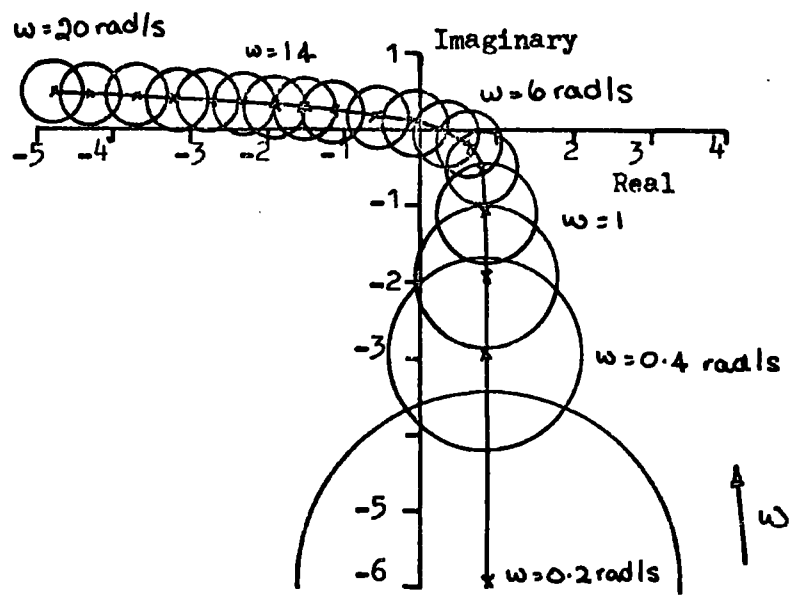


Fig. 7.4 Rotor Angle Time Response Using Non-Linear Model. Data Appendix H. Direct Control of Pm Assumed. Fault Pm(2)=1.4 p.u. For 0.1secs.

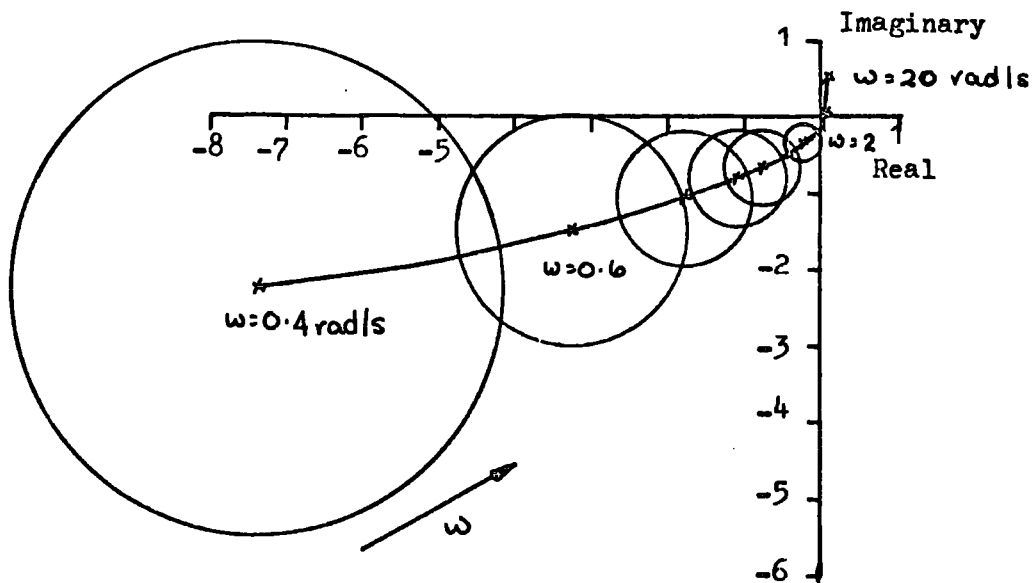


(a) $\hat{q}_{11}(p)$

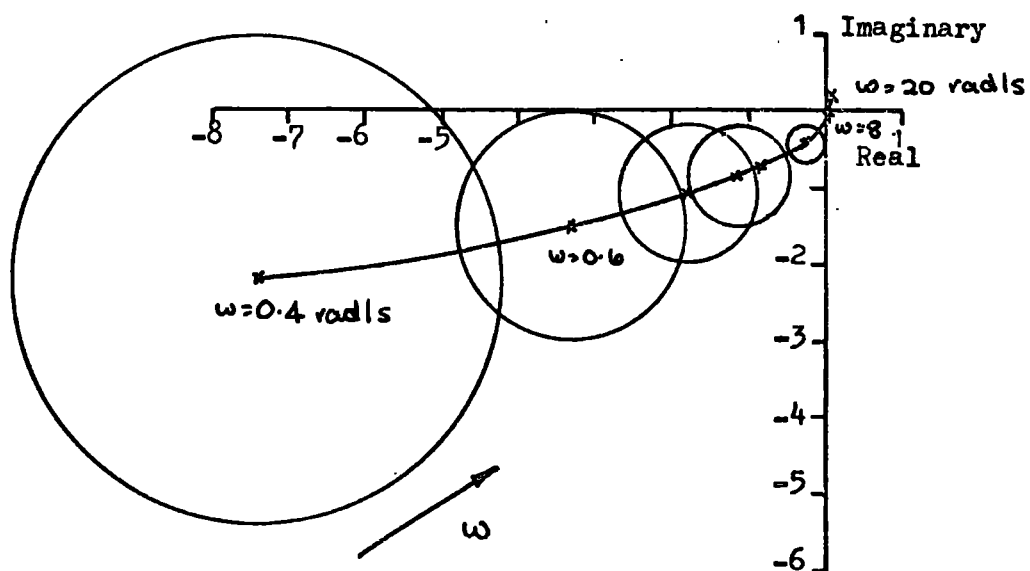


(b) $\hat{q}_{22}(p)$

Fig. 7.5 Inverse Nyquist Plots Showing d-Circles for Input Power Control with Velocity Feedback. Regulator Modelled by a First Order Lag.

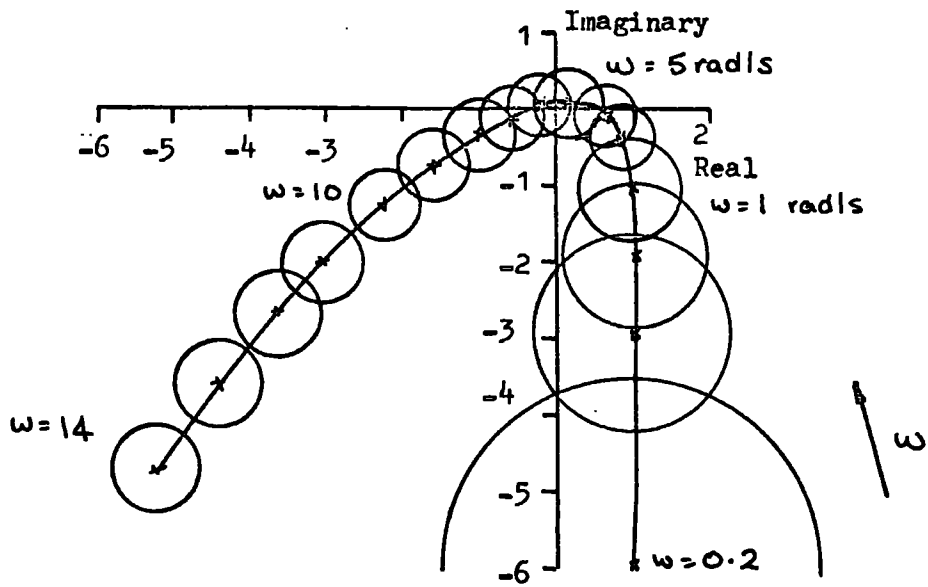


(a) $\hat{q}_{11}(p)$

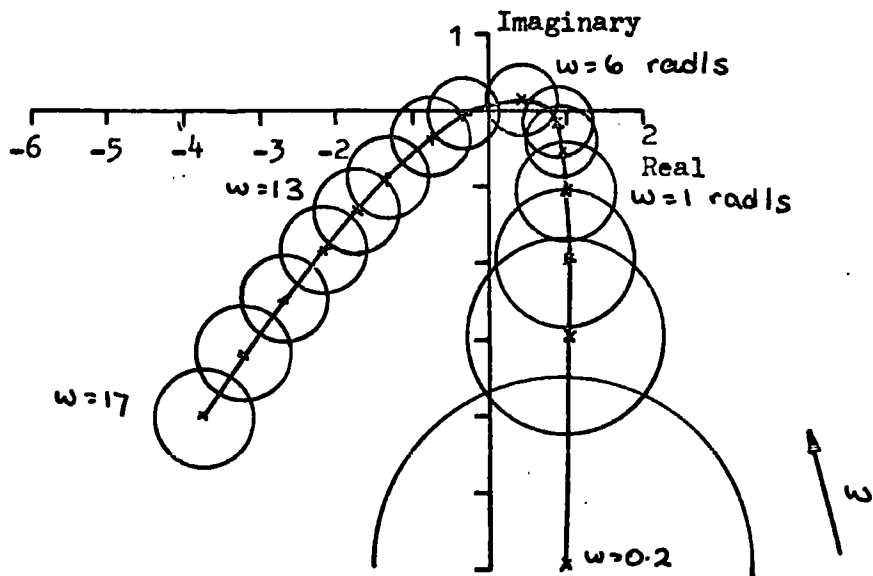


(b) $\hat{q}_{22}(p)$

Fig. 7.6 Inverse Nyquist Plots Showing d-Circles for Input Power Control with Acceleration Feedback. Regulator Modelled by a First Order Lag.

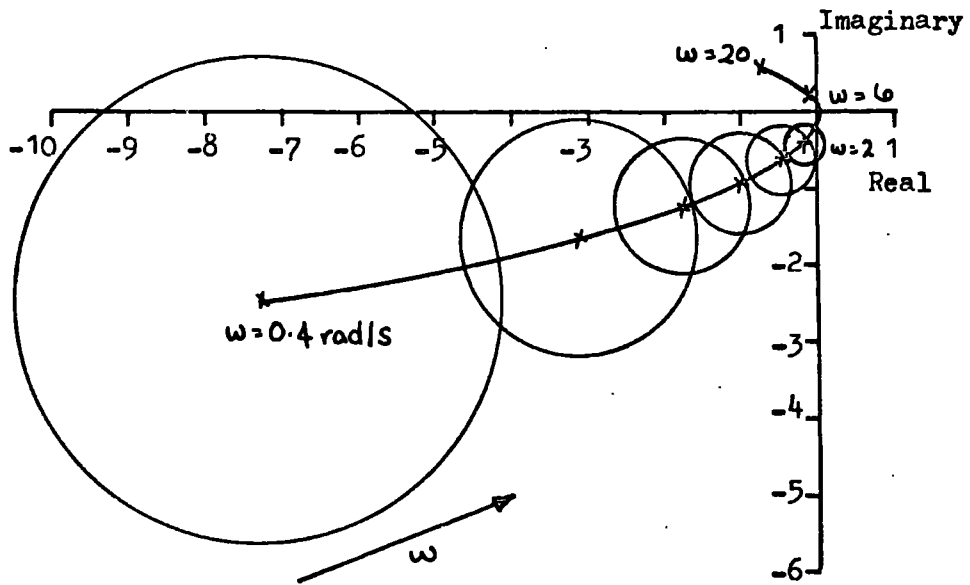


(a) $\hat{q}_{11}(p)$

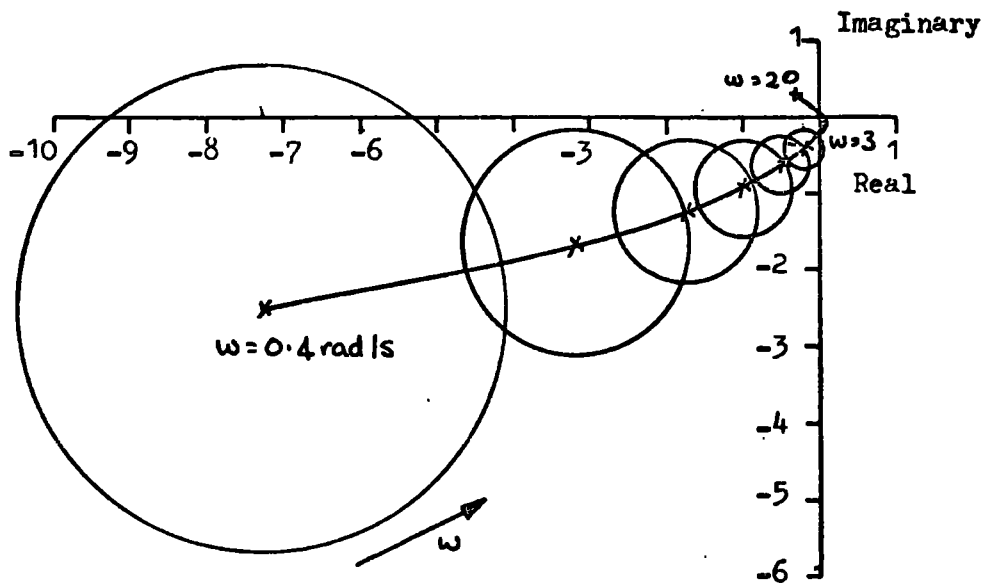


(b) $\hat{q}_{22}(p)$

Fig. 7.7 Inverse Nyquist Plots Showing d-Circles for Input Power Control with Velocity Feedback. A Second Order Regulator Model Assumed.

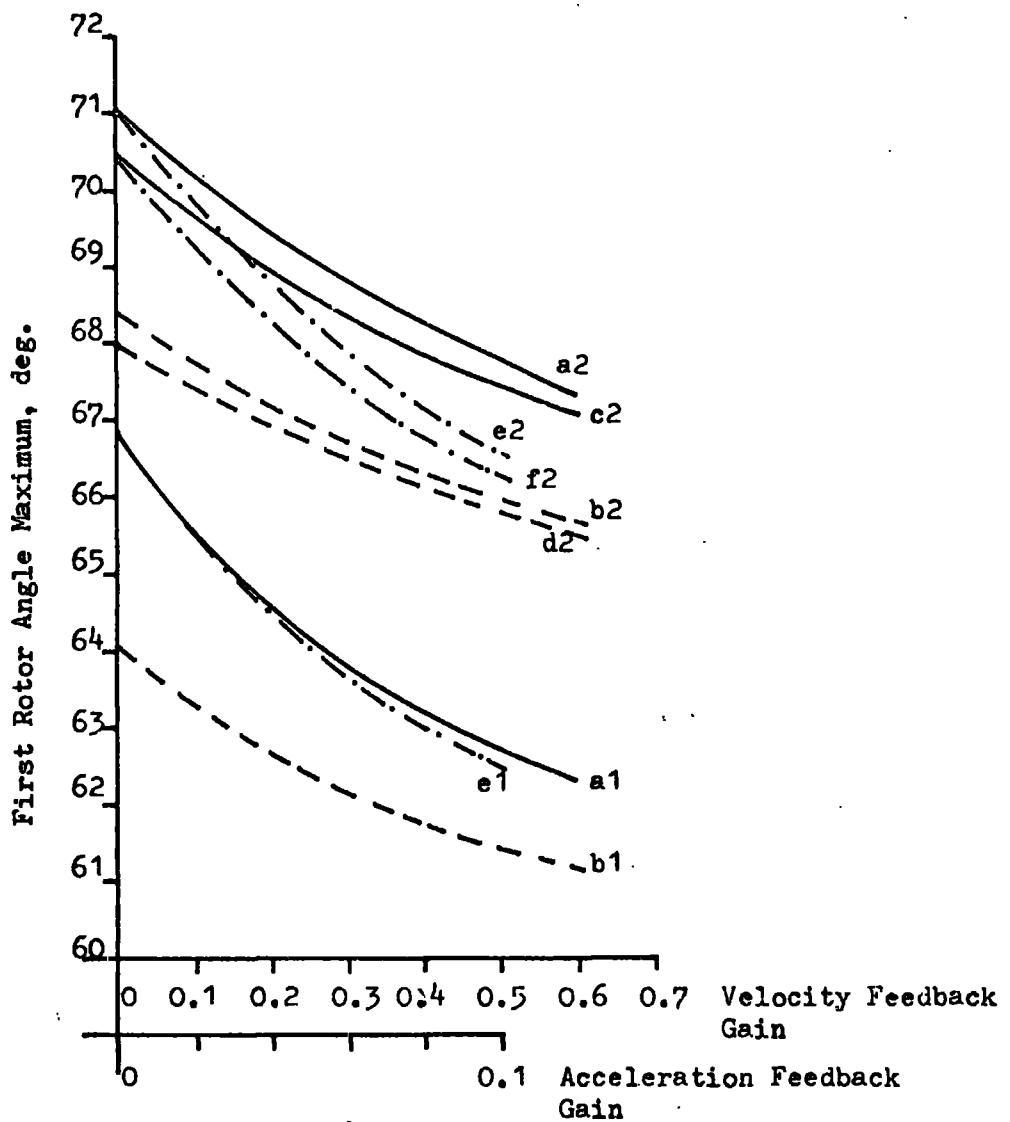


(a) $\hat{q}_{11}(p)$



(b) $\hat{q}_{22}(p)$

Fig. 7.8 Inverse Nyquist Plots Showing d-Circles for Input Power Control with Acceleration Feedback. A Second Order Regulator Model Assumed.



1 - M/c 1; 2 - M/c 2

- a1, a2 - Velocity Feedback, Interaction Present.
- b1, b2 - Velocity + 0.05 Acceleration Feedback, Interaction Present.
- c2 - Velocity Feedback, Interaction Removed.
- d2 - Velocity + 0.05 Acceleration Feedback, Interaction Removed.
- e1, e2 - Acceleration Feedback, Interaction Present.
- f2 - Acceleration Feedback, Interaction Removed.

Fig. 7.9 The Effect of Different Input Power Control Schemes on the First Rotor Angle Maximum for Small Perturbations. A Second Order Input Power Regulator Assumed.

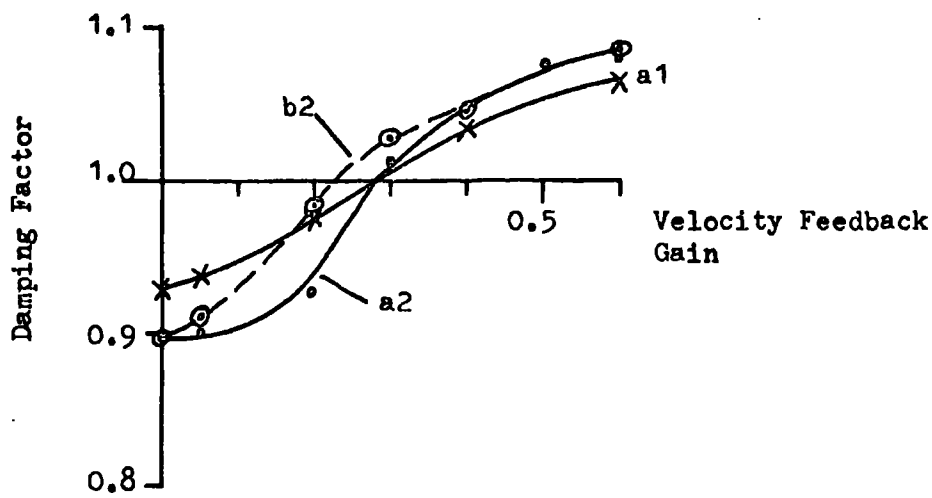


Fig. 7.10(a) The Effect of Velocity Feedback on System Damping

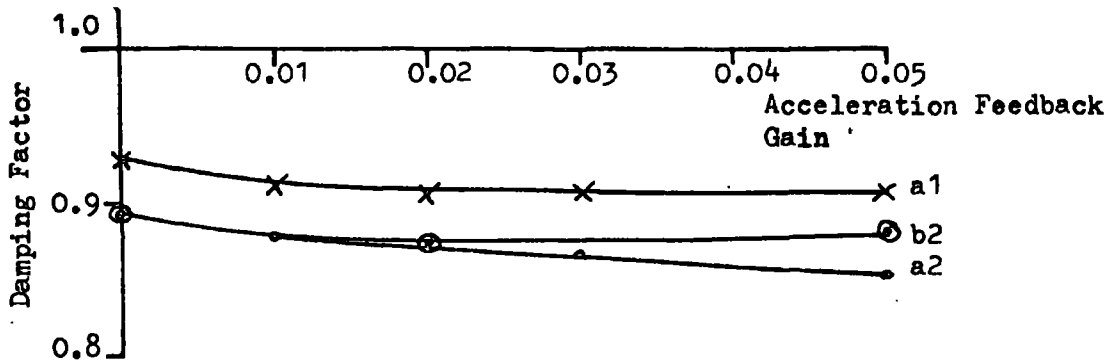


Fig. 7.10(b) The Effect of Acceleration Feedback on System Damping.

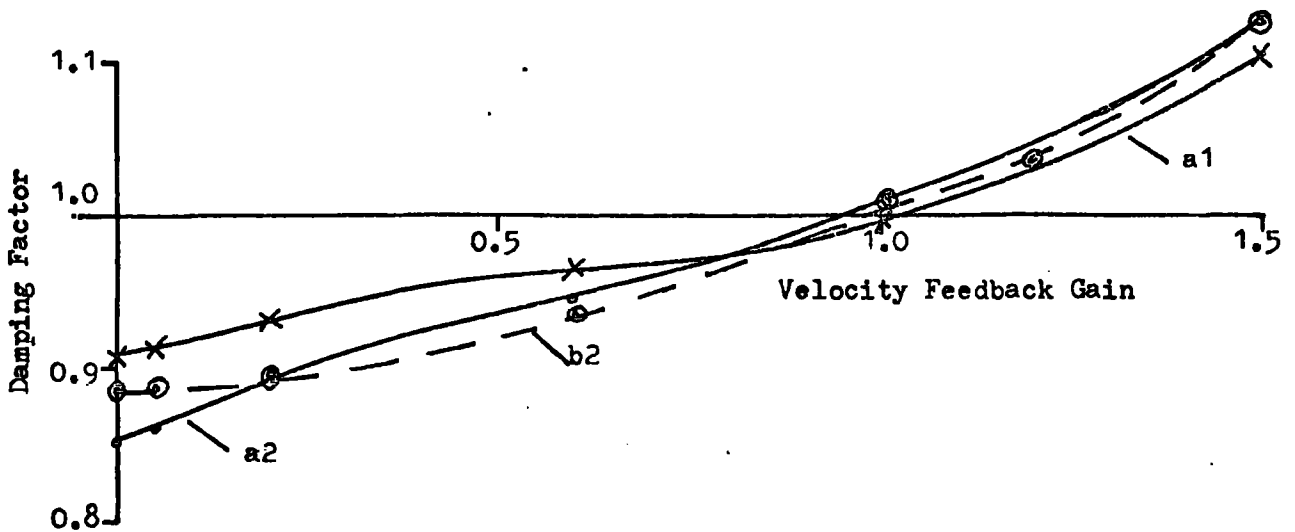


Fig. 7.10(c) The Effect of Velocity Feedback on System Damping When Stabilised by 0.05 Acceleration Feedback Signal.

a1 - M/c 1; a2 - M/c 2; Interaction Present.
 b2 - M/c 2; Interaction Removed.

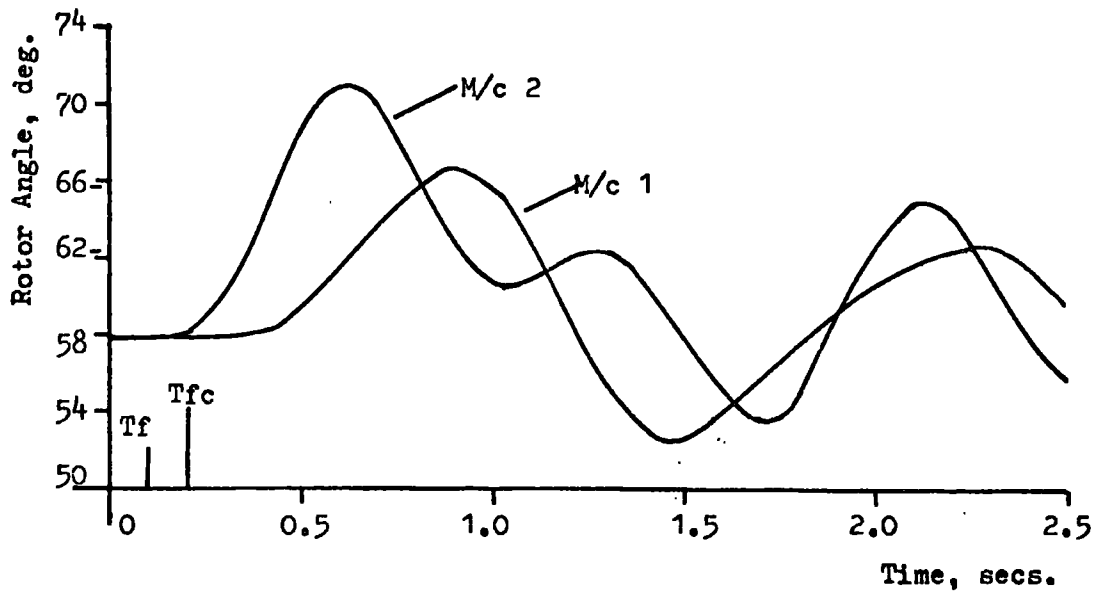


Fig. 7.11(a) No Control

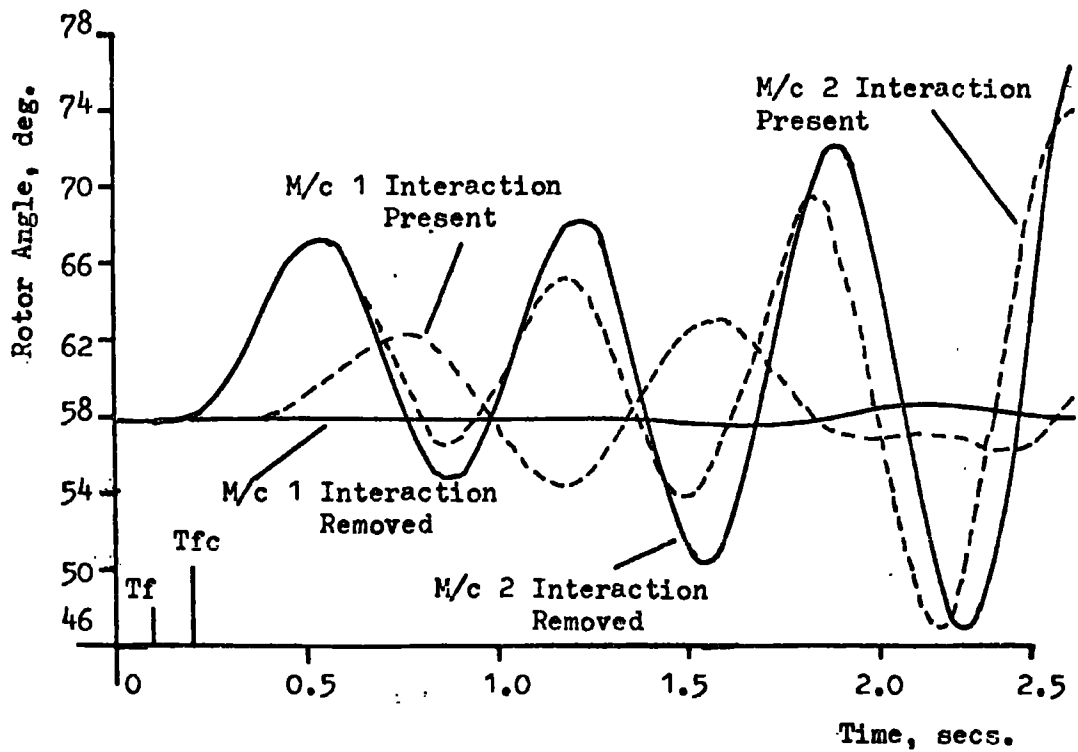


Fig. 7.11(b) Velocity Feedback
 $K_{fb1} = K_{fb2} = 0.6$

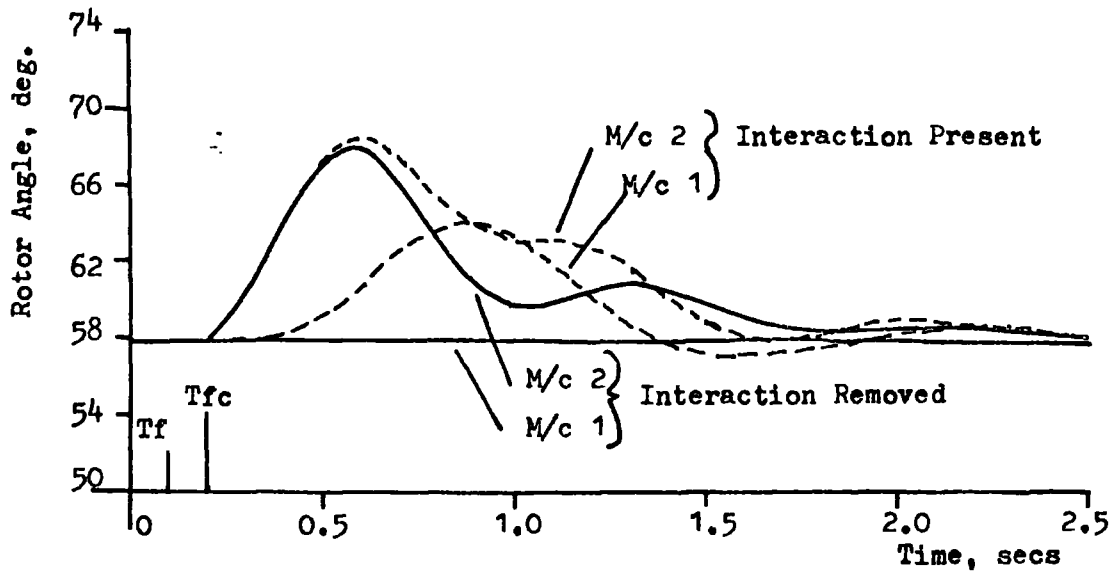


Fig. 7.11(c) Acceleration Feedback, $K_{fb1}=K_{fb2}=0.05$

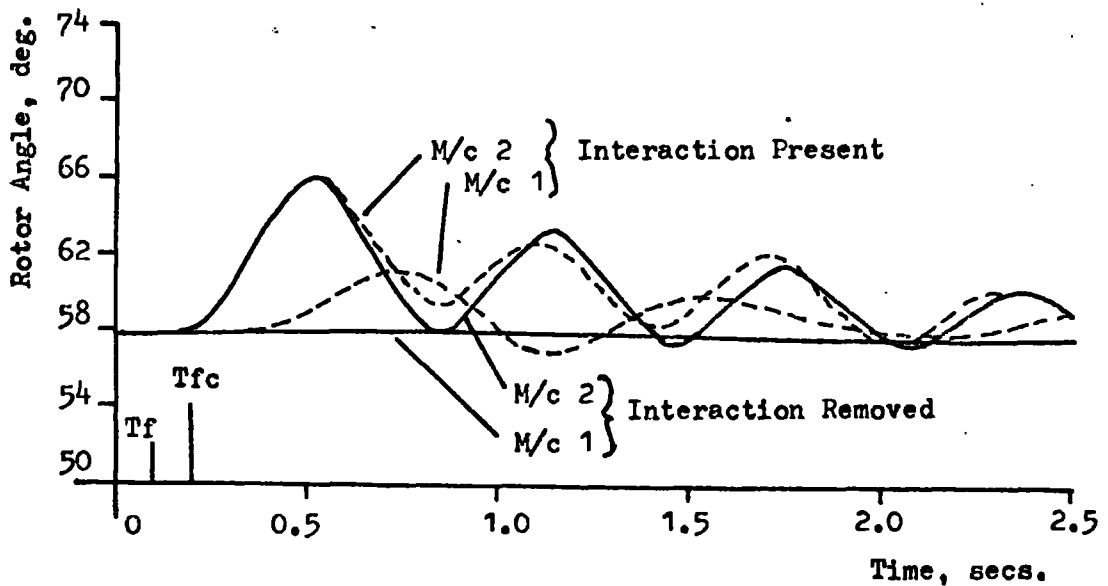


Fig. 7.11(d) Velocity Feedback, $K_{fb1}=K_{fb2}=0.6$, Stabilised by an Acceleration Signal of Gain=0.05.

Fig. 7.11 Rotor Angle Time Responses Using Non-Linear Model. Data Appendix H. Second Order Input Power Regulator Assumed. Fault, $P_m(2)=2.1$ p.u. for 0.1 secs.

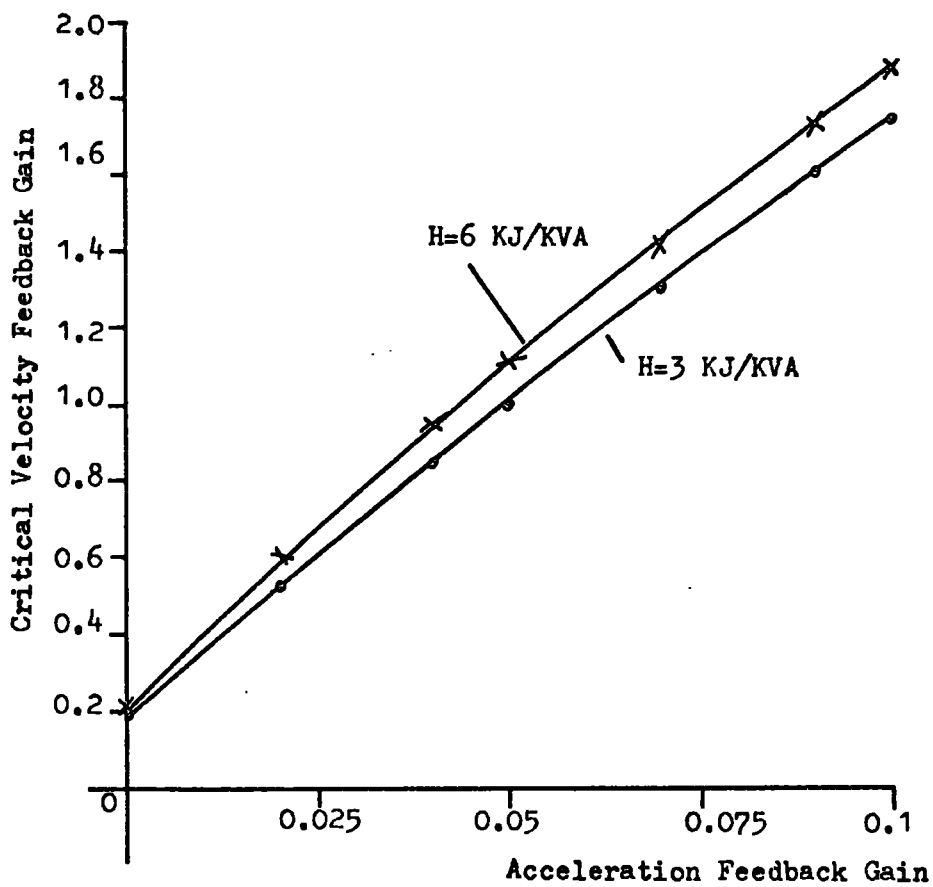


Fig. 7.12 Variation of the Critical Velocity Feedback Gain with Acceleration Stabilising Signal For The Second Order Input Power Regulator. Data Appendix H.

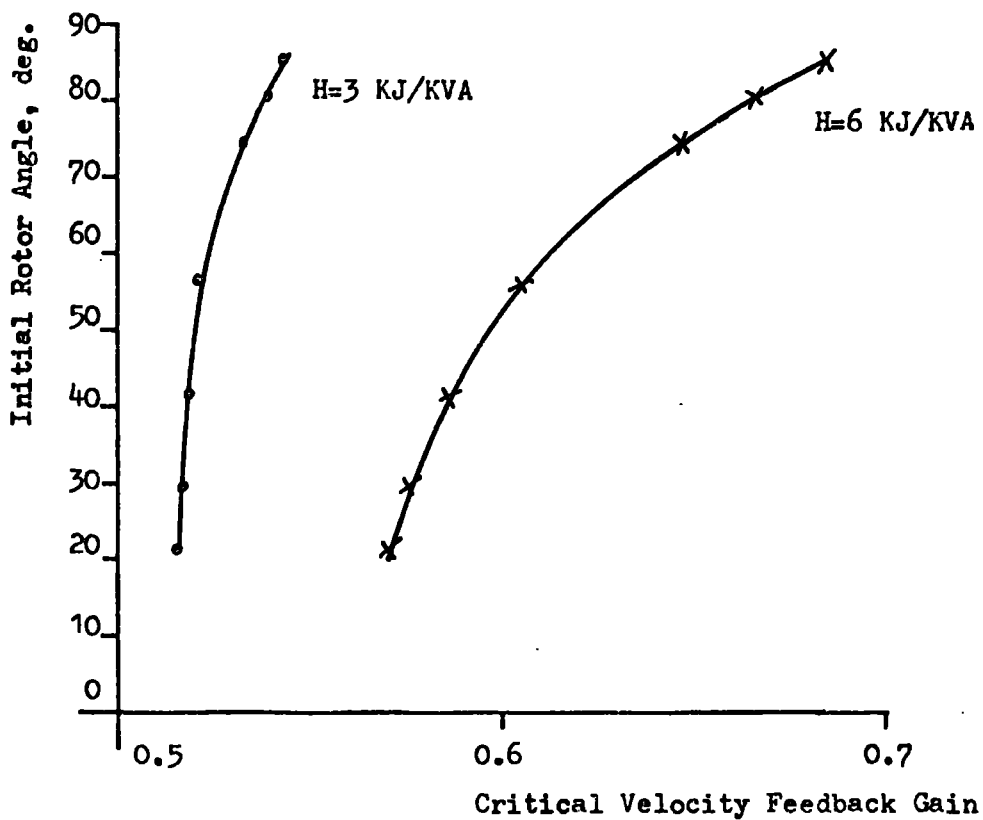


Fig. 7.13 Variation of Critical Velocity Feedback Gain with Initial Rotor Angle for the Second Order Input Power Regulator. Data Appendix H.

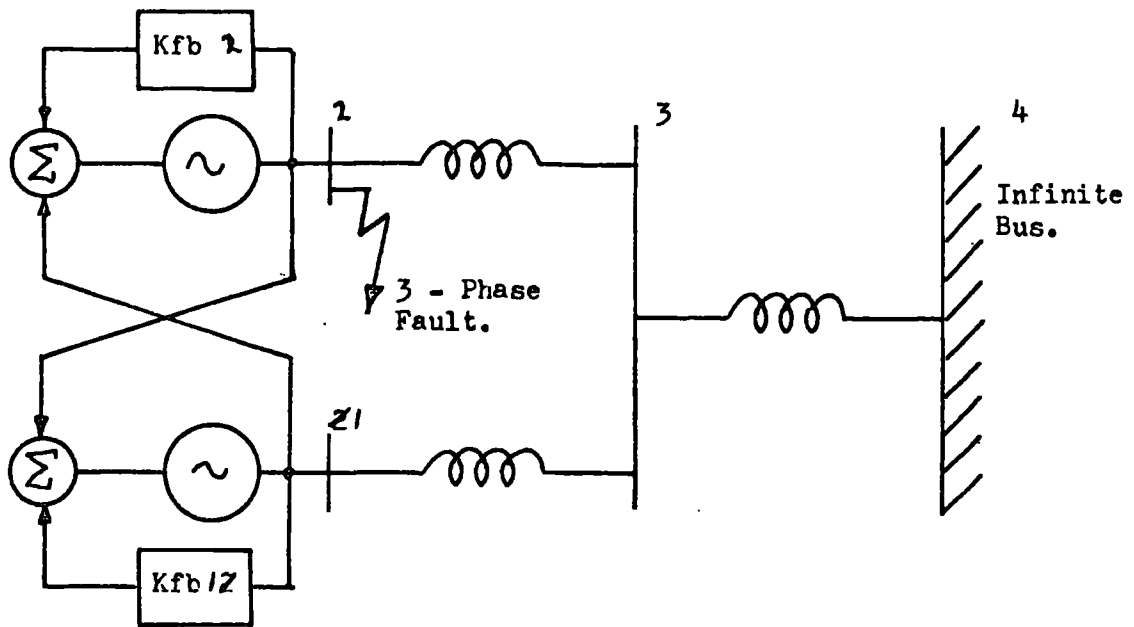


Fig 7.14(a)

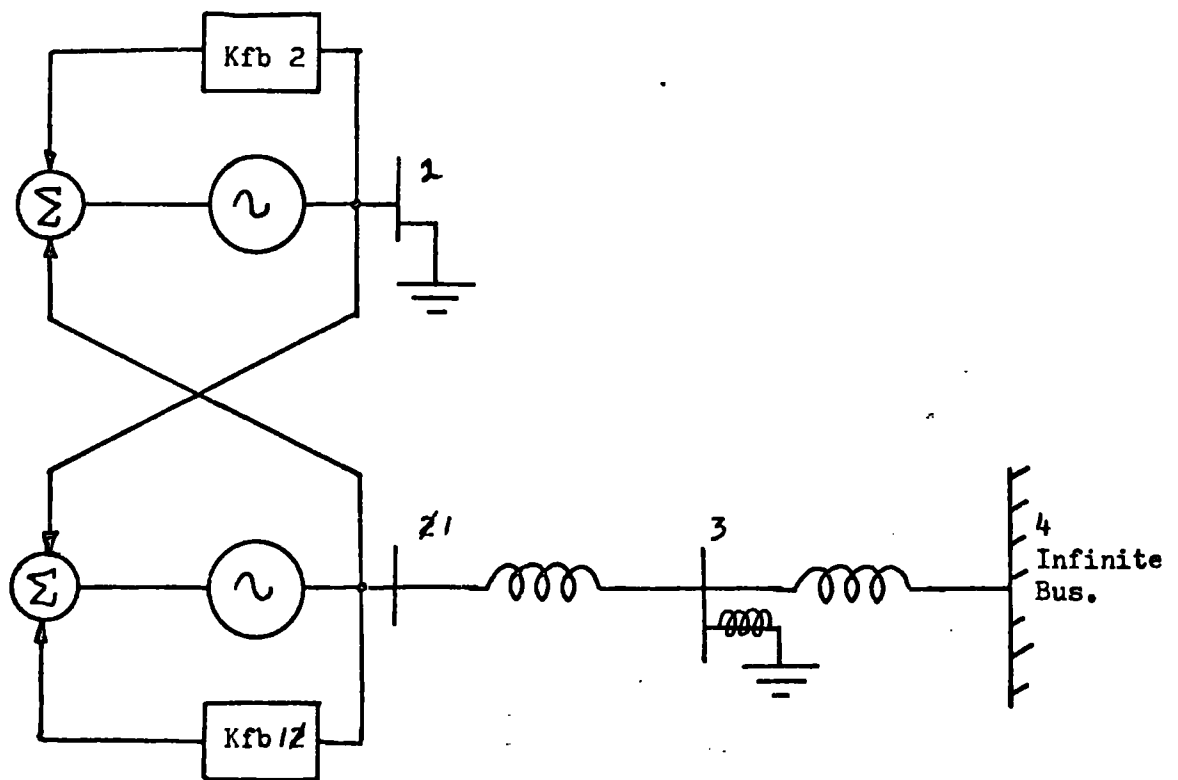


Fig. 7.14(b)

Fig. 7.14 The Power of Fig. 2.7 Under Fault Conditions.

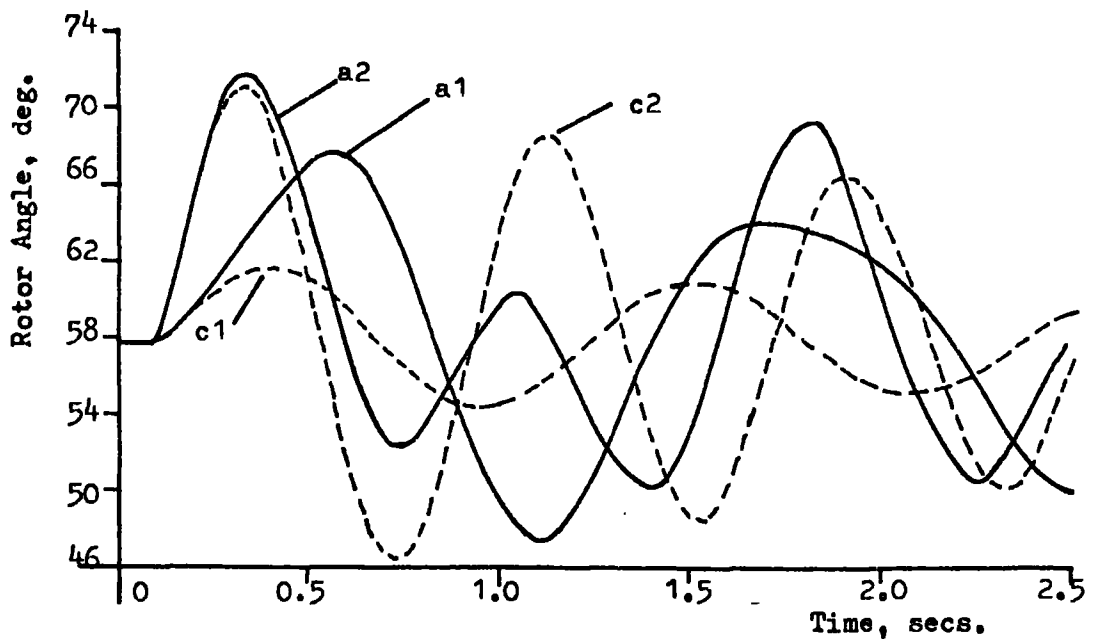


Fig. 7.15(a)

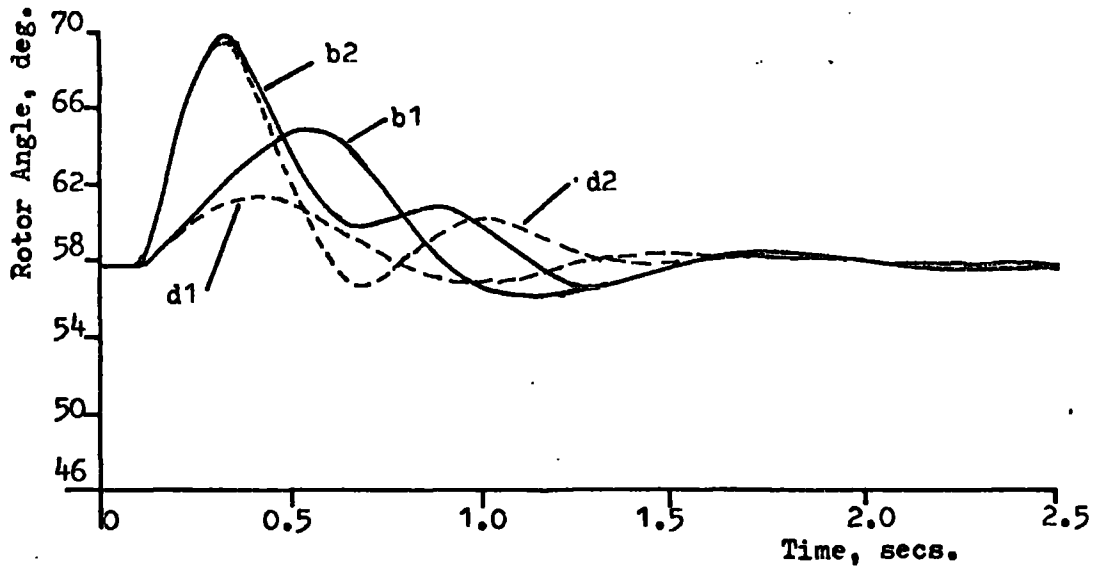


Fig. 7.15(b)

- a1 - M/c 1; a2 - M/c 2; No Control.
- b1 - M/c 1; b2 - M/c 2; Acceleration Feedback Gain = 0.07
Interaction Present.
- c1 - M/c 1; c2 - M/c 2; Interaction Removed.
- d1 - M/c 1; d2 - M/c 2; Acceleration Feedback Gain = 0.07
Interaction Removed.

Fig. 7.15 Rotor Angle Time Responses for Model System Fig. 2.7, Data Appendix H, Subjected to a 3-Phase Fault at The Terminals of M/c 2 for 0.05 secs. Second Order Input Power Regulator Modelled.

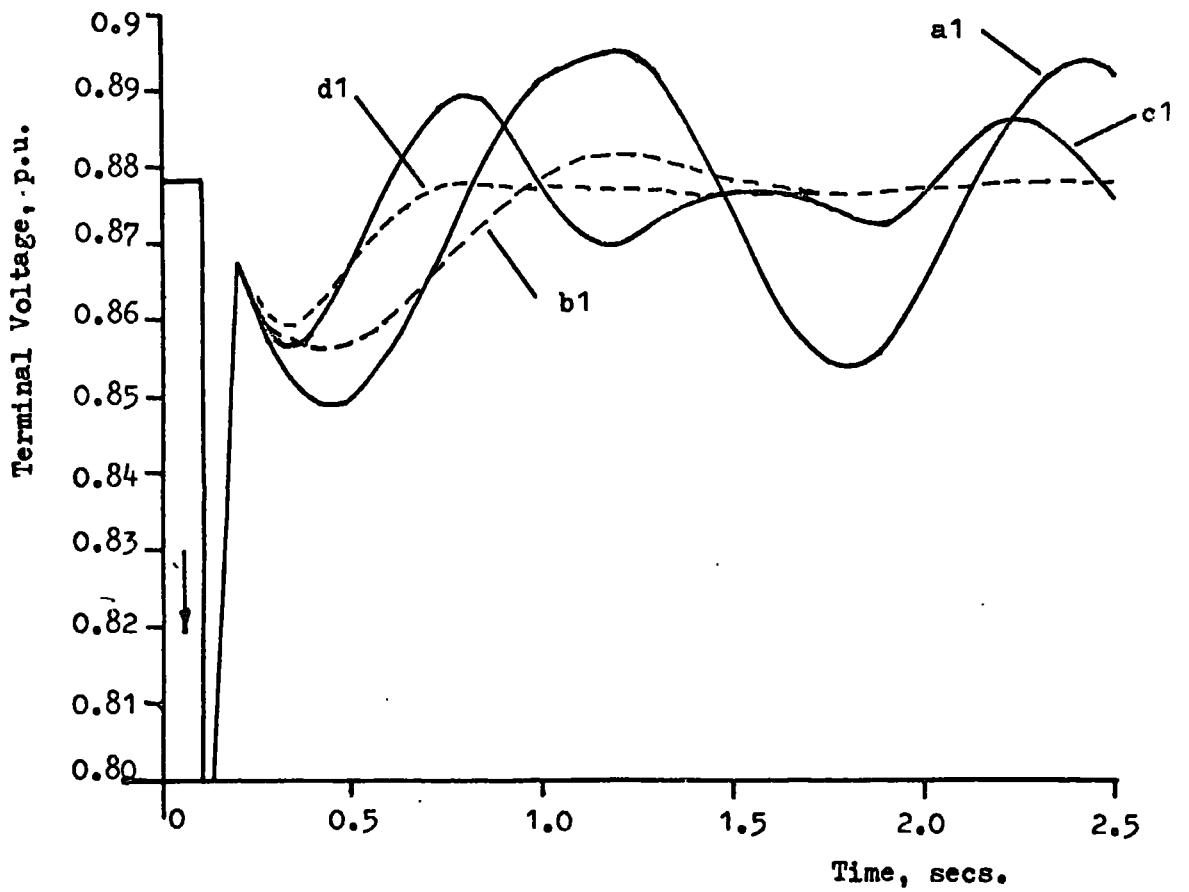


Fig. 7.16(a)

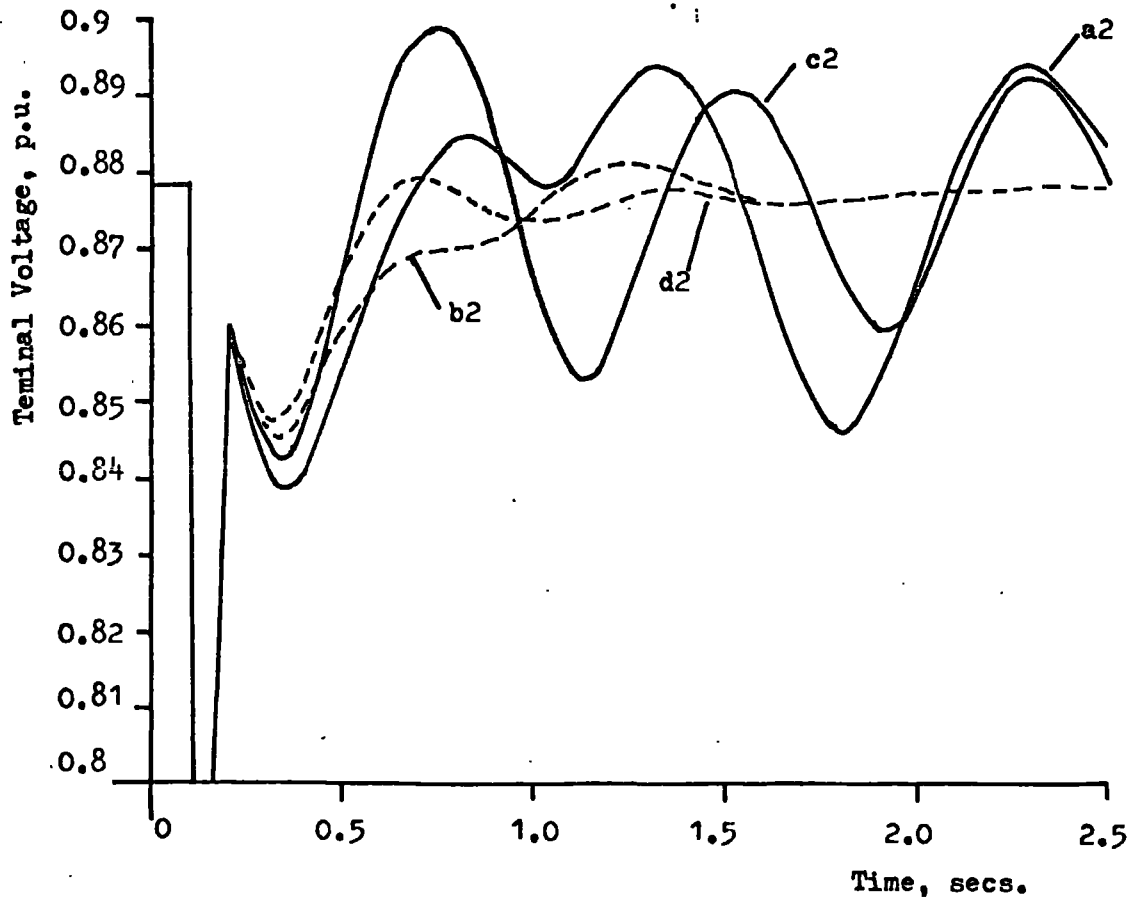


Fig. 7.16 Variation of Terminal Voltage with Time Corresponding to The Rotor Angle Responses of Fig. 7.15

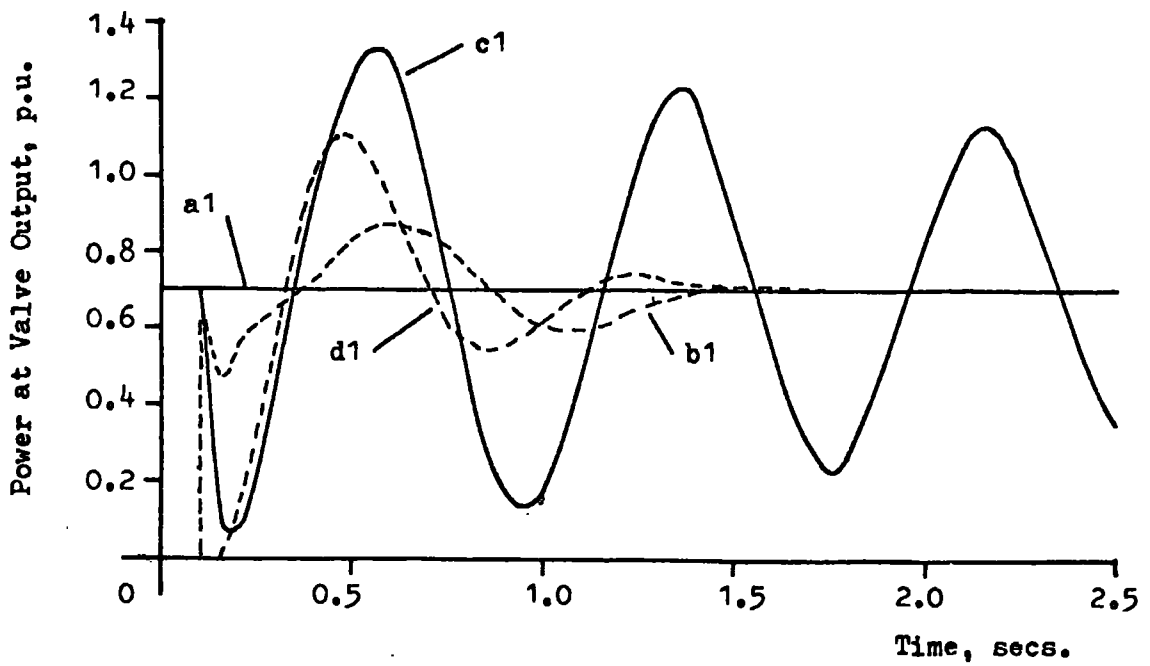


Fig. 7.17(a)

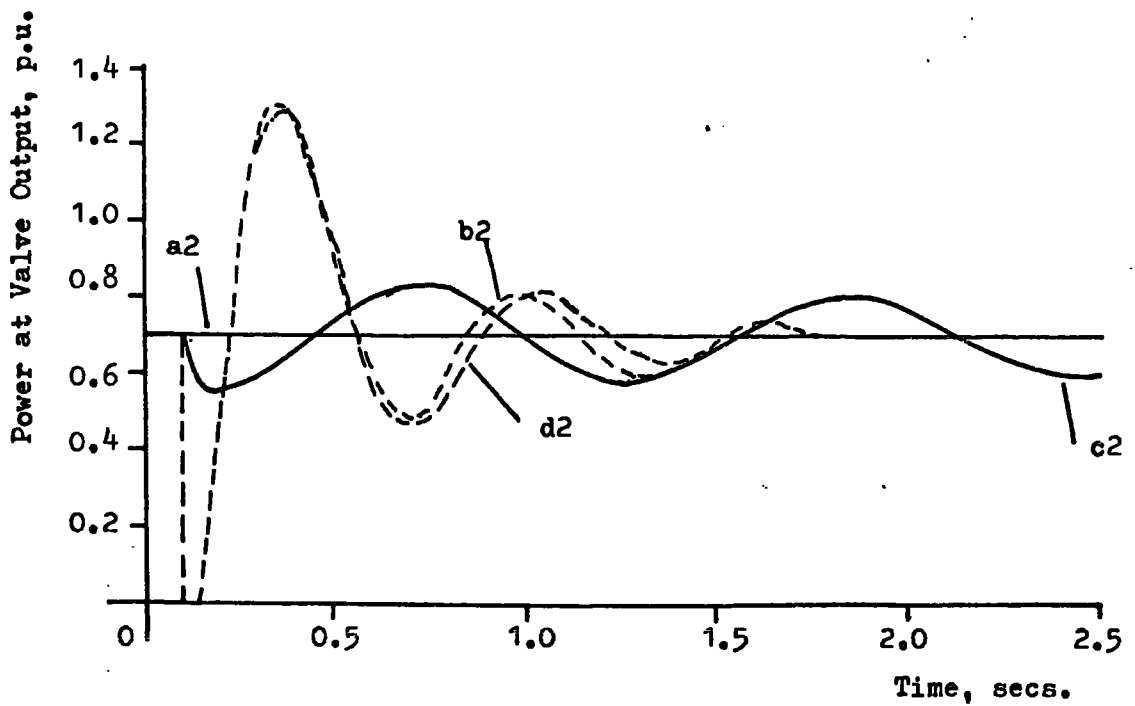


Fig. 7.17(b)

Fig. 7.17 Variation of Valve Output Power With Time Corresponding to The Rotor Angle Responses of Fig. 7.15

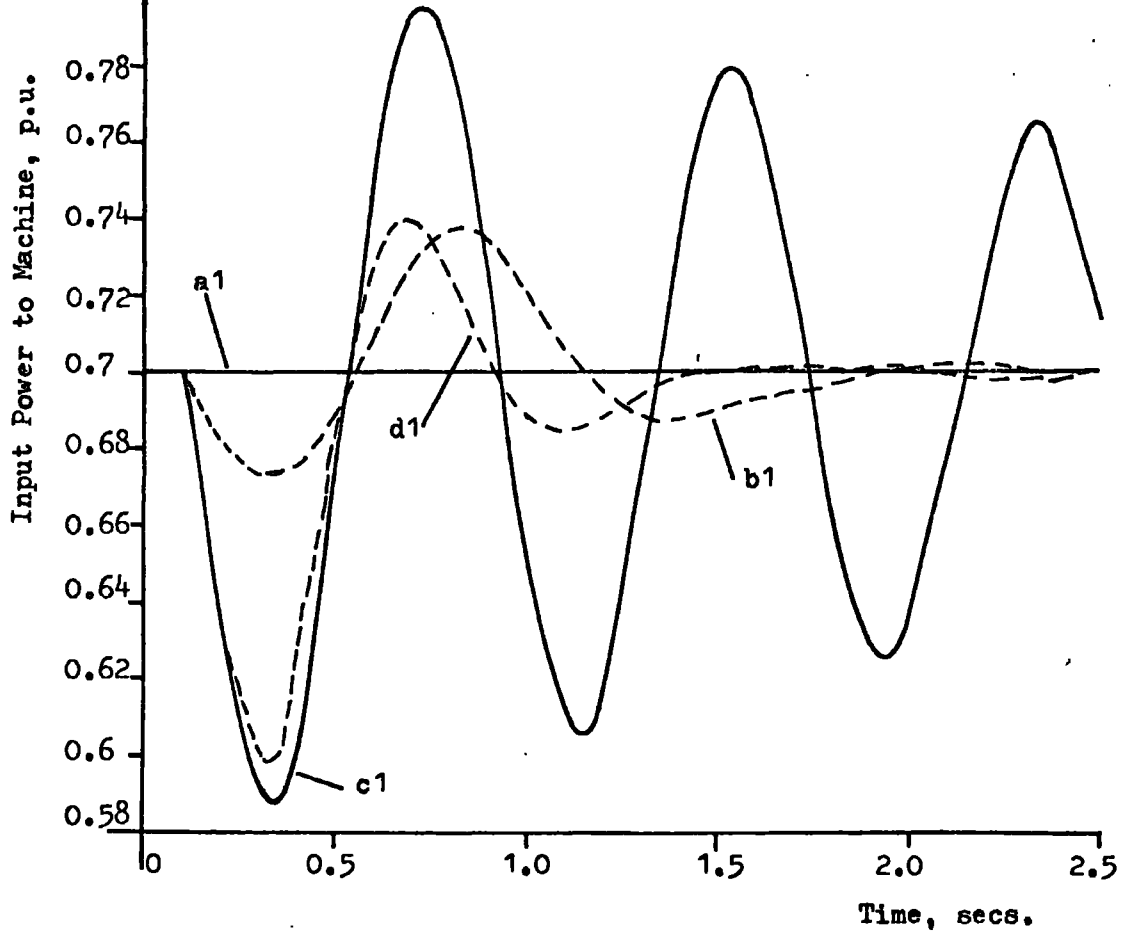


Fig. 7.18(a)

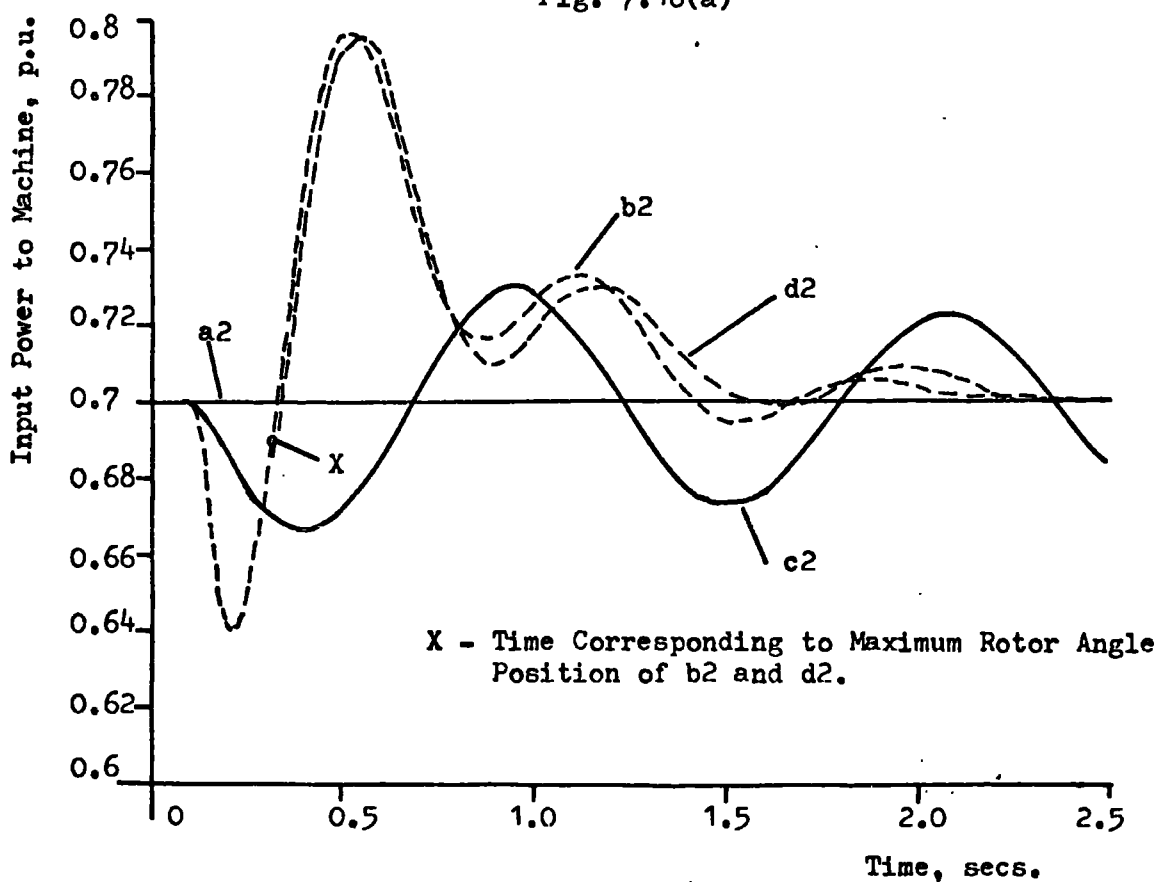
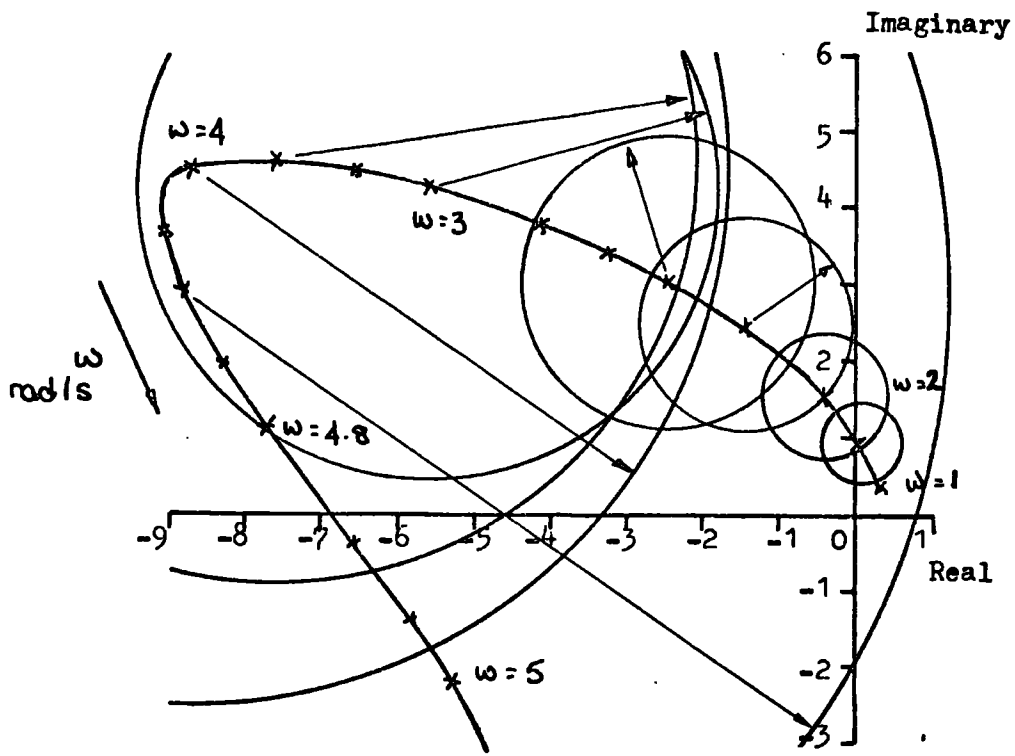
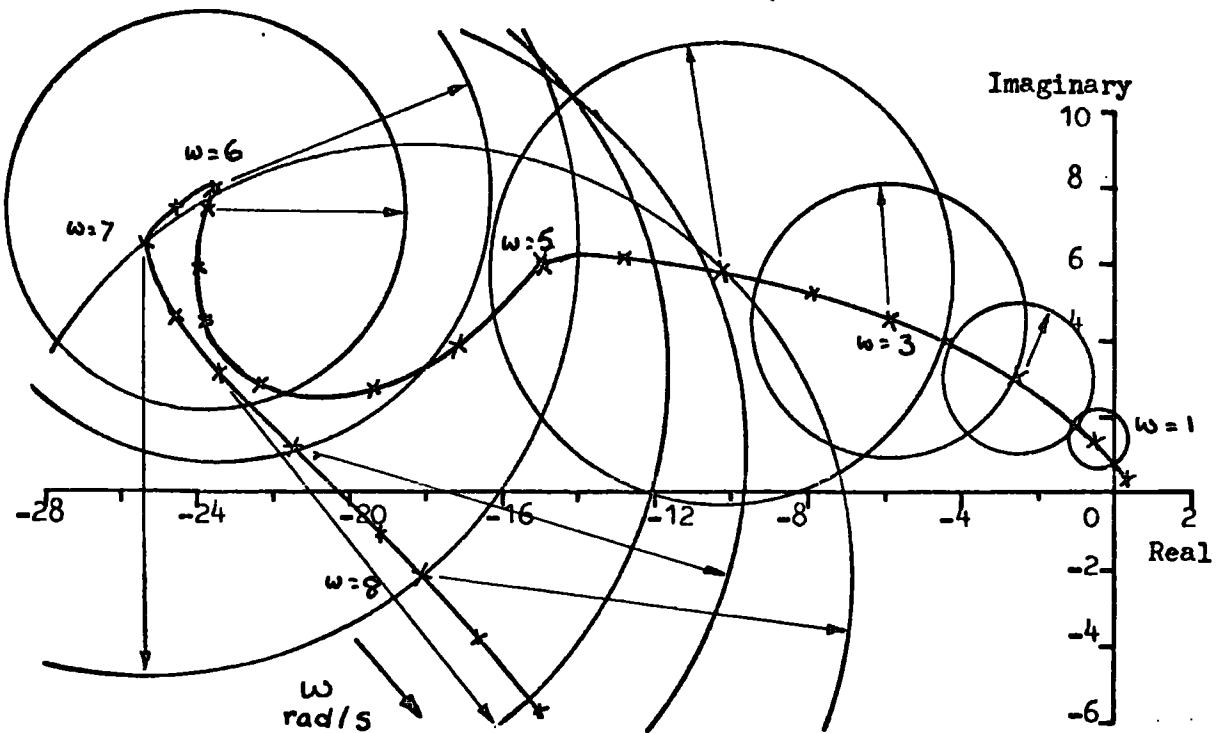


Fig. 7.18(b)

Fig. 7.18 Variation of Machine Input Power with Time Corresponding to The Rotor Angle Responses of Fig. 7.15

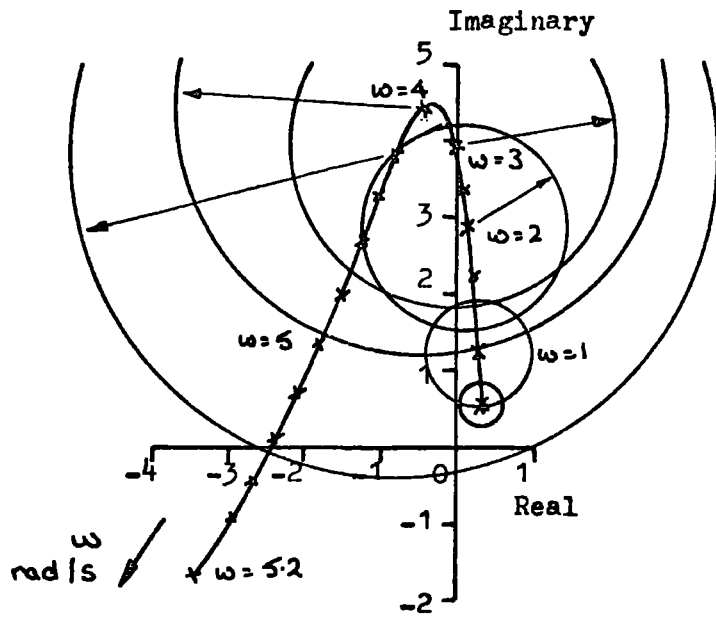


(a) $\hat{q}_{11}(p)$

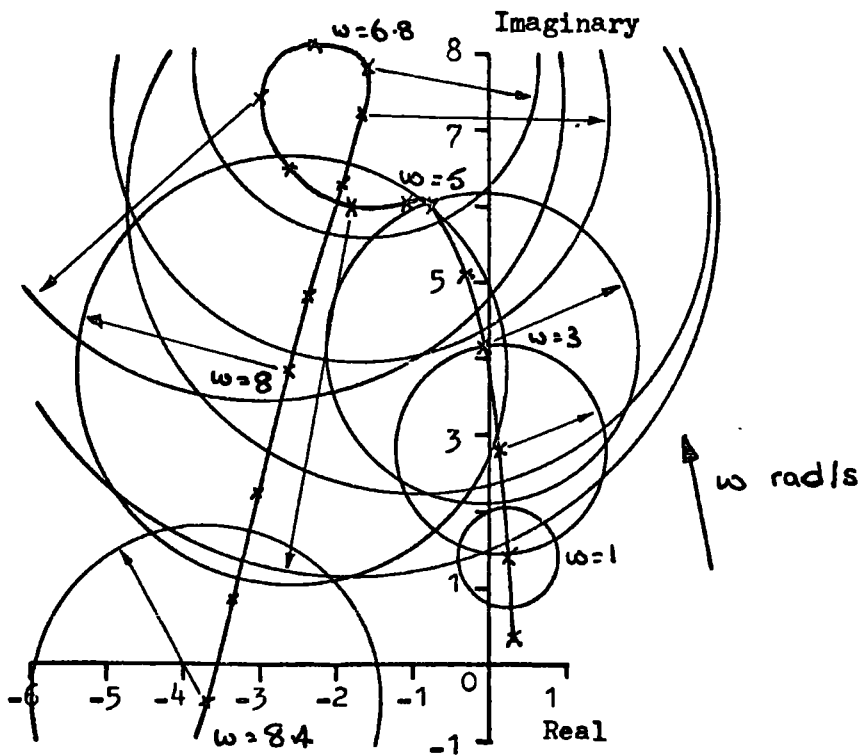


(b) $\hat{q}_{22}(p)$

Fig. 7.19 Inverse Nyquist Plots Showing d-Circles For Excitation Control for Voltage Feedback to The Rotating Exciter.

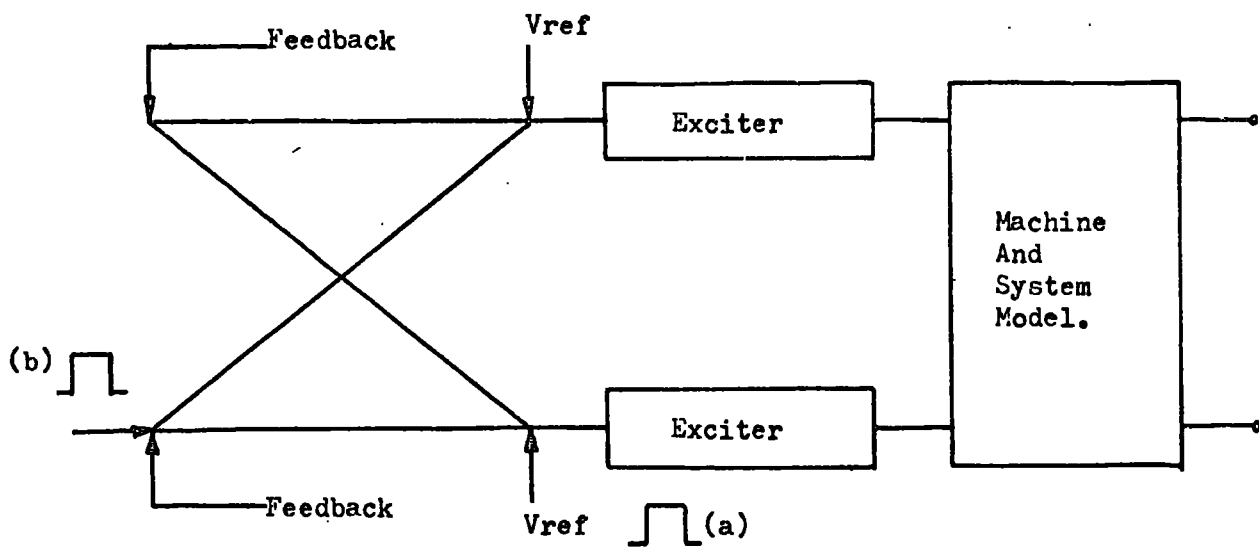


(a) $\hat{q}_{11}(p)$



(b) $\hat{q}_{22}(p)$

Fig. 7.20 Inverse Nyquist Plots Showing d-Circles for Excitation Control with Voltage Feedback to The Static Exciter.



(a) Practical Situation (b) Interaction Completely Removed

Fig. 7.21 Disturbances Imposed On The Excitation System.

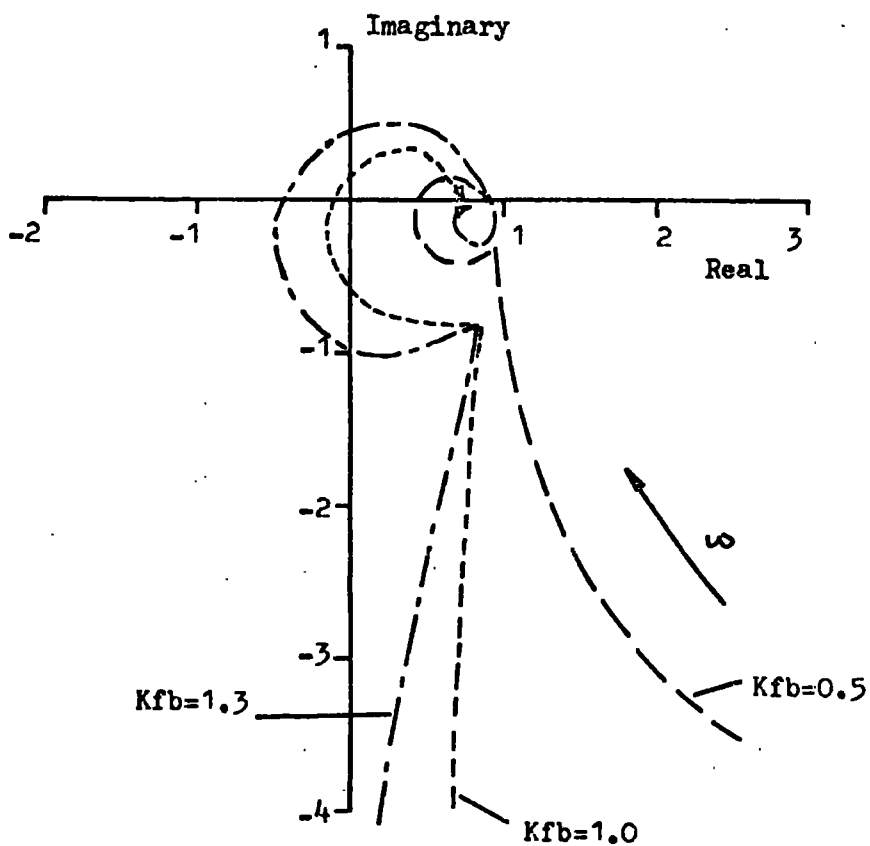
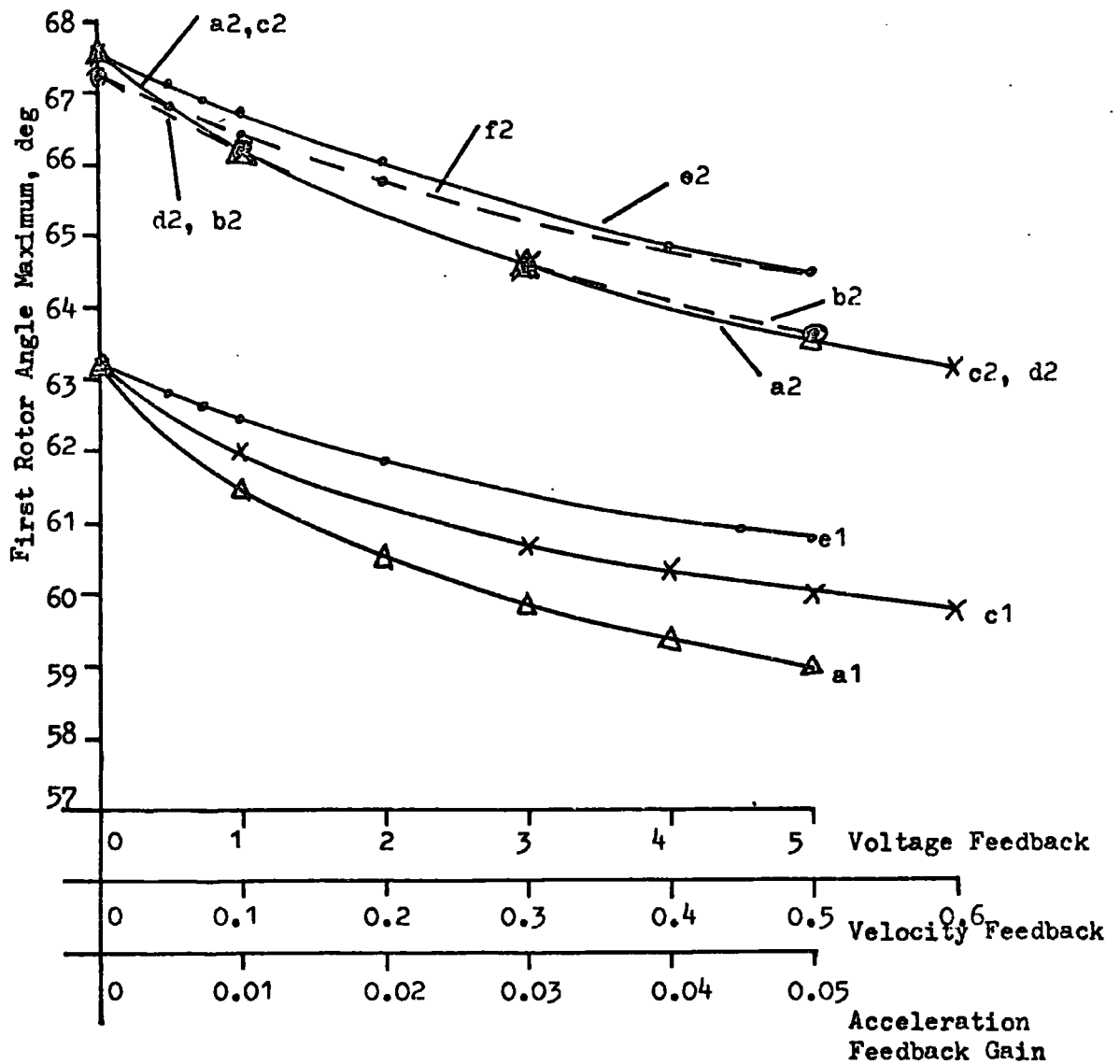


Fig. 7.22 Voltage Feedback To The Static Exciter. Plots Of Det. $T(p)$



1 - M/c 1; 2 - M/c 2

- a1, a2 - Voltage Feedback, Interaction Present.
- b2 - Voltage Feedback, Interaction Removed.
- c1, c2 - Velocity Feedback, Interaction Present.
- d2 - Velocity Feedback, Interaction Removed.
- e1, e2 - Acceleration Feedback, Interaction Present.
- f2 - Acceleration Feedback, Interaction Removed.

Fig. 7.23 The Effect Of Different Excitation Control Schemes On First Rotor Angle Maximum For Small Perturbations. Static Excitation System Modelled.

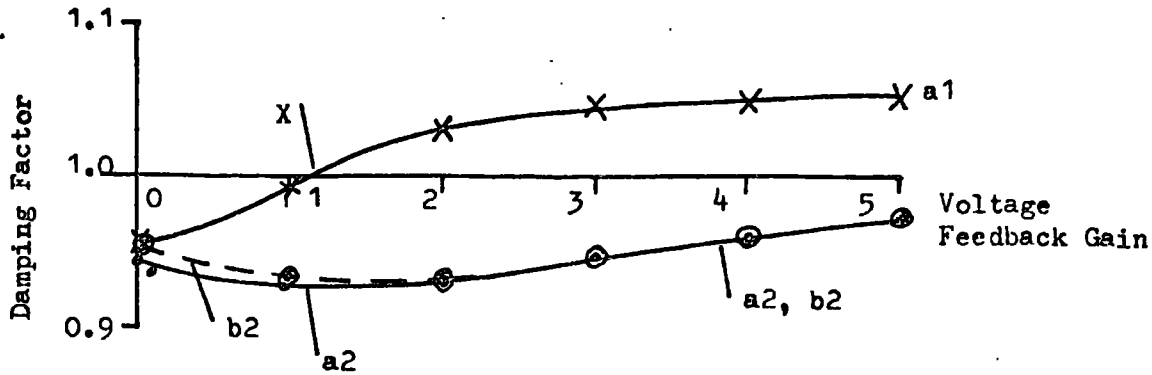


Fig. 7.24(a) The Effect of Voltage Feedback On System Damping

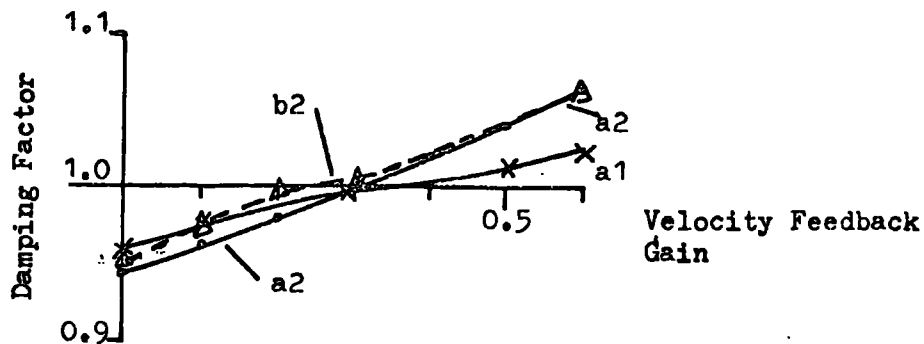


Fig. 7.24(b) The Effect Of Velocity Feedback On System Damping.

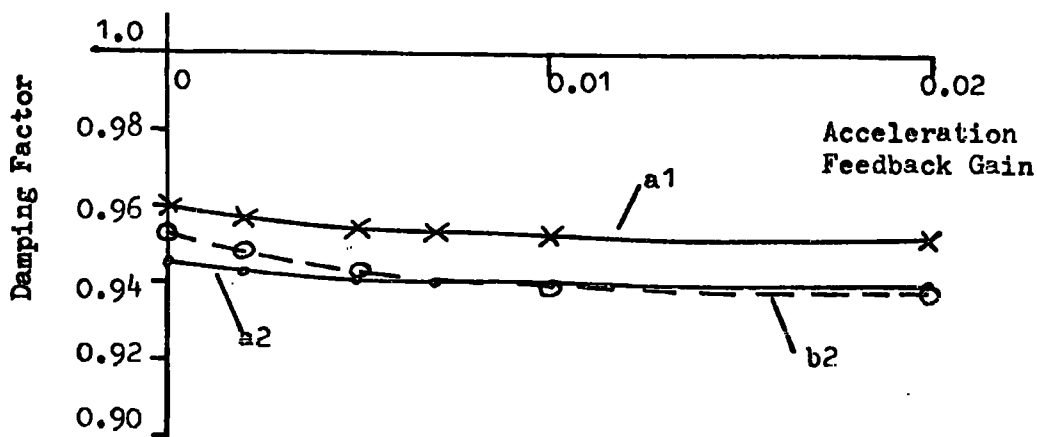
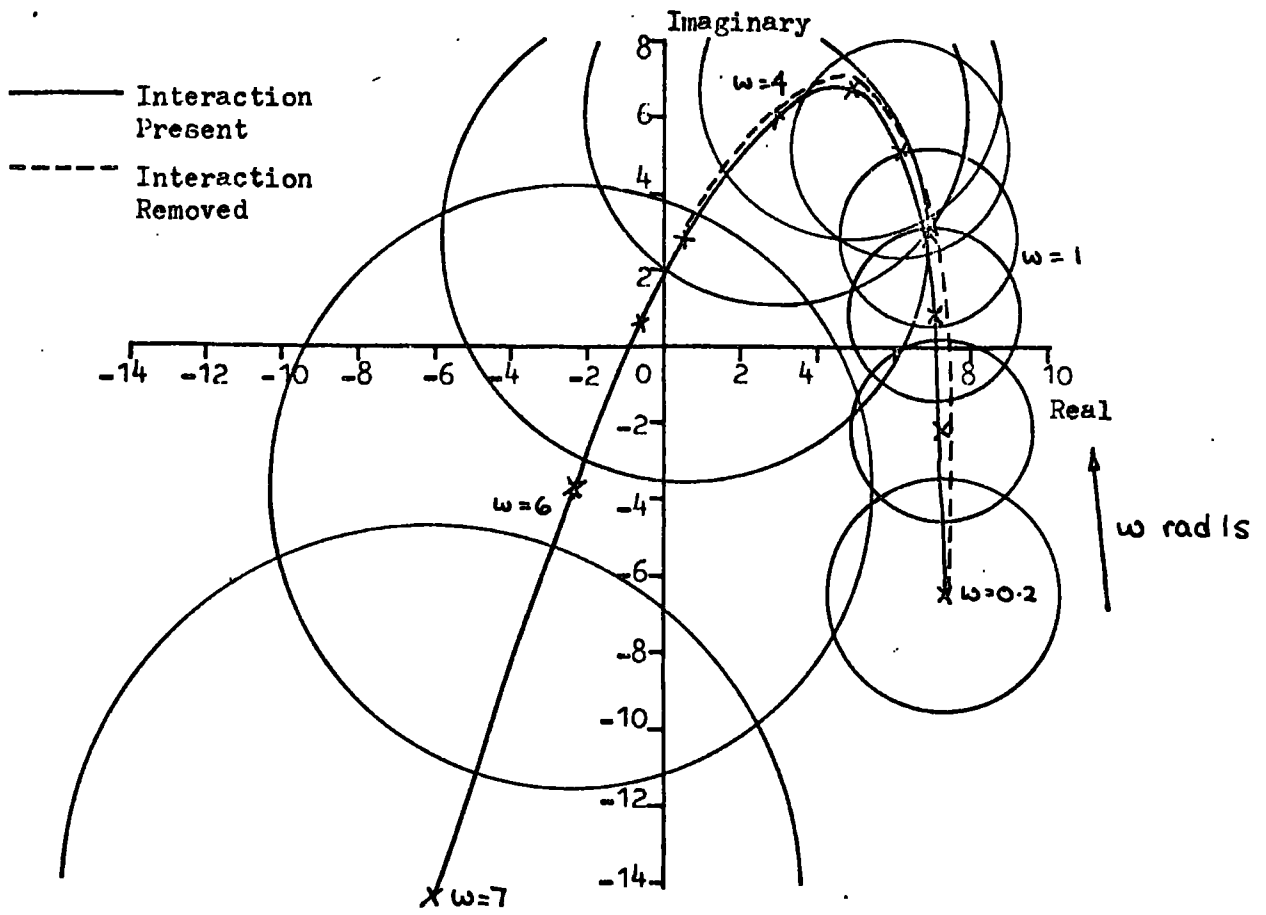
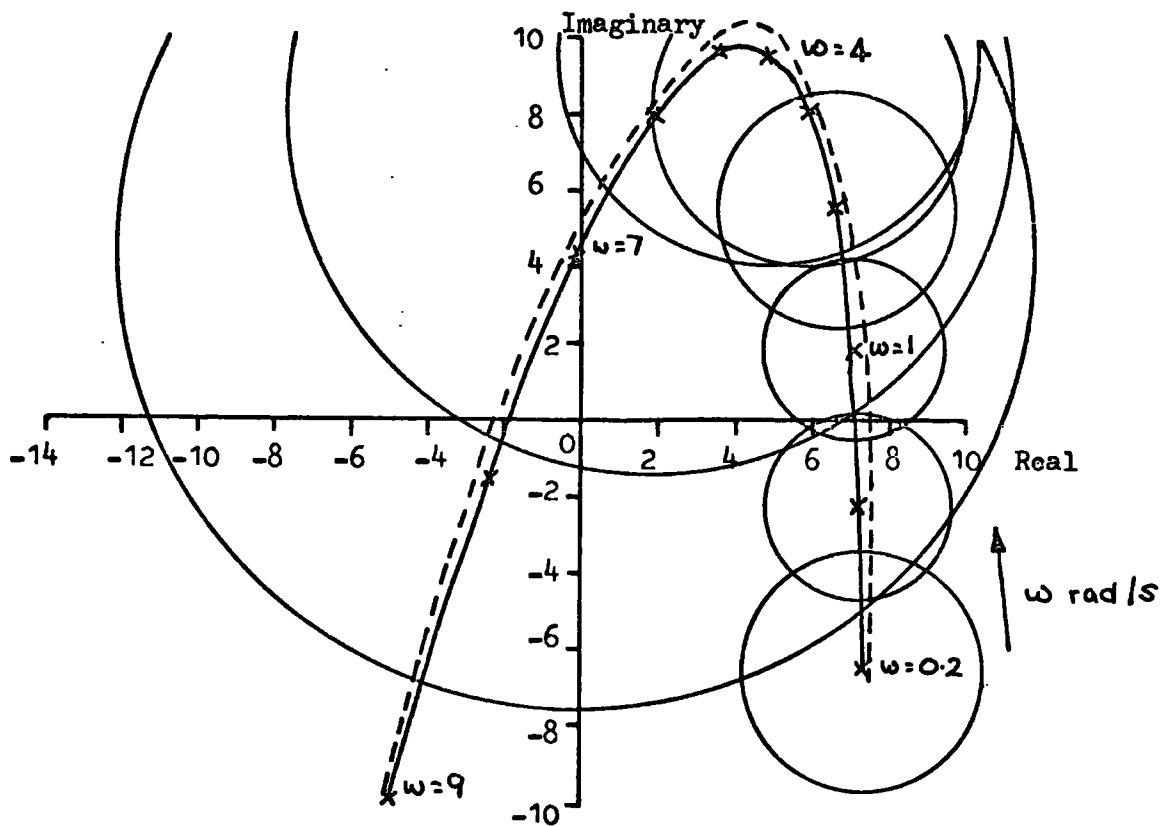


Fig. 7.24(c) The Effect Of Acceleration Feedback On System Damping.

a1 - M/c 1; a2 - M/c 2; Interaction Present.
 b2 - M/c 2; Interaction Removed.

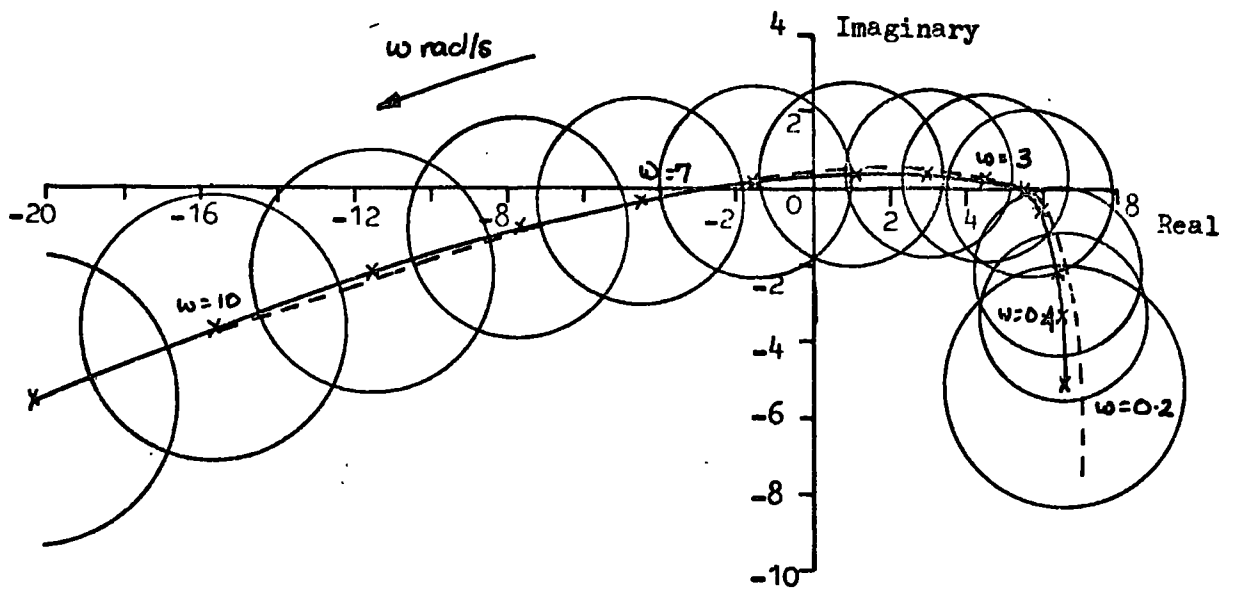


(a) $\hat{q}_{11}(p)$

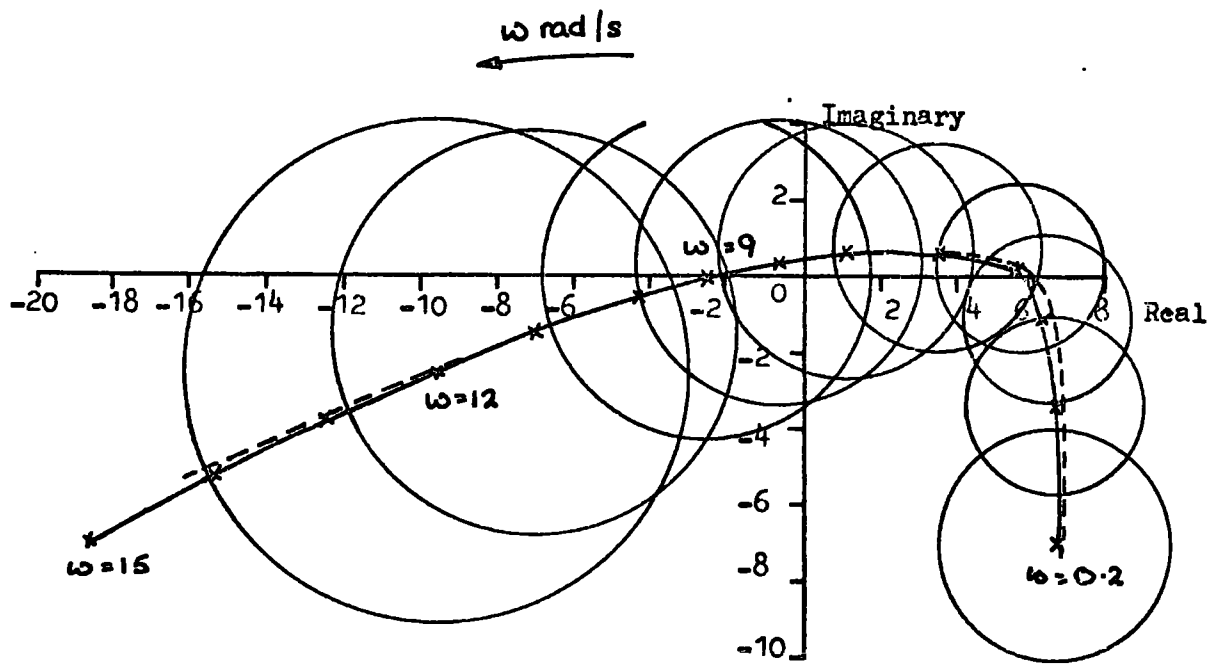


(b) $\hat{q}_{22}(p)$

Fig. 7.25 Inverse Nyquist Plots Showing d-Circles For Excitation Control. Velocity Feedback To A Rotating Exciter.



(a) $\hat{q}_{11}(p)$



(b) $\hat{q}_{22}(p)$

————— Interaction Present.

- - - - - Interaction Removed

Fig. 7.26 Inverse Nyquist Plots Showing d-Circles For Excitation Control. Velocity Feedback To A Static Exciter.

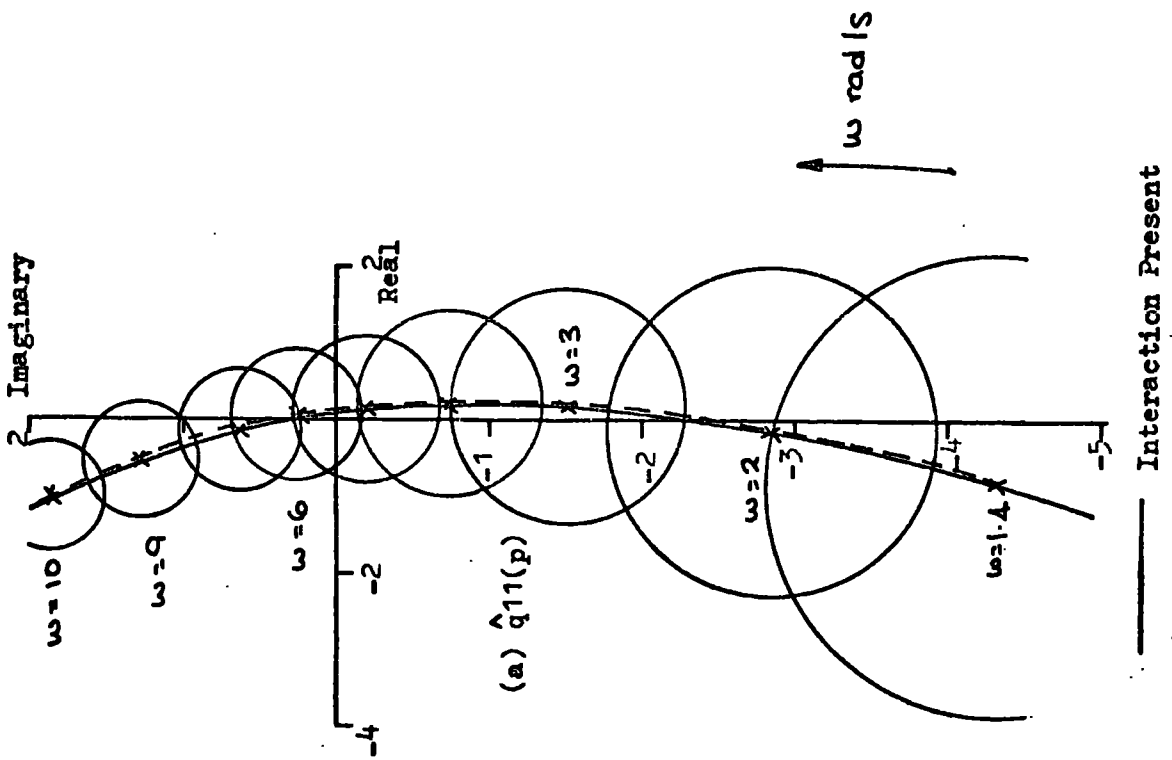
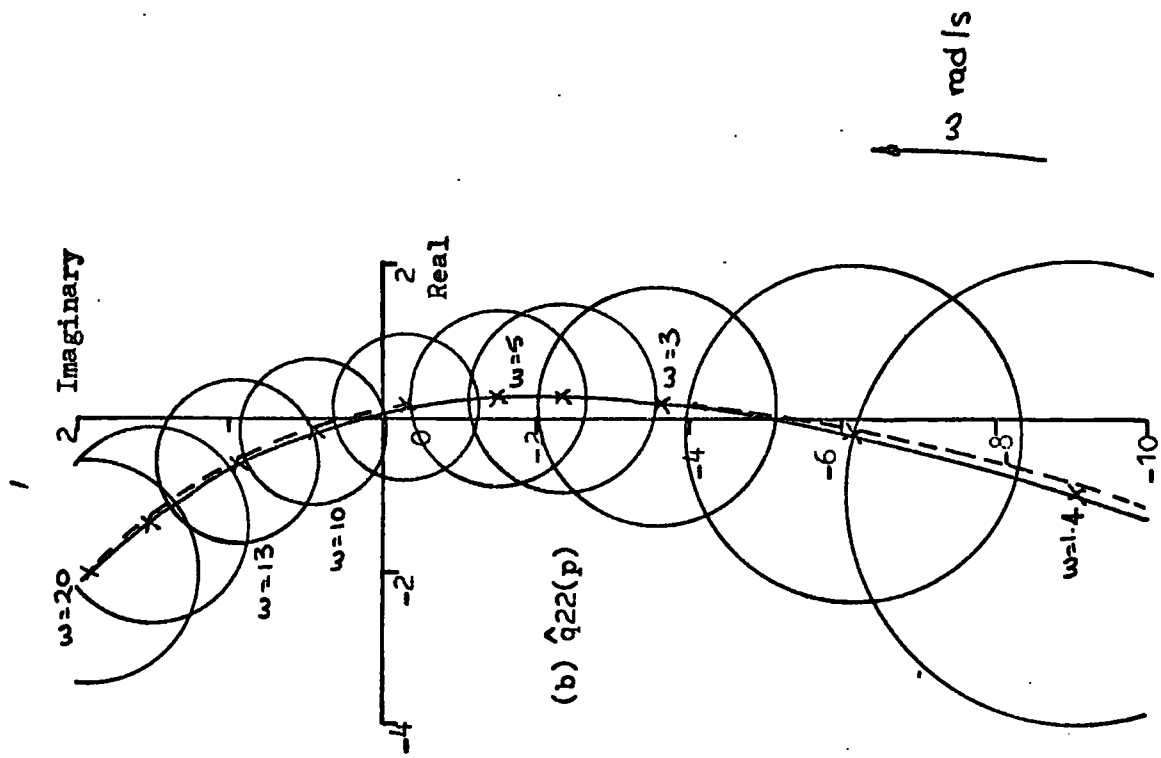


Fig. 7.28 Inverse Nyquist Plots Showing d-Circles For Excitation Control With Acceleration Feedback To The Static Exciter.

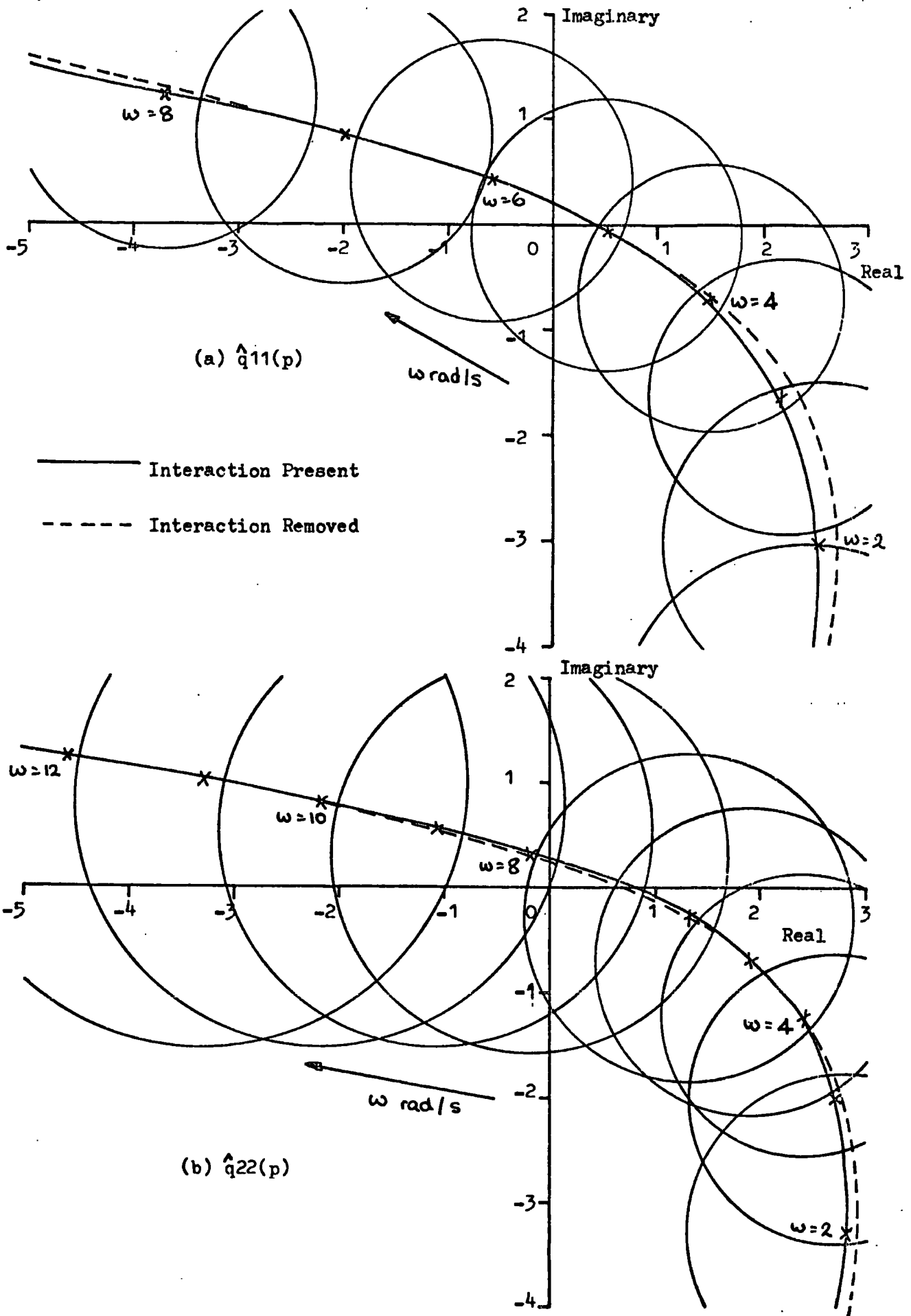


Fig. 7.29 Inverse Nyquist Plots Showing d-Circles For Excitation Control. Acceleration Feedback To a Rotating Exciter.

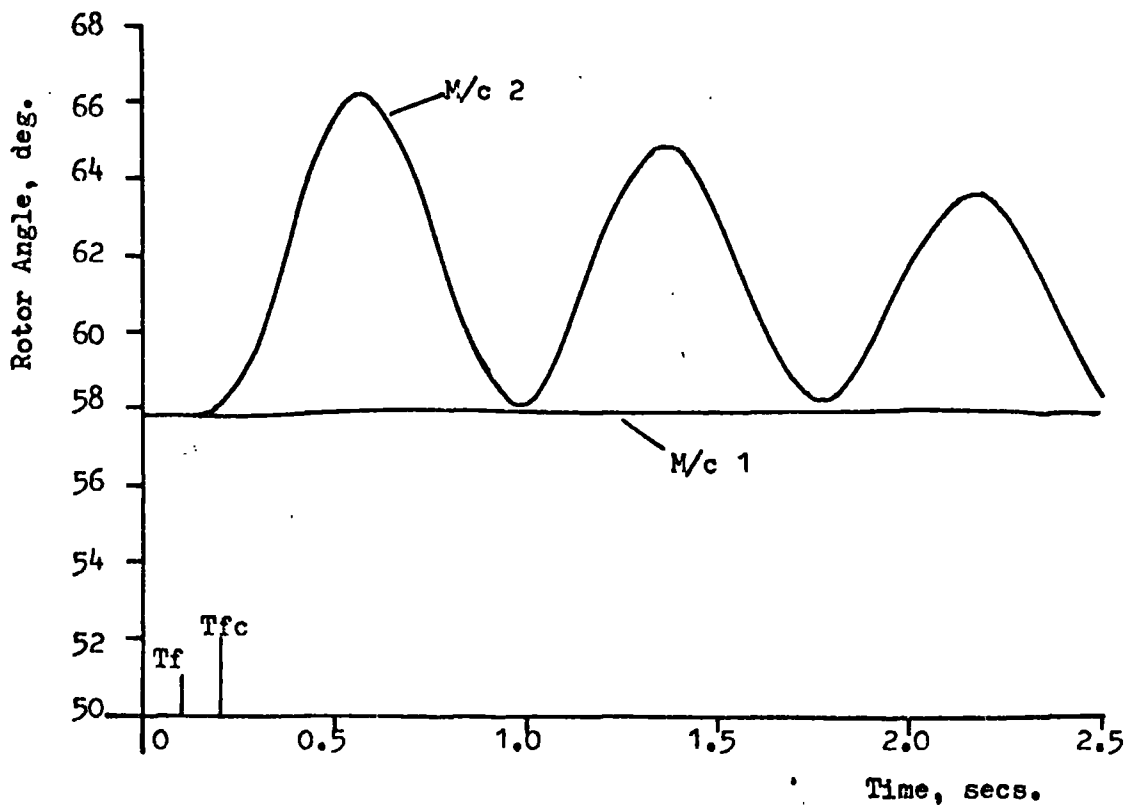


Fig. 7.30(a) Rotor Angle Response For a Step on The Input To The Control Unit. Linear Equations Used.

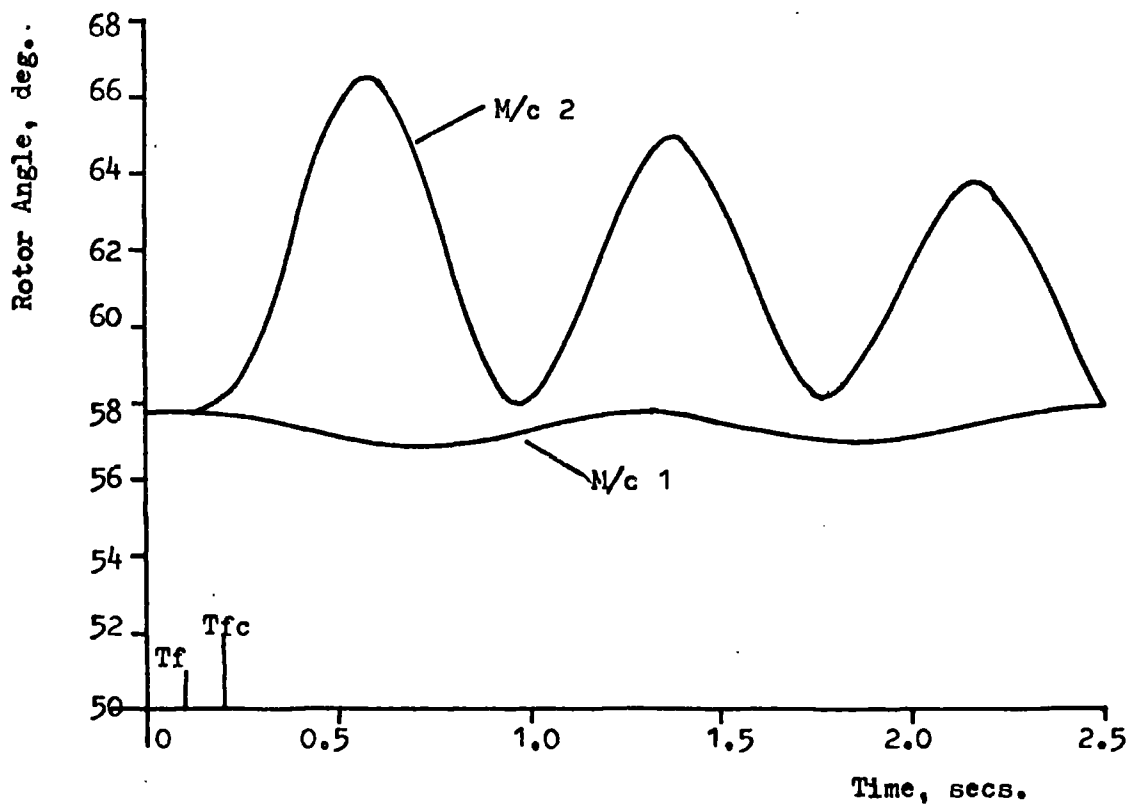


Fig. 7.30(b) Rotor Angle Time Response For A Step Change On $V_{ref}(2)$. Linear Equations Used.

Model System Fig. 2.7, Data Appendix H.

CHAPTER 8.

A NON-INTERACTIVE CONTROL SCHEME - LARGE DISTURBANCES

8.1 GENERAL

In the previous Chapter regulator limits had little effect on the system response as disturbances imposed were only small. By imposing a three phase fault on the terminals of machine 2 in fig. 2.7 for 0.21s, the critical clearing time for the uncontrolled system, large rotor angle oscillations are produced. This allows the effect of the regulator limits on the system response, with and without interaction present to be investigated for different feedback arrangements.

The damping effect of different feedback signals is related to the Nyquist stability of the system and was studied in detail via the I.N. diagrams in the last chapter and consequently does not constitute a major investigation here.

To study the effect of a combined velocity and acceleration feedback signal an acceleration feedback gain of $K_{fb,2} = 0.05$ was used as this produced large, first rotor angle reductions with good subsequent damping when the velocity feedback gain was zero (see fig. 8.3). Further this acceleration feedback gain compensates for the improper phasing introduced by the non-interactive control unit.

8.2 FAST VALVING

8.2.1 ACCELERATION FEEDBACK

For large disturbances increasing the feedback gain initially reduces the first load angle maximum but then causes it to increase curves (e) and (f2) in fig. 8.1(b). This is associated with the mechanical input power to the machine being reversed at the wrong moment in time.

Hughes⁽⁴⁵⁾ states that by using Pontryagin's maximum principle the minimum possible rotor angle swing is obtained by applying the full closing signal to the steam valves on the occurrence of the fault and removing it when the maximum value of rotor swing is obtained. Acceleration feedback closes the valve on the occurrence of a fault but tends to remove this closing signal on fault clearance. By using a large feedback gain it is possible for P_m , the mechanical input power, to increase to such an extent, while δ is still increasing, that the machine tends to accelerate and increase its load angle as demonstrated for a feedback gain of 0.1 by fig. 8.1(b) curves (e). Fig. 8.8(a) shows the increase in P_m causing the increase in first rotor angle swing where point (A) corresponds to the time at which the maximum value of δ_2 is reached.

The flow of synchronising power between the machines causes an increase in the first rotor angle excursion of the unfaulted machine at high feedback gains even though the power limits of this machine may not be met. This effect is shown by curve (e1) in fig. 8.1(b) while fig. 8.8(b) shows the variation of power at the turbine valve with time for an acceleration feedback gain of 0.1, note that the power limits for machine 1 are not reached. Removing interaction counteracts the flow of synchronising power and removes this effect shown by curve (f1) in fig. 8.1(b).

The effect of a non-interactive control unit at low feedback gains (less than 0.01 in this case study) is to increase future rotor angle swings, an effect attributed to the differences between the linear and non-linear models. The linear, non-interactive controller produces a control signal of such magnitude that the power regulator limits of the non-linear model are continually met and improper phasing results. An example of this in fig. 8.11 shows the variation of power at the valve corresponding to the rotor angle response of fig. 8.5.

The control effect of the non-interactive control unit can be thought of as an apparent total feedback signal of varying gain acting round each individual machine. The improper phasing causes this gain, at certain instants, to change sign and introduce negative damping into the system. This results in the increased rotor angle oscillations. Increasing the individual machine acceleration feedback gain partially compensates for the improper phasing by reducing the number of times the power regulator limits are reached, as in fig. 8.9(a). This produces the positively damped response of fig. 8.3. Note the response of machine 2 in fig. 8.3 is more oscillatory than in fig. 8.2, where interaction was present, because of the cross-feedback tending to produce the improper phasing.

The main advantage of the non-interactive controller is its ability to produce a large, beneficial, reduction in the first load angle maximum of the unfaulted machine. This is demonstrated in fig. 8.1(B) where curve (f1) shows lower first load angle maximums than (e1), the corresponding plot for the interactive study. Because of the low fault clearing time used in section 7.8 the effect of the cross feedback from machine 1 had no significant effect on machine 2. Now, however, with the increase in the clearing time cross feedback from machine 1 is of sufficient magnitude to have a positive effect in its tendency to hold the control valve of machine 2 closed on fault removal; point A in fig. 8.9(b) showing a lower value of F_m than the corresponding point in the interactive plot of fig. 8.7. This is responsible for the further decrease in first rotor angle maximum of machine 2, at low feedback gains, shown by curve (f2) in fig. 8.1(b). After fault clearance the cross feedback signal counteracts a substantial amount of the synchronising power flowing from the directly faulted machine, machine 2, to machine 1 producing an increase in the instantaneous difference between the load angles. A greater transfer of synchronising power from machine 2 is allowed producing a further reduction

in the first load angle maximum of machine 2. This effect was discussed in Chapter 7.

If the acceleration feedback gain, k_{fb_i} , is further increased the limits again tend to cause an increase in the first load angle excursion of the directly faulted machine, curve (f2) in fig. 8.1(b).

8.2.2 VELOCITY FEEDBACK

Increasing the velocity feedback gain continually reduces the first load angle maximum as shown by curves (a) in fig. 8.1(a). However this gain has to be limited because of the tendency towards self-induced oscillations as discussed in Chapter 7.

The self-induced oscillations for large disturbances can be related to the I.N. diagrams of fig. 7.7. The Nyquist stability limit deduced from rotor angle time responses for the large three phase fault yields a maximum feedback gain slightly in excess of 0.2, which is comparable with that predicted from the Nyquist diagram of fig. 7.7 and the damping curves of fig. 7.10(A). This is further verification of both the method of representing damping effects in Chapter 7 and the connection between self-induced oscillations and the I.N. diagrams. Fig. 8.6 demonstrates the tendency towards self-induced oscillations with a feedback gain $k_{fb_{1,2}} = 0.2$ while points A1 and A2 are examples of the interaction effects discussed in Chapter 5.

By removing interaction the improper phasing introduced by the controller cannot be compensated for by velocity feedback before self-induced oscillations set in. It is therefore concluded that the use of this non-interacting control scheme with velocity feedback is unsatisfactory for large disturbances.

8.2.3 COMBINED VELOCITY AND ACCELERATION FEEDBACK

The advantages of using a combined feedback signal were discussed in section 7.7. When the system is subjected to a three phase fault the velocity signal tries to hold the valve closed on fault removal but can only slightly reduce the opening signal to the valve produced by the dominant acceleration term. This results in a slight reduction in the first load angle maximum as the velocity gain increases; curves (b) in fig. 8.1(a). This effect is more noticeable in machine 1, curve (b1), as the fault energy associated with this machine is not great enough for the effect of the velocity term to be completely overshadowed by the acceleration signal.

For the reasons discussed previously the removal of interaction produces a substantial reduction in the first load angle maximum of the unfaulted machine. Again because of the dominating behaviour of the acceleration terms in the control signal the velocity feedback gain has little effect on the first load angle maximums as shown by the near horizontal lines, (d1) and (d2) in fig. 8.1(A).

8.3 EXCITATION CONTROL

8.3.1 THE ALTERATION OF FIRST LOAD ANGLE MAXIMUM

Hughes⁽⁴⁵⁾ and Dineley et al⁽⁹⁾ found that using a static exciter and a feedback signal incorporating a term proportional to acceleration higher first swing excursions resulted than in the uncontrolled case. This is demonstrated in fig. 8.12 by points (x) and (u) when the system of fig. 2.7 was subjected to a three phase fault at the common bus, bus 3, for 0.15s (Data Appendix H).

Three factors contribute to this rotor angle increase;

- (i) The acceleration term tends to remove the signal to the exciter on fault removal, as shown by curve (a) in fig. 8.13, whereas

optimum reduction is achieved when a full increasing signal is maintained on the exciter until the initial rotor angle swing reaches its maximum. (45)

- (ii) A static exciter is normally powered from the machine terminal voltage, which, during the fault interval is low giving a low ceiling voltage.
- (iii) The response of a static exciter is very fast providing a large excitation forcing signal.

Consequently during the fault period there is a tendency to provide a high forcing signal which is severely limited by the ceiling voltage. On fault removal the terminal voltage increases providing a "buck" ceiling limit of large magnitude. This allows the acceleration term, on fault removal, to produce high negative field forcing and a reduction in the height of the operating locus, beneath its steady state operating value, while the load angle is still increasing.

This effect could be removed, producing a substantial reduction in first load angle maximum, if high ceiling limits were used with the static exciter. Alternatively a partial solution to the problem is to limit the buck ceiling at 0.0 and hence reduce the negative field forcing producing the reduction in the height of the operating locus. These two solutions are demonstrated by curves (a) in fig. 8.12 where a significant decrease in first load angle is obtained with infinite limits, point (z), while with a buck ceiling limit of 0.0 first load angle excursions comparative with the uncontrolled case are obtained, point (u).

If a rotating exciter is used Hughes (45) has shown that with an acceleration term stabilizing the voltage signal first swing maximum is only slightly greater than if just voltage feedback is used. This is due to the rotating exciter having both a slow speed of response and high working ceiling voltages, typically +6 p.u. and 0.0 p.u.



The advantage of using an acceleration signal is that it increases the positive damping within the system as discussed in section 7.9.4.

With a feedback signal proportional to either terminal voltage or rotor velocity the optimum forcing signal is applied to the exciter during the critical first swing. This produces a reduction in the first load angle maximum as shown by curves (b) and (c) in fig. 8.12. Because the instantaneous magnitude of these signals is never of the same large magnitude as the acceleration term the effect of the ceiling voltages is not so drastic and a reduction in load angle is achieved with the practical working values of ceiling voltage. However as was seen in Chapter 7 the feedback gain must be limited or else self-induced oscillations will be produced.

Implementing the non-interactive controller tends to apply a forcing signal nearer the optimum to the exciter during the critical period and reduces the first load angle maximum. This reduction in first load angle produced by the non-interactive controller with an acceleration feedback gain, $k_{fb,2} = 0.02$, is shown in fig. 8.12, curves (d). With all limit values large reductions are obtained relative to the interactive case, curves (a). However as in the interactive study changing the ceiling limits determines the value reached during the first load angle swing. The field forcing required by this controller to produce maximum load angle reduction is large, typically greater than 10.0 p.u. which is substantially greater than the practical working ceiling voltages. Consequently the more the boost ceiling is limited greater is the first load angle swing. Because the optimum forcing signal is applied during the critical period the buck ceiling limit has little effect on the first load angle swing, see points p and q in fig. 8.12.

8.3.2 SUBSEQUENT LOAD ANGLE REDUCTIONS

The introduction of damping by the different feedback signals was discussed in Chapter 7 where the tendency towards self-induced oscillations with velocity and/or voltage feedback was observed. These feedback signals had to be limited or Nyquist instability resulted. In comparison the limit imposed on the acceleration feedback was to prevent an overdamped response from being produced.

For large disturbances with interaction present the acceleration feedback forces the exciter to operate in a partial bang-bang mode until the increase in the positive damping forces the excitation voltage from the ceiling limit to its steady state value over a short time period, fig. 8.14(b). The slow response of the field winding to this change, caused by the large field open circuit time constant, T_{do}' , results in a slow decay in the height of the operating locus. This slow decay produces an apparent final load angle value less than the steady state value, see fig. 8.14(a). However as shown in fig. 8.14(a) this load angle value will slowly rise to its steady state position as the height of the operating locus decays. A buck ceiling limit of 0.0 was used to obtain fig. 8.14. If, however, the buck ceiling limit has a negative value, as in fig. 8.17(a), a similar effect is observed with the apparent final value reached by the rotor angle being greater than the steady state value. To guarantee this effect does not become excessive and produce a distorted response it is necessary to impose a limit on the acceleration feedback gain, depending on both the system and regulator parameters, particularly the ceiling voltages.

The effect of the non-interactive control unit is similarly dependent on the exciter ceiling voltages. With infinite limits two substantially non-interacting curves are produced, fig. 8.15. However using practical ceiling limits there is a tendency for the field forcing

to continually reach the ceiling voltages, as in fig. 8.16(b), which results in improper phasing and distorted response similar to fig. 8.16(a). The improper phasing can be substantially reduced if an acceleration feedback signal is used whereas neither velocity or voltage signals can provide the necessary compensation before self-induced oscillations set in. The effect of acceleration feedback and velocity feedback relative to fig. 8.16 is shown in fig. 8.17 and fig. 8.18 respectively.

Consequently the non-interactive control unit should only be employed if high ceiling limits are available and then either velocity, acceleration or voltage feedback can be used to shape the response as improper phasing does not exist. However if the exciter is subject to low ceiling limits an acceleration feedback signal is necessary to compensate for the improper phasing produced by the limits.

Similar results are obtained when a rotating exciter is used.

8.4 THE EFFECT OF INTERACTION REMOVAL ON THE STABILITY LIMIT

The control methods have been shown to reduce first load angle maximums and introduce positive damping into the system. Because of the increase in the positive damping the danger of multiswing instability is reduced and critical clearing time becomes dependent on the first load angle excursion. Consequently any change in the stability boundary can be related to the change in first load angle maximum resulting from the different control arrangements.

An example of this is demonstrated for control of input power in fig. 8.19 where the change in the stability limit can be related to the change in first load angle maximum of machine 2 in fig. 8.1. As the fault is applied to the terminals of machine 2 it is this machine that is most susceptible to instability and is consequently the limiting factor in determining the overall system stability limit.

Fig. 8.19 demonstrates that in increasing the system stability boundary the use of the combined acceleration and velocity signal, with interaction removed, line (e), is the best control scheme for input power control. With this control arrangement the increase in critical clearing time over the uncontrolled case is 0.06s or 3 cycles. Further fig. 8.19 only considers the change in the first load angle of machine 2 and takes no account of the drastic reduction in the first load angle of the indirectly faulted machine, machine 1. This is one of the most beneficial effects produced by interaction removal and helps substantiate the argument for the added control complexity of interaction removal.

8.5 CONCLUSION

The positive damping of individual alternators is increased by the use of an acceleration feedback signal. This signal has to be limited or else both an increase in the first load angle maximum and a distorted response will be obtained. These effects are associated with the practical output limits of the regulator. The increase in the load angle is most pronounced when a static exciter is used as such an excitation system is powered from the machine terminal voltage giving a low ceiling voltage during the fault period. The increase in first load angle oscillation is small compared with the substantial positive damping introduced into the system by the static exciter and is thus preferred to the rotating exciter.

The limit on the acceleration feedback gain is dependent not only on the regulator limits but also on the fault size, position and duration. Increasing the regulator limits will produce both a well damped response and reduced first load maximum. However for practical and economic reasons the use of regulator limits much above 6 p.u. is not feasible. In the case of excitation control limiting the buck ceiling limit helps reduce the first load angle maximum.

If a velocity signal to the input power regulator and either a velocity or voltage signal to the exciter is used the optimum signal for first load angle reduction is applied. However this signal has to be limited because of the tendency towards self-induced oscillations. Thus the optimum signal for first load angle reduction does not necessarily produce the best subsequent response.

Good overall control is obtained if a velocity and acceleration signal is applied to the input power regulator. The acceleration signal stabilises the velocity term and produces good subsequent damping while during the first swing the velocity term tends to apply a more optimum control signal than acceleration feedback alone. This reduces the first load angle maximum. This feedback control can be further strengthened by removing interaction.

If interaction is removed the discrepancies between the linear and non-linear models, particularly the use of regulator limits, produces improper phasing giving a distorted response. This improper phasing can be largely compensated for by an acceleration feedback signal. Velocity and/or voltage feedback, depending on the regulator, cannot compensate the improper phasing. Consequently the beneficial effect of removing interaction is limited, for large excursions, to the cases where an acceleration stabilising signal can be used.

When considering first load angle reduction, interaction removal tends to apply a control signal nearer the optimum during the critical first swing. This produces a reduction in the first swing maximum and a corresponding increase in the stability limit. This reduction in the first swing maximum is particularly noticeable in the machine, or machines, not directly affected by the fault and is one of the major advantages of the non-interactive controller.

In general improved response is obtained if interaction is removed with an acceleration signal producing the correct compensation. This improvement in response being more pronounced when control is applied to the input power regulator than to field excitation.

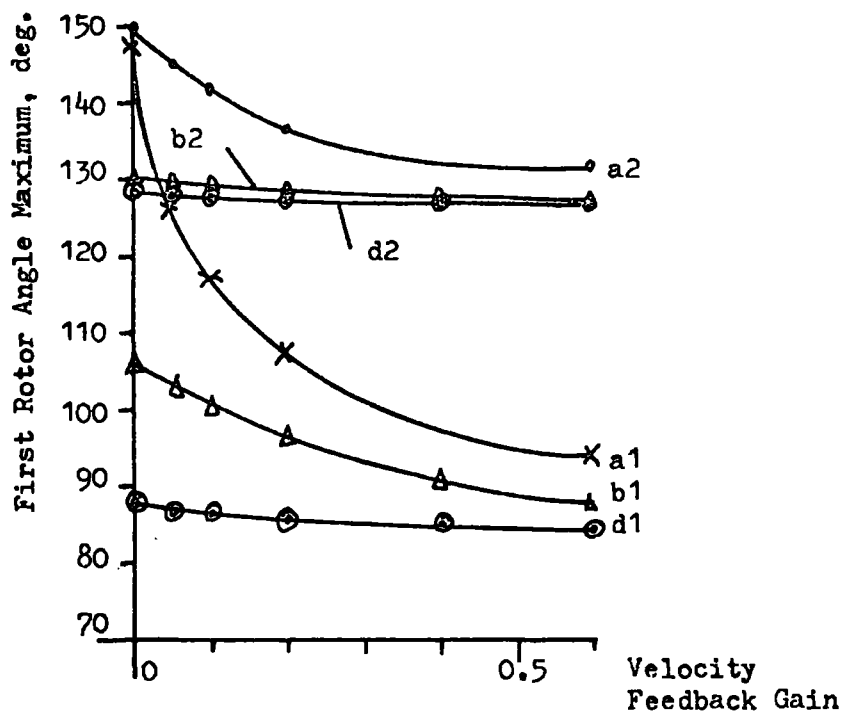


Fig. 8.1(a)

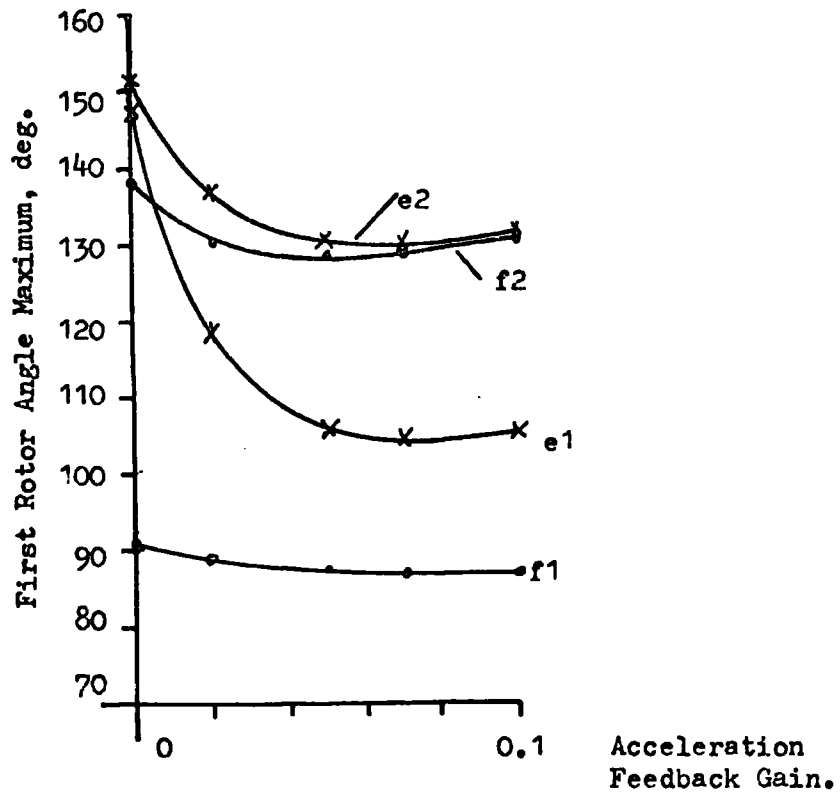


Fig. 8.1(b)

1 - M/c 1; 2 - M/c 2

a1, a2 - Velocity Feedback, Interaction Present.

b1, b2 - Velocity + 0.05 Acceleration Feedback, Interaction Present.

d1, d2 - Velocity + 0.05 Acceleration Feedback, Interaction Removed.

e1, e2 - Acceleration Feedback, Interaction Present.

f1, f2 - Acceleration Feedback, Interaction Removed.

Fig. 8.1 The Effect of Input Power Control Schemes on First Rotor Angle Maximum for A 3-Phase Fault To Earth On The Terminals Of Machine 2. A Second Order Input Power Regulator Assumed.

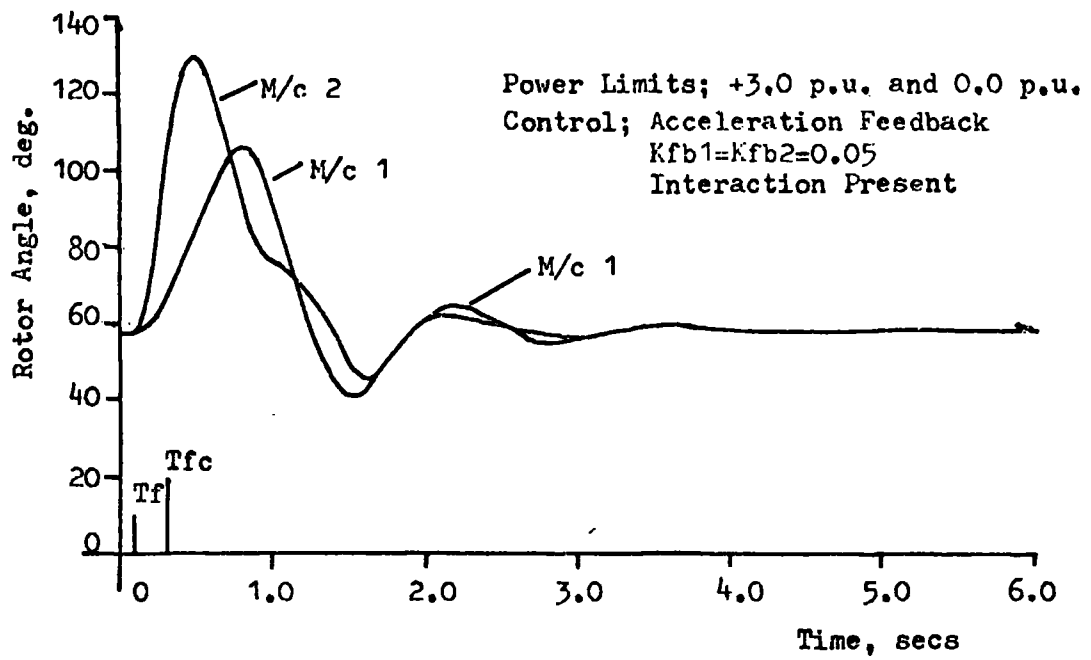


Fig. 8.2 Rotor Angle Time Response For A 3-Phase Fault At The Terminals Of Machine 2 For 0.21 secs.

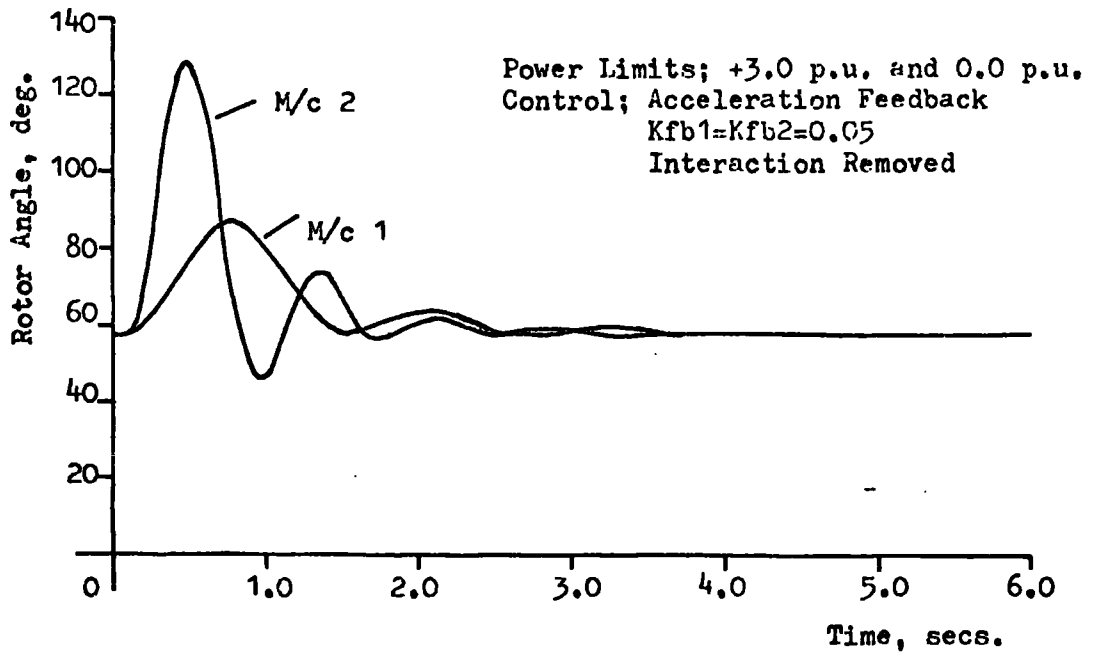


Fig. 8.3 Rotor Angle Time Response For A 3-Phase Fault At The Terminals Of Machine 2 For 0.21 secs.

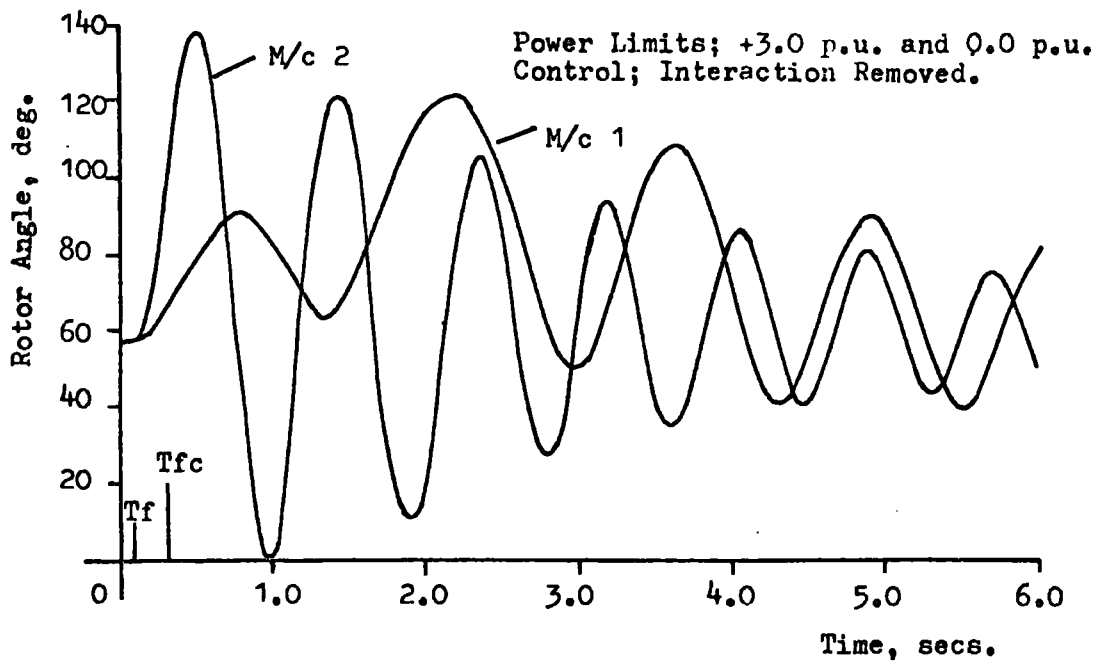


Fig. 8.5 Rotor Angle Time Response For A 3-Phase Fault At The Terminals Of Machine 2 For 0.21 secs.

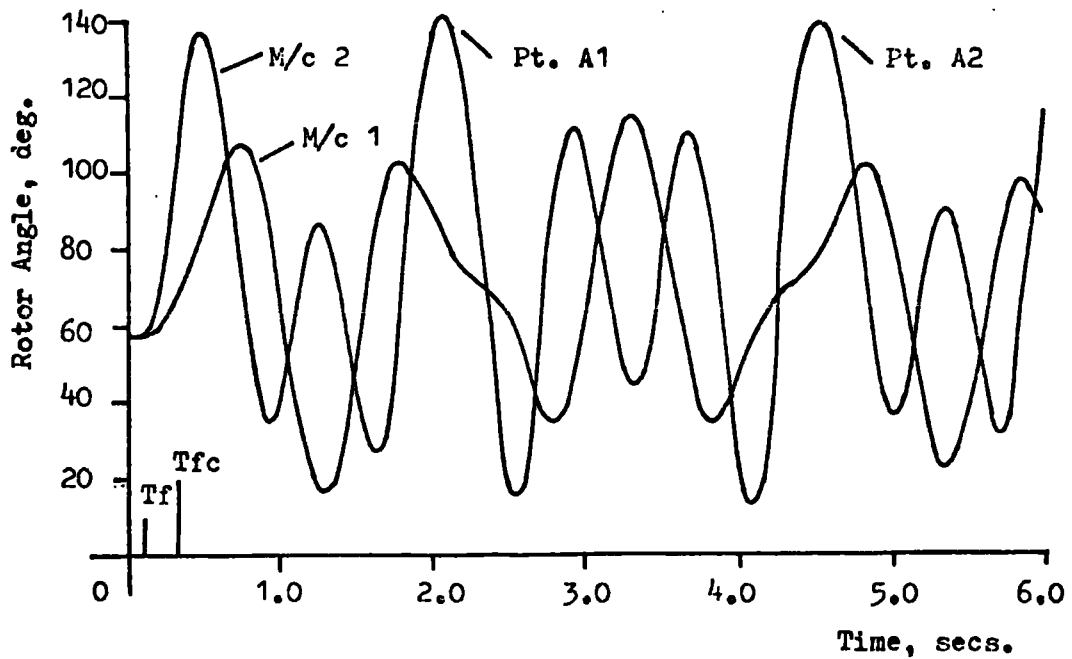


Fig. 8.6 Rotor Angle Time Response For A 3-Phase Fault At The Terminals Of Machine 2 For 0.21 secs. Control; Velocity Feedback, $K_{fb1}=K_{fb2}=0.2$, Interaction Present. Power Limits; +3.0 p.u. and 0.0 p.u.

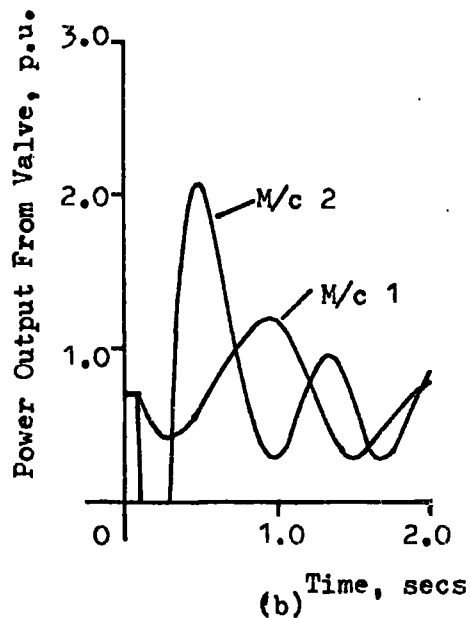
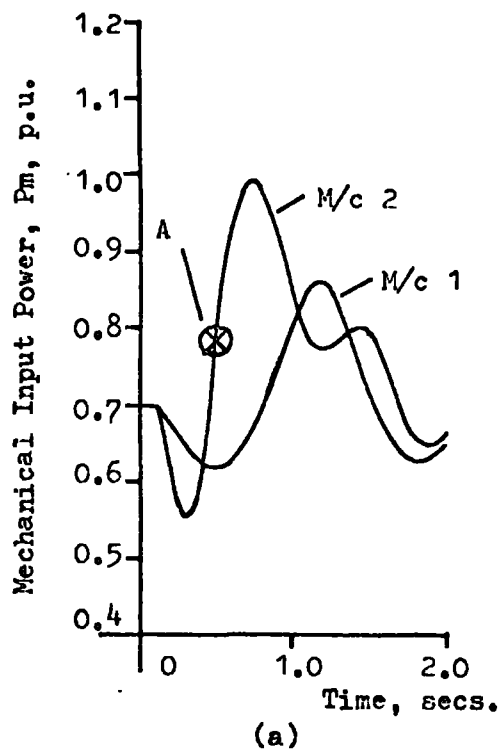


Fig. 8.7 Variation of Machine Input Power and Power At Valve Output Corresponding To The Rotor Angle Response Of Fig. 8.2

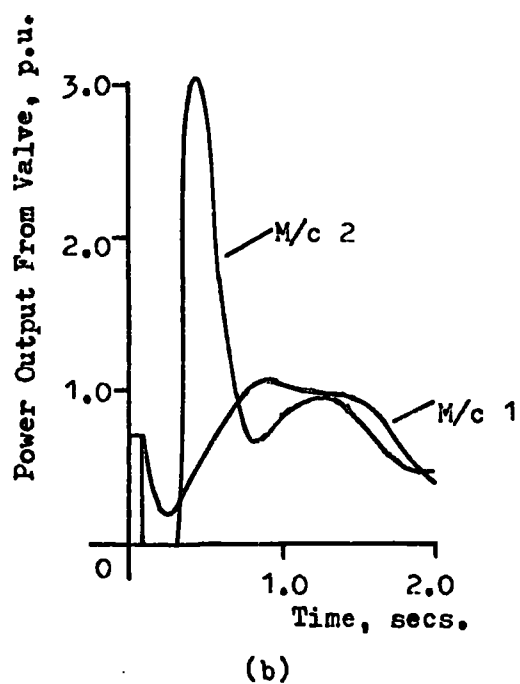
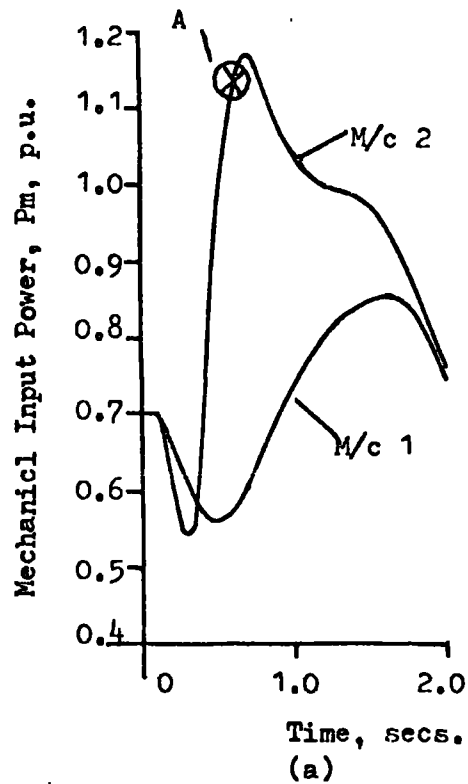


Fig. 8.8 Variation of Machine Input Power and Power At Valve Output For A 3-Phase Fault On The Terminals Of Machine 2 For 0.21 secs. Power Limits +3.0 p.u. and 0.0 p.u. Acceleration Feedback Gain $K_{fb1}=K_{fb2}=0.1$. Interaction Present.

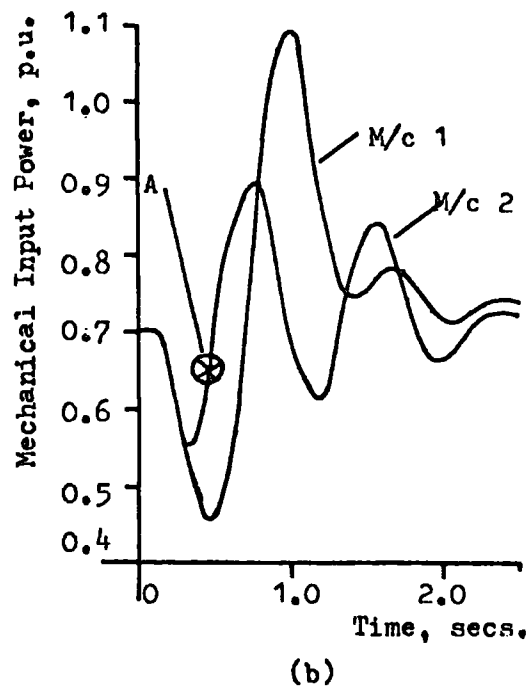
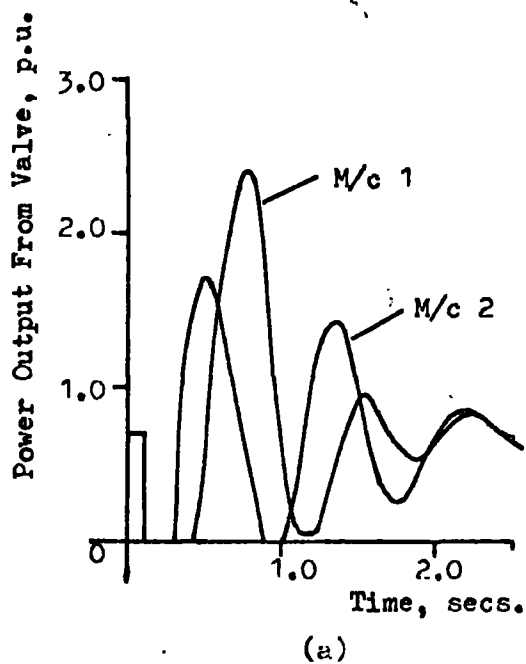


Fig. 8.9 Variation of Machine Input Power and Power At Valve Output Corresponding To The Rotor Angle Response Of Fig. 8.3. Power Limits; +3.0 p.u. and 0.0 p.u. Acceleration Feedback Gain $K_{fb1}=K_{fb2}=0.05$. Interaction Removed.

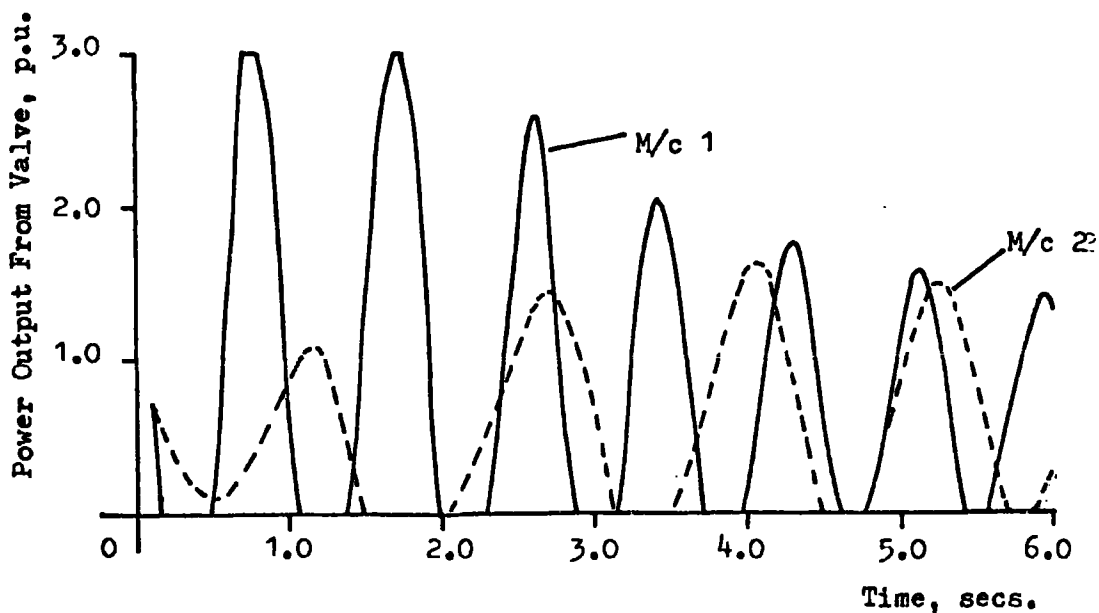
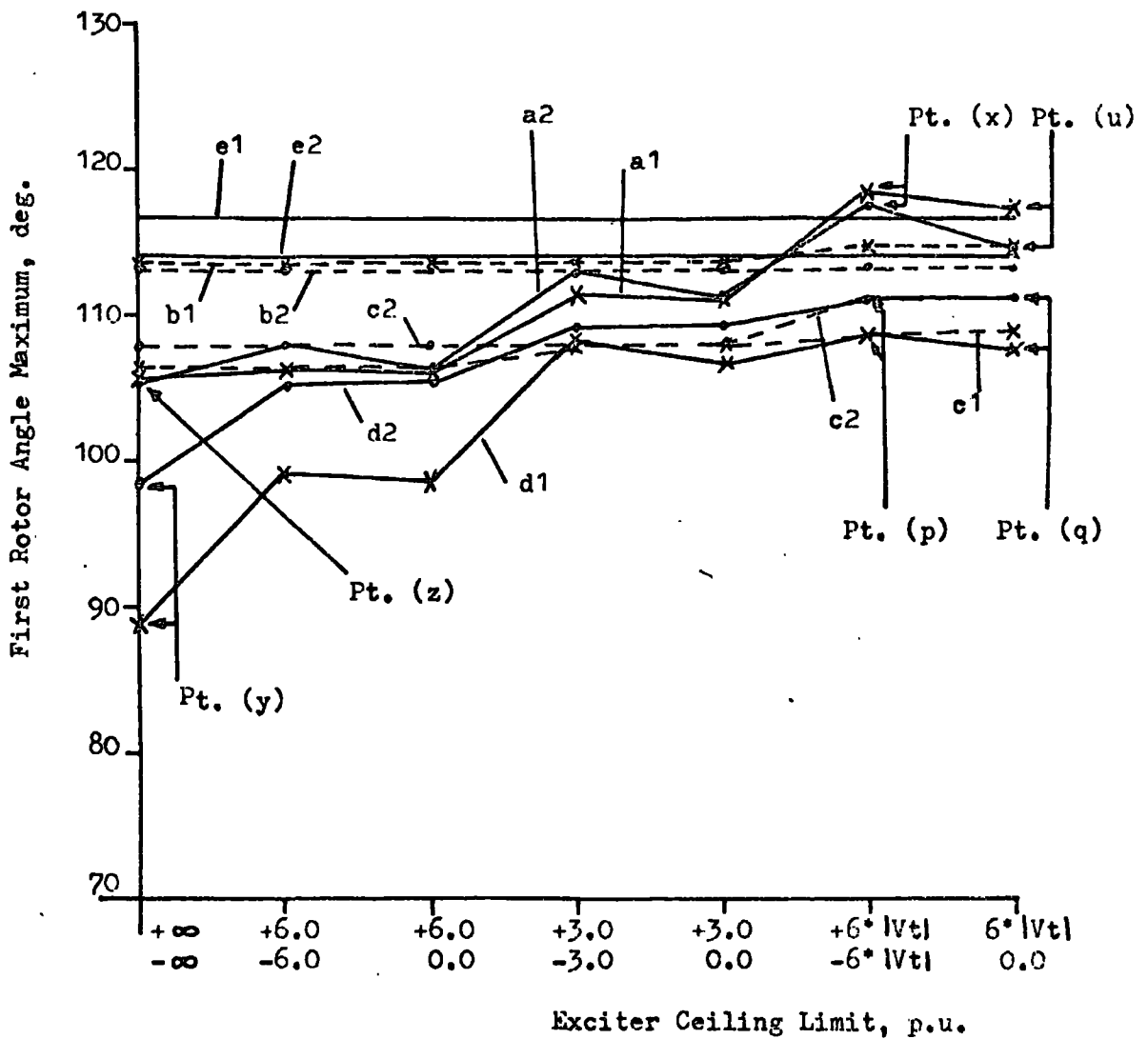


Fig. 8.11 Variation Of Power Output Of Valve Corresponding To The Rotor Angle Response Of Fig. 8.5. Power Limits 3.0 p.u. And 0.0 p.u. Interaction Removed.



1 - M/c 1; 2 - M/c 2.

- a1, a2 - Acceleration Feedback, $Kfb1=Kfb2=0.02$. Interaction Present.
- b1, b2 - Voltage Feedback, $Kfb1=Kfb2=0.1$. Interaction Present.
- c1, c2 - Velocity Feedback, $Kfb1=Kfb2=0.1$. Interaction Present.
- d1, d2 - Acceleration Feedback, $Kfb1=Kfb2=0.02$. Interaction Removed.
- e1, e2 - No Control. Interaction Present.

Fig 8.12 The Effect Of Ceiling Limits In A Static Exciter On First Rotor Angle Maximum For Various Feedback Arrangements.

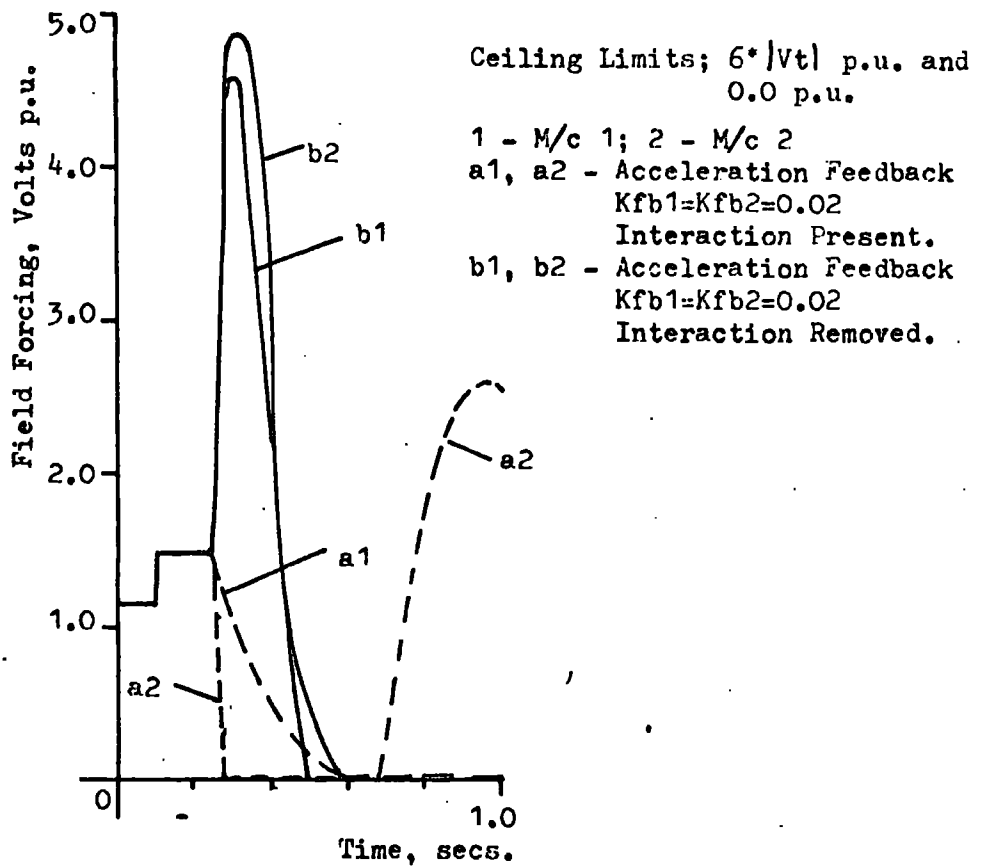


Fig. 8.13 Variation Of Excitation Voltage As A Result Of Acceleration Feedback To The Static Exciter. 3-Phase Fault On Bus 3 Of Fig. 2.7 For 0.15 secs. Data Appendix H.

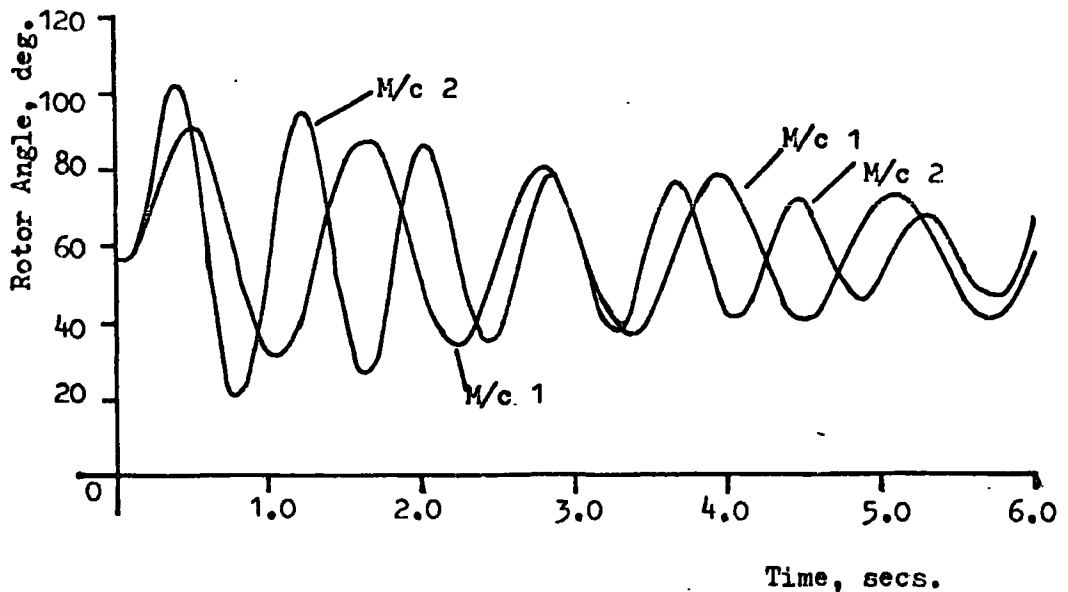


Fig. 8.15 Rotor Angle Response Demonstrating The Effect Of The Non-Interactive Control Unit In Conjunction With A Static Exciter Operating With Infinite Limits.

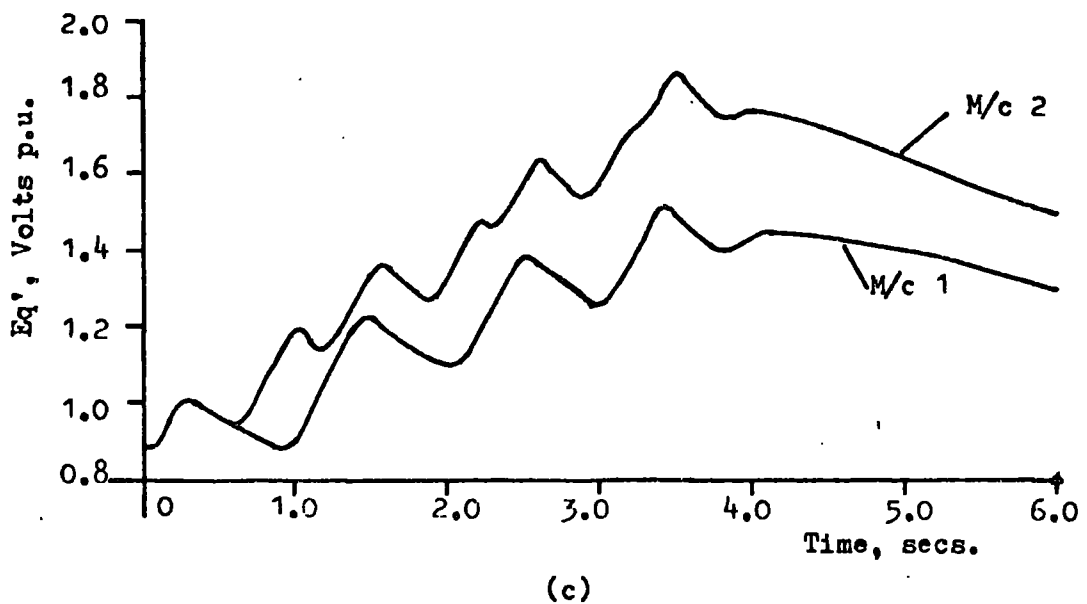
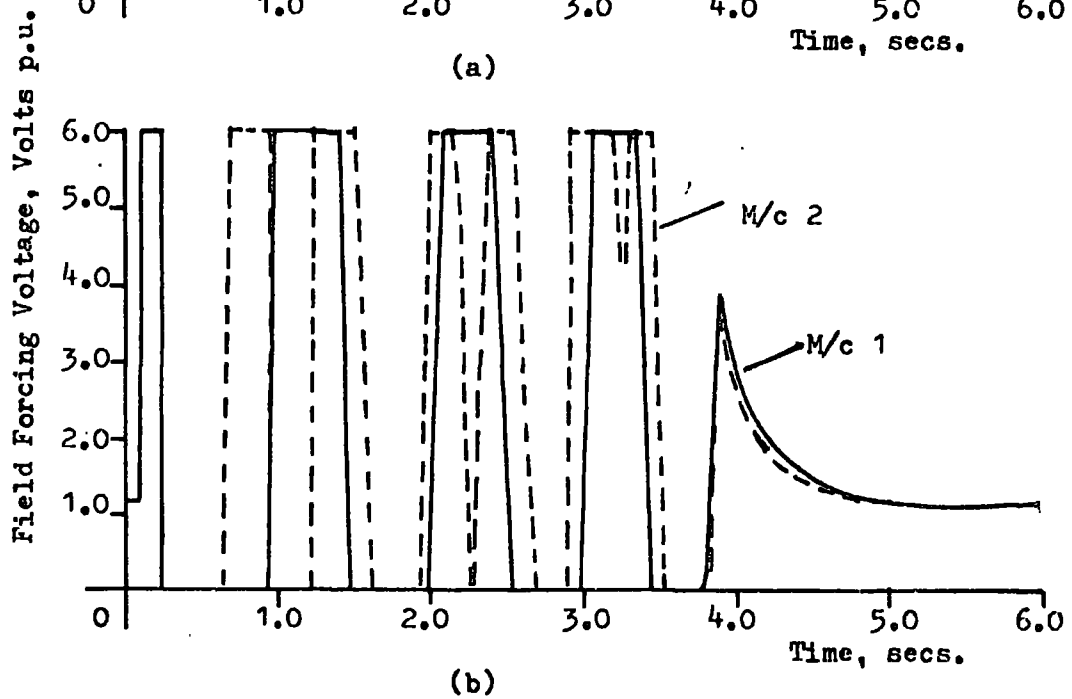
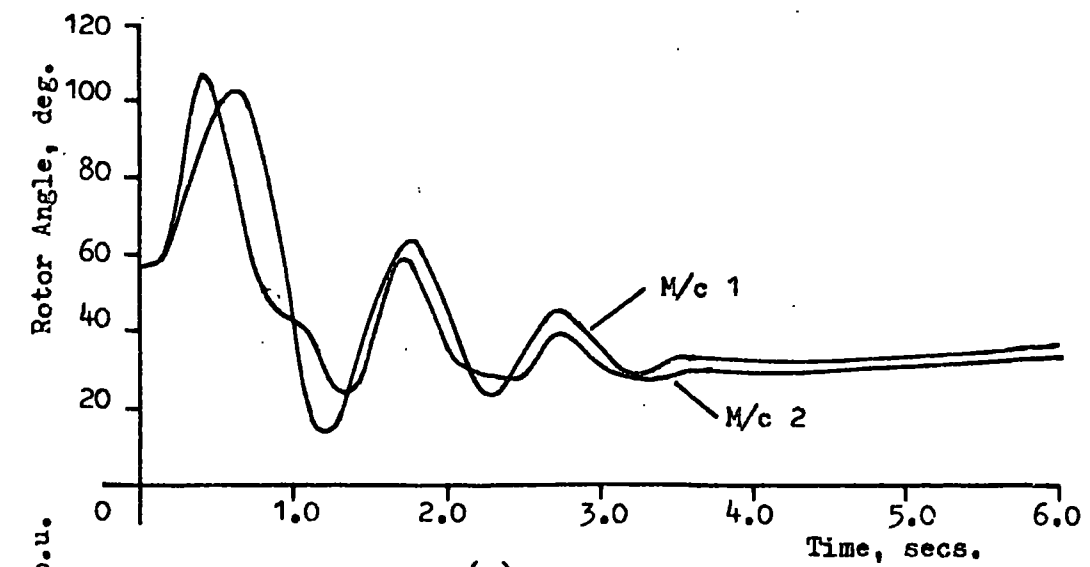
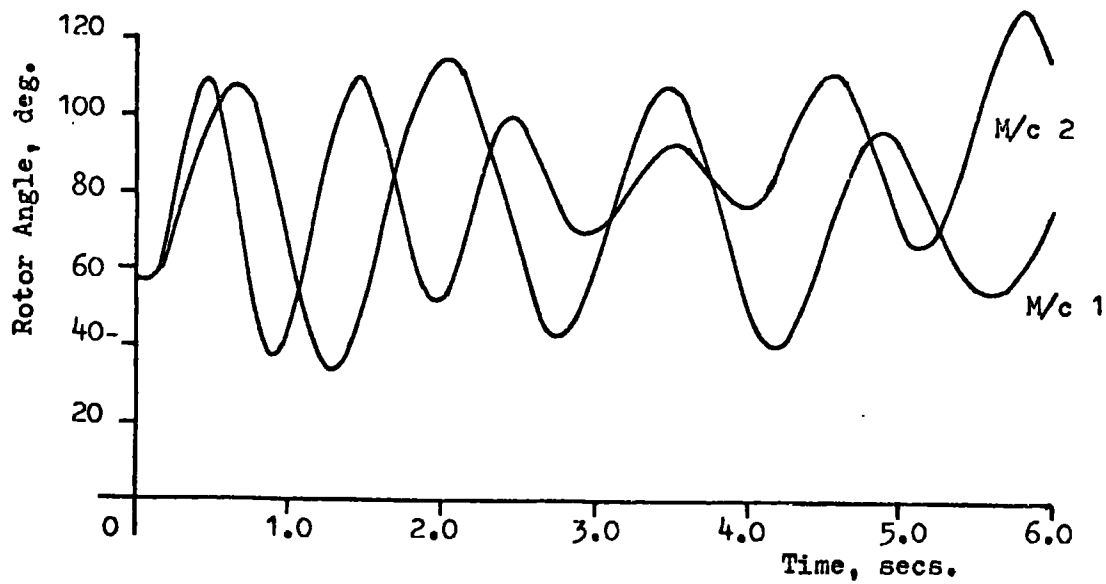
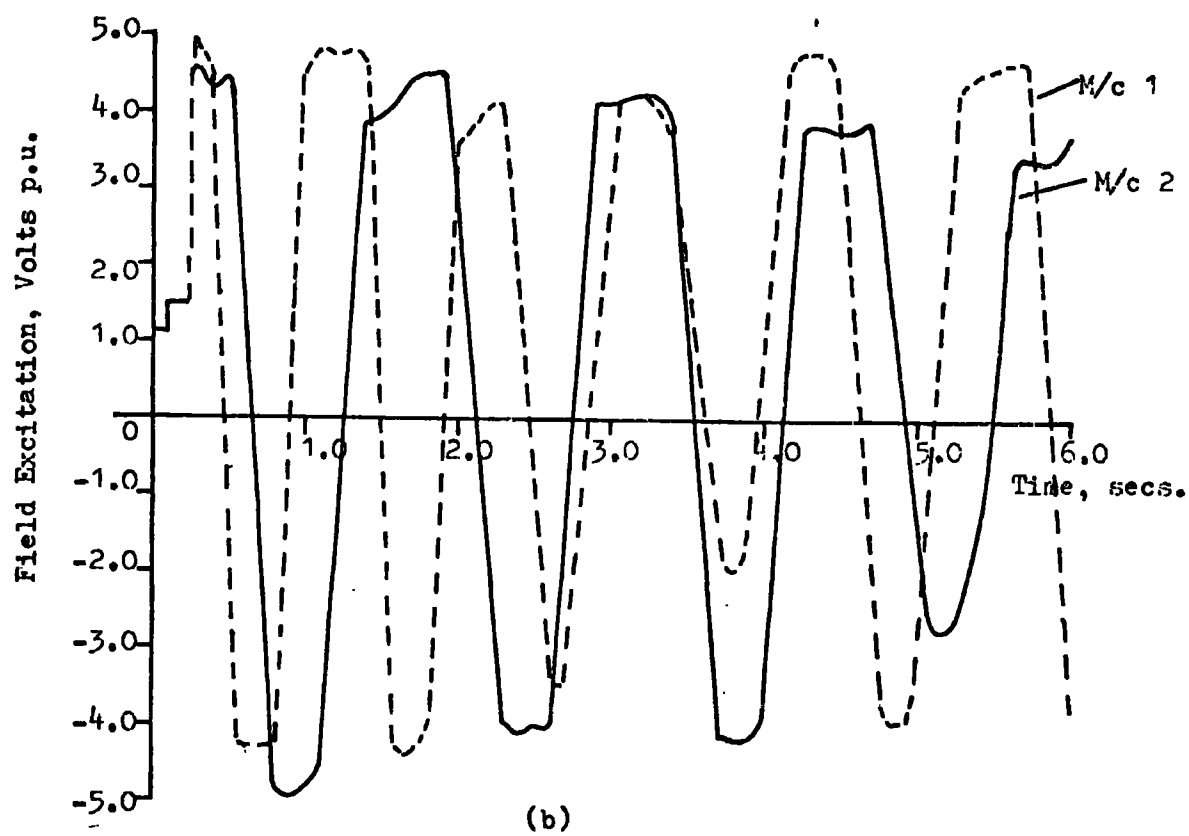


Fig. 8.14 Rotor Angle And Static Exciter Response For A Three Phase Fault On Bus 3 Of Fig. 2.7 For 0.15 secs. Data Appendix H. Exciter Ceiling Limits 6.0 and 0.0 p.u. Acceleration Feedback $K_{fb1}=K_{fb2}=0.05$. Interaction Present.



(a)



(b)

Fig. 8.16 Rotor Angle And Field Excitation Responses Demonstrating The Effect Of Exciter Ceiling Limits On The Non-Interactive Control Scheme. Static Exciter With Ceiling Limits $+6.0 \cdot |V_t|$ and $-6.0 \cdot |V_t|$ p.u.

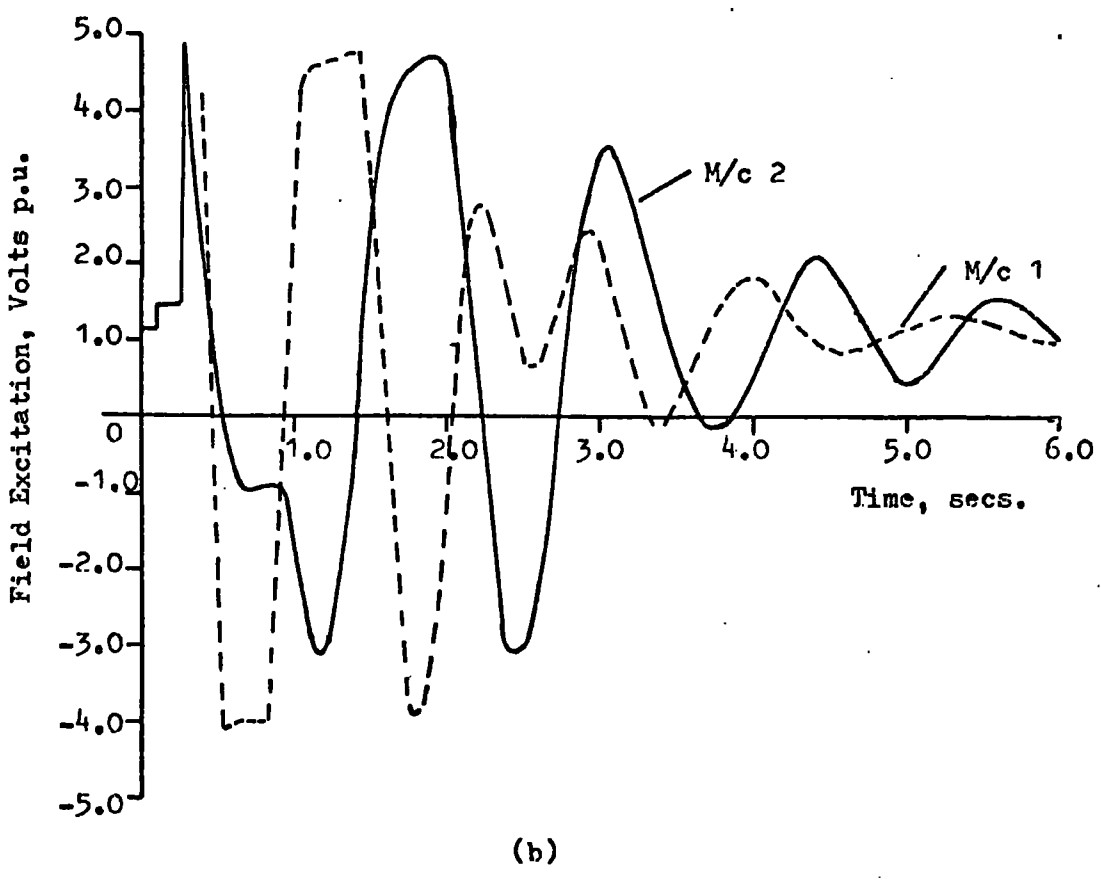
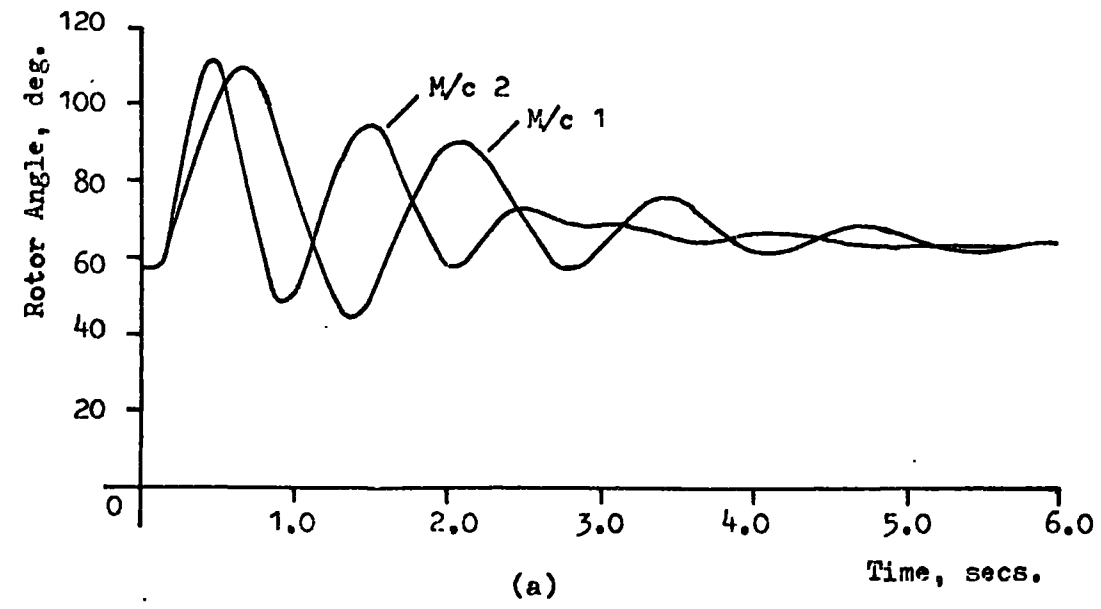


Fig. 8.17 Rotor Angle And Field Excitation Responses Demonstrating The Stalling Effect Of Acceleration Feedback, $K_{fb1}=K_{fb2}=0.02$, On The Non-Interactive Control Scheme. Static Exciter With Ceiling Limits $+6.0 \cdot |V_t|$ and $-6.0 \cdot |V_t|$ p.u.

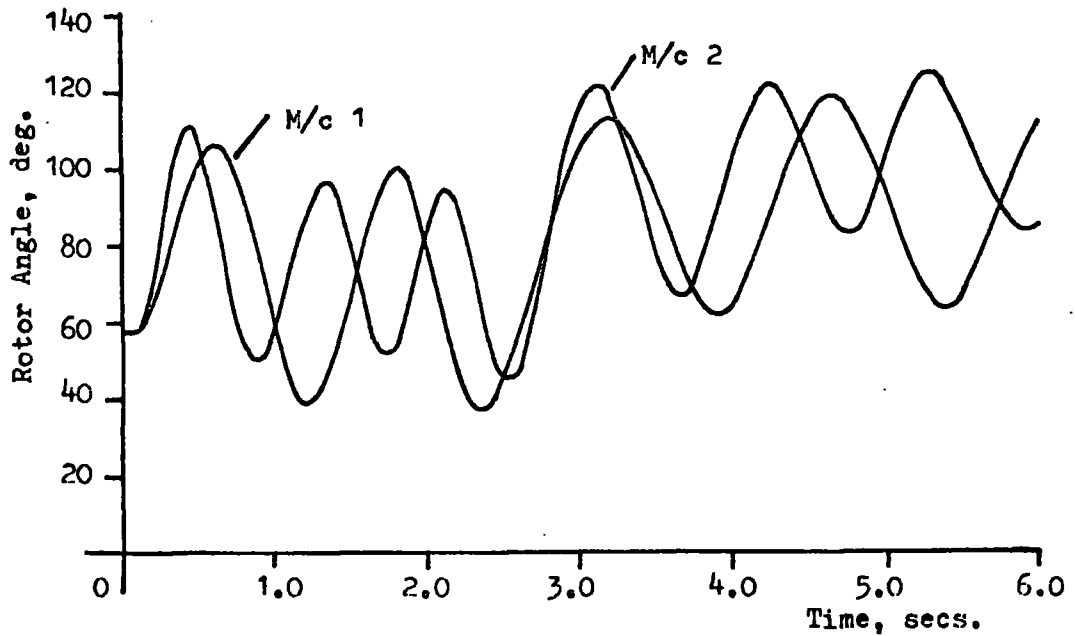
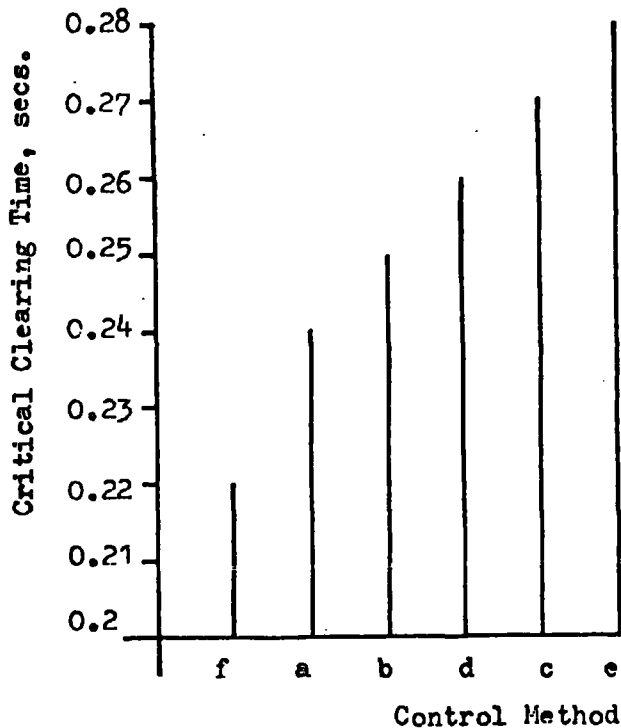


Fig. 8.18 Rotor Angle Response Demonstrating The Effect Of Velocity Feedback, $K_{fb1}=K_{fb2}=0.3$, To The Non-Interactive Control Unit. Static Exciter With Ceiling Limits $+6.0^{\circ}|V_t|$ And $-6.0^{\circ}|V_t|$ p.u.



- a - Velocity Feedback, $K_{fb1}=K_{fb2}=0.1$. Interaction Present.
- b - Acceleration Feedback, $K_{fb1}=K_{fb2}=0.05$. Interaction Present.
- c - Acceleration Feedback, $K_{fb1}=K_{fb2}=0.05$. Interaction Removed.
- d - 0.05 Acceleration Feedback + 0.1 Velocity Feedback. Interaction Present.
- e - 0.05 Acceleration Feedback + 0.1 Velocity Feedback. Interaction Removed.
- f - No Control. Interaction Present.

Fig. 8.19 The Variation In Critical Clearing Time With Different Feedback Control Schemes.

CHAPTER 9

RELIABILITY OF THE NON-INTERACTIVE CONTROL METHOD

9.1 GENERAL

The benefits gained from using a non-interactive control scheme have been discussed. The reliability of the non-interactive control method in terms of overall stability and interaction effects is now investigated with particular reference to the second order input power regulator.

When interaction is removed the system behaves like two single input/output systems and the feedback gains can be increased to their limit without affecting the other channel. The I.N. plots are lines.

If part of the feedback across the machines is lost interaction between channels will exist. The amount of this interaction can be assessed by the width of the band produced by drawing the d-circles.

The oscillation frequency of the load angle in previous time response plots is between 3 and 12 rad/s, depending on the inertia. It will be shown that the feedback arrangements that produce the smallest d-circles within this frequency band have the least amount of interaction. This will be seen to apply even though the d-circles at lower or higher frequencies may be of greater magnitude.

9.2 THE EFFECT OF THE CROSS FEEDBACK COMPONENTS

The presence of the different cross-feedback terms in the control signal can be described by the connection of the cross-feedback links (a) to (c) in fig. 7.2(a).

If links (a) in fig. 7.2(a) are closed an acceleration component is included in the cross-feedback signal which reduces the radius of the

d-circles and hence interaction at high frequencies. However at low frequencies it is the position component, links (c) that is the dominant term. This effect of frequency on interaction is demonstrated in fig. 9.1. At high frequency curves (e), (f) and (d), which contain an acceleration cross-feedback signal, show the lowest d-circle radius whereas at low frequencies it is curves with a position term included in the cross-feedback signal, curves (c) and (e), that have the lowest d-circle radius.

If a velocity term is included in the cross-feedback signal, corresponding to the closure of links (b) in fig. 7.2(a), interaction effects are considerably reduced, relative to the interactive study, as illustrated in fig. 9.2 by comparing curves (d), (c) and (h) with curve (a). Comparable graphs in fig. 9.1 show a reduction in the radius of the d-circles during the critical middle frequencies. It is the velocity term that is dominant in removing interaction in the practical system. If the velocity term, links (b) in fig. 7.2(a) is not included in the cross-feedback signal interaction effects are only slightly reduced relative to the uncontrolled case. This is illustrated in fig. 9.1 by comparing curves (e) and (f) with (a). The only exception to this is if position cross-feedback alone is applied by closing link (c) in fig. 7.2(a) when the system becomes more interactive than the uncontrolled case. Shown in fig. 9.1 by comparing curves (g) and (a). Transient plots demonstrated that with individual machine acceleration feedback gains, $Kfb_{1,2} = 0.0$, and position cross feedback only the system was unstable. This was verified by plotting $\det T(p)$ as in fig. 9.3. Increasing the feedback gain Kfb_2 to 0.05 resulted in a stable system.

The increase in interaction produced by the position cross feedback term is further emphasised by comparing curves (c) and (h) in figs. 9.1 and 9.2 where curve (c) for velocity and position cross-feedback produces more

interaction than just velocity cross-feedback alone, curve (h). If link (a) is closed in fig. 7.2(a) an acceleration term is included in the control signal and helps stabilise the position cross-feedback term. This is illustrated in fig. 9.1 by comparing curves (e) and (f) which produce d-circles of the same radius within the middle frequency band.

From the above discussion if the non-interactive control unit fails the only unstable condition will exist if position cross-feedback is retained alone with no individual acceleration feedback gain, k_{fb_i} . Feedback round each individual alternator as a response shaping mechanism will generally be used and unless this has been lost the system will be stable in the Nyquist sense.

If complete cross feedback between the machines is lost, in one direction only, then depending on the fault the machine may or may not be affected by the flow of synchronising power. Consider fig. 9.4 where curve (a) shows the load angle response for a three phase fault on bus 2 with interaction between machine 2 and machine 1 only. Because the synchronising power flowing to machine 1 is not counteracted by a change in input power the benefits described in section 7.8 are lost. However in curve (b), fig. 9.4, interaction is removed between machine 2 and machine 1 counteracting the flow of synchronising power and giving the improved response.

9.3 APPLICATION OF THE NON-INTERACTIVE CONTROLLER TO REP 6

For small perturbation studies where there is a step change in the input power no significant benefits are obtained by using the non-interactive control unit over just acceleration damping, fig. 9.5. The effect of the cross feedback is to produce a reverse swing in the load angle of machine 1, an effect caused by incorrect gain settings in the cross feedback elements.

If the disturbance takes the form of a three phase fault on the terminals of machine 2, the tendency to reverse swing in machine 1 is utilised producing a substantial reduction in the first load angle maximum of machine 1, curve b, fig. 9.6. Interaction is substantially reduced on later excursions giving the improved response of curves (b) over just acceleration damping, curves (a), fig. 9.6.

9.4 SENSITIVITY OF THE CONTROL UNIT TO CHANGES IN THE INITIAL OPERATING POINT.

9.4.1 SMALL PERTURBATIONS

The difference in the response of the linear and non-linear models for small perturbations has been shown in previous sections to be insignificant. The maximum amount of interaction will be removed when a controller is designed and used about one specific operating point. In the case of the linear model the interaction removal will be complete. The influence on overall system response of controllers designed for different system conditions, than in which they are operated, can be assessed by plotting the radius of the d-circles against frequency as in section 9.3.

The data of Appendix H, with the model system of fig. 2.7, was used in conjunction with a second order input power regulator. Non-interactive control units were designed for three different initial rotor angle settings. The values of the cross-feedback gains for these control designs are shown in the table of fig. 9.8. Application of these control units, at initial rotor angles different to their design values, were found to substantially reduce interaction effects as demonstrated by curves (c) and (d) in fig. 9.7. Curve (b), where interaction is removed completely, and curve (a) of the uncontrolled machine are reproduced for comparison. The pertinent frequency range is again between 3 to 12 rad/s.

The importance of this result is that it will not be necessary to change the feedback values in the control unit with every change of loading condition, even with the synchronous machine operating at rotor angles in excess of 60° .

These points are further emphasised when considering large three phase faults.

9.4.2 LARGE DISTURBANCES

The small changes in the cross feedback gains of the different control units produced little effect on the interaction phenomena between machines for large disturbances as demonstrated by comparing figs. 9.9 and 8.3 where no significant differences are obvious. The improper phasing discussed in section 8.2 again being compensated for by an acceleration feedback gain of 0.05 round each individual alternator. The danger of multiswing instability has now been eliminated and the transient stability limit can be related to first swing maximum.

Fig. 9.10 demonstrates that the different control units have negligible effect on the first rotor angle maximum of either machine and consequently does not greatly affect the transient stability limits. The importance being that the gain settings in the control unit need not be altered as the system loading changes to produce the required transient stability limit.

9.5 CONCLUSION

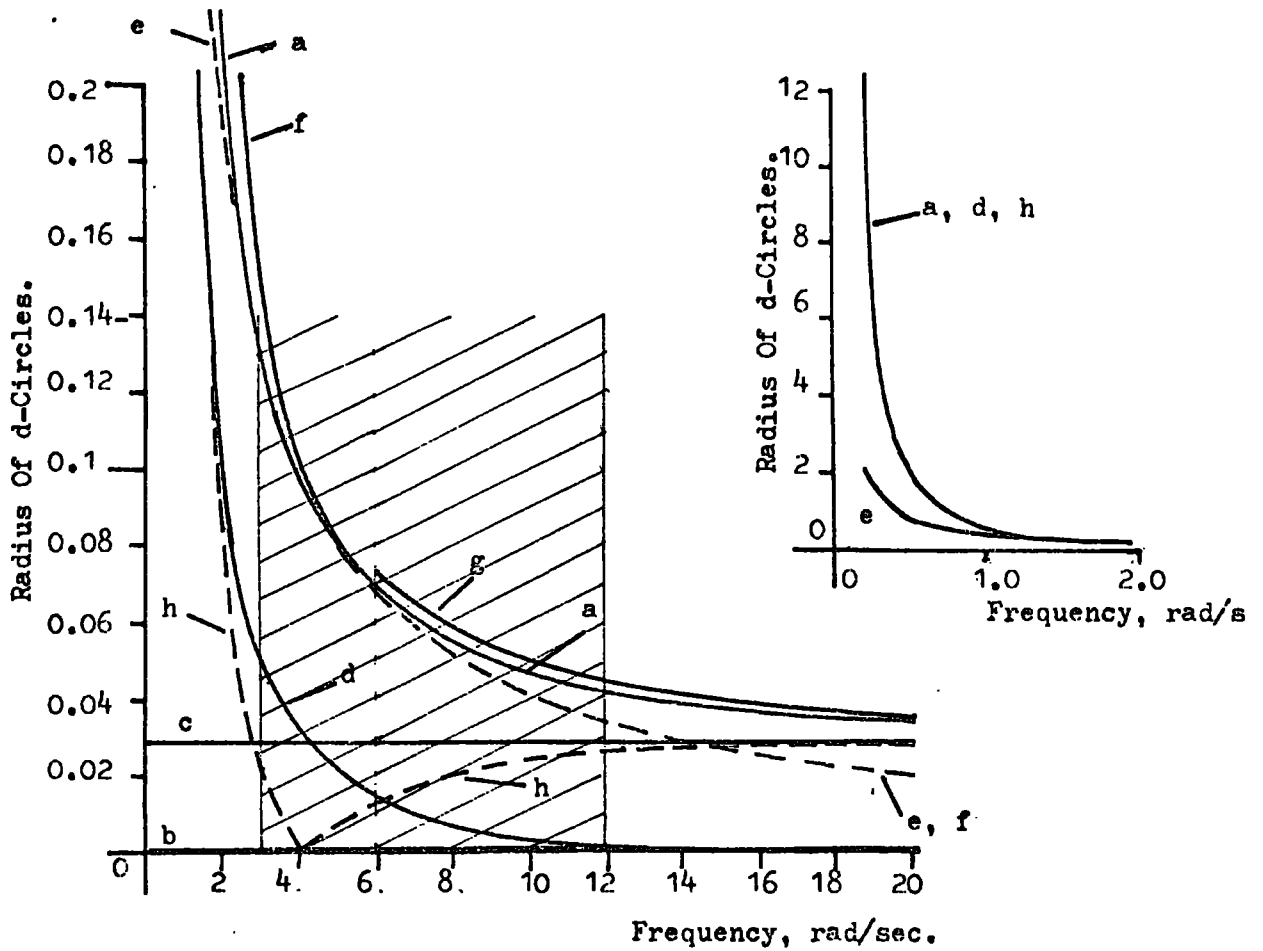
The velocity term included in the cross-feedback signal was shown to remove a substantial amount of interaction between oscillation frequencies of 3 to 12 rad/s. It is the interaction effects within these frequencies which are most prominent. Consequently it is the velocity cross feedback term that is most important and, if retained, always reduces the system interaction.

The only case when more interaction is present than in the uncontrolled case is if only position cross feedback is retained. This would produce Nyquist instability. However if an acceleration damping signal, k_{fb} , is used the system would be stable. In general, feedback round each individual machine would be used to shape the response.

If the non-interacting control is lost in one direction the actual effect it would have on the system is very dependent on the position of the fault. If the ultimate failure in the group control scheme occurs where the cross-feedback signals are completely lost the machines will still have their individual feedback controls operative and will simply revert to this conventional mode of operation.

If the non-interactive controller is applied to the machine model of REP 6 interaction effects are substantially reduced especially in the case of the three phase fault. The author feels that if the design model parameters of REP 2 are adjusted to give a load angle response similar to REP 6 further reduction in interaction effects would be achieved.

The versatility of the design method was demonstrated when it was shown that the control unit could adequately cope with changes in system loading without losing its non-interactive properties. This was shown to be true with the machine operating at load angle in excess of 60° . Consequently it is not necessary to change the gain settings in the control unit every time there is a change in the system loading conditions.



- a - No Cross Feedback
- b - Interaction Removed; Velocity, Acceleration and Position Cross-Feedback.
- c - Velocity and Position Cross-Feedback.
- d - Velocity and Acceleration Cross-Feedback.
- e - Acceleration and Position Cross-Feedback.
- f - Acceleration Cross-Feedback.
- g - Position Cross-Feedback.
- h - Velocity Cross-Feedback.

Fig. 9.1 The Change In d-Circle Radius With Frequency For Different Cross-Feedback Arrangements. Data Appendix H.

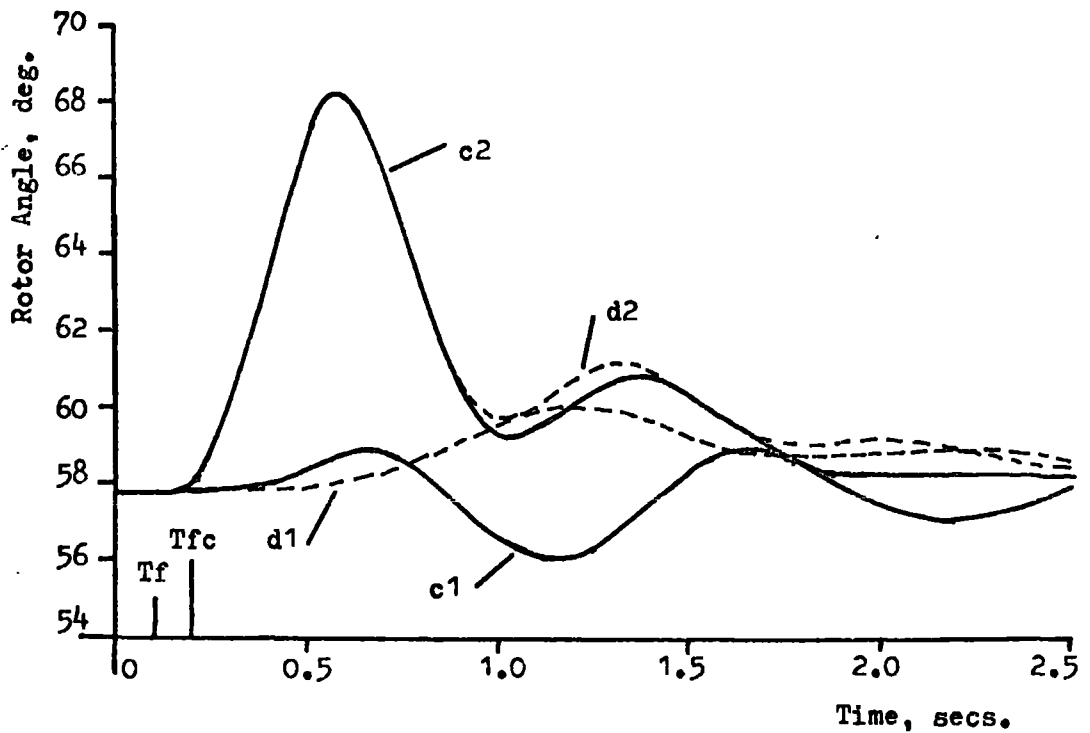
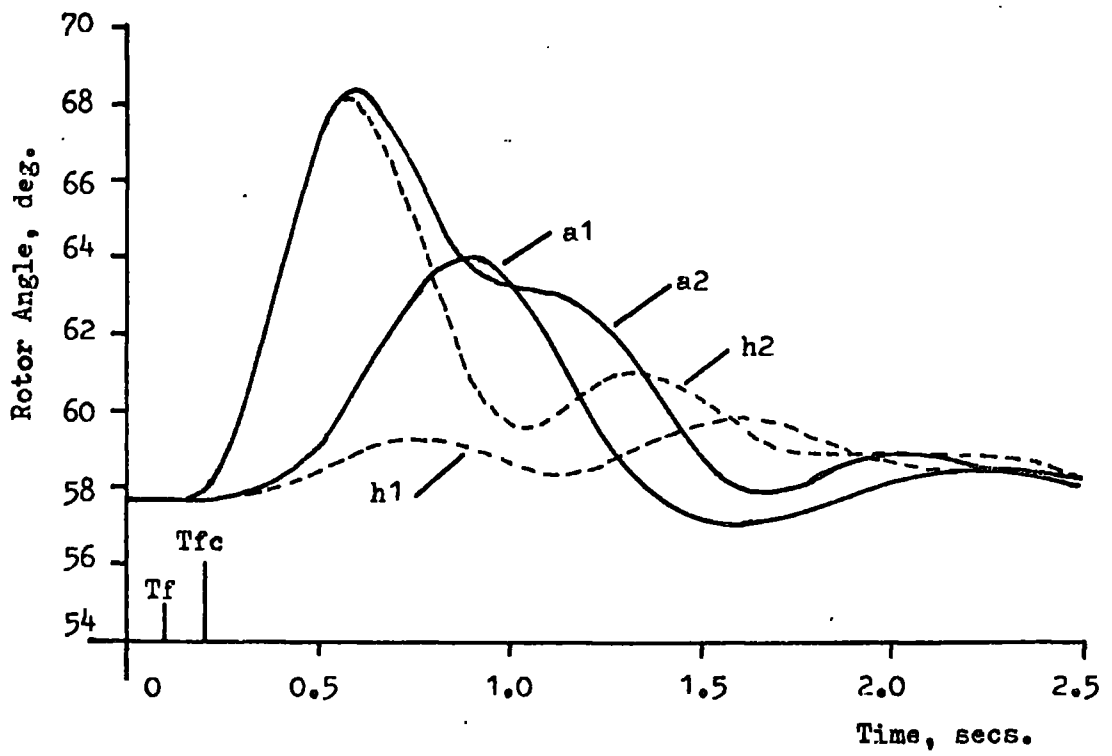
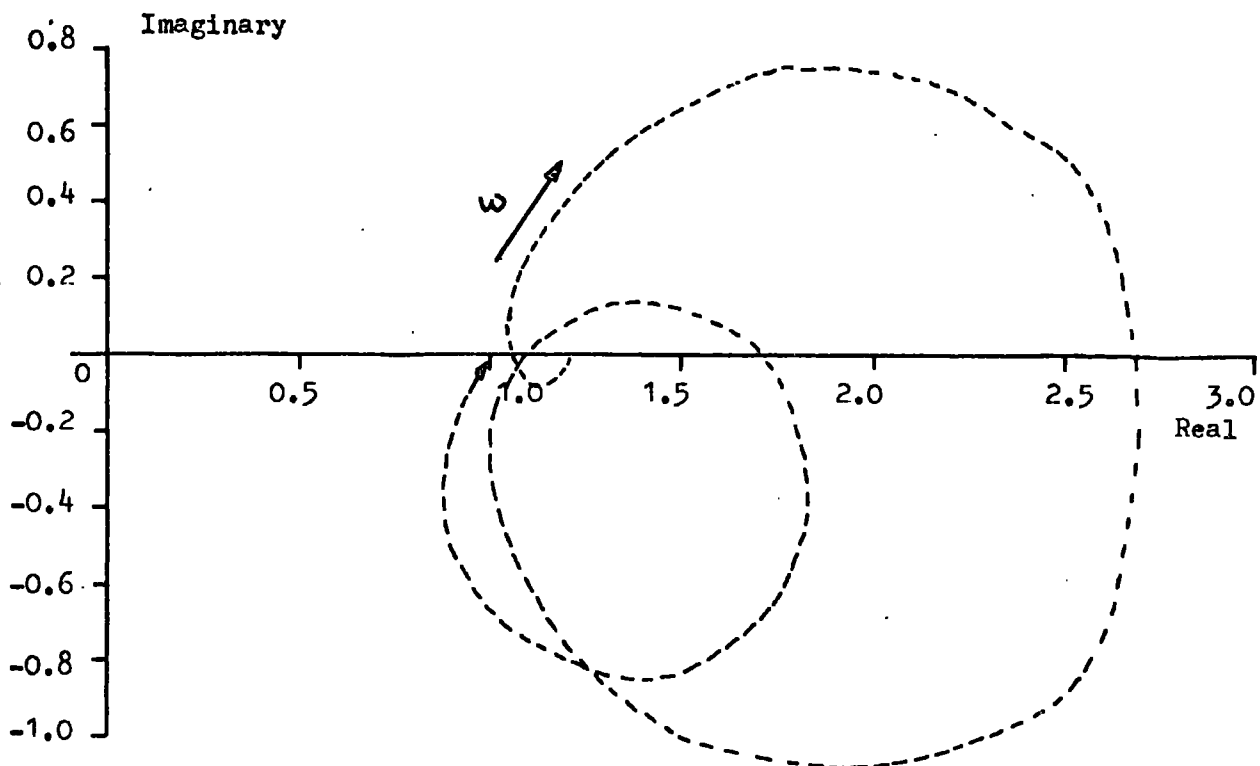
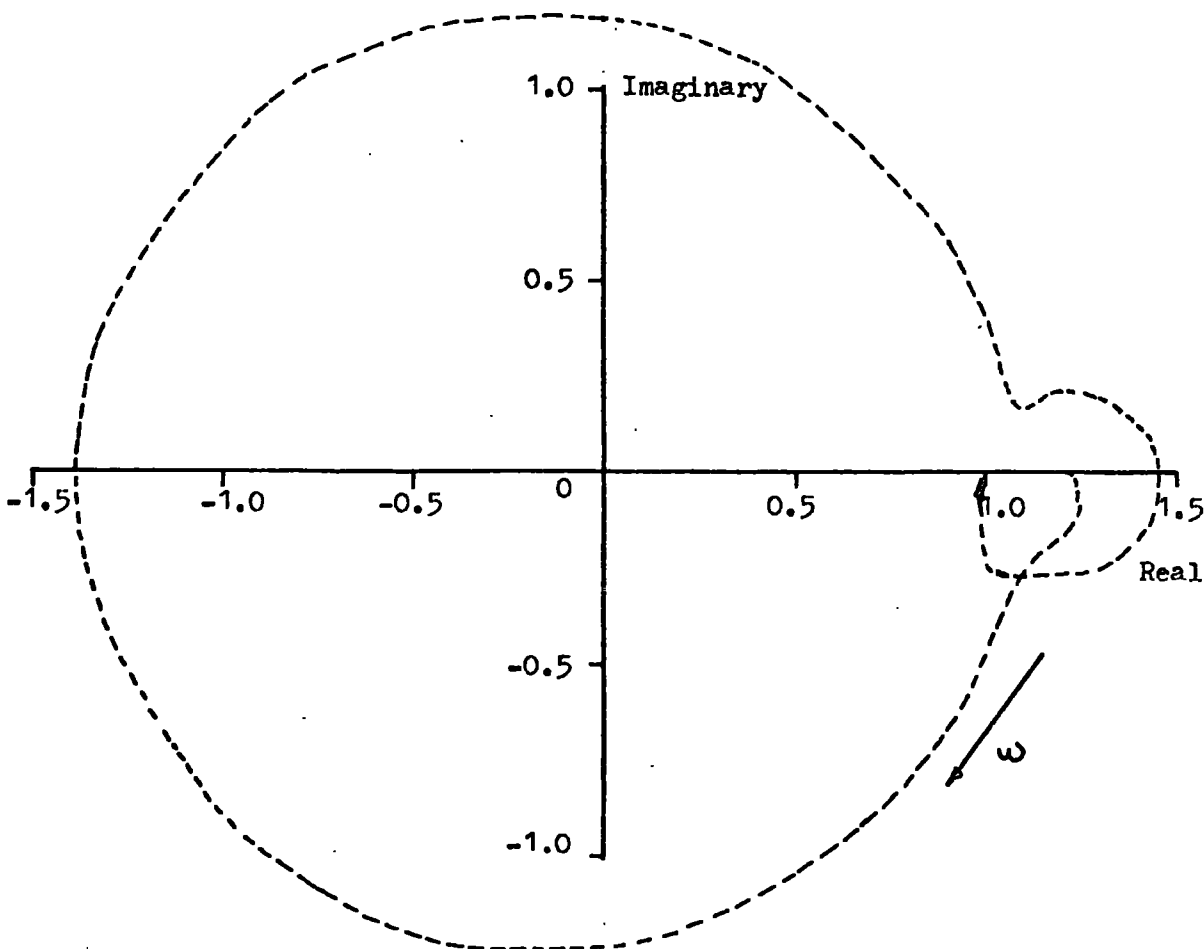


Fig. 9.2 Rotor Angle Responses Showing The Effect Of Different Cross Feedback Arrangements. Control Key As For Fig. 9.1 Acceleration Feedback $K_{fb1}=K_{fb2}=0.05$. Data Appendix H. Input Power To Machine 2 Stepped From 0.7 p.u. To 2.1 p.u. During Fault Interval.

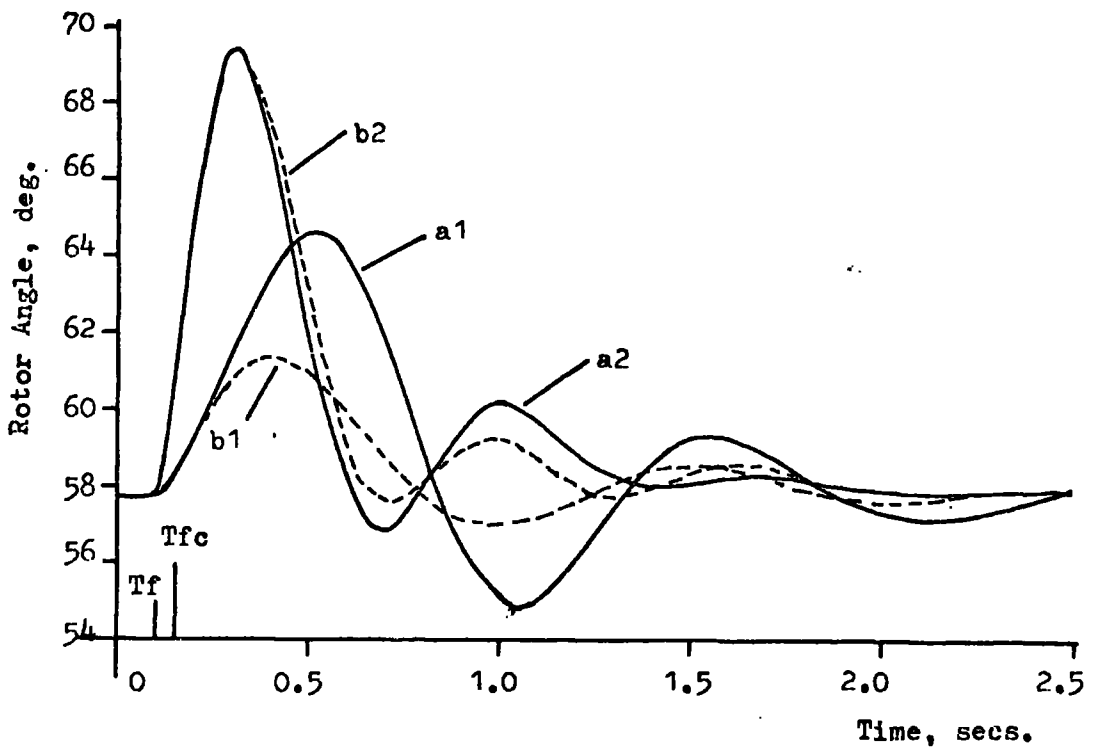


(a) $K_{fb1} = 0.05, K_{fb2} = 0.0$



(b) $K_{fb1} = K_{fb2} = 0.0$

Fig. 9.3 Stability Plots Of Det. $T(p)$ For Different Acceleration Feedback Gains. Interaction Partly Removed In The System Of Fig. 2.7 By Position Cross-Feedback.



1 - M/c 1; 2 - M/c 2

a1; a2 - Interaction Removed Between M/c1 and M/c 2 Only.
Acceleration Feedback, $K_{fb1}=K_{fb2}=0.07$.

b1, b2 - Interaction Removed Between M/c 2 and M/c 1 Only.
Acceleration Feedback, $K_{fb1}=K_{fb2}=0.07$.

Fig. 9.4 Rotor Angle Response Showing The Effect Of Interaction Removal In 1 Direction Only. 3-Phase Fault On The Terminals Of M/c 2 For 0.05 secs. Data Appendix H.

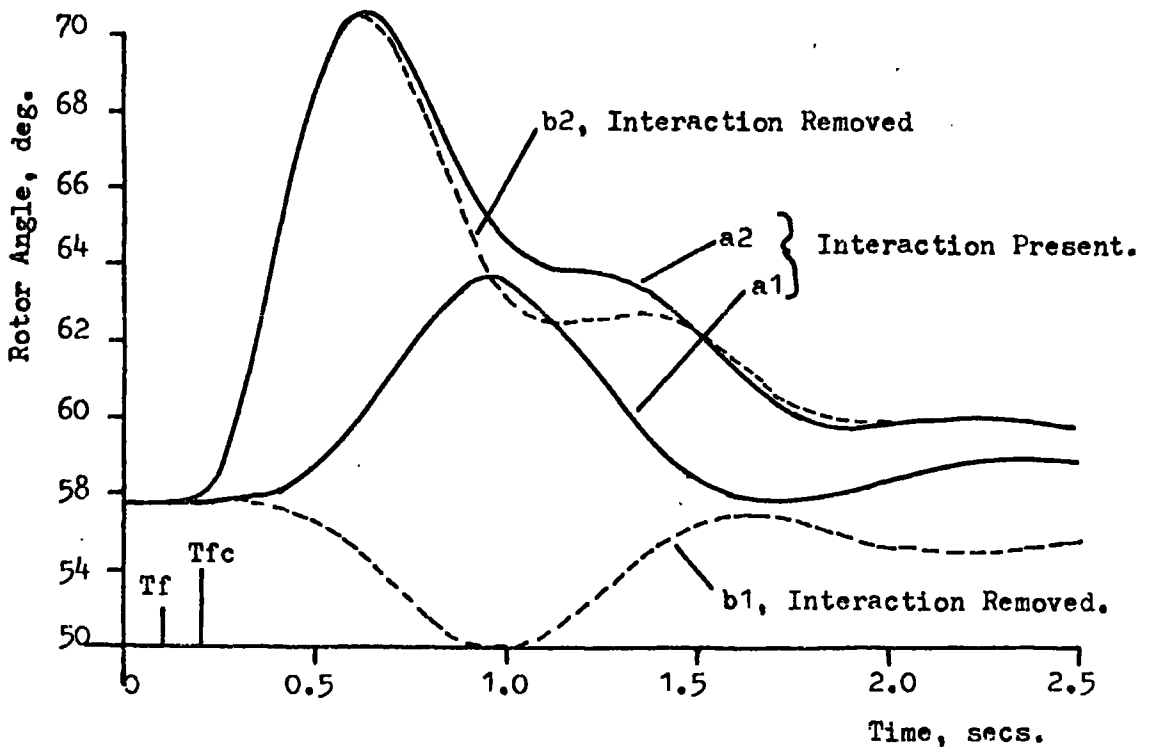
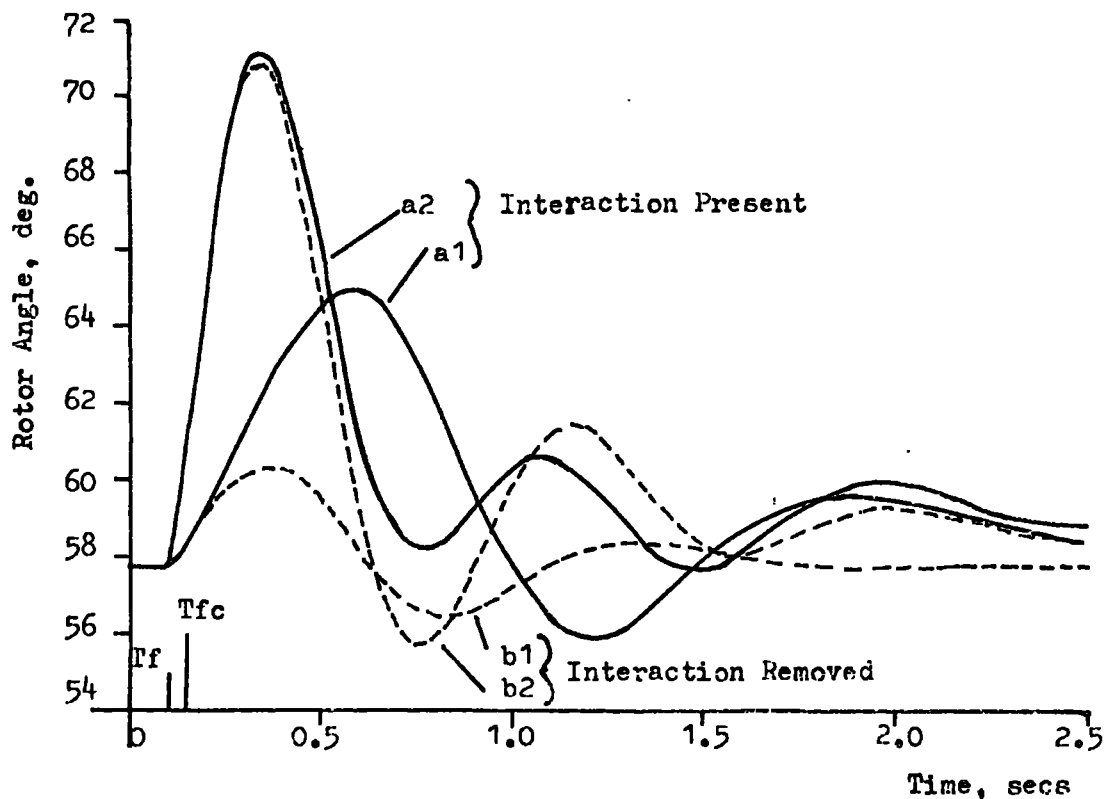
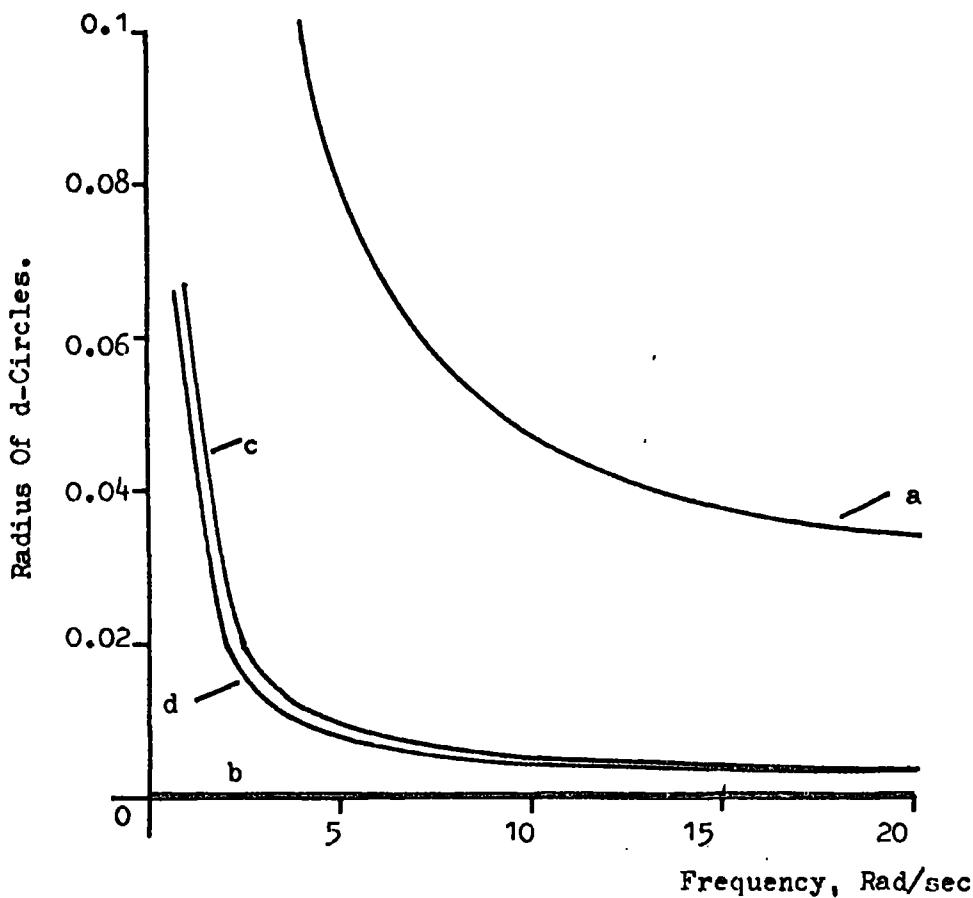


Fig. 9.5 Rotor Angle Response For REP 6 Showing The Effect Of The Non-Interactive Controller. Data Appendix H. Input Power To M/c 2 Stepped From 0.7 p.u. To 2.1 p.u. During Fault. Acceleration Feedback, $K_{fb1}=K_{fb2}=0.05$.



1 - M/c 1; 2 - M/c 2

Fig. 9.6 Rotor Angle Response For REP 6 Showing The Effect Of The Non-Interactive Control Unit. Data Appendix H. 3-Phase Fault On The Terminals Of Machine 2 For 0.05 secs. Acceleration Feedback, $K_{fb1}=K_{fb2}=0.05$.

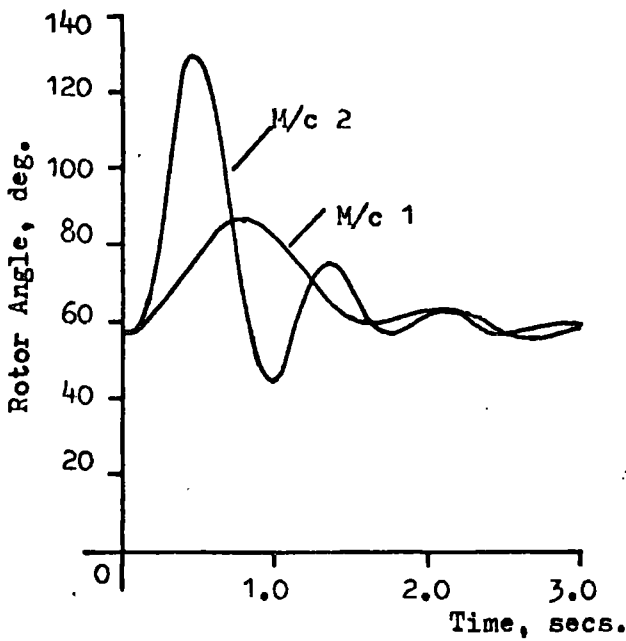


- a - No Cross Feedback
- b - Complete Removal Of Interaction. Controller Designed At 57.78 deg. Operated At $\delta_o=57.78$ deg.
- c - Interaction Removed. Controller Designed At 74.47 deg. Operated At $\delta_o=57.78$ deg.
- d - Interaction Removed. Controller Designed At 41.80 deg. Operated At $\delta_o=57.78$ deg.

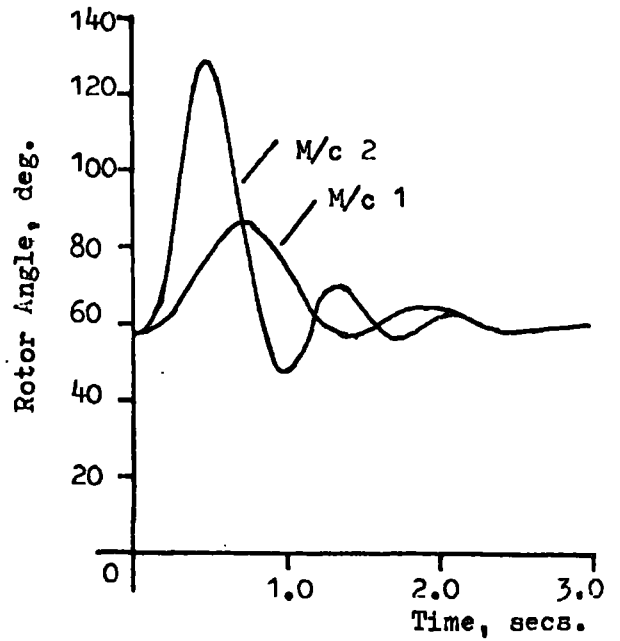
Fig 9.7 Interaction Effects, As A Function Of d-Circle Radius Produced By Non-Interactive Control Units Designed At Different Initial Loadings But Operating At $\delta_o=57.78$ deg.

Initial Rotor Angle. deg.	Position Gain	Velocity Gain	Acceleration Gain
41.80	0.532	0.441	0.0319
57.78	0.489	0.405	0.029
74.47	0.435	0.361	0.0261

Fig. 9.8 Cross-Feedback Gains For Different Initial Loading Conditions.

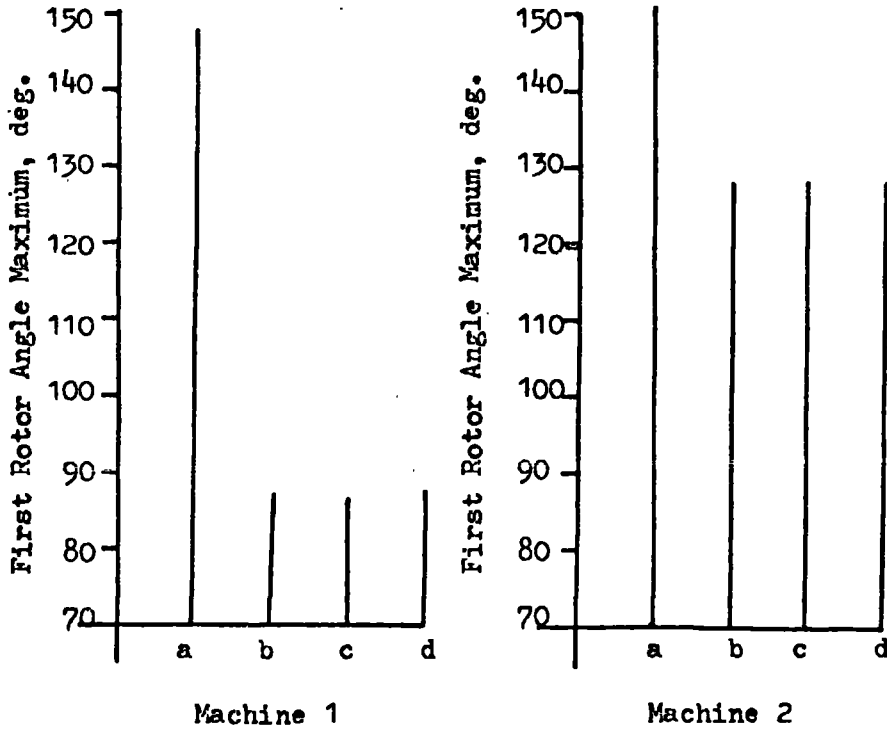


(a) Design Angle = 41.80 deg.



(b) Design Angle = 74.47 deg.

Fig. 9.9 The Effect On Rotor Angle Response Of A Controller Designed At A Differant Loading Condition To Which It Is Operated. Acceleration Feedback, $K_{fb1} = K_{fb2} = 0.05$.



- a - Uncontrolled
- b - Interaction Removed + 0.05 Acceleration Feedback. Controller Designed At 57.78 deg.
- c - Interaction Removed + 0.05 Acceleration Feedback. Controller Designed At 74.47 deg.
- d - Interaction Removed + 0.05 Acceleration Feedback. Controller Designed At 41.80 deg.

Fig. 9.10 The Reduction In First Rotor Angle Maximum Due To The Different Non-Interactive Control Units.

CHAPTER 10

CONCLUSION

10.1 CONTROL DESIGN METHOD

The likelihood of transient instability limits the amount of electrical loading that a power system can be subjected to; consequently any control method that improves the transient stability margin is economically worth investigation. The control methods evolved in this work for multi-machine power systems, through the use of Linear Multivariable Control Theory, produced an increase in the transient stability limit and improved system response, over the uncontrolled system, at all disturbance levels.

Multivariable control methods are developed because they allow investigation of a control scheme in the frequency plane by well established classical techniques, notably Nyquist methods, which allows correct dynamic compensation to be easily predicted. Further they offer advantages over optimum control methods in that they do not require access to all the system states. Neglecting a system state in an optimum design method can render an inherently stable system unstable. (56)

A convenient method of qualifying and quantifying the amount of interaction present in any multi-input/output system can be achieved by plotting the d-circles on the I.N. diagram. This method of quantifying the interaction was used extensively in Chapter 9 and yielded results in excellent agreement with the time response plots. It should be noted that the time response only allows a qualitative assessment of interaction to be made.

One of the difficulties of the design method was that the d-circles occasionally tended to hinder assessment of the critical feedback gain, see Section 7.9.2., but experience taught the relative importance of the locus of the d-circle band to the locus of the d-circle centres.

10.2 IMPEDANCE SWITCHING

To obtain a working knowledge of the Linear Multivariable Design Method a delta connection of three machines was initially investigated. Although not a practical interconnection of machines such a system was used for its ease in mathematical modelling. Working from this mathematical background control schemes involving impedance changing at times determined by the control unit were evolved.

One control scheme used capacitor insertion to quench machine transients. This is similar in manner to schemes suggested by other authors, for single machine systems, when working from either a practical knowledge of the systems behaviour⁽⁵¹⁾⁽⁵²⁾⁽⁷⁵⁾⁽⁸⁴⁾ or by optimum control techniques.⁽⁸¹⁾

One of the dangers of mathematical simulation is that the engineer can lose sight of the physical system under study. This is especially important in the context of impedance switching where high power levels, typically kilowatts or megawatts are involved. It is thus necessary, as was done throughout this work, to relate any control scheme back to the physical system and to consider the practical difficulties involved in its implementation.

10.3 A COMPARISON BETWEEN EXCITATION CONTROL AND FAST VALVING

Investigations into input power regulator modelling demonstrated that to obtain representative results a model of at least second order had to be used. With this second order input power regulator model the machine and associated controls are of equivalent order to the machine with excitation control; only the time constants of the different control stages differ. However certain feedback signals show the same general tendency in both exciter and fast valve control.

Two exciters were considered; the classical rotating exciter and the newer static exciter which is powered from the machine terminal voltage.

For the multimachine power system both excitation and input power control using feedback signals describing the machines state improved the overall response at all disturbance levels. Similar observations were recorded for excitation control (Dineley et al⁽⁹⁾) and input power control (Dineley and Kennedy⁽³⁴⁾) when the control of a single machine system subjected to a 3-phase fault was being investigated. However the feedback gain has to be limited or, as in the case of velocity feedback, self-induced oscillations leading ultimately to instability will result while too large an acceleration feedback gain tends to produce an overdamped response and slow voltage recovery on fault clearance.

Conventional voltage feedback to the exciter was also limited as it tended to produce a self-induced instability. This effect was more noticeable with the static exciter than the slower acting rotating exciter. This phenomena was noted to have been the reason for previous authors⁽⁶⁾⁽⁷⁸⁾⁽⁷⁹⁾ using a stabilising signal dependent on the machines state in the overall control signal to the exciter.

The effect of excitation control on first rotor angle maxima was found to be very dependent on the exciter used, feedback parameter, feedback gain, fault and ceiling limits. Dineley et al⁽⁹⁾ demonstrated that acceleration feedback to the static exciter of a single machine power system actually increases first rotor angle swings during 3-phase short circuit whereas other control signals slightly reduced the first swing maximum. The work presented in Chapter 8 also demonstrated this to be true in the case of multimachine power systems. The reason for the increase in first swing is attributed to the low ceiling limits of the static exciter during the

fault interval and that on fault removal the acceleration signal tends to reverse the field forcing. This effect can be reduced by decreasing the buck ceiling limit. However subsequent control was improved by using an acceleration feedback signal.

This tendency towards an increase in the first rotor angle swing with acceleration feedback to either the input power regulator or the rotating exciter was also noted. However it is not so apparent as in the static exciter. The actual magnitude of the effect is again very dependent on regulator limits and feedback gain.

Implementing the non-interactive controller improves individual machine control in the multimachine power system by substantially reducing any harmful interaction effects within the system. This interaction removal being nearly total for small perturbations. This then allows any change in the input to, say, machine 1 to only affect this machine while the other machines are undisturbed.

For large disturbances the linear design method produced improper phasing due to the incorrect values of cross-feedback gain at high rotor angles. However, this improper phasing can be adequately compensated for in both fast valving and excitation control by acceleration feedback round each individual machine. An improved system response results with interaction effects being kept to a minimum.

Using the input power regulator improved system control over excitation methods was achieved in the multimachine system both with and without interaction present as the effect of any exciter is severely restricted by the large value of the field open circuit time constant, T_d' . Hughes⁽⁴⁵⁾ has demonstrated a similar improved control over excitation methods for the single machine system using fast valving.

10.4 FUTURE TRENDS

With the further development of turbine fast valving inevitable⁽⁸²⁾ the control schemes developed in this work for both excitation and input power control become a practical possibility. How, then, will such schemes influence the future development program of electric generation and transmission ?

In the underdeveloped countries new power systems are continually being built with the load centre electrically and physically remote from the generating areas. This is an ideal situation for interaction effects leading ultimately to multiswing instability to exist. In Chapters 7 and 8 control methods were designed which eliminated the tendency towards multiswing instability, by reducing interaction effects to a minimum, by either excitation or input power control schemes. Thus, it has been shown possible to control this harmful interaction phenomena by supplementary feedback signals to control units that already exist on the generator.

In the area of electric generation conventional turbo-generators are reaching their maximum ratings. Turbo-alternators of 1300 MW are being designed with a possible extension to a 2000 MW limit.⁽⁹²⁾ This maximum power rating can be substantially increased by using superconducting generators. Such generators not only allow increased power output but also demonstrate improved efficiency over the conventional machine.

With the superconducting A.C. generator many new technical problems have to be solved, but here let us briefly examine the excitation control limitations of a 2000 MVA superconducting generator. For such a machine the rated field voltage will be of the order of 5 volts while the rated field energy will be approximately 25 MJ.⁽⁹⁰⁾ Consequently to provide any significant field forcing exciter ceiling limits of 10 KV may well be necessary. Also any practical superconducting machine design must shield the superconducting field winding from alternating fluxes.⁽⁹¹⁾ This is achieved by means of

an eddy - current screen round the field winding, as shown in the I.R.D. design in reference (91). This not only shields the field winding but means any change in field flux will take a long time in penetrating this shield. Further there will be a severe limit on the rate at which the field voltage can be changed due to the inherent physical properties of superconducting windings.

A superconducting winding consists of filaments of superconductor within a copper matrix. If the change in field voltage is too rapid localised hot spots are formed within the copper matrix resulting in the superconductor going normal.

This then suggests that control of prime-mover power will be the best way of providing control to the superconducting A.C. machine. It has been demonstrated that there is adequate capability in turbine fast valving to control not only first rotor angle swing but also subsequent swings and to give good voltage regulation.

10.5 FAST VALVING

Fast valving techniques have been shown to produce a stronger control action than excitation methods in both multimachine and single machine power systems because of the small time constants involved with this form of control action.

Capacitor switching can produce large reductions in the first rotor angle excursion but subsequent control is difficult because of the number of high power switching operations involved. However fast valving can produce both a substantial reduction in first rotor angle maximum and good subsequent control action and is thus preferred.

Input power control in the multimachine system can be further strengthened by removing interaction effects.

The strongest form of input power control in the multimachine system is achieved by using a combined feedback signal incorporating both velocity and acceleration feedback round each individual alternator; a conclusion also reached by Dineley and Kennedy⁽³⁴⁾ for the single machine system. The acceleration signal stabilises the velocity term and helps produce good subsequent control while the velocity signal helps produce a more optimum control action during the first rotor angle swing. Further reduction of first rotor angle maxima result if interaction effects are removed when a near optimum control signal is achieved. Subsequent control is also improved.

However with both interaction present and interaction removed the acceleration signal has to be limited or else slow voltage recovery on fault removal would result. With a correctly selected acceleration feedback gain good control can be achieved giving good voltage regulation especially in the case of the non-interactive system. Similar results showing improved voltage regulation using fast valving have been published by Dineley and Fenwick⁽⁸⁹⁾ for the single machine system when a machine model including stator transients was used. A detailed simulation of the prime-mover and governor was also incorporated. However the similarity in the results obtained by Dineley and Fenwick and those presented in this work suggest that the models used in this multimachine program are adequate for overall control investigations.

REFERENCES

1. Anderson, J.H., Proc. I.E.E.E., Vol. 59, No. 1, Jan. 1971, pp. 25-35, "The Control of a Synchronous Machine using Optimal Control Theory."
2. Adkins, B., "The General Theory of Electrical Machines", pub. by Chapman and Hall, 1964.
4. Colombo, A. et al "Determination of the Dynamic Response of Electrical Systems by means of a Digital Program", I.E.E.E. Trans. on Power App. and Systems, Vol. PAS-87, No. 6, June 1968, pp. 1411-1418.
5. Cushing, E.W. et al, "Fast valving as an aid to Power System Transient Stability and Prompt Resynchronization and rapid reload after full load rejection", I.E.E.E. Trans. on Power App. and Systems, July/Aug. 1972, Vol. PAS-91, No. 4.
6. Dandeno, P.L. et al, "Effect of High-Speed Rectifier Excitation Systems on Generator Stability limits", I.E.E.E. Trans. on Power App. and Systems, Vol. PAS-87, No. 1, Jan. 1968, pp. 190-201.
7. Glavitsch, H., Discussion on "Effect of High Speed Rectifier Excitation Systems in Generator Stability Units", I.E.E. Trans. on Power App. and Systems, Vol. PAS-87, No. 1, Jan. 1968, pp. 190-201.
8. Dandeno, P.L. and Kundur, P., "Simulation of the Dynamic Non-Linear Response of Interconnected Synchronous Machine - Pt. II. Network Solution Procedures and Comparisons of Particular Computational Methods", I.E.E.E. Trans. on Power App. and Systems, Vol. PAS-91, No. 5, Sept/Oct. 1972.
9. Dineley, J.L. et al "Optimized Transient Stability from excitation control of Synchronous Generators", I.E.E.E. Trans. on Power App. and Systems, Vol. PAS-87, No. 8, Aug. 1968, pp. 1696-1705.

10. Griscom, S.B., "A Mechanical Analogy to the problem of Transmission Stability". The Electric Journal, Vol. 23, No. 5, May 1926, pp. 230-235.
11. Janischewskyj, W. and Kundur, P. "Simulation of the non-linear Dynamic response of Interconnected Synchronous Machines. Pt. I - Machine Modelling and Machine Network Interconnection Equations", I.E.E.E. Trans. on Power App. and Systems, Vol. PAS-91, No. 5, Sept./Oct. 1972.
12. Kimbark, E.W., "Power System Stability - Vol I. Elements of Stability Calculations", pub. by John Wiley and Sons 1948.
13. Kimbark, E.W., "Power System Stability - Vol III. Synchronous Machines" pub. by John Wiley and Sons 1948.
14. Kreyszig, E., "Advanced Engineering Mathematics", pub. by John Wiley and Sons 1967.
15. Lapidus, L. and Seinfeld, J.H., "Numerical solution of ordinary Differential Equations", Vol. 74 in Mathematics in Science and Engineering, Academic Press 1971.
16. Laughton, M.A. and Humphrey-Davies, M.W., "Numerical techniques in solution of power-system load-flow problems" Proc. I.E.E. Vol. III, No. 9, Sept. 1964, pp. 1575-1588.
17. Lockay, H.E. and Bolger, R.L. "Effect of turbine-generator Representation in System Stability Studies", I.E.E.E. Trans. on Power App. and Systems, Vol. PAS-84, No. 10, Oct. 1965.
18. Olive, D.W. "New Techniques for the Calculation of Dynamic Stability". Trans. I.E.E.E. on Power App. and Systems, Vol. 85, 1966, pp. 767-777.

19. Park, R.H. "Two-reaction theory of Synchronous Machines. Generalized method of Analysis Pt. I", Trans. A.I.E.E., Vol. 48, No. 2, July, 1929, pp. 716-731.
20. Park, R.H. "Two-reaction theory of Synchronous Machines Pt. II", Trans. A.I.E.E., 1933, Vol. 52, p. 352.
21. Freece, C., "The Application of Analogue techniques to the digital study of transient stability problems in Power Systems", Ph.D. Thesis, Newcastle-upon-Tyne University, Jan. 1968.
22. Stagg, G.W. and El-Abiad, A.H., "Computer Methods in Power systems analysis", pub. McGraw-Hill, 1968.
23. Taylor, D.G., "Analaysis of synchronous machines connected to power-system networks", Proc. I.E.E., July 1962, pp. 606-610.
24. Young, C.C., "Equipment and System modelling for large-scale stability studies". I.E.E.E. Trans. on Power App. and Systems. Vol. PAS-91, No. 1, Jan/Feb 1972, pp. 99-110.
25. McCracken, D.D., "A Guide to Fortran IV programming", pub. John Wiley and Sons Inc., 1965.
26. Hamdy A.M. Moussa and Yao-nan Yu, "Optimal Power System stabilization through excitation and/or governor control", Trans. I.E.E.E. on Power App. and Systems, Vol. PAS-91, No. 3, May/June 1972, pp.1116-1174.
27. Jenkins, K., Reyrolle-Parsons Ltd., Private Communication.
28. James, M.L. and Smith, G.M. and Wolford, J.C., "Applied Numerical methods for digital Computation", pub. International Textbook Co. Ltd., 1967.

29. Doherty, R.E. and Nickle, C.A., "Synchronous Machines I",
T.A.I.E.E. 1926, Vol. 45.
30. Doherty, R.E. and Nickle, C.A., "Synchronous Machines II",
T.A.I.E.E., 1926, Vol. 45.
31. Gless, G.E. "Direct method of Liapunov applied to transient power
system stability", I.E.E.E. Trans. on Power App. and Systems,
Vol. PAS-85, No. 2, Feb. 1966.
32. Siddiquee, M.W., "Transient stability of an A.C. generator by Lyapunov's
direct method", Int. J. Control, 1968, Vol. 8, No. 2., pp. 131-144.
33. Willems, J.L., "Optimum Lyapunov functions and Stability regions for
Multimachine power Systems", Proc. I.E.E., Vol. 117, No. 3, March 1970.
34. Dineley, J.L. and Kennedy, M.W., "Influence of governors on Power-
System transient stability", Proc. I.E.E., Vol III, No. 1, Jan. 1964.
35. El-Abiad, A.H. and Nagappan, K., "Transient Stability regions of
Multimachine Power Systems", I.E.E.E. Trans. on Power App. and
Systems, Vol. PAS-85, No. 2, Feb. 1966.
36. Shackshaft, G., "General purpose turbo-alternator model",
Proc. I.E.E., Vol. 110, No. 4, April 1963, p. 703.
37. Dineley, J.L. and Morris, A.J., "Synchronous Generator transient
Control: Pt. I - Theory and evaluation of alternative mathematical
models", I.E.E.E. Trans. Power App. and Systems, March/April 1973,
Vol. PAS-92, No. 2, p.417.
38. Hammons, T.J. and Winning, D.J., "Comparisons of synchronous-machine
models in the study of the transient behaviour of electrical Power
Systems", Proc. I.E.E., Vol. 118, No. 10, Oct. 1971, p.1442.

39. Adkins, B. Discussion on "Comparisons of synchronous-machine models in the study of the transient behaviour of electrical power systems", Proc. I.E.E., Vol. 119, No. 9, Sept. 1972, p.1329.
40. Devotta, J.B.X., Discussion on "Comparisons of synchronous-machine models in the study of the transient behaviour of electrical power systems", Proc. I.E.E., Vol. 119, No. 9, Sept. 1972, p.1330.
41. Harley, R.G. and Adkins, B., "Calculation of the angular back swing following a short circuit of a loaded alternator", Proc. I.E.E., Vol. 117, No. 2, Feb. 1970.
42. Hammons, T.J., "Transient behaviour of synchronous-generator models employing two damper windings on each axis", Paper presented at Eighth Universities Power Engineering Conference 1973, Bath.
43. Mehta, D.B. and Adkins, B., "Transient torque and load angle of a synchronous generator following several types of system disturbance", Proc. I.E.E., 1960, 107A, pp. 61-74.
44. Rogers, G.J. and Smith, J.R. "Synchronous-machine model including eddy currents", Proc. I.E.E., April 1973, Vol. 120, No. 4, p.461.
45. Hughes, F.M., "Improvement of turbogenerator transient performance by control means", Proc. I.E.E., Vol. 120, No. 2, Feb. 1973, p.233.
46. Nicholson, H. "Dynamic Optimisation of a boiler turboalternator model". Proc. I.E.E., Vol. 113, No. 2, Feb. 1966, pp.385-399.
47. Laughton, M.A., "Matrix analysis of dynamic stability in synchronous multimachine systems", Proc. I.E.E. 1966, 113(2), pp.325-336.

48. Aldred, A.S. and Shackshaft, G., "A frequency response method for the predetermination of synchronous-machine stability", Proc. I.E.E. 1960, 107c, p. 2-10.
49. Faruqi, F.A., "Improvement of Power System Transient behaviour using feedback control", Paper at SUPEC 1972, Jan. Bradford.
50. Concordia, C., "Steady-State Stability of Synchronous Machines as affected by voltage-Regulator characteristics", Trans. Amer. Inst. Elect. Eng., May 1944, Vol. 63, pp. 215-220.
51. Kimbark, E.W., "Improvement of system stability by switched series capacitors", I.E.E.E. Trans. on Power App. and Systems, Vol. PAS-85, No. 2, Feb. 1966.
52. Smith, O.J.M., "Power System transient control by Capacitor switching", I.E.E.E. Trans. Power App. and Systems, Vol. PAS-88, No. 1, Jan. 1969, pp. 28-35.
53. Smith, O.J.M., "Optimal removal in a power system", I.E.E.E. Trans. power App. and Sys., Vol. PAS-84, No. 5 and 6, pp. 361-374 and 528-531, June and May 1965.
54. Wood, T.C., "Algorithm 42, Invert", Comm. ACM, Apr. 1961.
55. Prime, H.A., "Modern concepts in Control Theory", pub. McGraw-Hill
1969.
56. Hamdy A.M. Moussa and Yao-nan Yu, "Optimal Stabilization of a Multimachine system", I.E.E.E. Trans. on Power App. and Systems, May/June 1972, Vol. PAS-91, No. 3, pp. 1174-1182.
57. Dineley, J.L. and Morris, A.J., "The Dynamic Interaction of closely-coupled synchronous Generators", I.E.E.E. Trans. on Power App. and Systems, Sept./Oct. 1971, Vol. PAS-90, No. 5, p. 2158.

58. McLain, D.K., Discussion on (33). Proc. I.E.E., Vol. 118, No. 3/4, March/April, 1971.
59. Bumby, J.R. and Preece, C., Discussion on (33) and (58), Vol. 118, No. 11, Nov. 1971.
60. Bumby, J.R. and Preece, C., "Transient Interaction between close coupled generators and its implication for control scheduling", Paper presented at the Eighth Universities power Engineering Conference, Bath, Jan. 1973.
61. De Sarkar, A.K. and N. Dharma Row, "Stabilization of a Synchronous Machine through output feedback control", Trans. I.E.E.E. Power App. and Systems, Vol. PAS-92, No. 1, Jan/Feb 1973.
62. Nicholson, H., "Dynamic Optimisation of a Multimachine power system", Proc. I.E.E., Vol. 113, No. 5, May 1966.
63. Magnusson, P.C., "The Transient-energy method of calculating Stability" A.I.E.E. Trans., 1947, Vol. 66, pp. 747-755.
64. Aylett, P.D., "The Energy-Integral Criterion of Transient Stability limits of a Power System", Proc. I.E.E., July 1958, pp. 527-537.
65. Rosenbrock, H.H., "Design of multivariable Control Systems using the Inverse Nyquist Array", Proc. I.E.E., Vol. 116, No. 11, Nov. 1969, pp. 1929-1936.
66. Rosenbrock, H.H., "Progress in the design of Multivariable control Systems", Measurement and Control, Vol. 4, Jan. 1971, p.9.
67. Mac Farlane, A.G.J., "Multivariable control system design techniques, a guided tour", Proc. I.E.E., Vol. 117, No. 5, pp. 1039, May 1970.

68. Mac Farlane, A.G.J., "Return-difference and return-ratio matrices and their use in analysis and design of multivariable feedback control systems", Proc. I.E.E., Vol. 117, No. 10, Oct. 1970.
- 69A. Munro, N., "Design of controllers for open-loop unstable multivariable systems using inverse Nyquist Array", Proc. I.E.E., Vol. 119, No. 9, Sept. 1972, p.1377.
- 69B. Luntz, R., Munro, N., McLeod, R.S., "Computer aided design of multi-variable control systems", 4th UKAC Control Convention, Sept. 1971, p. 59.
70. Rosenbrock, H.H., "State space and Multivariable Theory", pub. by Nelson 1970.
71. Mc Morran, P., "Application of the Inverse Nyquist Method to a distillation column model", 4th UKAC Control Convention.
72. Rosenbrock, H.H., "On the design of linear multivariable control systems", Proc. 3rd IFAC Congress, London, 1966.
73. Willems, J.L., "Direct Methods for transient Power System stability analysis", 4th UKAC, Control Convention, 1-3 Sept. 1971, pp. 30-34.
74. Edminister, "Electric Circuits", pub. Schaum Publishing Co., 1965.
75. Mittelstadt, W.A., "Four methods of Power System Damping", I.E.E.E. Trans. on Power App. and Systems, Vol. PAS-87, No. 5, May 1968, pp. 1323-1329.
76. Lokay, H.E. and Thoits, P.O., "Effects of Future turbine-generator characteristics on transient stability", I.E.E.E. Trans. on Power App. and Systems Nov./Dec. 1971, Vol. PAS-90, No. 6, p.2427.

77. Butler, J.W. and Concordia, C., "Analysis of series Capacitor Application Problems", A.I.E.E. Trans., Aug. 1937, pp. 975-989.
78. Watson, W. and Mandur, G., "Experience with Supplementary Damping Signals for Generator Static excitation Systems", Trans. I.E.E.E. Power App. and Sys., Jan./Feb. 1973, pp. 199-203.
79. Schleif, F.R., Hunkins, H.D., Martin, G.G., and Hattan, E.E., "Excitation Control to Improve Powerline Stability", I.E.E.E. Trans. on Power App. and Sys., Vol. PAS-87, No. 6, June 1968.
80. Kashkari, C.N., "Effects of feedback signals on transient stability-phase plane approach", I.E.E.E. Trans. on Power App. and Systems, Sept./Oct. 1971, Vol. PAS-90, No. 5, p. 2228.
81. Dineley, J.L. and Morris, A.J., "Synchronous Generator Transient Control Pt. II; Theory and evaluation of new control techniques", March/April 1973, Vol. PAS-92, No. 2, p.423-432.
82. Park, R.H., "Fast Turbine Valving", I.E.E.E. Trans. on Power App. and Systems, May/June 1973, Vol. PAS-92, No. 3, pp. 1065-1073.
83. I.B.M. Application Program, "System 1360 Continuous Modelling Program Users Manual".
84. Webster, R.H., Mane, A.P. and Smith, O.J.M., "Series Capacitor switching to quench electromechanical transients in Power Systems", I.E.E.E. Trans. on Power App. and Systems, Vol. PAS-90, No. 2, March/April 1971, pp. 427-432.
85. Kimbark, E.W. and Middlestadt, W.A., Discussion on "Series Capacitor Switching to quench electromechanical transients in Power Systems", I.E.E.E. Trans. on Power App. and Systems, Vol. PAS-90, No. 2, March/April 1971, p. 432.

86. Taylor, E.R., Discussion on "Series Capacitor Switching to quench electromechanical transients in Power Systems", I.E.E.E. Trans. on Power App. and Systems, Vol. PAS-90, No. 2, March/April 1971, p.432.
87. Shackshaft, G., "Effect of oscillatory torques on the movement of generator rotors", Proc. I.E.E., Vol. 117, No. 10, October 1970, pp. 1969-1974.
88. Smith, O.J.M., "Power System Transient Control by Capacitor Switching", I.E.E.E. Trans. on Power App. and Systems, Vol. PAS-88, No. 1, Jan. 1969, pp. 28-35.
89. Dineley, J.L., Fenwick, P.J., "Voltage Regulation Effects of Fast-Acting Speed Governors on Steam Turbine Generators", I.E.E.E. P.E.S. Summer Meeting and E.H.V./U.H.V. Conference, Vancouver, Canada, July 15-20, 1973.
90. Jefferies, M.J., Gibbs, E.E., Fox, G.R., Holley, C.H., Willyoung, D.M., "Prospects for Superconductive Generators in The Electric Utility Industry", I.E.E.E. Trans. on Power App. and Systems, Vol. PAS-92, No. 5, Sept./Oct. 1973, pp.1659-1666.
91. Richardson, P., Discussion on "Prospects for Superconductive Generators in The Electric Utility Industry", I.E.E.E. Trans. on Power App. and Systems, Vol. PAS-92, No. 5, Sept./Oct. 1973, p. 1666-1669.
92. Appleton, A.D. and Anderson, A.F., "A Review of The Critical Aspects of Superconducting A.C. Generators", Applied Superconductivity Conference, Annapolis, U.S.A., May 1972, paper M-2.

APPENDIX A

DEVELOPMENT OF THE SYNCHRONOUS MACHINE MODEL

A.1 5-WINDING MODEL

Park's equations⁽²⁾ for a synchronous machine with rotor damping effects represented by two short-circuited damper windings (fig. A.1) with saturation effects neglected are given by Hammons and Winning⁽³⁸⁾ and derived by Adkins⁽²⁾ as

e_d	=	$-\left(r_a + \frac{p}{\omega_0} x_d\right)$	$\dot{\nu} x_q$	$\frac{p}{\omega_0} x_{ad}$	$\frac{p}{\omega_0} x_{ad}$	$-\dot{\nu} x_{aq}$	*	i_d
e_q		$-\dot{\nu} x_{cd}$	$-\left(r_a + \frac{p}{\omega_0} x_q\right)$	$\dot{\nu} x_{ad}$	$\dot{\nu} x_{ad}$	$\frac{p}{\omega_0} x_{aq}$		i_q
e_f		$-\frac{p}{\omega_0} x_{ad}$	0	$\left(r_f + \frac{p}{\omega_0} x_f\right)$	$\frac{p}{\omega_0} x_{fd}$	0		i_f
0		$-\frac{p}{\omega_0} x_{ad}$	0	$\frac{p}{\omega_0} x_{fd}$	$\left(r_D + \frac{p}{\omega_0} x_D\right)$	0		i_D
0		0	$-\frac{p}{\omega_0} x_{aq}$	0	0	$\left(r_Q + \frac{p}{\omega_0} x_Q\right)$		i_Q

(A.1)

where $p = d/dt$, x_D , x_q , x_{fd} , x_D and x_Q are complete reactances, x_{ad} and x_{aq} are mutual reactances and $\omega_0 = 2\pi f_0$.

The mechanical equation of motion is

$$\frac{d\omega}{dt} = (P_M - P_T - P_e) \cdot \frac{\pi f_0}{H} \tag{A.2}$$

$$\frac{d\delta_q}{dt} = \omega - 2\pi f \tag{A.3}$$

Neglecting mechanical losses the mechanical input power is equal to the air-gap power

$$P_M = P_T + |I_T|^2 r_a \tag{A.4}$$

P_T , the real power at the machine terminals is given by

$$P_T - jQ_T = I_T \cdot E_T^* \tag{A.5}$$

The negative sign and the complex conjugate being used so as to conform to the convention of capacitive reactive power as positive.⁽¹²⁾

The speed equation is given by

$$\mathcal{N} = 1 + \frac{p \cdot \mathcal{E}}{\omega_0} \quad (\text{A.6})$$

The fluxes linking the respective windings are

$$\Phi_d = -x_d \cdot i_d + x_{ad} \cdot i_f + x_{ad} \cdot i_D \quad (\text{A.7})$$

$$\Phi_f = -x_{ad} \cdot i_d + x_f \cdot i_f + x_{fd} \cdot i_D \quad (\text{A.8})$$

$$\Phi_D = -x_{ad} \cdot i_d + x_{fd} \cdot i_f + x_D \cdot i_D \quad (\text{A.9})$$

$$\Phi_q = -x_q \cdot i_q + x_{aq} \cdot i_Q \quad (\text{A.10})$$

$$\Phi_Q = -x_{aq} \cdot i_q + x_Q \cdot i_Q \quad (\text{A.11})$$

and the electrical torque is given by

$$P_T = (\Phi_d \cdot i_q - \Phi_q \cdot i_d) \cdot \frac{\mathcal{N}}{2\omega_0} \quad (\text{A.12})$$

These equations can be simplified by approximating $x_{fd} = x_{ad}$ in equation (A.1). This simplification used by Hammons and Winning⁽³⁸⁾ and further explained by Adkins⁽²⁾ gives

$$\Phi_d = -x_d(p) \cdot i_d + \frac{x_{ad}}{r_f} \cdot G(p) \cdot e_f \quad (\text{A.13})$$

$$\Phi_q = -x_q(p) \cdot i_q \quad (\text{A.14})$$

where $x_d(p)$, $x_q(p)$ and $G(p)$ are operational impedances approximated by

$$x_d(p) = \frac{x_d \cdot (1 + p \cdot T_d') (1 + p \cdot T_d'')}{(1 + p \cdot T_{d0}') (1 + p \cdot T_{d0}'')} \quad (\text{A.15})$$

$$x_q(p) = x_q \cdot \frac{(1 + p \cdot T_q'')}{(1 + p \cdot T_{q0}'')} \quad (\text{A.16})$$

$$G(p) = \frac{(1 + p \cdot T_D)}{(1 + p \cdot T_{D0}') (1 + p \cdot T_{D0}'')} \quad (\text{A.17})$$

If a base assuming unit excitation produces unit armature voltage then equation (A.13) becomes

$$\Phi_d = -x_d(p) \cdot i_d + G(p) \cdot e_f \quad (\text{A.18})$$

Equations (A.13) and (A.14) can be expanded and written using the unit excitation/unit armature voltage base per unit system as

$$\begin{aligned} \phi_d = & \frac{-A}{1+p.Td_0'} . i_d - \frac{B}{1+p.Td_0''} i_d - x_d'' . i_d \\ & + \frac{G'}{1+p.Td_0'} . e_f - \frac{G''}{1+p.Td_0''} . e_f \end{aligned} \quad (A.19)$$

$$\phi_q = -\frac{(x_q - x_q'')}{(1+p.Tq_0'')} i_q - x_q'' . i_q \quad (A.20)$$

where

$$\begin{aligned} A & \approx x_d - x_d' & x_d'' & = x_d' . \frac{T_d''}{T_d_0''} \\ B & \approx x_d' - x_d'' & & \\ x_d' & = x_d . \frac{T_d'}{T_d_0'} & x_q'' & = x_q . \frac{T_q''}{T_q_0''} \\ G' & = \frac{T_d_0' - T_D}{T_d_0' - T_d_0''} & G'' & = \frac{T_d_0'' - T_D}{T_d_0' - T_d_0''} \end{aligned} \quad (A.21)$$

Further simplification and Hammons and Winning⁽³⁸⁾ introducing the variables

$$e_q' = \frac{G'}{1+p.Td_0'} . e_f - \frac{x_d - x_d'}{1+p.Td_0'} . i_d \quad (A.22)$$

$$e_q'' = \phi_d + x_d'' . i_d \quad (A.23)$$

$$e_d'' = -(\phi_q + x_q'' . i_q) \quad (A.24)$$

yields a simplification of the voltage equations (see (A.1))

$$e_d = -r_a . i_d + \frac{p}{\omega_0} \phi_d - \dot{\nu} . \phi_q \quad (A.25)$$

$$e_q = -r_a . i_q + \frac{p}{\omega_0} \phi_q + \dot{\nu} . \phi_d \quad (A.26)$$

to

$$e_d = -r_a . i_d + \frac{p}{\omega_0} e_q'' + \dot{\nu} . e_d'' + x_q'' . i_q \quad (A.27)$$

$$e_q = -r_a \cdot i_q - \frac{P}{\omega_0} e_d'' + \nu \cdot e_q'' - x_d'' \cdot i_d \quad (\text{A.28})$$

where

$$P \cdot e_q' = \frac{1}{T_{d0}'} (G' \cdot e_f - (x_d - x_d') \cdot i_d - e_q') \quad (\text{A.29})$$

$$P \cdot e_q'' = \frac{1}{T_{d0}''} (-G'' \cdot e_f - (x_d' - x_d'') \cdot i_d - e_q'' + e_q') + P \cdot e_q' \quad (\text{A.30})$$

$$P \cdot e_d'' = \frac{1}{T_{q0}''} ((x_q - x_q'') \cdot i_q - e_d'') \quad (\text{A.31})$$

After rearrangement of equation (A.22) and substitution of equations (A.30) and (A.31) into (A.19) (A.20) and (A.29)

Finally substituting Φ_d and Φ_q from equations (A.23) and (A.24) into (A.12) yields

$$P_T = e_d'' \cdot i_d + e_q'' \cdot i_q + (x_q'' - x_d'') \cdot i_d \cdot i_q \quad (\text{A.32})$$

A.2 3 WINDING MODEL

If the damper circuits D and Q in fig. (A.1) are omitted then i_D and i_Q in equation (A.1) are set equal to zero then the equations similar to (A.19) and (A.20) after substitution become

$$\Phi_d = \frac{-x_d - x_d'}{1 + p \cdot T_{d0}'} \cdot i_d - x_d' \cdot i_d + \frac{1}{1 + p \cdot T_{d0}'} \cdot e_f \quad (\text{A.33})$$

$$\Phi_q = -x_q \cdot i_q \quad (\text{A.34})$$

Introducing e_q'

$$e_q' = \frac{1}{1 + p \cdot T_{d0}'} \cdot e_f - \frac{x_d - x_d'}{1 + p \cdot T_{d0}'} \cdot i_d \quad (\text{A.35})$$

Again using the simplification used by Hammons and Winning⁽³⁸⁾ yields from (A.25) and (A.26)

$$e_d = -r_a \cdot i_d + x_q \cdot i_q \quad (\text{A.36})$$

$$e_q = -r_a \cdot i_q - x_d' \cdot i_d + e_q' \quad (\text{A.37})$$

Rearranging (A.35) gives

$$p \cdot e_q' = \frac{1}{T_{d0}'} (e_f - (x_d - x_d') \cdot i_d - e_q') \quad (\text{A.38})$$

Further substitution into (A.12) yields

$$P_T = (e_q' + (x_q - x_d') \cdot i_d) \cdot i_q \quad (\text{A.39})$$

An equivalent damping coefficient can be incorporated in equation (A.2) in the form of a velocity dependent term to account for positive sequence damping such that

$$\frac{d\omega}{dt} = (P_M - P_T - P_e - K_d \cdot \dot{\delta}) \cdot \frac{\pi \cdot f_0}{H} \quad (\text{A.40})$$

During the steady state equations (A.36) and (A.37) become

$$E_{Td} = -r_a \cdot I_d + x_q \cdot I_q \quad (\text{A.41})$$

$$E_{Tq} = -r_a \cdot I_q - x_d \cdot I_d + E_{q0} \quad (\text{A.42})$$

Because the stator quantities can be represented by slowly changing phasors the steady state equations are still valid during the transient period.

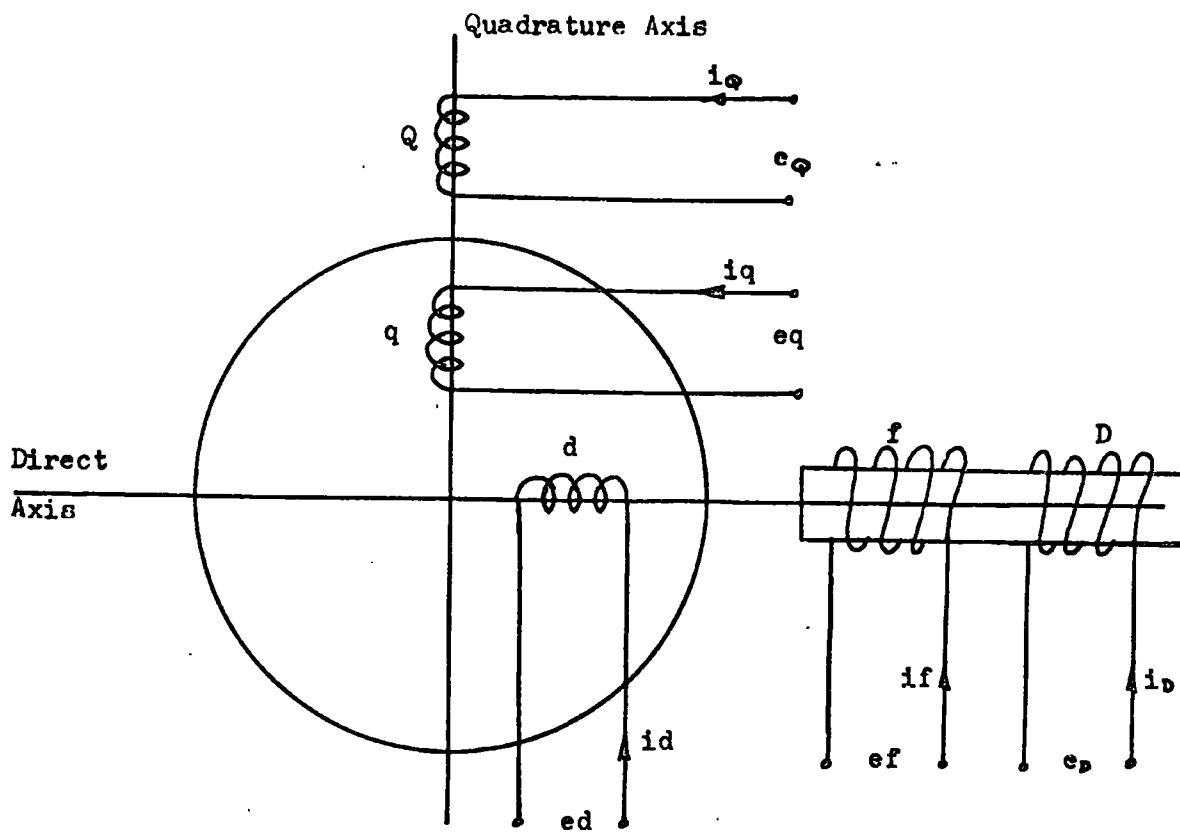


Fig. A.1 5 - Winding Synchronous Machine Model

APPENDIX B

THE NETWORK EQUATIONS

B.1 STEADY STATE

The real and reactive power at any bus k , is

$$P_k - j \cdot Q_k = E_k^* \cdot I_k \quad (B.1)$$

$$\therefore I_k = \frac{P_k - j \cdot Q_k}{E_k^*} \quad (B.2)$$

The performance of the network is given by

$$I_{BUS} = Y_{BUS} \cdot E_{BUS} \quad (B.3)$$

As ground is selected as the reference node (n-1) simultaneous equations of the form

$$E_k = \frac{1}{Y_{kk}} \left(I_k - \sum_{\substack{\ell=1 \\ \ell \neq k}}^n Y_{k\ell} \cdot E_\ell \right) \quad \begin{matrix} k=1, 2, \dots, n \\ k \neq s \end{matrix} \quad (B.4)$$

are set up.

Substituting (B.2) into (B.4)

$$E_k = \frac{1}{Y_{kk}} \left(\frac{P_k - j \cdot Q_k}{E_k^*} - \sum_{\substack{\ell=1 \\ \ell \neq k}}^n Y_{k\ell} \cdot E_\ell \right) \quad \begin{matrix} k=1, 2, \dots, n \\ k \neq s \end{matrix} \quad (B.5)$$

Equation (B.5) provides a set of simultaneous equations that must be solved by an iterative process to obtain the final bus voltages.

$$Y_{kk} = \sum_{\substack{\ell=1 \\ \ell \neq k}}^n y_{k\ell} + y_k \quad (B.6)$$

where

$$y_k = \sum_{\substack{\ell=1 \\ \ell \neq k}}^n y'_{k\ell} / 2 + y_{kSHUNT} \quad (B.7)$$

where

$\frac{y'_{k\ell}}{2}$ = the line charging between buses k and ℓ assumed as a shunt impedance split in two and lumped at both ends of the line.

Y_{KSHUNT} = any shunt admittances at bus k.

and $Y_{kl} = -y_{kl}$ (B.8)

When the final bus voltages have been obtained the power flow down each line and the power loss in each line is calculated

$$I_{kl} = (E_k - E_l) \cdot y_{kl} + E_k \cdot \frac{y'_{kl}}{2} \quad (B.9)$$

where $E_k \cdot \frac{y'_{kl}}{2}$ = current contribution at bus k due to line charging then

$$P_{kl} - j \cdot Q_{kl} = E_k^* \cdot I_{kl} \quad (B.10)$$

$$P_{lk} - j \cdot Q_{lk} = E_l^* \cdot I_{kl} \quad (B.11)$$

The power loss in line kl is given by the algebraic sum of equations (B.10) and (B.11)

B.2 TRANSIENT STATE

By representing loads as static admittances to ground

i.e. $y_{ko} = \frac{P_{Lk} - j \cdot Q_{Lk}}{E_k^* \cdot E_k}$ (B.12)

equation (B.5) is modified as now the impressed current at the bus is zero and (B.5) becomes

$$E_k = - \sum_{\substack{l=1 \\ l \neq k}}^{n+m} \frac{Y_{kl}}{Y_{kk}} \cdot E_l \quad \begin{array}{l} k=1, 2, \dots, n \\ k \neq s \\ \text{and during fault, if} \\ \text{3 phase } k \neq f \end{array} \quad (B.13)$$

and

$$Y_{kk} = \sum_{\substack{l=1 \\ l \neq k}}^{n+m} y_{kl} + y_k + y_{ko} \quad (B.14)$$

$$Y_{kl} = -y_{kl} \quad (B.15)$$

APPENDIX C

DEVELOPMENT OF THE LINEAR SYSTEM MODEL

C.1 MACHINE EQUATIONS

The machine equations for REP 2 are for the k^{th} machine

$$I_{TK} = \frac{E'_k - E_{TK}}{j \cdot x d'_k} \quad (C.1)$$

$$P_{TK} - j Q_{TK} = I_{TK} \cdot E'_k{}^* \quad (C.2)$$

$$e'_k = |E'_k| \cdot \cos \delta_k \quad (C.3)$$

$$f'_k = |E'_k| \cdot \sin \delta_k \quad (C.4)$$

$$E'_k = e'_k + j \cdot f'_k \quad (C.5)$$

$$\dot{\omega}_k = (P_{mk} - P_{TK} - K d_k \cdot \dot{\delta}_{qk}) \frac{f \cdot \pi}{H_k} \quad (C.6)$$

$$\dot{\delta}_{qk} = \omega_k - 2 \cdot \pi \cdot f \quad (C.7)$$

$$\frac{|E_{q'}|_k}{|E_{fd}|_k} = \frac{G_k}{1 + p \cdot T d o'_k} \quad (C.8)$$

where

$$G_k = \frac{|E_{q_0'}|_k}{|E_{fd_0}|_k} \quad (C.9)$$

$$|E'|_k = \sqrt{|E_{q'}|_k^2 + |E_{d'}|_k^2} \quad (C.10)$$

$$\tan \delta_{hk} = \frac{|E_{d'}|_k}{|E_{q'}|_k} \quad (C.11)$$

$$\delta_{qk} - \delta_{hk} = \delta_k \quad (C.12)$$

The phasor diagram described by these equations is shown in

fig. C.1.

Linearising by using a first order Taylor expansion around the initial operating point yields

$$\Delta I_{TK} = \frac{\Delta E'_k - \Delta E_{TK}}{j \cdot x_{d'k}} \quad (C.13)$$

$$\Delta (P_{TK} - j Q_{TK}) = \Delta I_{TK} \cdot E_{o'k}^* + I_{T0k} \cdot \Delta E'_k \quad (C.14)$$

$$\Delta e'_k = \Delta |E'_k| \cdot \cos \delta_{ok} - |E_{o'k}| \cdot \sin \delta_{ok} \cdot \Delta \delta_k \quad (C.15)$$

$$\Delta f'_k = \Delta |E'_k| \cdot \sin \delta_{ok} + |E_{o'k}| \cdot \cos \delta_{ok} \cdot \Delta \delta_k \quad (C.16)$$

$$\Delta E'_k = \Delta e'_k + j \cdot \Delta f'_k \quad (C.16a)$$

$$\Delta \dot{\omega}_k = (\Delta P_{mk} - \Delta P_{TK} - k d_k \cdot \Delta \dot{\delta}_{qk}) \cdot \frac{f \cdot \pi}{H_k} \quad (C.17)$$

$$\Delta \dot{\delta}_{qk} = \Delta \omega_k \quad (C.18)$$

$$\Delta |\dot{E}_{q'k}| = \frac{|E_{q'o'k}|}{|E_{o'k}|} \cdot \Delta |E_{q'k}| \quad (C.19)$$

$$\Delta |E'k| = \frac{|E_{q'o'k}|}{|E_{o'k}|} \cdot \Delta |E_{q'k}| \quad (C.20)$$

$$\Delta \delta_{hk} = \frac{-\cos \delta_{hok} \cdot \sin \delta_{hok} \cdot \Delta |E_{q'k}|}{|E_{q'o'k}|} \quad (C.21)$$

Substituting (C.20) into (C.21)

$$\Delta \delta_{hk} = \frac{-1}{|E_{o'k}|} \frac{\sin(\delta_{qo} - \delta_o)}{\cos(\delta_{qo} - \delta_o)} \cdot \Delta |E'k| \quad (C.21a)$$

$$\Delta \delta_{qk} - \Delta \delta_{hk} = \Delta \delta_k \quad (C.22)$$

Substitution of equation (C.20) and (C.21) into (C.19)

$$\Delta |\dot{E}'k| = \frac{G_k \cdot \Delta |E_{fd'k}| - \Delta |E'k|}{T_{d'o'k}} \quad (C.23)$$

where

$$G_k = \frac{|E_{o'k}| \cdot \cos^2(\delta_{qo} - \delta_o)_k}{|E_{fd'o'k}|} \quad (C.24)$$

C.2 SYSTEM EQUATIONS

The network performance equations (B.13) are linearised to give for bus k

$$\Delta E_k = - \sum_{\substack{\ell=1 \\ \ell \neq k}}^{n+m} \frac{Y_{k\ell}}{Y_{kk}} \cdot \Delta E_\ell - \sum_{\substack{\ell=1 \\ \ell \neq k}}^{n+m} \Delta \left[\frac{Y_{k\ell}}{Y_{kk}} \right] \cdot E_{\ell_0} \quad (C.25)$$

Assuming no change in the line admittances on the occurrence of a fault and writing the voltages ΔE_ℓ , $\ell = n+1, n+2, \dots, n+m$ as $\Delta E'_\ell$, $\ell = 1, 2, \dots, m$ and ΔE_ℓ , $\ell = 1, 2, \dots, n$ as $\Delta E_{T\ell}$, $\ell = 1, 2, \dots, n$.

$$\Delta E_{Tk} + \sum_{\substack{\ell=1 \\ \ell \neq k}}^n \frac{Y_{k\ell}}{Y_{kk}} \cdot \Delta E_{T\ell} = - \sum_{\ell=1}^m \frac{Y_{k, \ell+n}}{Y_{kk}} \cdot \Delta E'_\ell \quad (C.26)$$

writing

$$y_{k\ell} = \frac{Y_{k\ell}}{Y_{kk}}$$

gives

$$\sum_{\ell=1}^n y_{k\ell} \cdot \Delta E_{T\ell} = - \sum_{\ell=1}^m y_{k, \ell+n} \cdot \Delta E'_\ell \quad (C.27)$$

Equation (C.27) assumes that each machine is connected to each and every other bus. In general only one machine will be connected to any one bus in the order that machine 1 is connected to bus 1, machine 2 connected to bus 2 etc. Then equation (C.27) becomes for bus k and machine k

$$\sum_{\ell=1}^n y_{k\ell} \cdot \Delta E_{T\ell} = - y_{k, n+k} \cdot \Delta E'_k \quad (C.28)$$

Let

$$y_{ki} = \frac{y_{k\ell}}{y_{k, n+k}} \quad \text{for } k \leq m \quad (C.29)$$

and

$$y_{ki} = y_{k\ell} \quad \text{for } k > m$$

then

$$\sum_{\ell=1}^n y_{ki} \cdot \Delta E_{T\ell} = - \Delta E'_k \quad (C.30)$$

which can be written in the matrix form

$$[Y] * [\Delta E_T] = -[\Delta E'] \quad (C.31)$$

or

$$[\Delta E_T] = -[Y]^{-1} * [\Delta E'] \quad (C.32)$$

which is similar to, for bus k and machine k

$$\Delta E_{Tk} = - \sum_{\ell=1}^M \hat{y}_{k\ell} \Delta E'_\ell \quad (C.33)$$

Equation (C.33) yields a direct relationship between the voltages at any of the buses and the machine internal voltages.

If an infinite bus is included in the network this bus becomes bus number n . Because of the nature of an infinite bus $\Delta E_{Tn} = 0$.

Consequently equation (C.30) would become

$$\sum_{\ell=1}^{n-1} y_{k\ell} \Delta E_{T\ell} = -\Delta E'_k, \quad k=1,2,\dots,n-1. \quad (C.34)$$

This changes the order of the Y matrix in equation (C.31) which would alter the matrix inversion in equation (C.32). The inclusion of an infinite bus is optional within the program.

C.3 CONNECTION OF THE MACHINE AND NETWORK EQUATIONS

The linear equations (C.13) - (C.24) and (C.33) are written with state variables and input vectors are described as

$$\begin{array}{ll} \Delta P_{m1} = \alpha_1 & \Delta w_1 = x_1 \\ \vdots & \vdots \\ \Delta P_{mm} = \alpha_m & \Delta w_m = x_m \\ \Delta E_{fd1} = u_1 & \Delta \delta q_1 = x_{m+1} \\ \vdots & \vdots \\ \Delta E_{fdm} = u_m & \Delta \delta q_m = x_{2m} \\ & \Delta |E'|_1 = x_{2m+1} \\ & \vdots \\ & \Delta |E'|_m = x_{3m} \end{array} \quad (C.35)$$

Assume initially

$$\begin{aligned} \Delta \delta_1 &= X_{m+1} \\ &\vdots \\ \Delta \delta_m &= X_{2m} \end{aligned} \quad (C.36)$$

Substituting (C.35) and (C.36) into (C.15), (C.16) and (C.5) for machine k

$$\begin{aligned} \Delta E'_k &= (\cos \delta_{0k} + j \sin \delta_{0k}) \cdot X_{2m+k} \\ &- |E_{0k}'| (\sin \delta_{0k} - j \cos \delta_{0k}) \cdot X_{m+k} \end{aligned} \quad (C.37)$$

Letting $\underline{\Phi}_k = \cos \delta_{0k} + j \sin \delta_{0k}$ (C.38)

Equation (C.37) becomes

$$\Delta E'_k = [\underline{\Phi}_k, |E_{0k}'| \cdot j \cdot \underline{\Phi}_k]_* \begin{bmatrix} X_{2m+k} \\ X_{m+k} \end{bmatrix} \quad (C.39)$$

and

$$\Delta E'_k{}^* = [\underline{\Phi}_k^*, -|E_{0k}'| \cdot j \cdot \underline{\Phi}_k^*]_* \begin{bmatrix} X_{2m+k} \\ X_{m+k} \end{bmatrix} \quad (C.40)$$

Substituting (C.39) into (C.33) and (C.13)

$$\begin{aligned} \Delta I_{Tk} &= \frac{1}{j \cdot x d'_k} [\underline{\Phi}_k, |E_{0k}'| \cdot j \cdot \underline{\Phi}_k]_* \begin{bmatrix} X_{2m+k} \\ X_{m+k} \end{bmatrix} \\ &+ \frac{1}{j \cdot x d'_k} \left[\sum_{\substack{e=1 \\ e \neq k}}^m \hat{y}_{ke} [\underline{\Phi}_e, |E_{0e}'| \cdot j \cdot \underline{\Phi}_e] \begin{bmatrix} X_{2m+e} \\ X_{m+e} \end{bmatrix} \right] \end{aligned} \quad (C.41)$$

Substitution of (C.41) into (C.14) and taking the REAL part only

$$\begin{aligned} \Delta P_{Tk} \cdot \frac{f \cdot \pi}{H_k} &= [\Gamma_{1k}, \Gamma_{2k}]_* \begin{bmatrix} X_{2m+k} \\ X_{m+k} \end{bmatrix} \\ &+ \sum_{\substack{e=1 \\ e \neq k}}^m [\gamma_{1ke}, \gamma_{2ke}] \begin{bmatrix} X_{2m+e} \\ X_{m+e} \end{bmatrix} \end{aligned} \quad (C.42)$$

where,

$$\begin{aligned} \Gamma_{1k} &= \text{REAL} \left[E_{0k}'^* \cdot \frac{1}{j \cdot x d'_k} \cdot \underline{\Phi}_k + \hat{y}_{kk} \cdot E_{0k}'^* \cdot \frac{1}{j \cdot x d'_k} \cdot \underline{\Phi}_k \right. \\ &\quad \left. + I_{T0k} \cdot \underline{\Phi}_k^* \right] \cdot \frac{f \cdot \pi}{H_k} \end{aligned}$$

$$\Gamma'_{2k} = \text{REAL} \left[E_{0k}'^* \cdot |E_{0k}'| \cdot j \cdot \Phi_k \cdot \frac{1}{j \cdot \alpha d'_k} + E_{0k}'^* \cdot \frac{1}{j \cdot \alpha d'_k} \cdot \hat{y}_{kk} \cdot |E_{0k}'| \cdot j \cdot \Phi_k \right. \\ \left. - I_{T0k} \cdot |E_{0k}'| \cdot j \cdot \Phi_k^* \right] \cdot \frac{f \cdot \pi}{H_k}$$

$$y_{1ke} = \text{REAL} \left[E_{0k}'^* \cdot \frac{1}{j \cdot \alpha d'_k} \cdot \hat{y}_{ke} \cdot \Phi_e \right] \cdot \frac{f \cdot \pi}{H_k}$$

$$y_{2ke} = \text{REAL} \left[E_{0k}'^* \cdot \frac{1}{j \cdot \alpha d'_k} \cdot \hat{y}_{ke} \cdot |E_{0e}'| \cdot j \cdot \Phi_e \right] \frac{f \cdot \pi}{H_k} \quad (C.43)$$

Substitute (C.42) into (C.17)

$$\dot{x}_k = \left[\frac{f \cdot \pi \cdot d_k}{H_k} - [\Gamma'_{1k}, \Gamma'_{2k}] \begin{bmatrix} x_{2m+k} \\ x_{m+k} \end{bmatrix} \right. \\ \left. - \sum_{\substack{l=1 \\ l \neq k}}^M [y_{1ke}, y_{2ke}] \begin{bmatrix} x_{2m+l} \\ x_{m+l} \end{bmatrix} - \frac{K d_k \cdot f \cdot \pi \cdot x_k}{H_k} \right] \quad (C.44)$$

Taking $\Delta \delta_h$ into account from (C.22) as

$$x_{m+l} = \Delta \delta_{he} = x_{m+l} \quad (C.45)$$

gives

$$\dot{x}_k = \frac{f \cdot \pi \cdot d_k}{H_k} - [\Gamma'_{1k}, \Gamma'_{2k}] \begin{bmatrix} x_{2m+k} \\ x_{m+k} \end{bmatrix} \\ - \sum_{\substack{l=1 \\ l \neq k}}^M [y_{1ke}, y_{2ke}] \begin{bmatrix} x_{2m+l} \\ x_{m+l} \end{bmatrix} - \frac{K d_k \cdot f \cdot \pi \cdot x_k}{H_k} \quad (C.46)$$

where

$$\Gamma'_{1k} = \Gamma_{1k} + \Gamma_{2k} \cdot \frac{1}{|E_{0k}'|} \cdot \frac{\sin(\delta_{q0} - \delta_0)_k}{\cos(\delta_{q0} - \delta_0)_k}$$

$$y_{1ke} = y_{1ke} + y_{2ke} \cdot \frac{1}{|E_{0e}'|} \cdot \frac{\sin(\delta_{q0} - \delta_0)_k}{\cos(\delta_{q0} - \delta_0)_k} \quad (C.47)$$

Rewrite (C.24) as

$$\dot{x}_{2m+k} = \frac{G_k}{T d'_{0k}} \cdot u_k - \frac{1}{T d'_{0k}} \cdot x_{2m+k} \quad (C.48)$$

and finally

$$\dot{x}_{m+k} = x_k \quad (C.49)$$

The final set of linear equations are given by (C.46), (C.48) and (C.49).

C.4 CALCULATION OF THE OUTPUT MATRIX FOR VOLTAGE FEEDBACK

The magnitude of the terminal voltage is given by,

$$|E_T|_k^2 = \text{REAL}(E_{Tk})^2 + \text{IMAG}(E_{Tk})^2 \quad (\text{C.50})$$

which on linearising gives

$$\Delta |E_T|_k = \frac{\text{REAL}(E_{Tk_0}) \cdot \Delta [\text{REAL}(E_{Tk})] + \text{IMAG}(E_{Tk_0}) \cdot \Delta [\text{IMAG}(E_{Tk})]}{|E_T|_{k_0}} \quad (\text{C.51})$$

Substituting equation (C.39) and (C.33) into (C.51) gives

$$y = \Delta |E_T|_k = \sum_{k=1}^M (k_{1ke}, k_{2ke}) \begin{bmatrix} x_{2m+l} \\ x_{m+l} \end{bmatrix} \quad (\text{C.52})$$

where

$$\begin{aligned} k_{1ke} &= \text{REAL} \left[\frac{-\text{REAL}(E_{Tk_0}) \cdot \hat{y}_{ke} \cdot \Phi_e}{|E_T|_{k_0}} \right] \\ &+ \text{IMAG} \left[\frac{-\text{IMAG}(E_{Tk_0}) \cdot \hat{y}_{ke} \cdot \Phi_e}{|E_T|_{k_0}} \right] \\ k_{2ke} &= \text{REAL} \left[\frac{-\text{REAL}(E_{Tk_0}) \cdot \hat{y}_{ke} \cdot |E_0'|_{e,j} \cdot \Phi_e}{|E_T|_{k_0}} \right] \\ &+ \text{IMAG} \left[\frac{-\text{IMAG}(E_{Tk_0}) \cdot \hat{y}_{ke} \cdot |E_0'|_{e,j} \cdot \Phi_e}{|E_T|_{k_0}} \right] \end{aligned} \quad (\text{C.53})$$

using (C.45) and (C.21) gives

$$y = \Delta |E_T|_k = \sum_{k=1}^M (k_{1ke}, k_{2ke}) \begin{bmatrix} x_{2m+l} \\ x_{m+l} \end{bmatrix} \quad (\text{C.54})$$

where

$$k_{1ke} = k_{1ke} + k_{2ke} \cdot \frac{1}{|E_0'|_e} \cdot \frac{\sin(\delta_{q_0} - \delta_0)_e}{\cos(\delta_{q_0} - \delta_0)_e} \quad (\text{C.55})$$

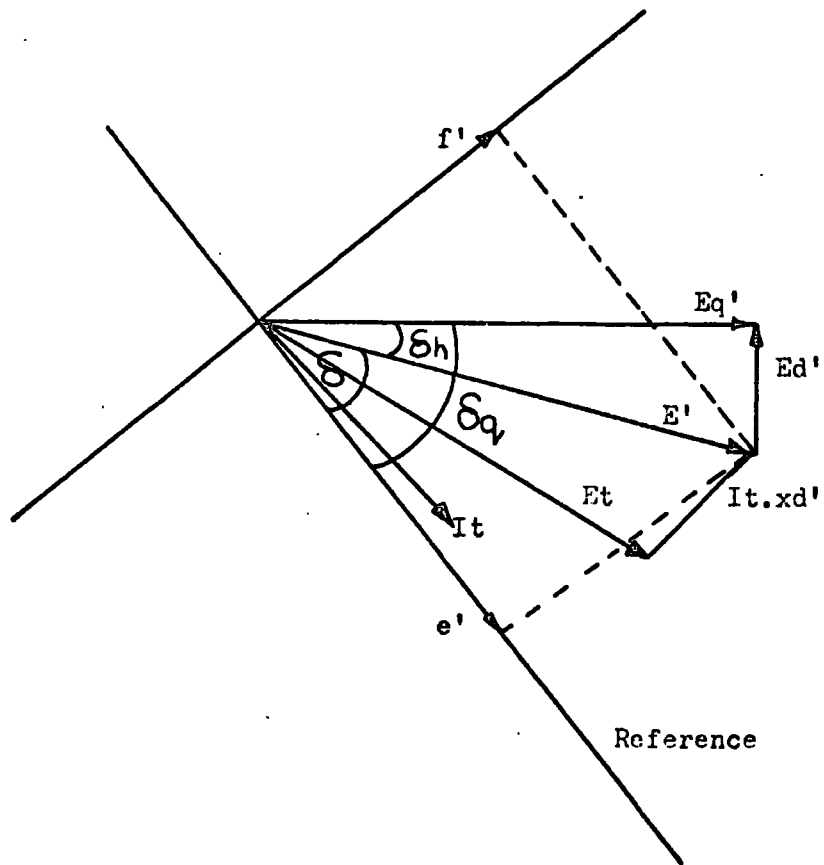


Fig. C.1 Phasor Diagram On Which The Linearised Model is Based.

APPENDIX D

A DESCRIPTION OF THE MULTIMACHINE DIGITAL PROGRAM

The high level language FORTRAN IV⁽²⁵⁾ and Double Precision complex variables used throughout. It was found that due to the integration and iteration the cumulative error was excessive when single precision variables were used.

SUBROUTINES CALLED

MAIN fig. D.1

Data is processed by the MAIN program. This section contains the machine model and also calls the other subroutines at the required moment.

MODAT fig. D.2

This forms the bus admittance matrix and also carries out any alterations to this matrix if necessary.

LFLOW fig. D.3

This carries out the load flow solutions in the steady and transient state.

EULER, MEULER, RKFIX, RKVAR

These are the four integration routines available.

PLOTTY

This plots out any specified three variables of the system. Scaling is pre-set.

DIMAG, DREAL

These are two function subprograms that find the real and imaginary parts of a number.

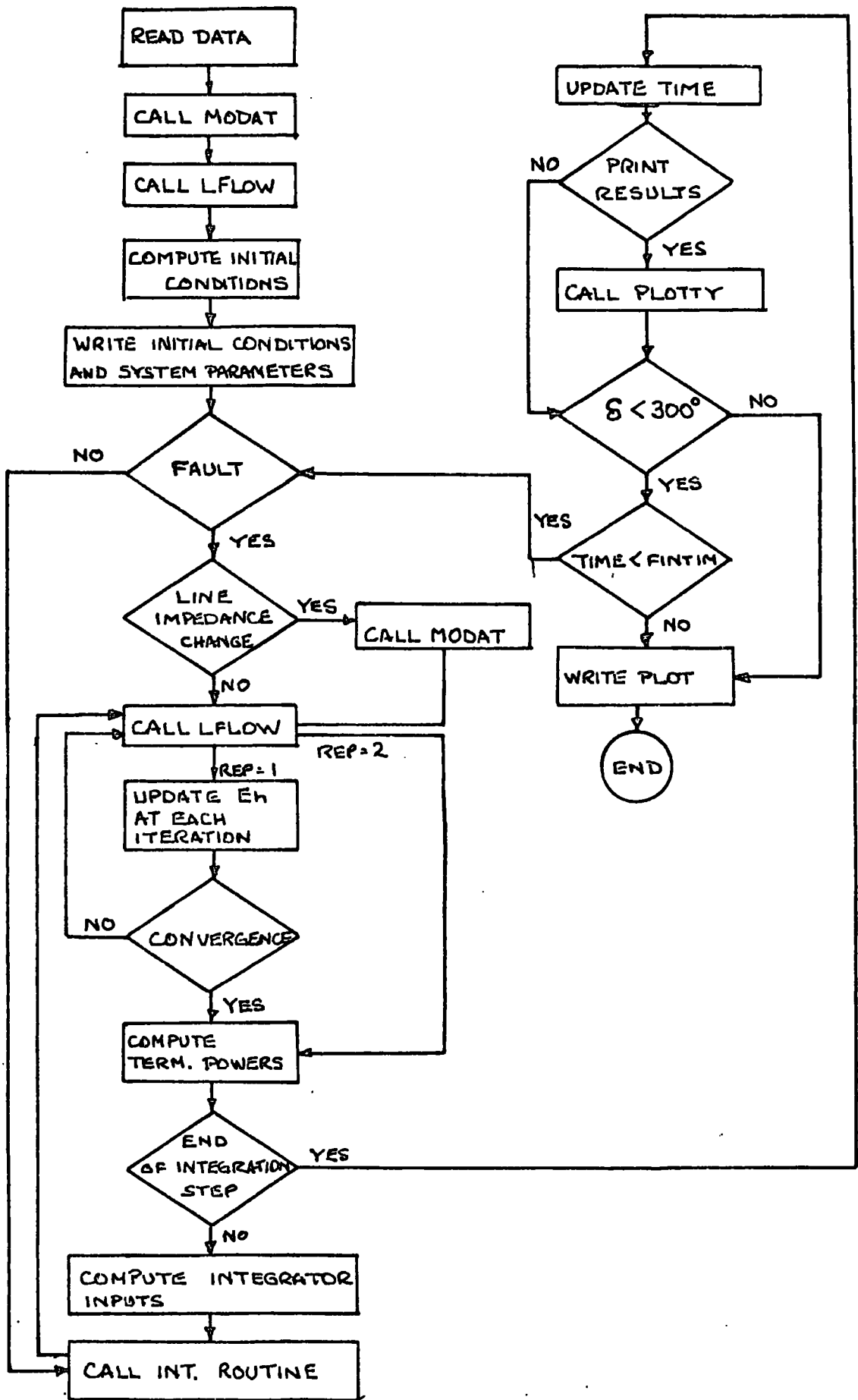
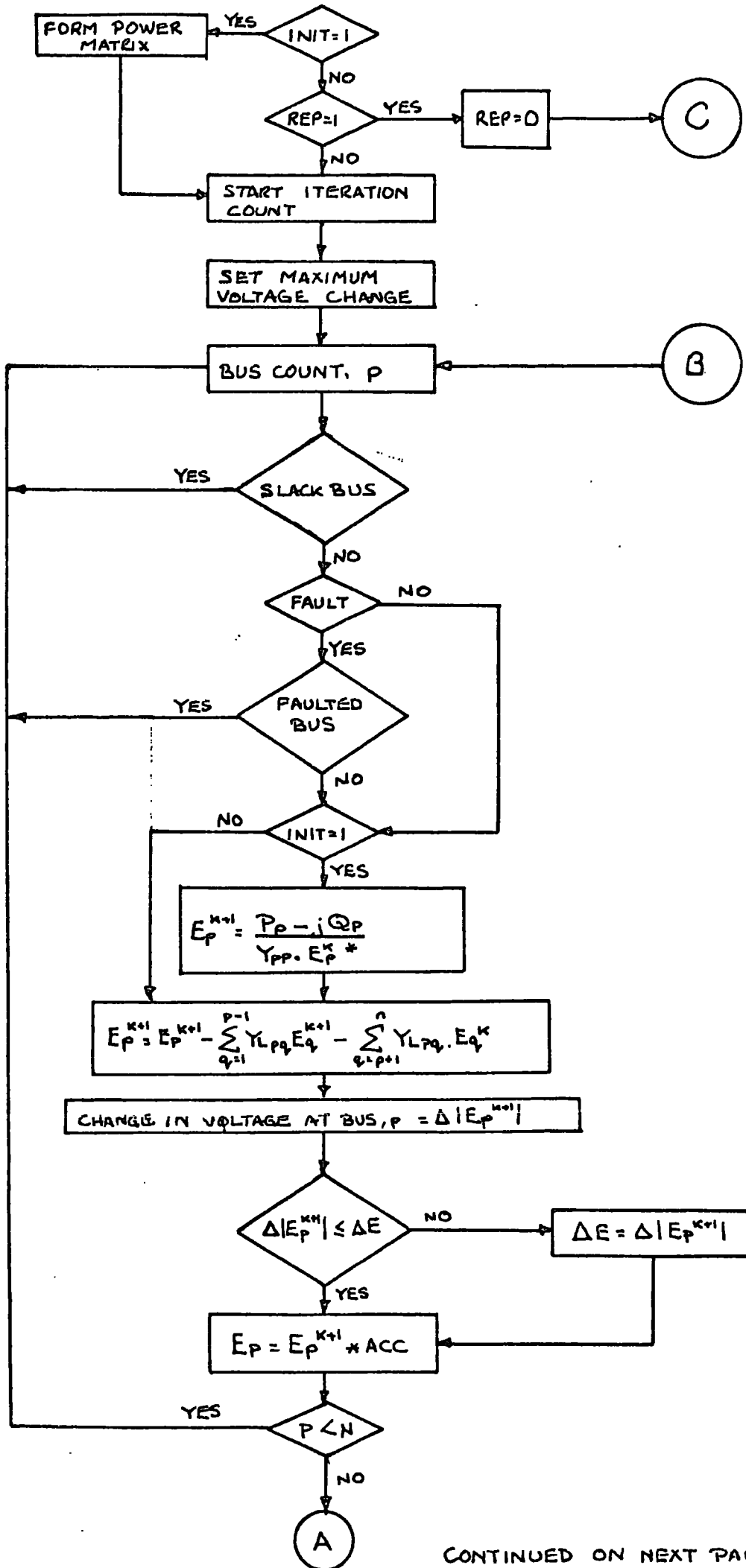


Fig. D.1 Flow Diagram Of The Non-Linear Multi-Machine Program



CONTINUED ON NEXT PAGE.

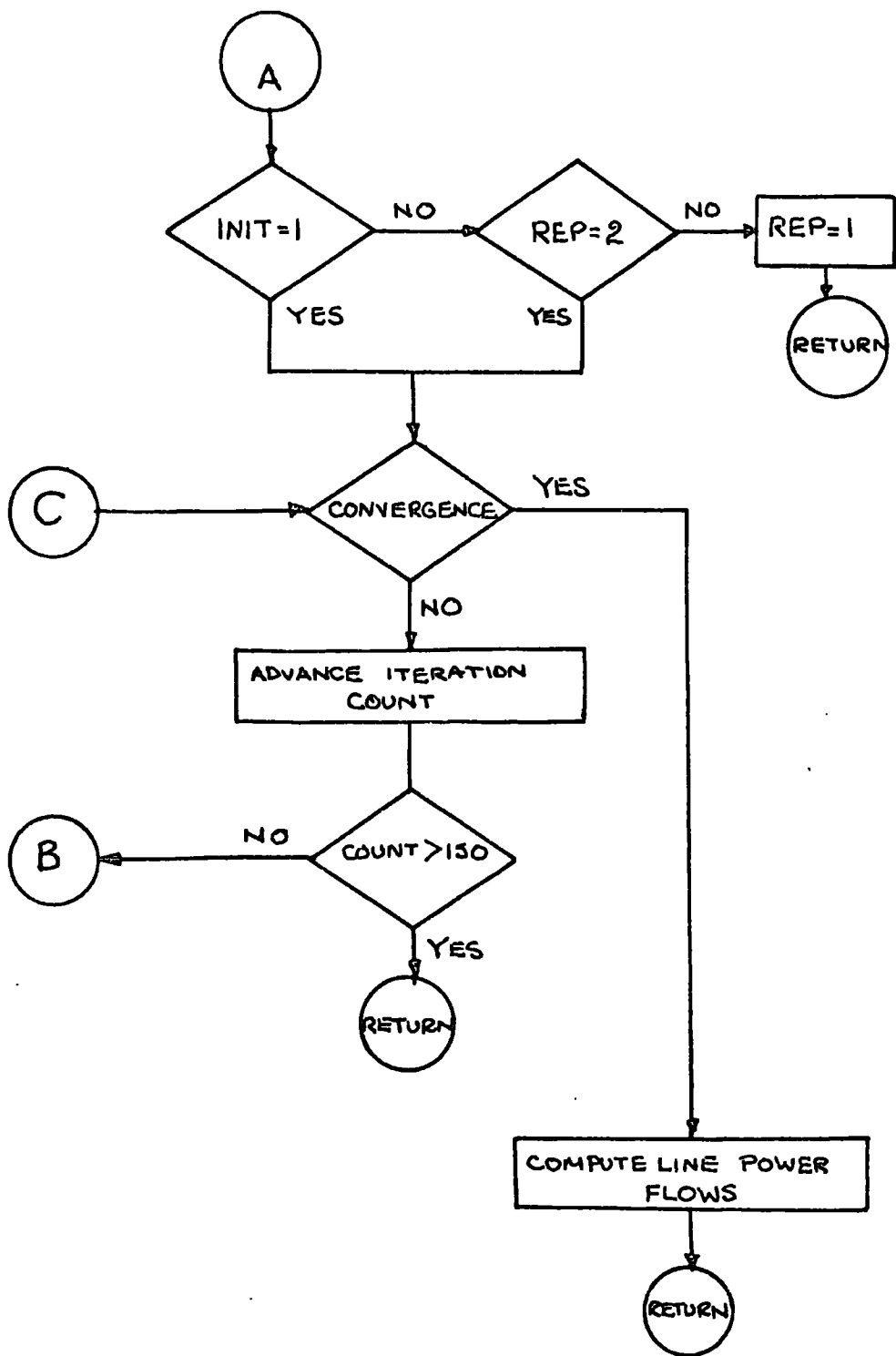


Fig. D.2 Flow Diagram For The Load Flow Subroutine, IFLOW.

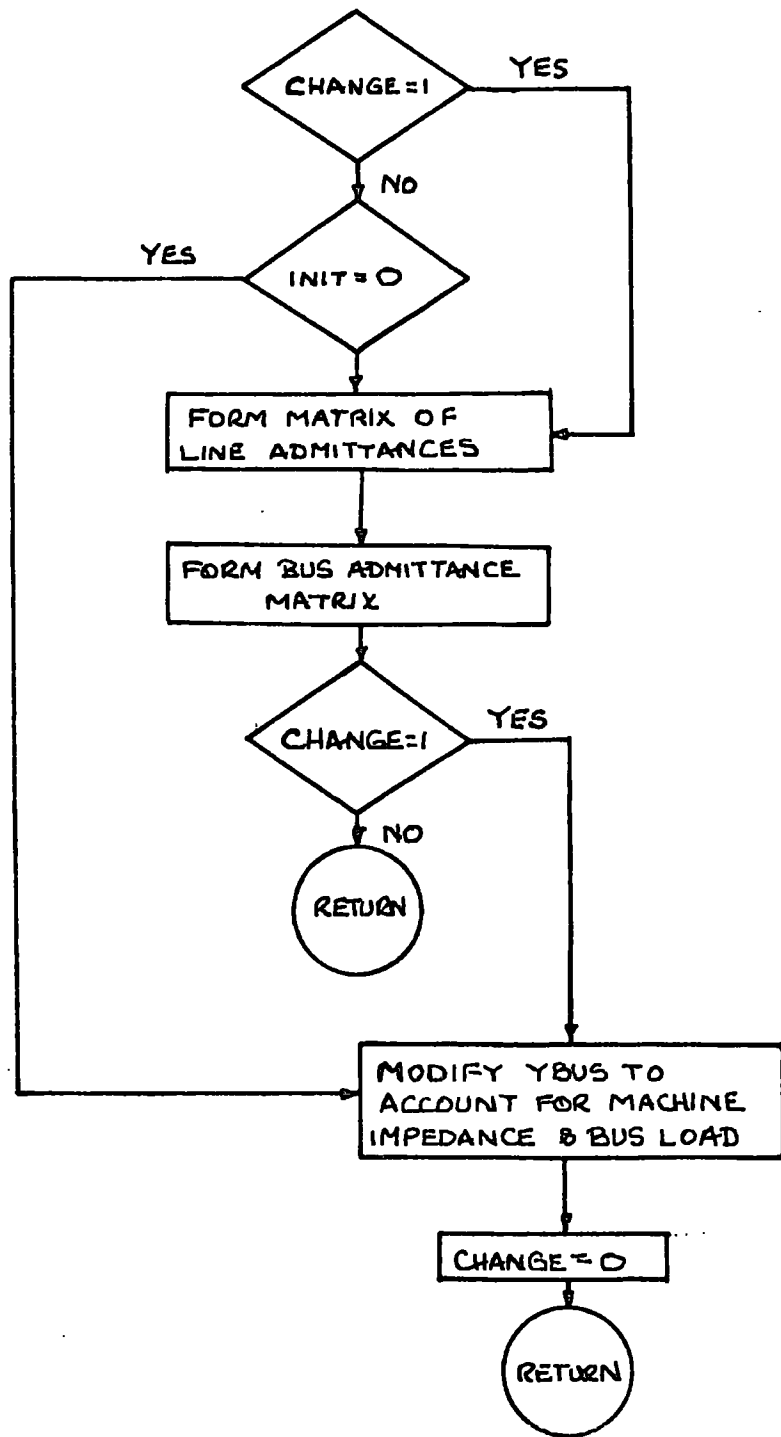


Fig. D.3 Flow Diagram Of The Subroutine MODAT.

APPENDIX E

A DESCRIPTION OF THE LINEAR PROGRAM

The high level language FORTRAN IV⁽²⁵⁾ and Double Precision complex variables were used throughout.

SUBROUTINES CALLED

MAIN fig. E.1

The MAIN program contains the machine model and calls the other subroutines at the required moment. The systems non-linear equations are solved to obtain the initial operating conditions about which the linearised model will operate.

INV.

Equations (C.32) require a matrix inversion. Complex line impedances are used and consequently the routine must have the ability to invert a complex matrix. The method used was based on the CACM Alogorithum 42.⁽⁵⁴⁾ This inverts a square matrix, A, by applying a series of elementary row operations to the matrix to reduce it to the identity matrix. When these operations are applied to the identity matrix the inverse of the matrix A results.

Other subroutines called are, MODAT, LFLOW, EULER, MEULER, RKFIX, RKVAR, PLOTYY and the function sub-programs DIMAG, DREAL. These are discussed in Appendix D.

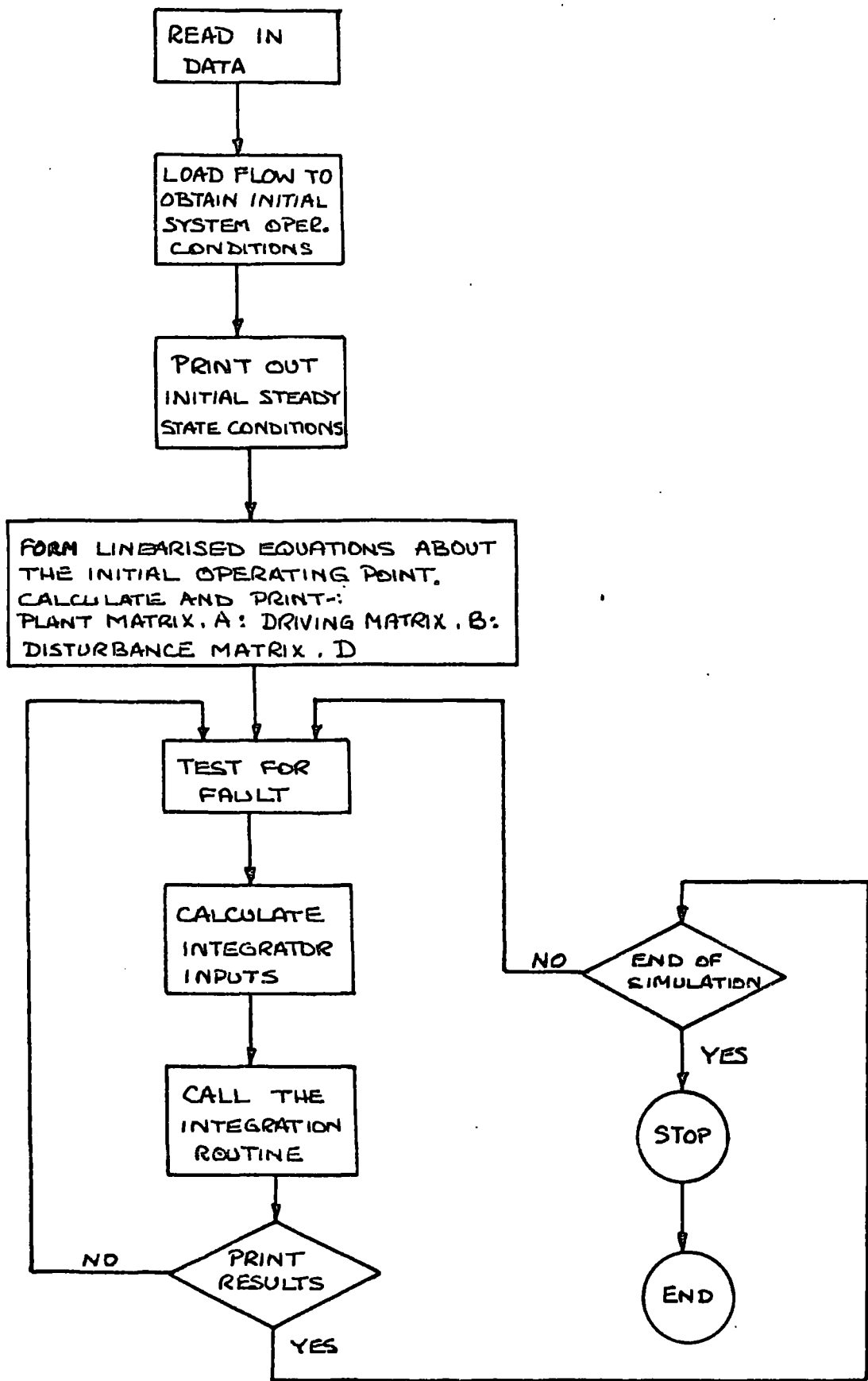
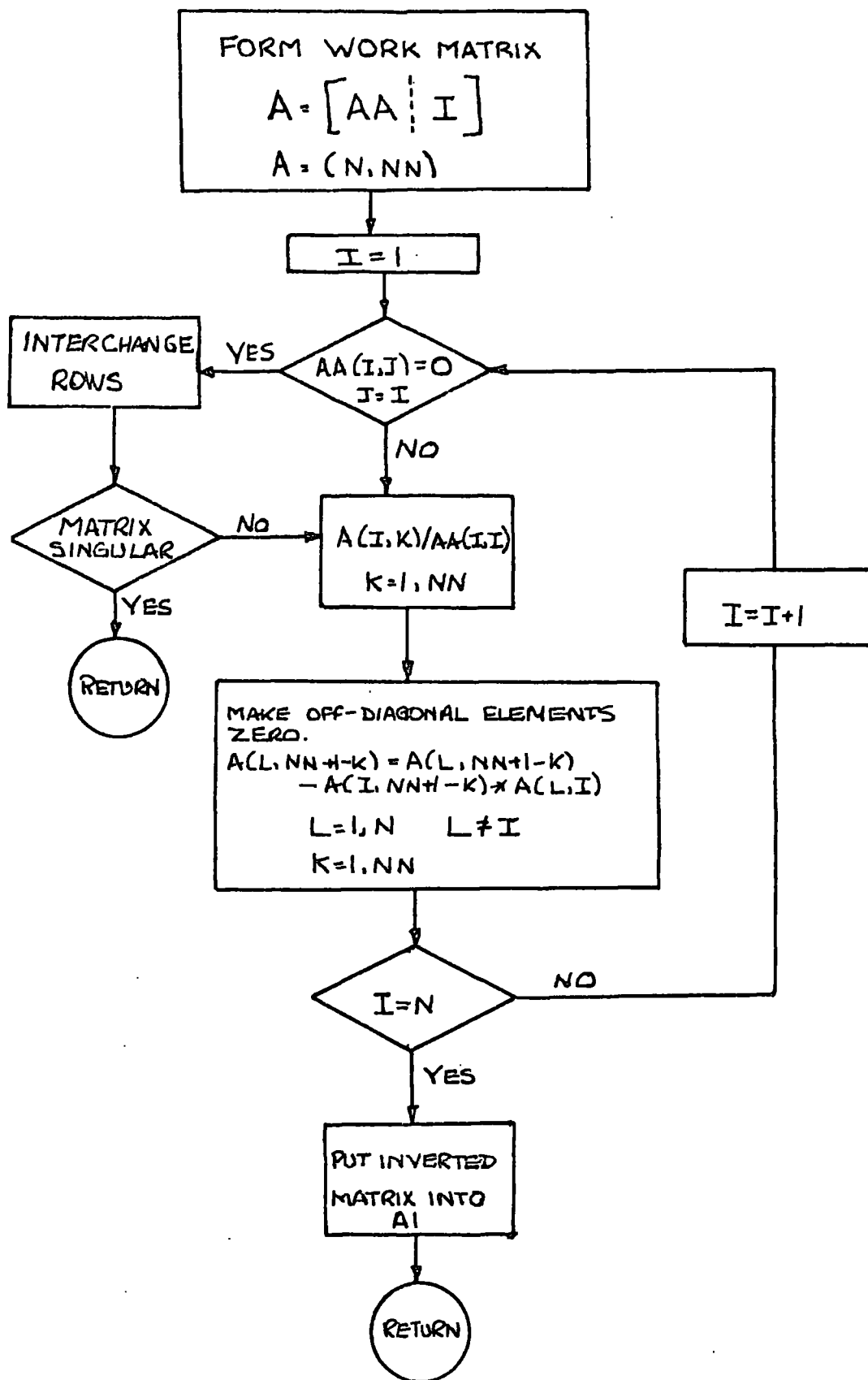


Fig. E.1 Flow Diagram For The Linearised Multi-Machine Program.



AA - MATRIX TO BE INVERTED.
A1 - INVERTED MATRIX.

Fig. E.2 Flow Diagram For The Complex Matrix Inversion Subroutine INV.

APPENDIX F

DIGITAL PROGRAM TO PLOT INVERSE NYQUIST DIAGRAMS

The high level language FORTRAN IV⁽²⁵⁾ and complex variables were used throughout.

SUBROUTINES CALLED

MAIN fig. F.1

Initial frequency data is read, and all output is printed, from this section. The other subroutines are called from the MAIN program at the required time.

The d-circles are not plotted by the computer because;

- (i) The plot comes out on the line printer and consequently a low accuracy is obtained. Typically for axis ± 5 , y is ± 0.25 and x is ± 0.1 .
- (ii) No graphical display terminals were available at Durham at the time of writing the program.

Fig. F.1 shows that the MAIN program is completed once for each diagonal element of $Q(p)$. Only one PLOT matrix is called. In designing the program two options were available;

- (i) Have $m \times m$ PLOT matrices available and deal with all the \hat{q}_{ij} elements together.
- (ii) Use one PLOT matrix and deal with each element \hat{q}_{ij} individually.

The latter method was selected as the computer time used was small relative to the large amount of memory storage needed with the first option.

INV.

See Appendix E.

PLOTTER fig. F.2

This plots the I.N. diagrams. Fixed scale values are used as with variable values the scale on each plot could be different.

TRFN

This specifies $G(p)$ in transfer function form and also specifies the elements in the controller matrices $K(p)$ and $L(p)$. If $G(p)$ is to be computed from the state space equations INFACE is called.

INFACE fig. F.3

This inputs the A, B and C matrices and forms $G(p)$.

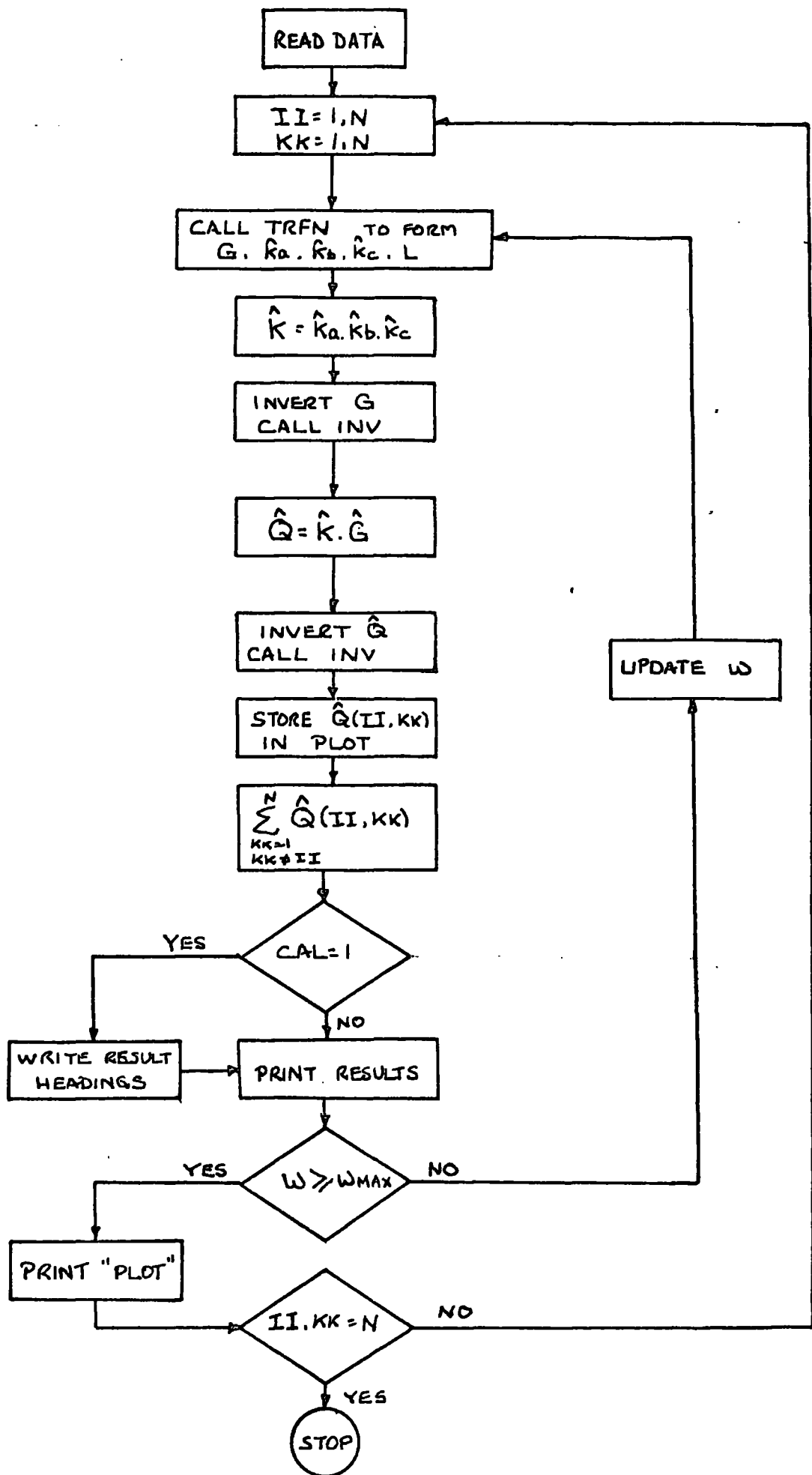


Fig. F.1 Flow Diagram For The Inverse Nyquist Array Design Program.

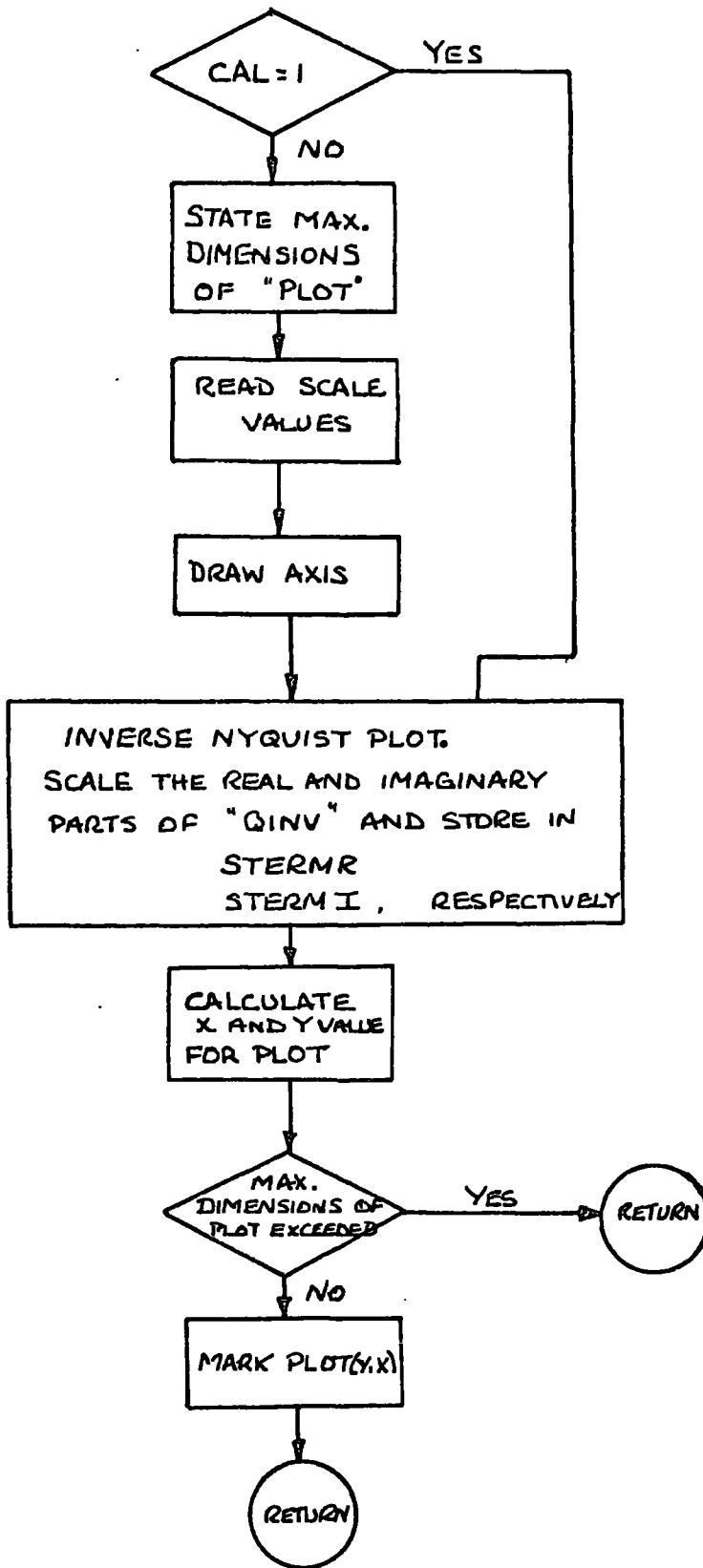


Fig. F.2 Flow Diagram For The Inverse Nyquist Plotting Subroutine PLOTTER.

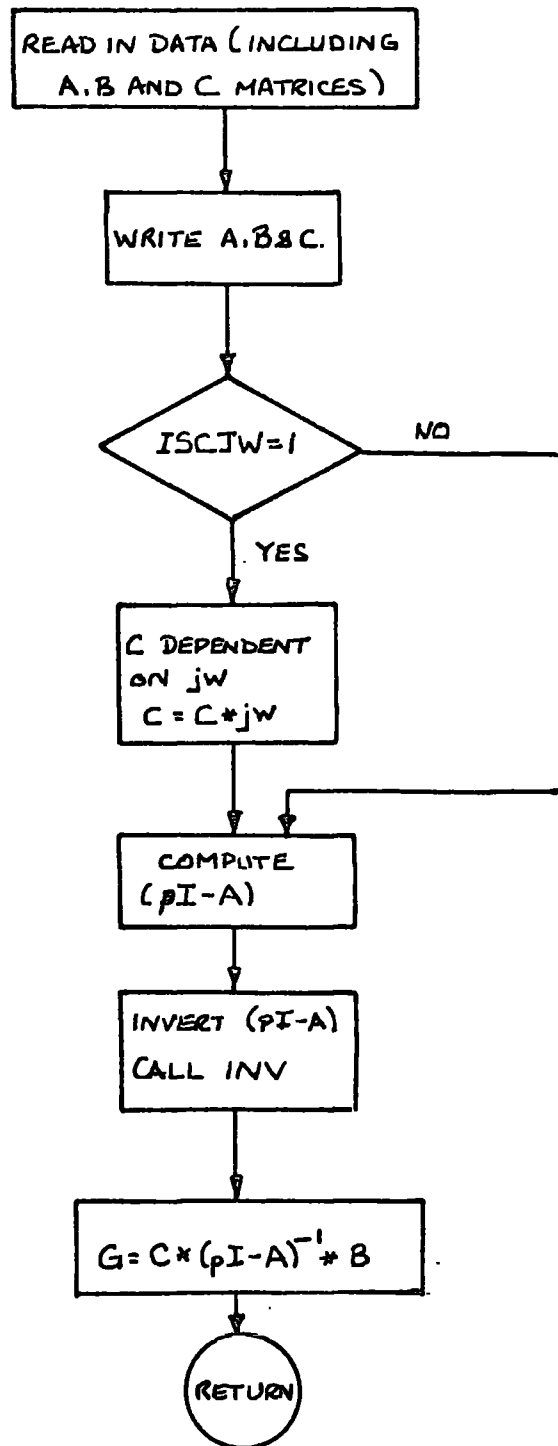


Fig. F.3 Flow Diagram For The Subroutine INFACE.
This Subroutine Computes The Plant Transfer Function
Matrix $G(p)$.

APPENDIX G

MACHINE AND SYSTEM PARAMETERS

The machine parameters have been used previously by Dandeno and Kundur. (8)

$$x_d = 0.978 \text{ p.u.}$$

$$x_q = 0.616 \text{ per unit}$$

$$x_d' = 0.325 \text{ p.u.}$$

$$T_{d0}' = 4.58 \text{ s.}$$

H varies between 2 - 6 KJ/KVA

K_d varies between 0 and 0.01

SYSTEM PARAMETERS

∇ - system (fig. 5.1)

$$Z_{12} = \text{varied between } 0.01 - 0.2 \text{ p.u.}$$

$$Z_{13} = 0.12 \text{ p.u.}$$

$$Z_{34} = 0.12 \text{ p.u.}$$

$$Z_{24} = 0.24 \text{ p.u.}$$

Bus 3 being subjected to a 3ϕ fault of varying time length.

λ - system (fig. 2.7)

$$Z_{13} = 0.12 \text{ p.u.}$$

$$Z_{23} = 0.12 \text{ p.u.}$$

$$Z_{34} = 0.28 \text{ p.u.}$$

Bus 3 being subjected to a 3ϕ fault of varying time length.

APPENDIX H

MACHINE DATA

$H_1 = 6 \text{ KJ/KVA}$	$H_2 = 3 \text{ KJ/KVA}$
$x_{d1} = 0.978 \text{ p.u.}$	$x_{d2} = 0.978 \text{ p.u.}$
$x_{q1} = 0.616 \text{ p.u.}$	$x_{q2} = 0.616 \text{ p.u.}$
$x_{d1}' = x_{q1}' = 0.325 \text{ p.u.}$	$x_{d2}' = x_{q2}' = 0.325 \text{ p.u.}$
$K_{d1} = 0.01$	$K_{d2} = 0.01$

SYSTEM DATA - Model system fig. 2.7

$Z_{13} = 0.12 \text{ p.u.}$
 $Z_{23} = 0.12 \text{ p.u.}$
 $Z_{34} = 0.24 \text{ p.u.}$
 $V_B = 1.0 \text{ p.u.}$

PLANT MATRIX, A

-0.261799	0.0	-31.121246	12.797647	-27.72003	3.168726
0.0	-0.523599	25.595294	-62.242492	6.337453	-55.440006
1.0	0.0	0.0	0.0	0.0	0.0
0.0	1.0	0.0	0.0	0.0	0.0
0.0	0.0	0.0	0.0	-0.218341	0.0
0.0	0.0	0.0	0.0	0.0	-0.218341

DRIVING MATRICES

B,	26.179939	0.0	D,	0.0	0.0
	0.0	52.359878		0.0	0.0
	0.0	0.0		0.0	0.0
	0.0	0.0		0.0	0.0
	0.0	0.0		0.165785	0.0
	0.0	0.0		0.0	0.165785

REGULATOR CONSTANTS

Input Power Regulator

$$T_v = 0.08 \text{ s} \quad T_s = 0.75 \text{ s} \quad K_p = 1.0$$

Limits = + 3.0 and 0.0 p.u.

Field Excitation Regulator

Static Exciter, $T_{ex} = 0.03 \text{ s}$

Rotating Exciter, $T_{ex} = 0.5 \text{ s}$

Gain, $k = 10.0$

